Home: www.HangGliderHistory.com

NASA TN D-1009

TECHNICAL NOTE

D-1009

TRANSONIC PRESSURE DISTRIBUTIONS ON THREE RIGID WINGS SIMULATING PARAGLIDERS WITH VARIED CANOPY CURVATURE AND LEADING-EDGE SWEEP

By Paul G. Fournier and B. Ann Bell

Langley Research Center
Langley Air Force Base, Va.

NATIONAL AERONAUTICS AND SPACE ADMINISTRATION

WASHINGTON

January 1962

1L

Home: www.HangGliderHistory.com

NATIONAL AERONAUTICS AND SPACE ADMINISTRATION

TECHNICAL NOTE D-1009

TRANSONIC PRESSURE DISTRIBUTIONS ON THREE RIGID WINGS SIMULATING PARAGLIDERS WITH VARIED CANOPY CURVATURE AND LEADING-EDGE SWEEP

By Paul G. Fournier and B. Ann Bell

L
1
8
6
5

SUMMARY

An investigation has been made in the Langley 8-foot transonic pressure tunnel to determine the transonic chordwise pressure distribution of three paraglider models through an angle-of-attack range from 10° up to 90°. Three rigid metal models simulated a paraglider which had a basic flat planform with leading edges swept back 45°. These configurations had leading-edge sweep angles of 61.6°, 52.5°, and 48.6°, which resulted in one-half-circle, one-third-circle, and one-quarter-circle curvature of the semispan trailing edges when viewed from downstream. The results of the investigation are presented as curves of chordwise pressure distributions at four spanwise locations for each model.

INTRODUCTION

The performance, stability, and control characteristics of paragliders at subsonic, transonic, and supersonic speeds are being studied at the Langley Research Center. Some preliminary work on the paraglider concept is presented in references 1 to 4.

Widespread interest in the paraglider for applications such as launch-vehicle recovery and terminal recovery of spacecraft has necessitated detailed load-distribution data over a range of Mach numbers. Observations of paraglider models in previous investigations have shown that the shape the canopy assumes in flight can be closely represented by portions of a conical surface. With this assumption, rigid metal models of varying curvature were constructed (one-half-circle, one-third-circle, and one-quarter-circle curvature of the semispan trailing edges when viewed from downstream) to measure the chordwise pressure distribution over a Mach number range from low subsonic to high supersonic.

The low-subsonic pressure-distribution data are presented in reference 5. Presented herein are results of an investigation at transonic speeds for an angle-of-attack range from 10° up to 90°. Some discussion on the applicability and general characteristics of the data is included.

SYMBOLS

The coefficients and symbols used in the presentation of the data herein are as follows:

L 1865

c local projected chord, in.

b span, in.

q dynamic pressure, $\frac{1}{2}\rho V^2$, lb/sq ft

x distance along local projected chord, in.

z distance above keel reference plane (horizontal plane through keel center line), in.

p_l local pressure, lb/sq ft

p free-stream static pressure, lb/sq ft

C_p pressure coefficient, $\frac{p_l - p}{q}$

M free-stream Mach number

V free-stream velocity, ft/sec

α nominal keel angle of attack, deg

ρ air density, slugs/cu ft

DESCRIPTION OF MODEL

Pressure distributions were obtained on three 1/10-inch-thick metal and plastic models constructed to simulate a range of conical shapes that the paraglider might assume in flight. These models are the same models that were used in the investigation of reference 5. The models had a basic flat planform with leading edges swept back 45° (area of 1 square foot). These configurations had leading-edge sweeps of 61.6°, 52.5°, and 48.6°, which resulted in one-half-circle, one-third-circle, and one-quarter-circle curvature of the semispan trailing edges when viewed from downstream. Photographs of the models are presented in figures 1 and 2.

L
1
8
6
5

The difference in curvature was accomplished by development of the panels of each model around a right-circular cone. (See fig. 3.) The resulting models with panels forming one-half of a conical surface, one-third of a conical surface, and one-fourth of a conical surface are designated as models 1, 2, and 3, respectively. Geometric characteristics of all three models are presented in figure 4.

The right and left panels for each model were welded to a hollow center keel which carried small pressure tubes to the canopy. The right panel had the lower-surface pressure orifices (including those on the leading edge and trailing edge), and the left panel had the upper-surface pressure orifices. The location of the orifices at each of the four spanwise stations, given in fraction of local projected chord, are presented in figure 5. In addition, these orifice locations are given in terms of vertical distance from the keel reference plane and horizontal distance along the paraglider keel.

Plastic leading edges of approximately 3/8-inch diameter were cast to each model. An auxiliary strut extended below the reference plane of the models. (See figs. 1 and 2.) Wires were attached from the strut to the leading edge of the models to reduce the flexure of the paraglider panels. It is believed that the strut had some effect on the pressure data at transonic speeds, especially at the higher angles of attack, but this effect was not evaluated.

APPARATUS, TESTS, AND CORRECTIONS

The sting-supported models were tested in the Langley 8-foot transonic pressure tunnel through a Mach number range from 0.80 to 1.20. This facility is rectangular in cross section with the upper and lower walls slotted longitudinally to allow continuous operation through the transonic speed region with negligible effects of choking and blockage.

All tests were made with the tunnel operating at a stagnation pressure of 0.25 atmosphere. The stagnation temperature and dewpoint were maintained at a level to preclude shock condensation effect.

The Reynolds number based on the paraglider keel length varied from approximately 1.11×10^6 to 1.25×10^6 for the range of test Mach numbers.

No corrections to the free-stream Mach number and dynamic pressure for the effects of model and wake blockage are necessary for tests in the slotted test section of the Langley 8-foot transonic pressure tunnel (ref. 6). There is a range of Mach numbers above a Mach number of 1.00 where the data are affected by reflected compressions and expansions from the test-section boundary. From considerations of the results of reference 7, it is believed that for Mach numbers up to approximately 1.03 the effects of these disturbances on the measurements made in the present investigation would be negligible. No test data are presented in the range where the reflected boundary disturbance might impinge upon the models.

L
1
8
6
5

The angles of attack have not been corrected for loads on the model; however, it was estimated that the maximum correction would be about 0.1° or 0.2°.

PRESENTATION OF DATA

Data on the three paraglider models through the Mach number range and angle-of-attack range are presented in figures 6 to 8 as plots of pressure coefficient C_p against fraction of local chord projected to the plane of the leading edges and keel x/c. A short discussion on the applicability of the pressure data is presented as well as a few comments on the general characteristics of the data. It should be kept in mind that the effect of the auxiliary strut has not been evaluated in the presentation of these data.

As pointed out in reference 5 for the subsonic pressure distribution of the paraglider models, the pressure data for angles of attack up to between 10° and 15°, depending on the model, will result in negative lift values on all stations. The data presented herein begin at an angle of attack of 10°.

DISCUSSION

Paragliders now being considered for launch vehicle and spacecraft application have either large inflatable keel and leading edges or small metal-tube keel and leading edges. It is believed that the data on the three rigid paragliders of the present paper will more closely simulate the loads expected on configurations with rigid keels and leading edges of small diameter.

L
1
8
6
5

The transonic pressure-distribution curves for these paraglider models indicate that the peak pressures near the leading edge of the inboard stations are in general somewhat lower and less defined than those shown in the subsonic data of reference 5. However, the maximum pressures for the outboard stations were slightly higher for the transonic data. The present data also indicate that the maximum pressure varies less with increasing Mach number. A comparison of the pressure at the various stations showed a loss of loading near the outboard chord which decreased with decreasing curvature of the canopy, as did the data of reference 5. These effects might be expected from consideration of the spanwise angle-of-attack variation shown in figure 5.

CONCLUDING REMARKS

An investigation has been made of the chordwise pressure distribution at transonic speeds of three rigid metal models simulating a paraglider. In general, the over-all local distribution characteristics shown in the present paper indicate that the peak pressures near the leading edge of the inboard stations are somewhat lower and less defined than those shown in the subsonic data of NASA Technical Note D-983. However, the maximum pressures for the outboard stations were slightly higher for the transonic data. Also, as expected, the present data indicated a loss of loading near the outboard chord which decreased with decreasing curvature of the canopy.

Langley Research Center,
National Aeronautics and Space Administration,
Langley Air Force Base, Va., October 25, 1961.

Home: www.HangGliderHistory.com

REFERENCES

1. Rogallo, F. M., and Lowry, J. G.: Flexible Reentry Gliders. Preprint No. 175C, Soc. Automotive Eng., Apr. 1960.

2. Rogallo, Frances M., Lowry, John G., Croom, Delwin R., and Taylor, Robert T.: Preliminary Investigation of a Paraglider. NASA TN D-443, 1960.

3. Naeseth, Rodger L.: An Exploratory Study of a Parawing as a High-Lift Device for Aircraft. NASA TN D-629, 1960.

4. Hewes, Donald E.: Free-Flight Investigation of Radio-Controlled Models With Parawings. NASA TN D-927, 1961.

5. Fournier, Paul G., and Bell, B. Ann: Low Subsonic Pressure Distributions on Three Rigid Wings Simulating Paragliders With Varied Canopy Curvature and Leading-Edge Sweep. NASA TN D-983, 1961.

6. Wright, Ray H., and Ward, Vernon G.: NACA Transonic Wind-Tunnel Test Sections. NACA Rep. 1231, 1955. (Supersedes NACA RM L8J06.)

7. Wright, Ray H., Ritchie, Virgil S., and Pearson, Albin O.: Characteristics of the Langley 8-Foot Transonic Tunnel With Slotted Test Section. NACA Rep. 1389, 1958. (Supersedes NACA RM L51H10 by Wright and Ritchie and RM L51K14 by Ritchie and Pearson.)

L
1
8
6
5

L-1865

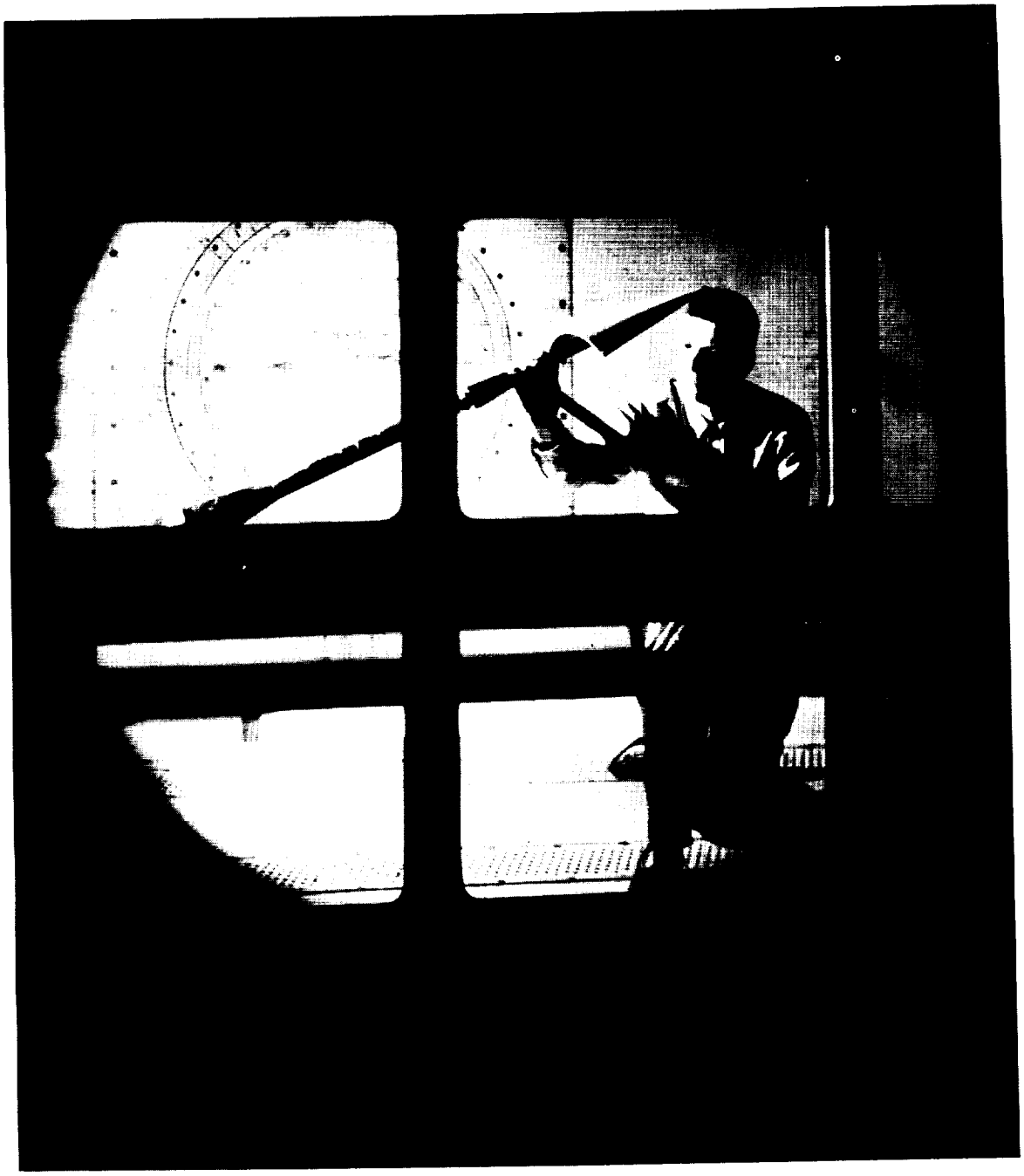

(a) Side view. L-61-1732

Figure 1.- Typical test setup.

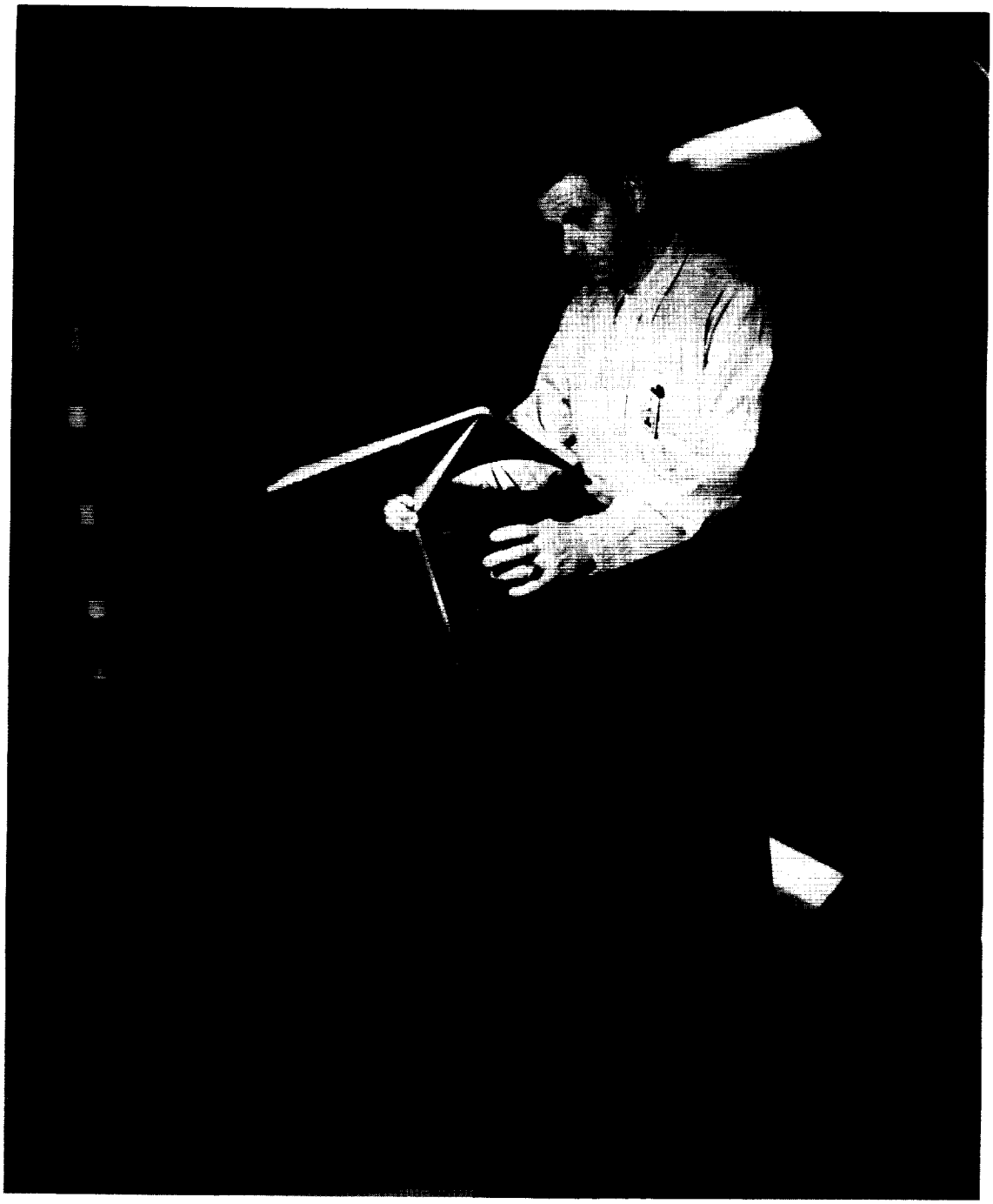

L-1865

(b) One-quarter front view. L-61-1731

Figure 1.- Concluded.

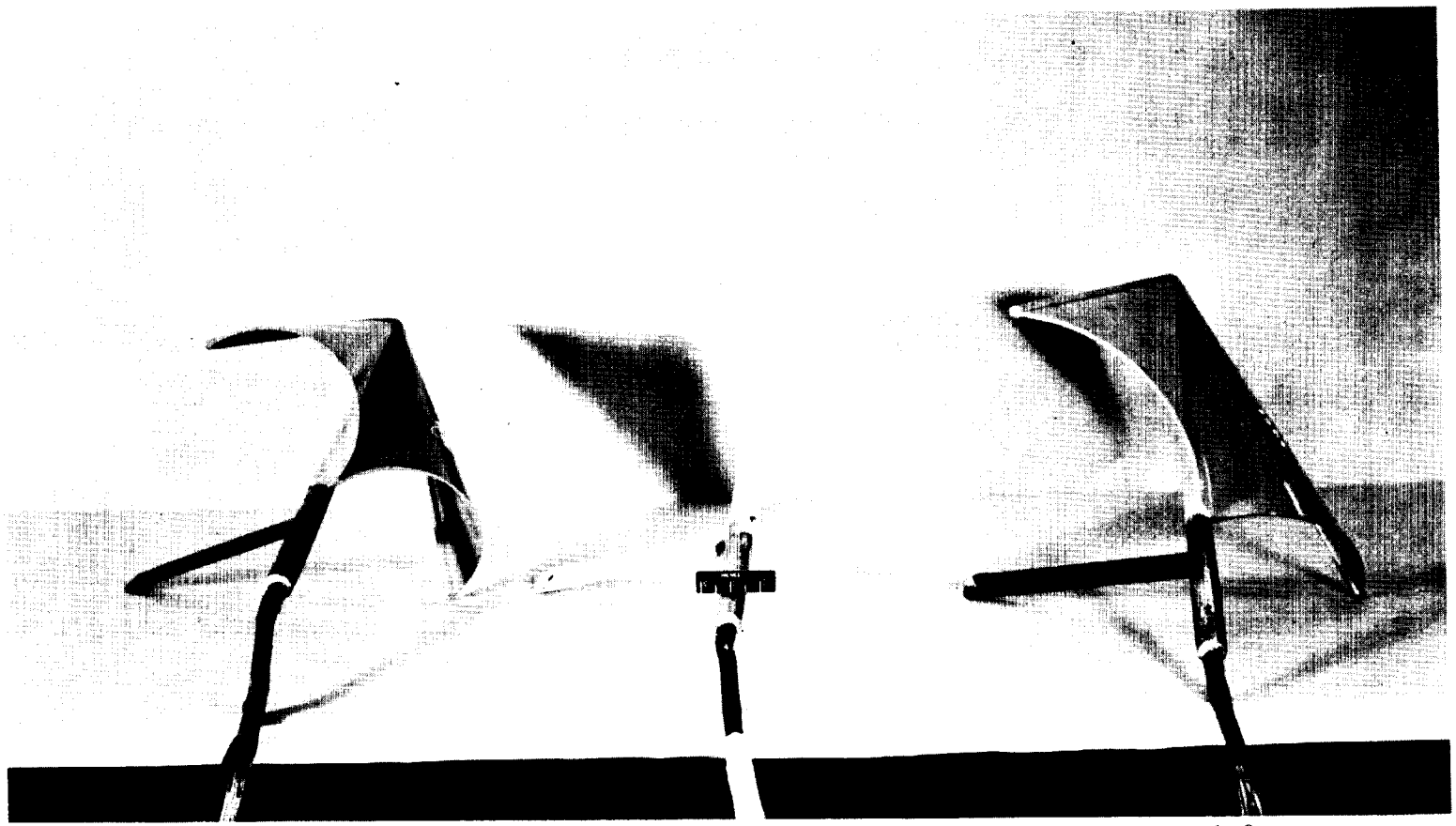

(a) One-quarter rear view. L-61-4687

Figure 2.- Photographs of the three models tested.

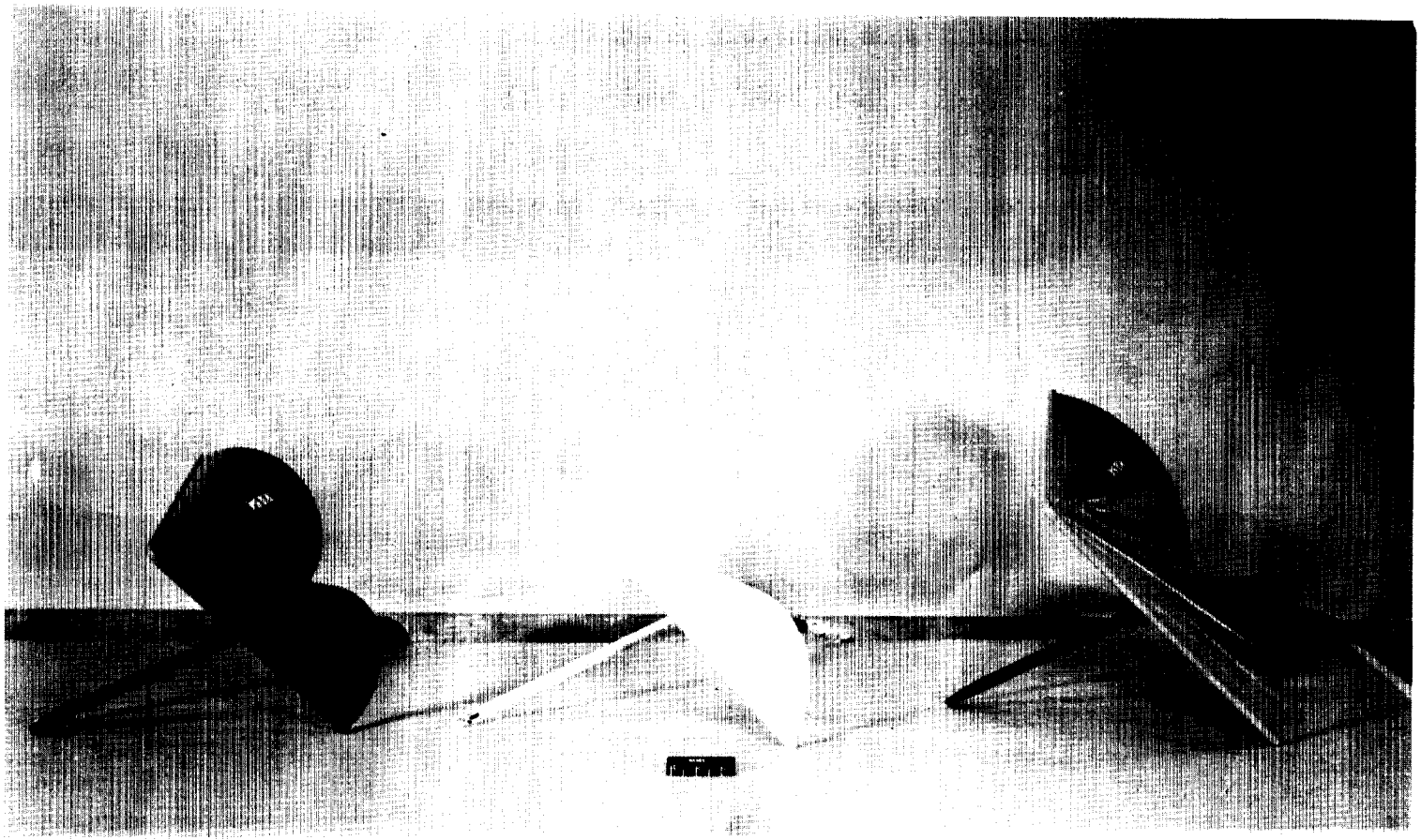

(b) Three-quarter front view. L-61-4689

Figure 2.- Concluded.

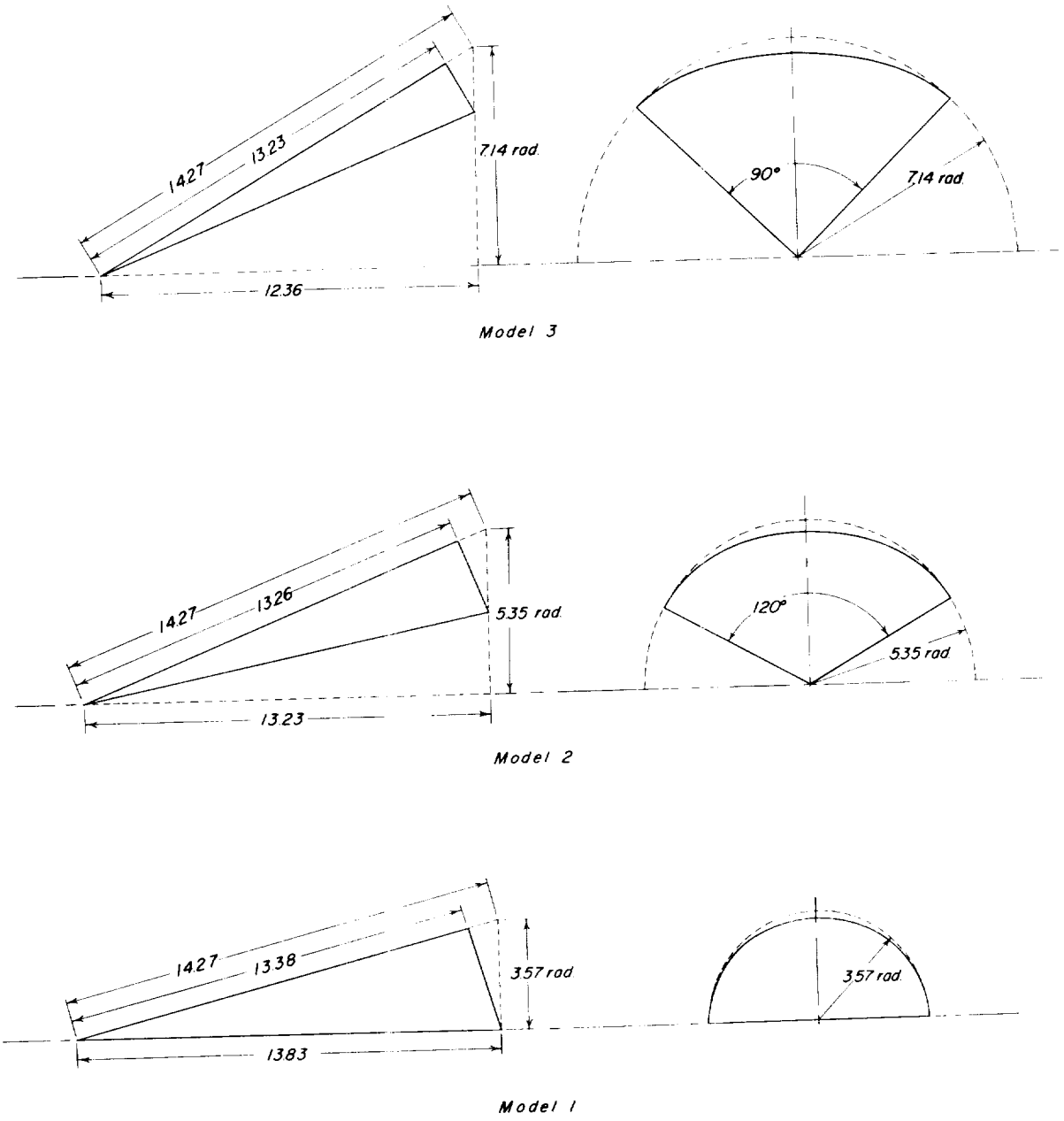

Figure 3.- Development of paraglider panels. Linear dimensions are in inches.

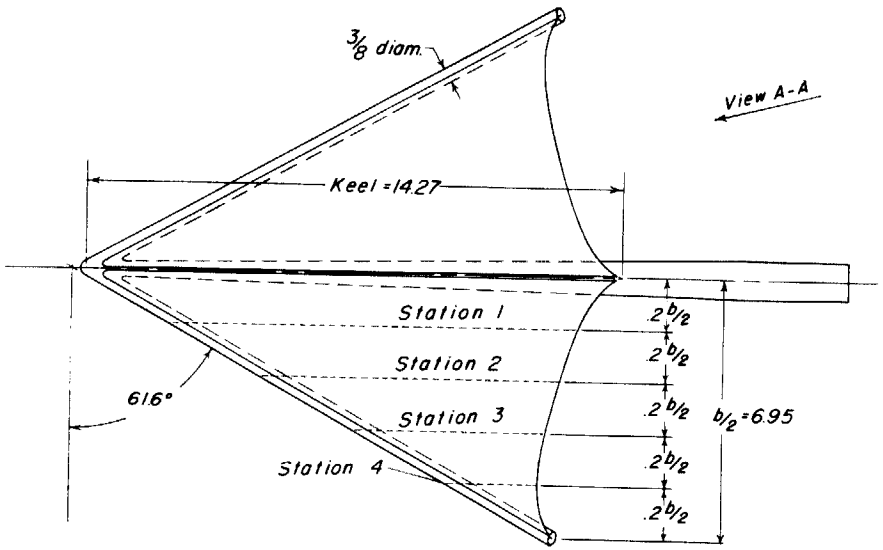

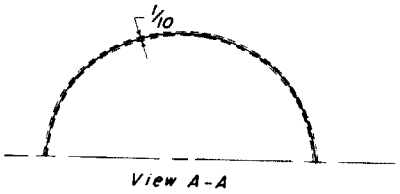

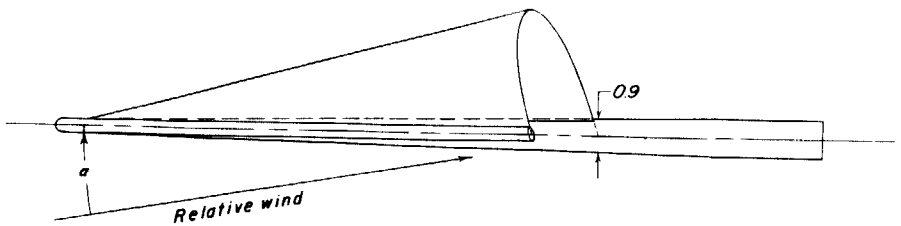

(a) Model 1.

Figure 4.- Geometric characteristics of rigid paraglider models. Linear dimensions are in inches.

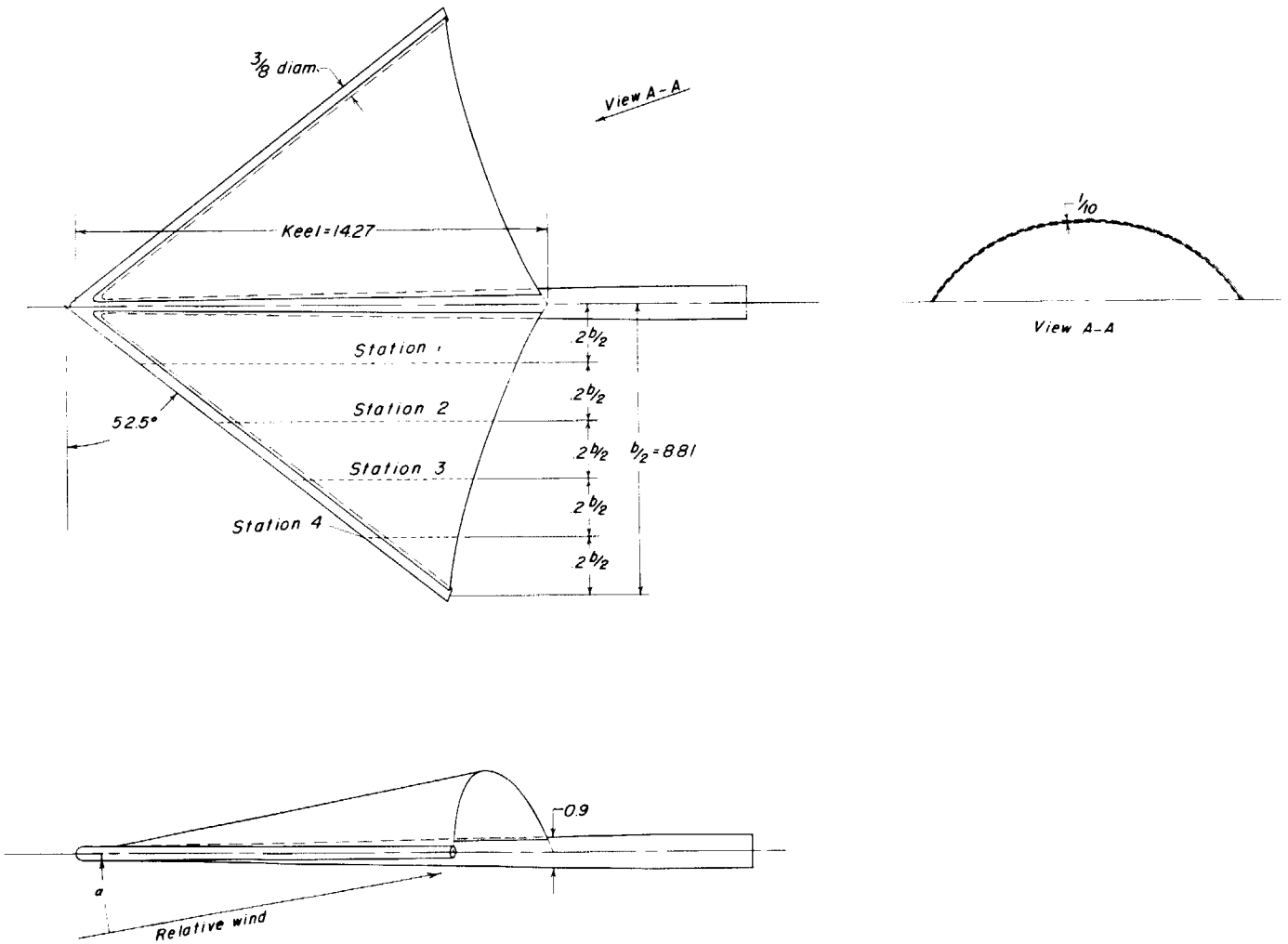

(b) Model 2.

Figure 4.- Continued.

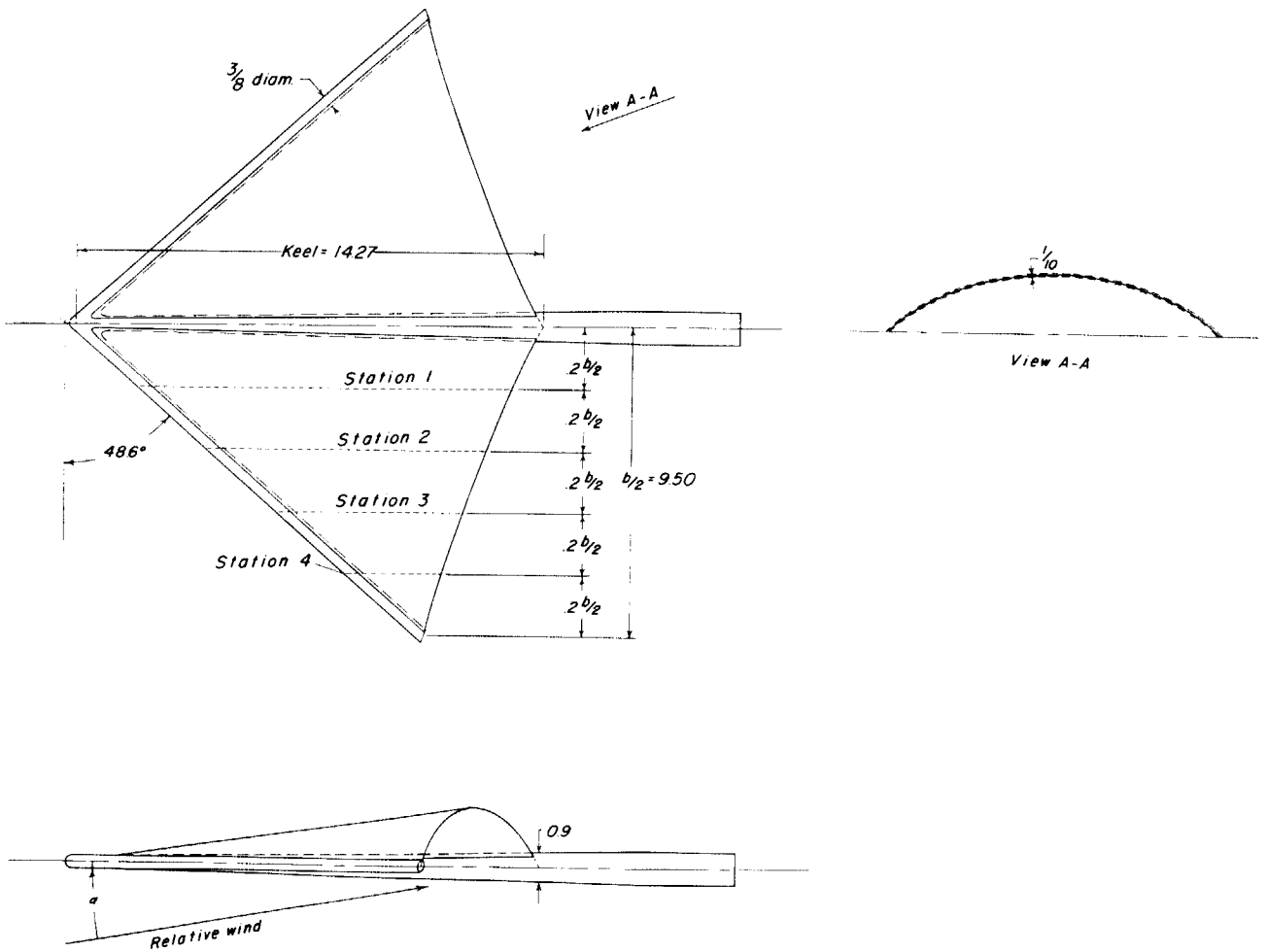

(c) Model 3.

Figure 4.- Concluded.

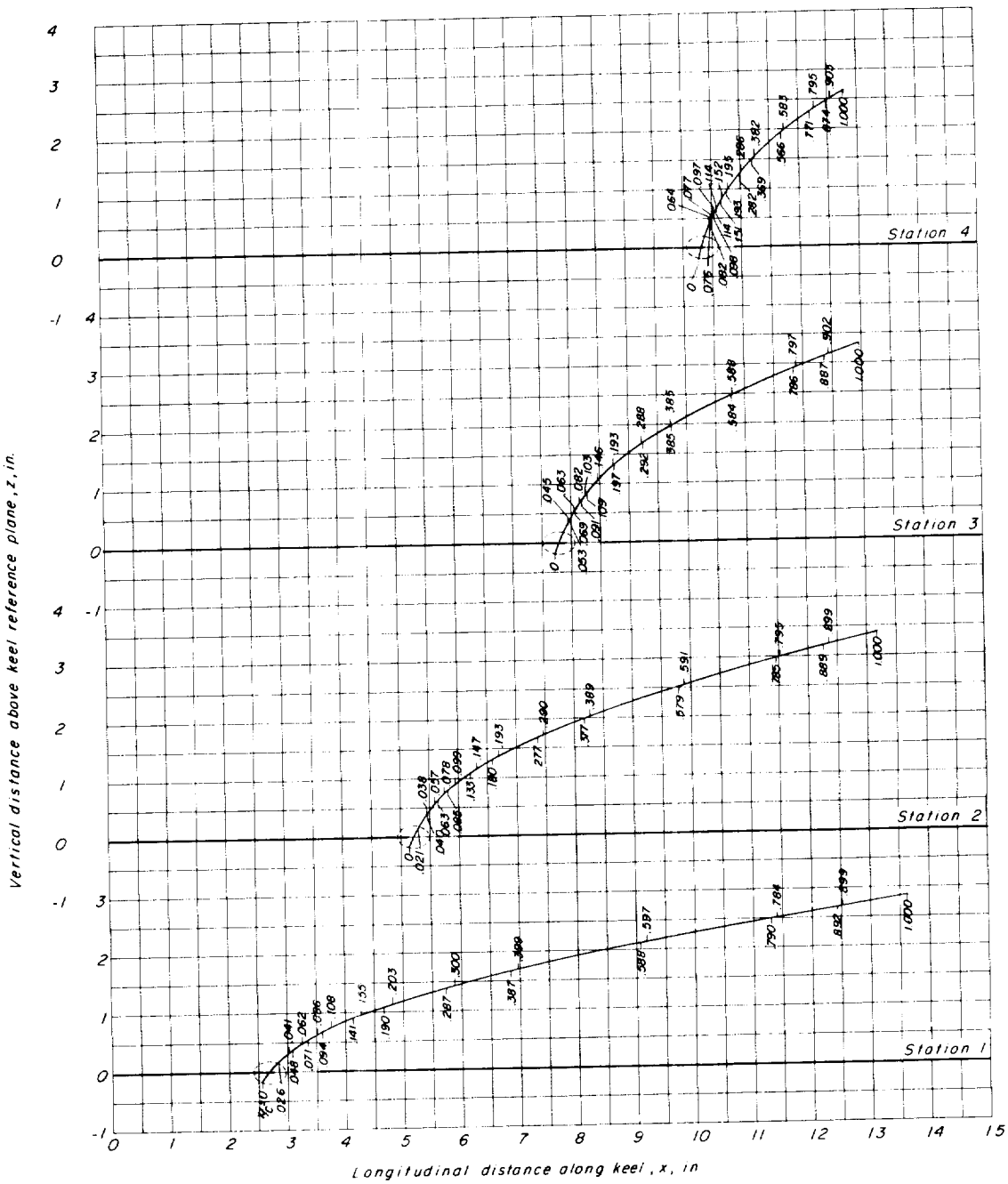

(a) Model 1.

Figure 5.- Location of lower- and upper-surface orifices designated in fraction of local projected chord c.

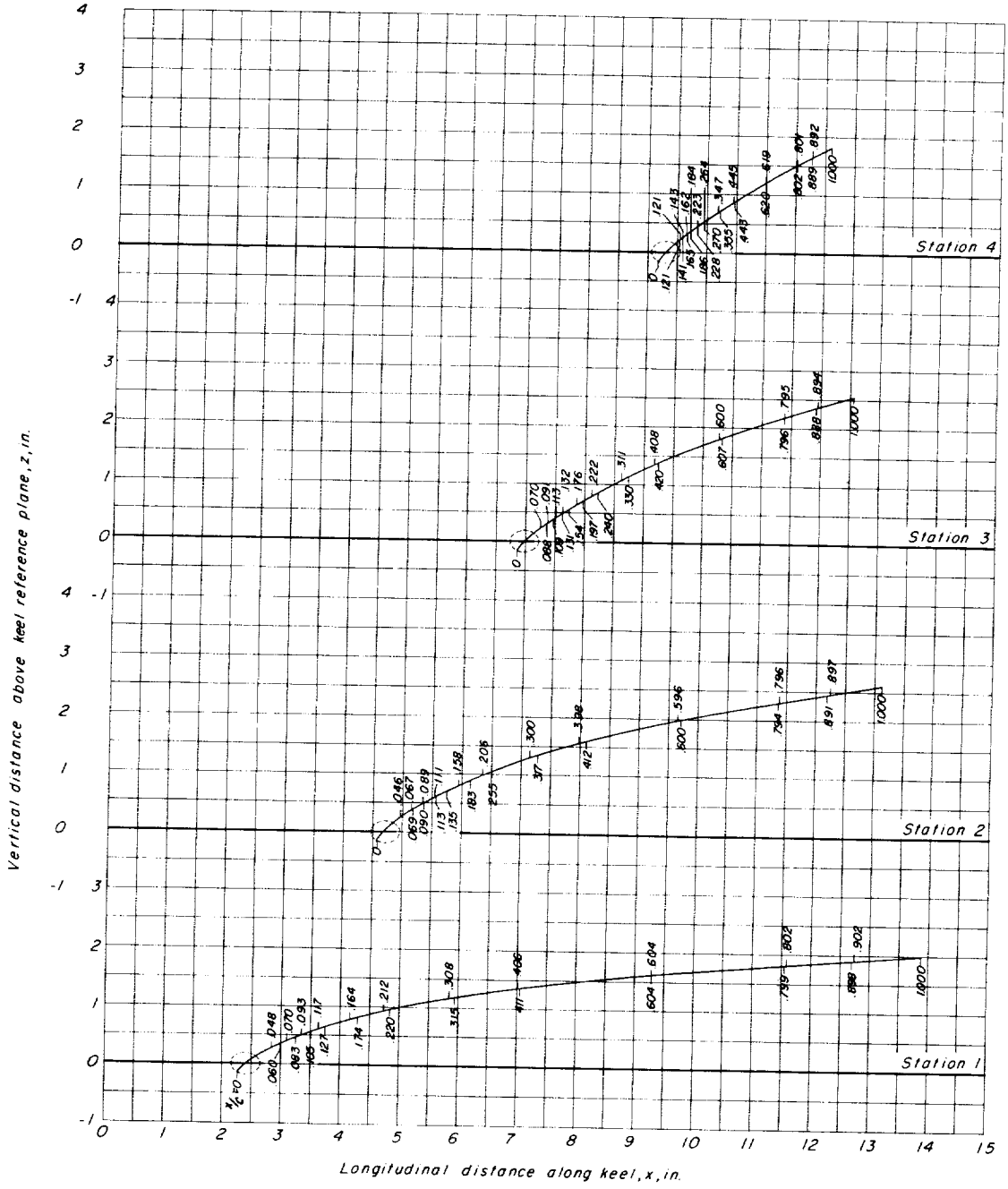

(b) Model 2.

Figure 5.- Continued.

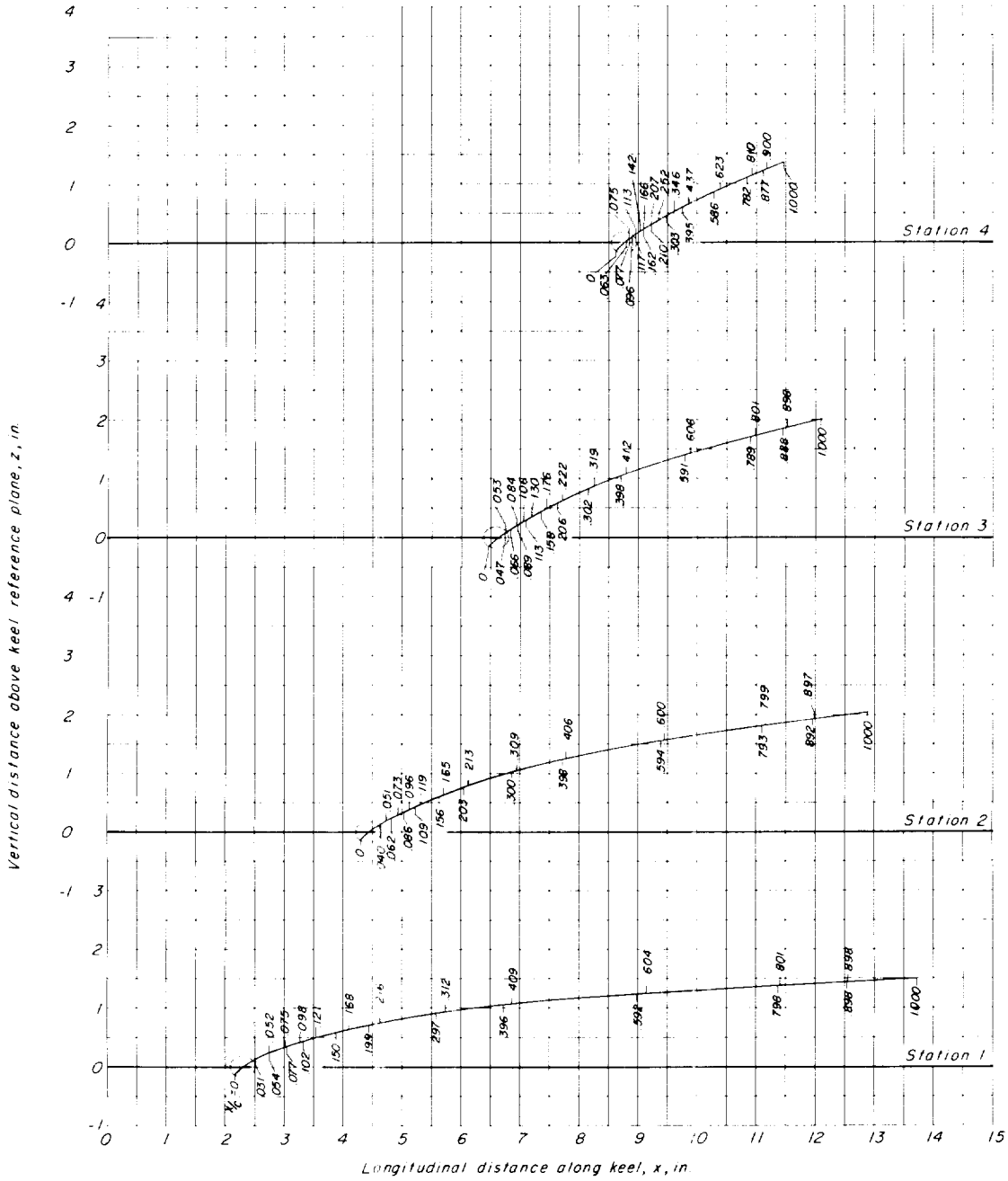

(c) Model 3.

Figure 5.- Concluded.

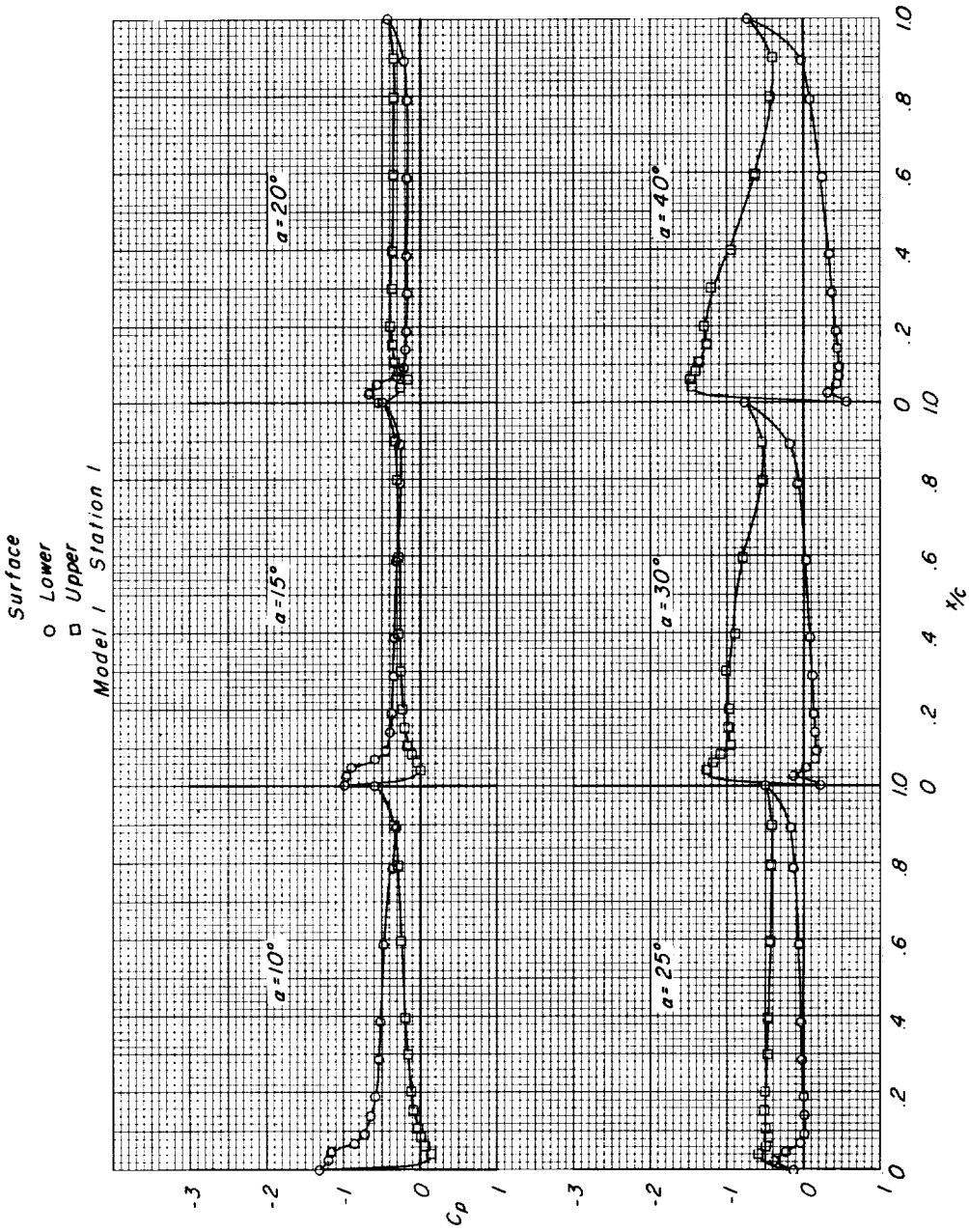

(a) M = 0.80.

Figure 6.- Pressure distributions on model 1 at various angles of attack and Mach numbers.

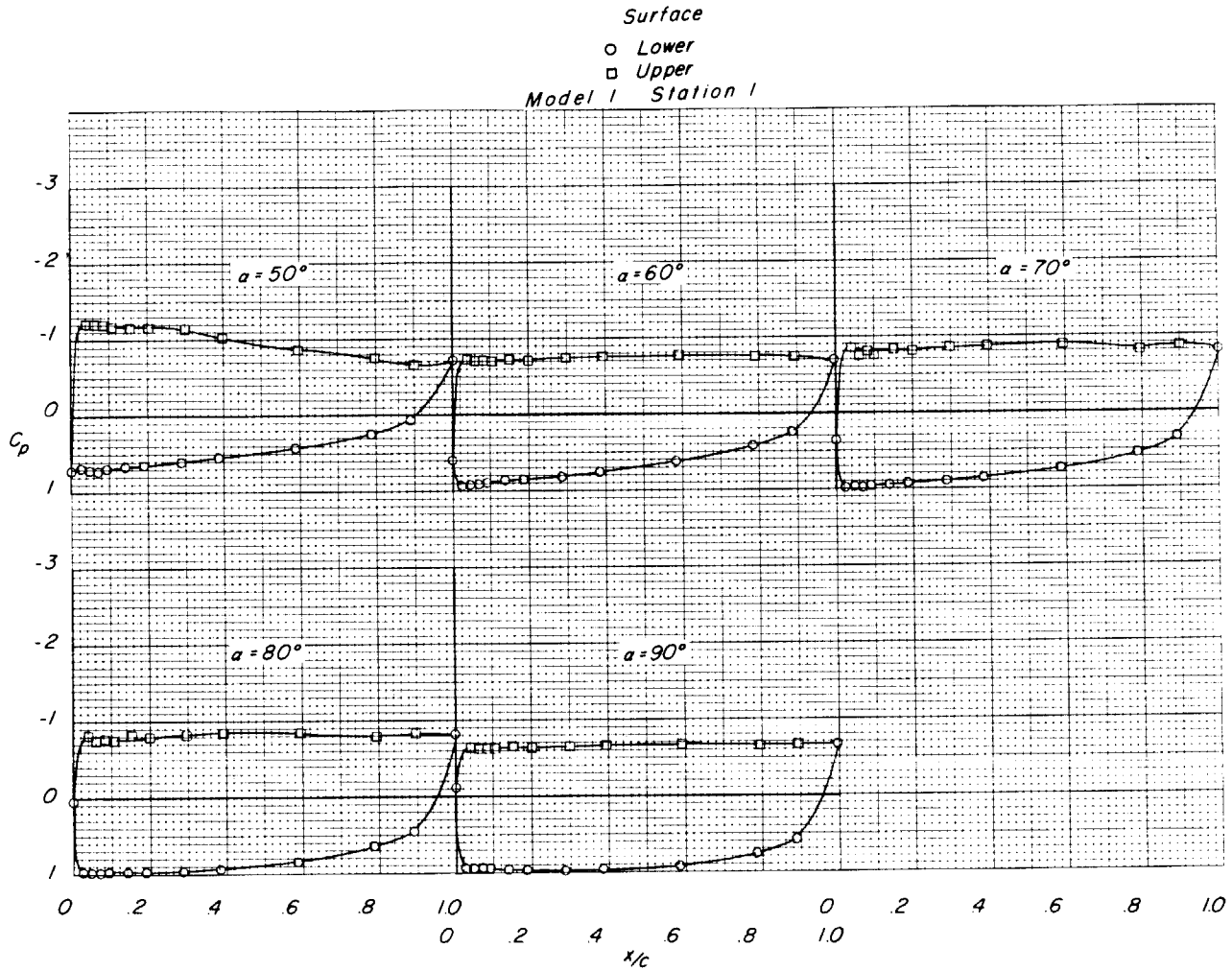

(a) M = 0.80. Continued.

Figure 6.- Continued.

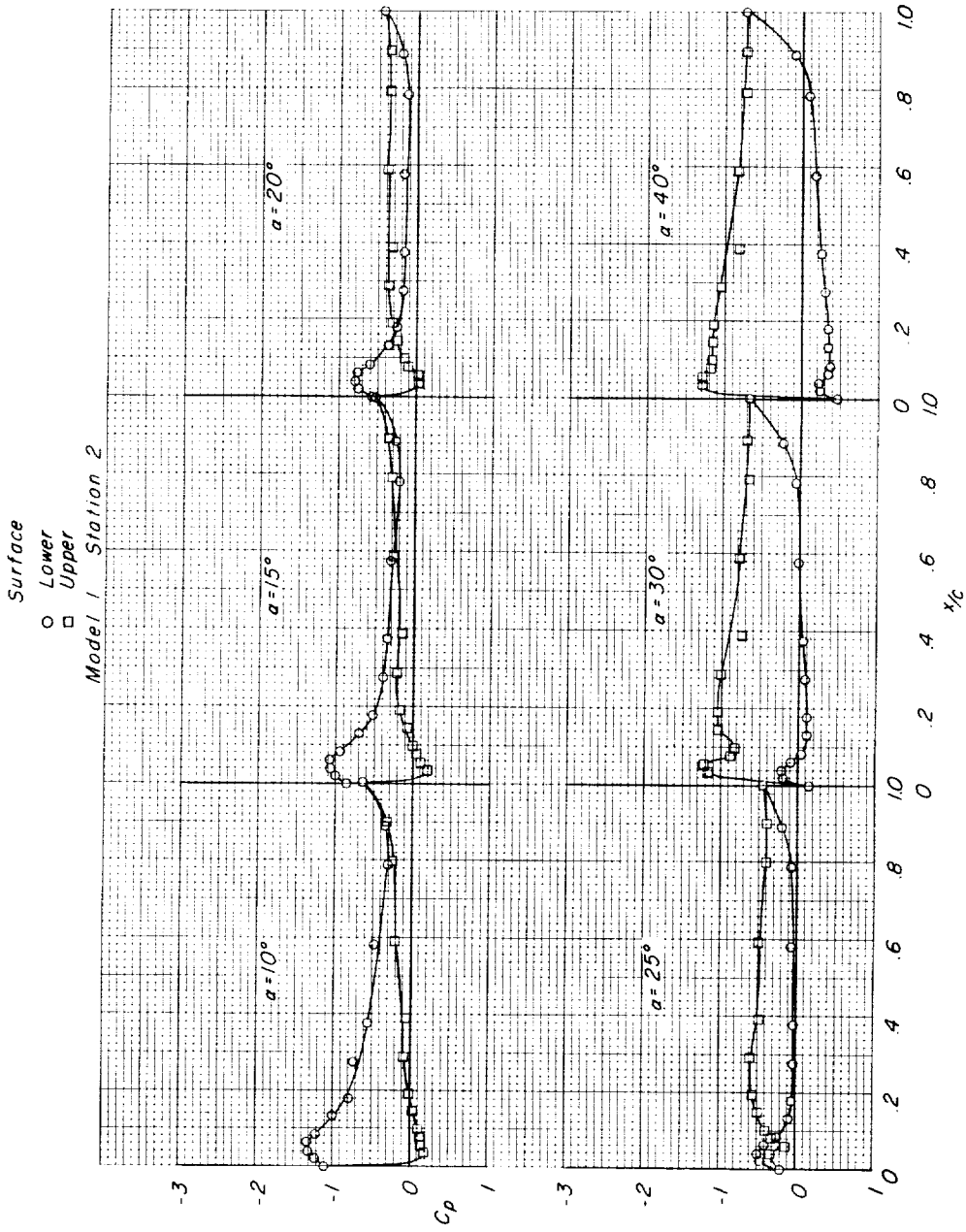

(a) M = 0.80. Continued.

Figure 6.- Continued.

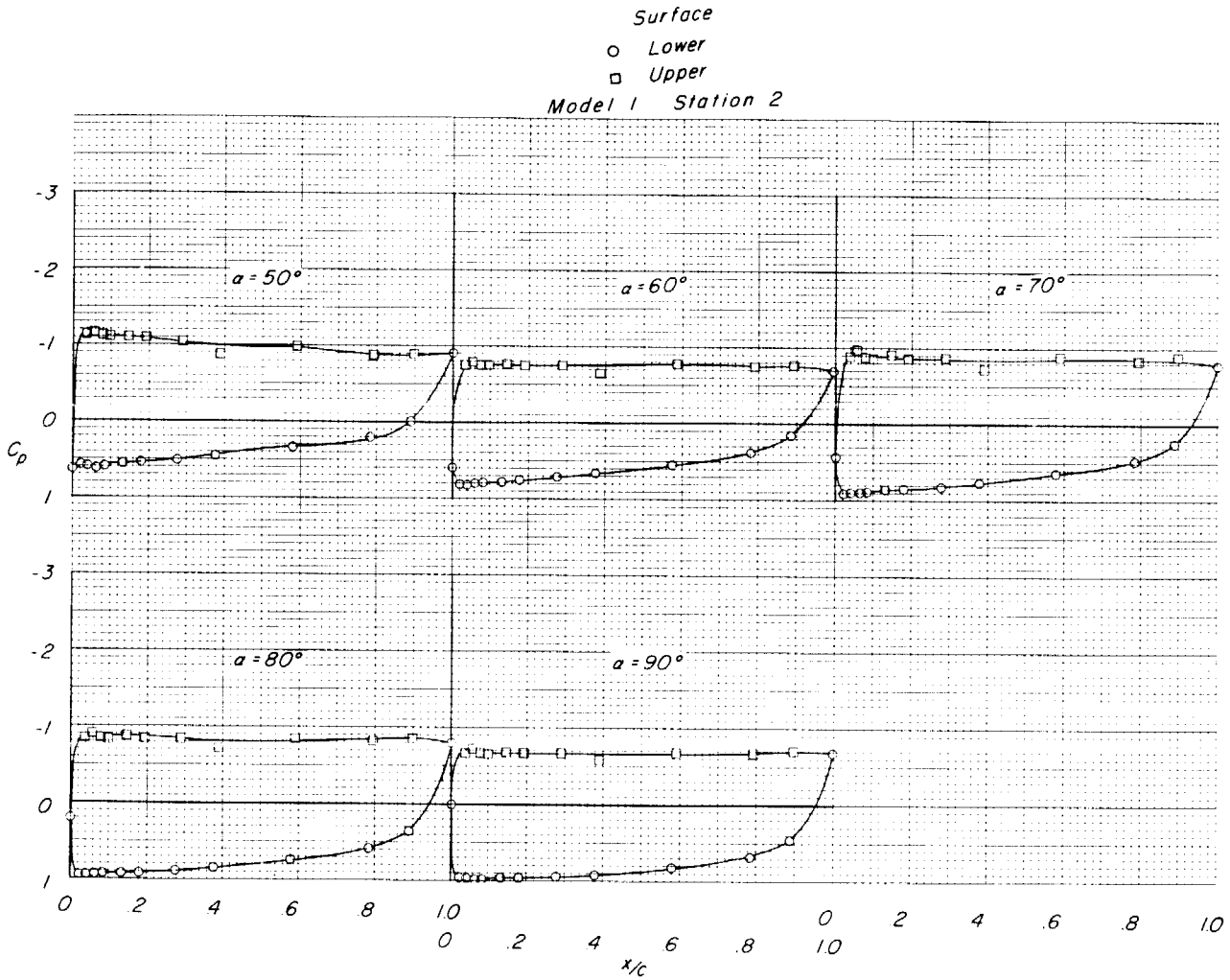

(a) **M** = 0.80. Continued.

Figure 6.- Continued.

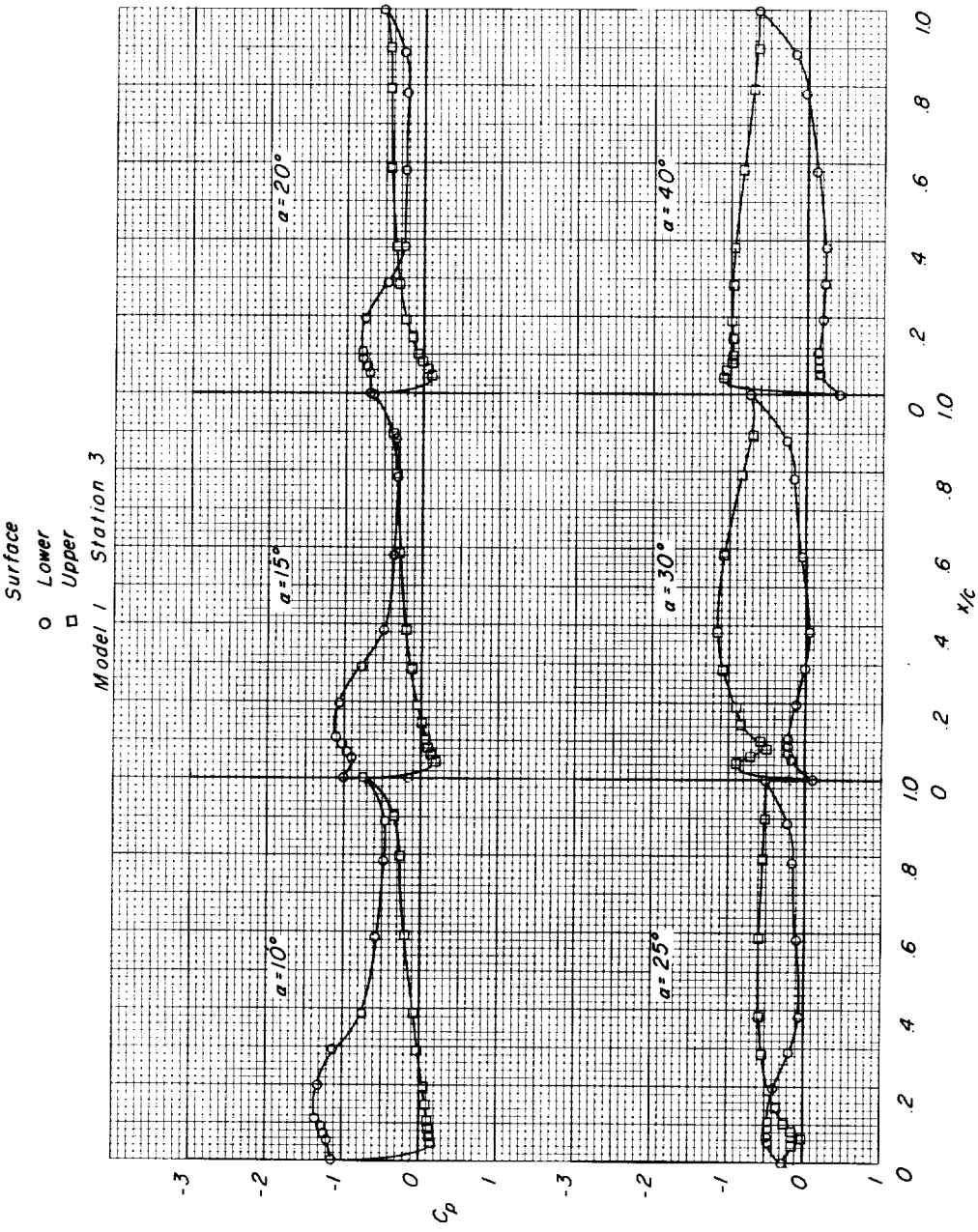

(a) M = 0.80. Continued.

Figure 6.- Continued.

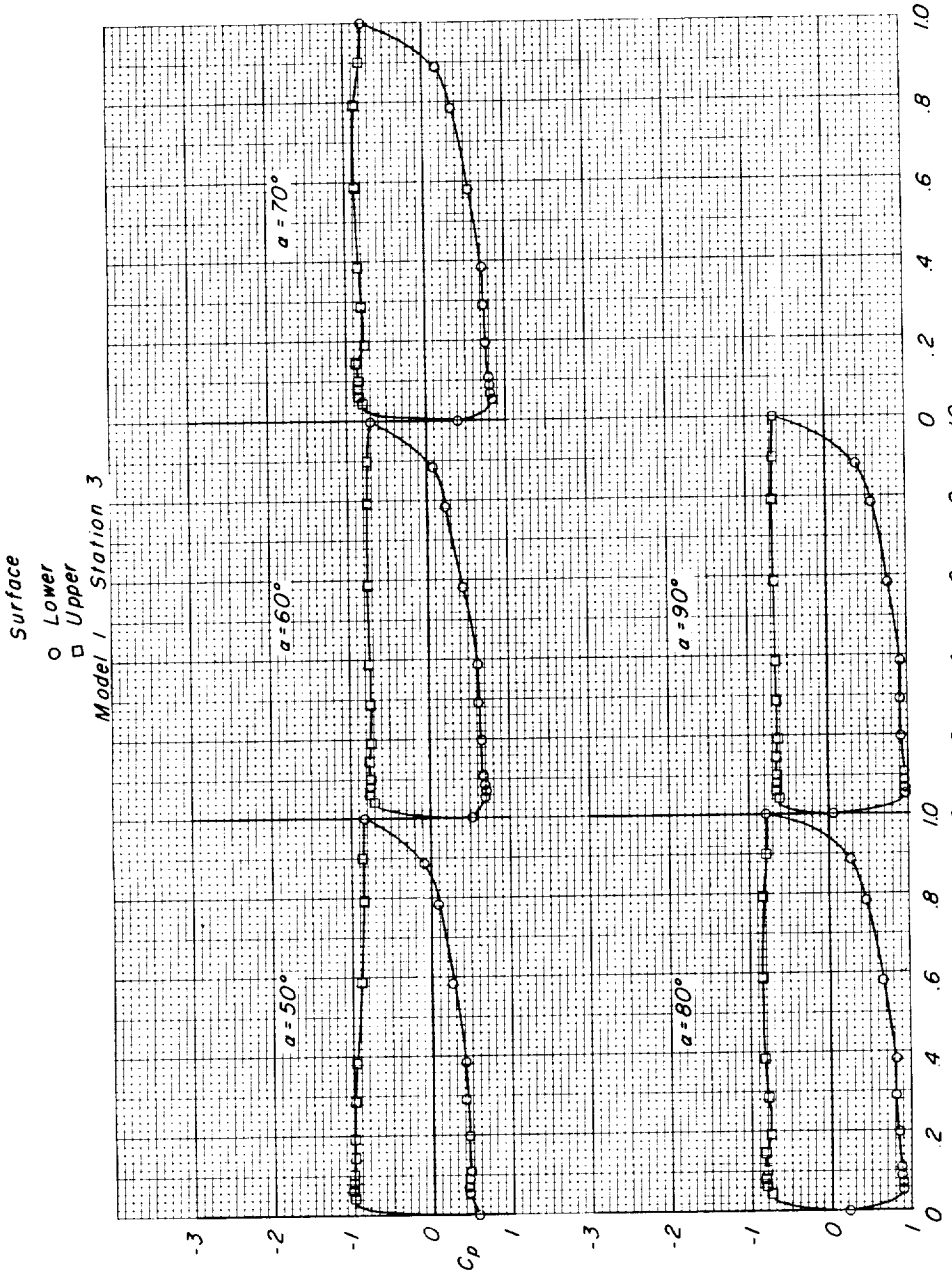

(a) M = 0.80. Continued.

Figure 6.- Continued.

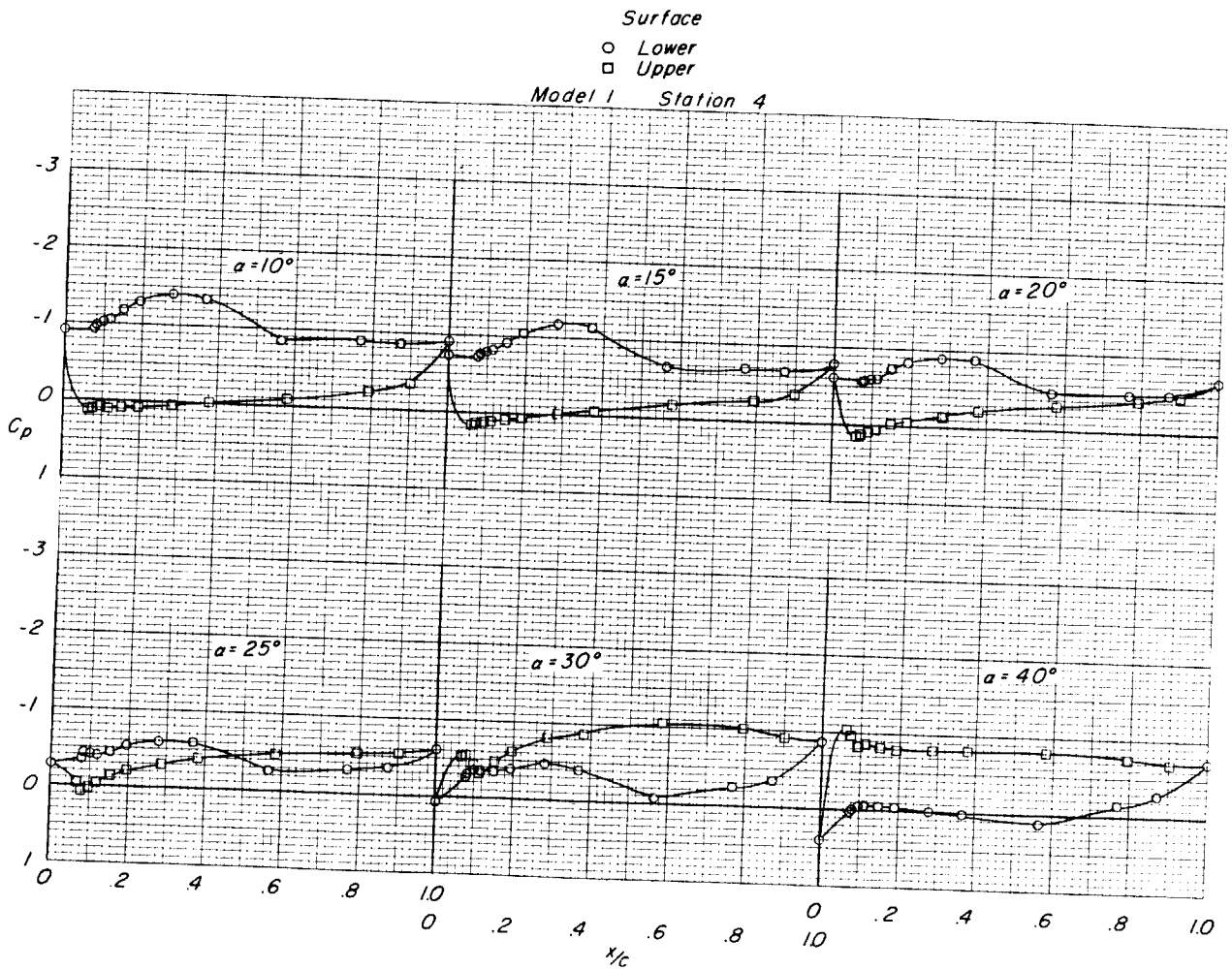

(a) M = 0.80. Continued.

Figure 6.- Continued.

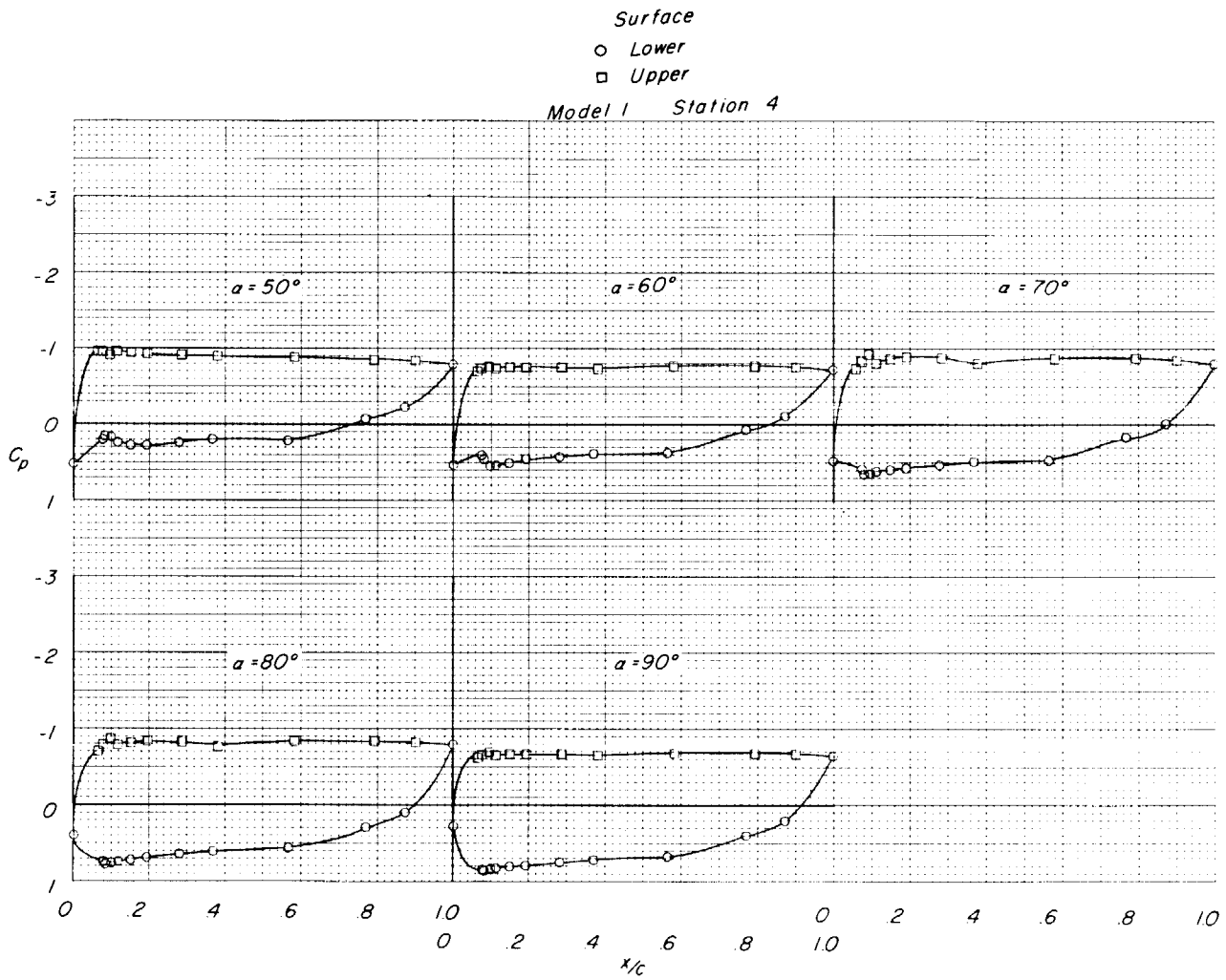

(a) M = 0.80. Concluded.

Figure 6.- Continued.

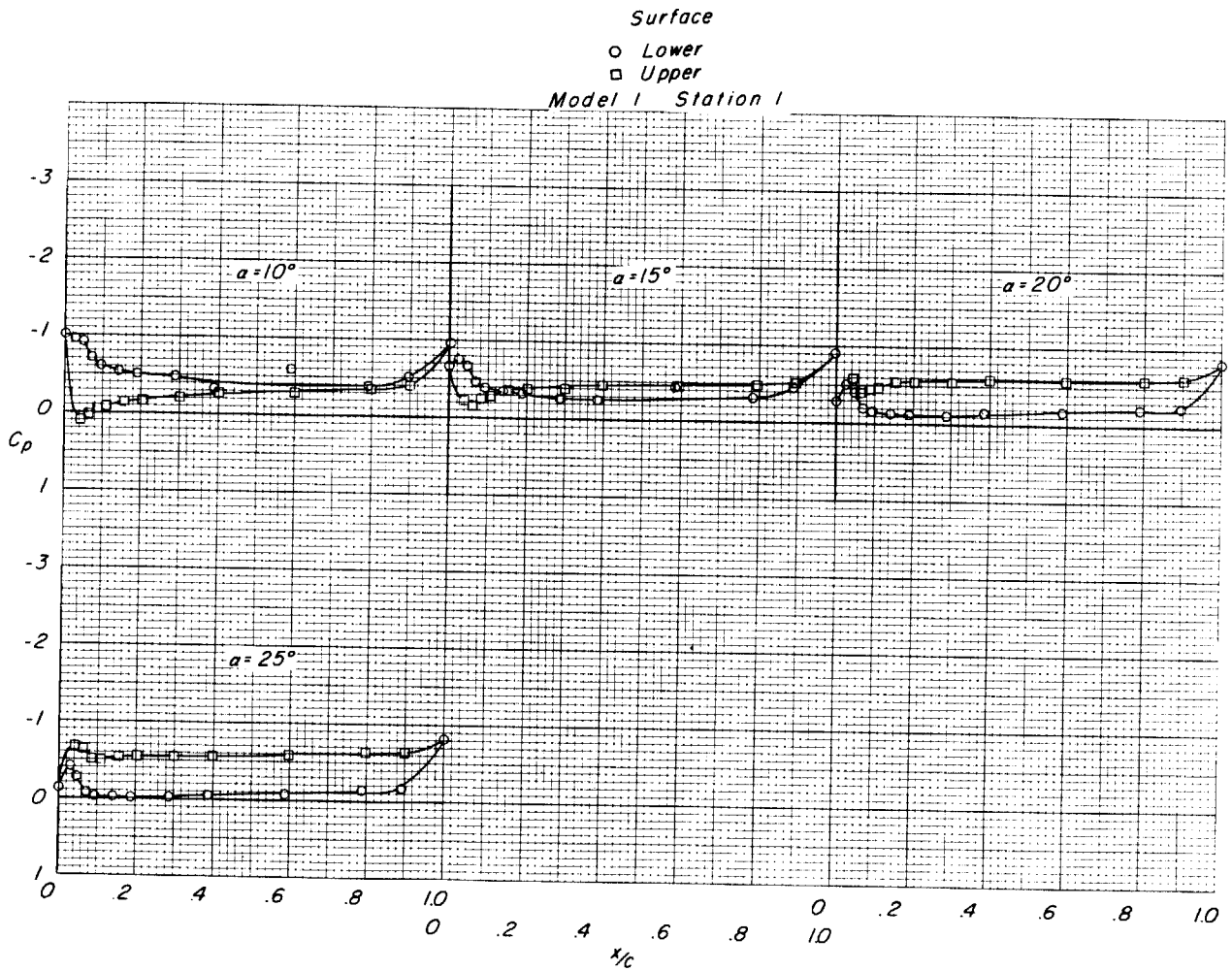

(b) M = 0.94.

Figure 6.- Continued.

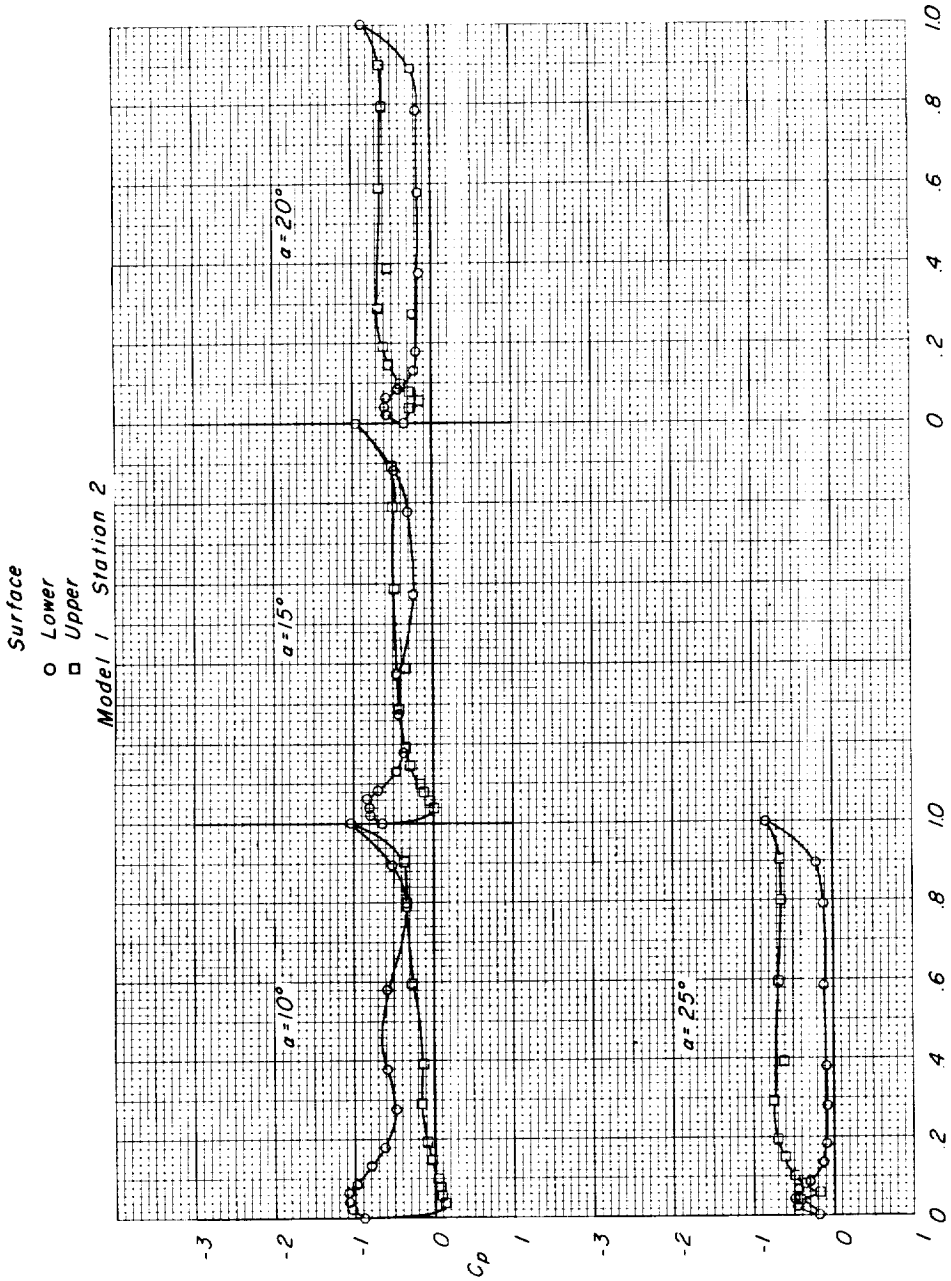

(b) M = 0.94. Continued.

Figure 6.- Continued.

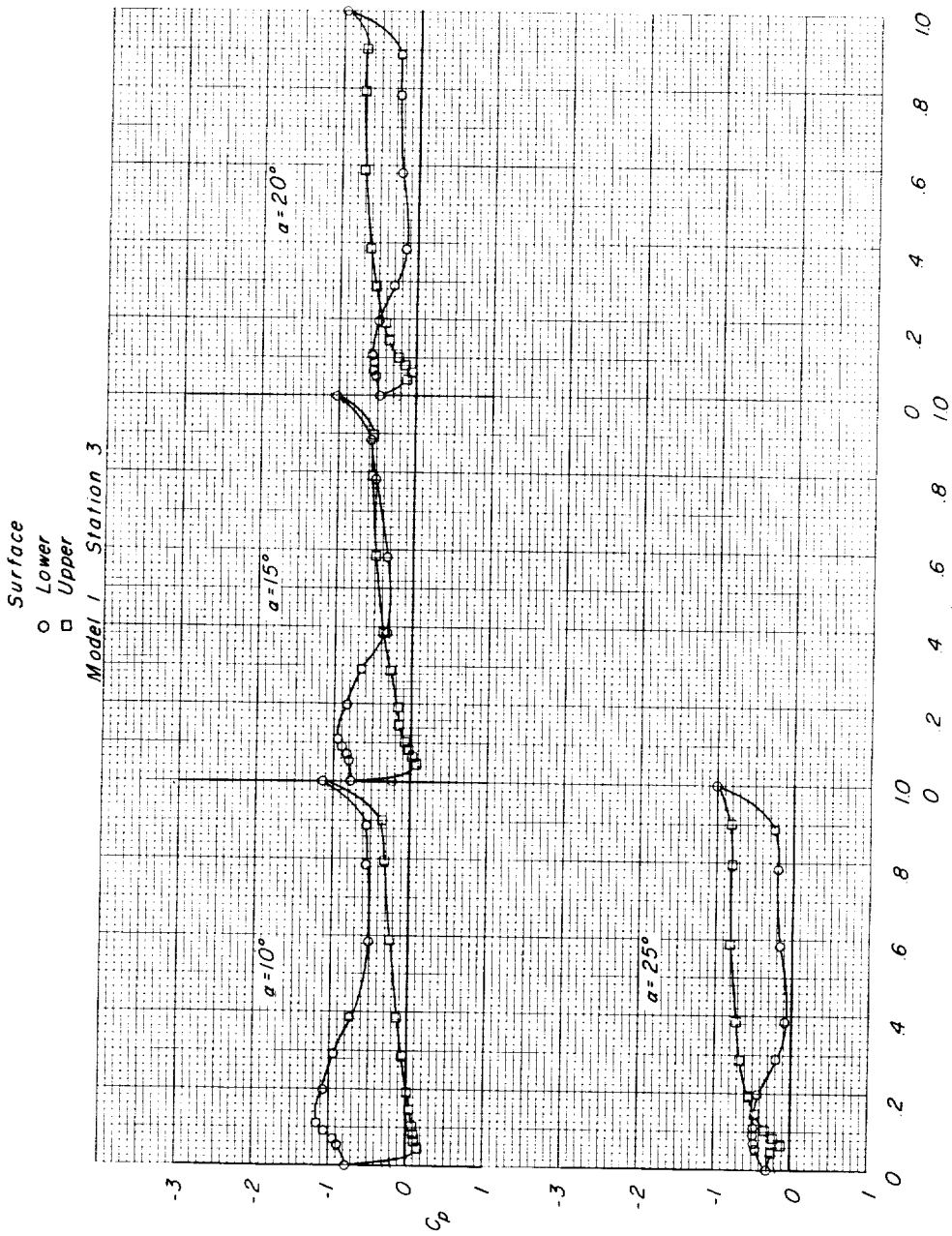

(b) M = 0.94. Continued.

Figure 6.- Continued.

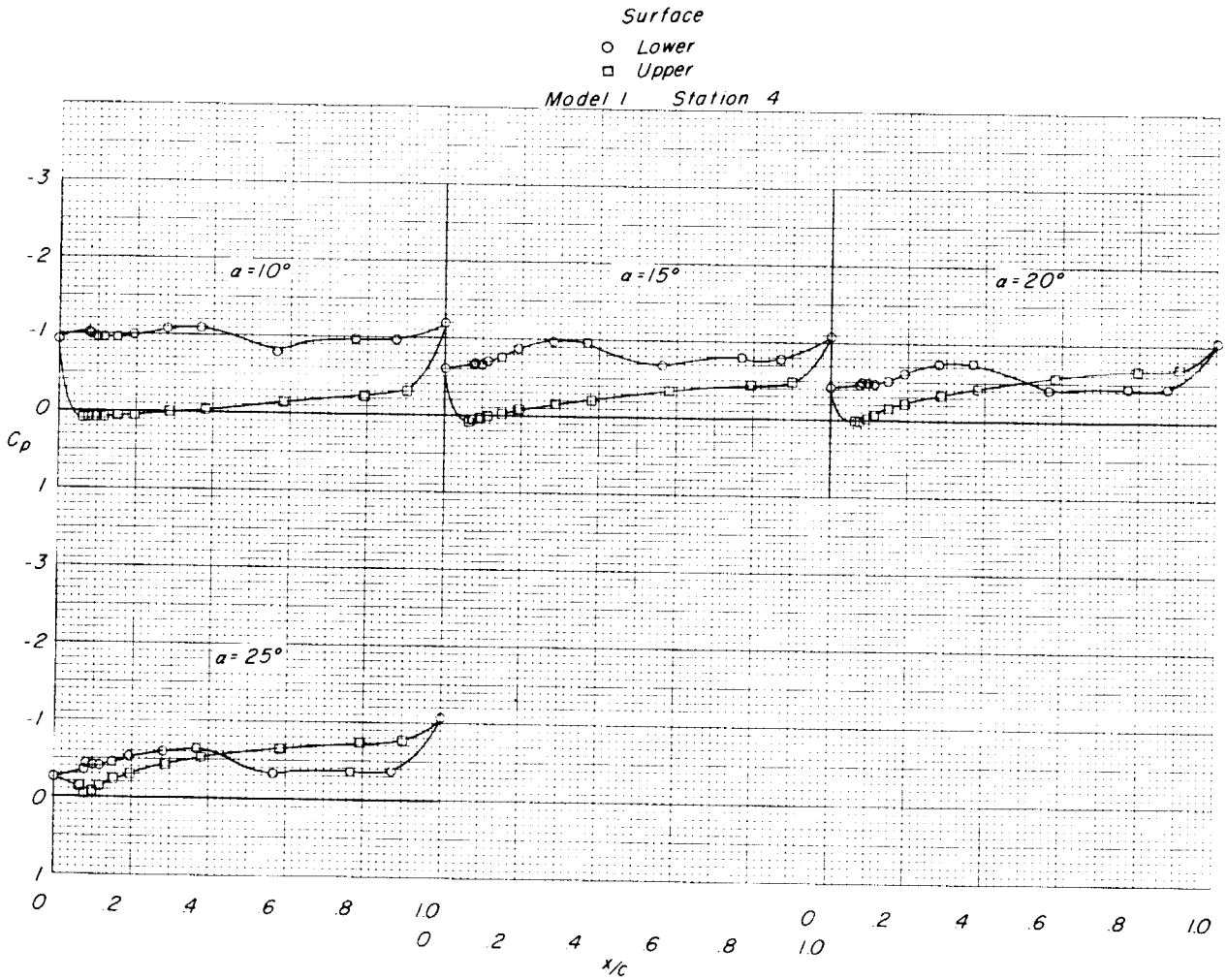

(b) M = 0.94. Concluded.

Figure 6.- Continued.

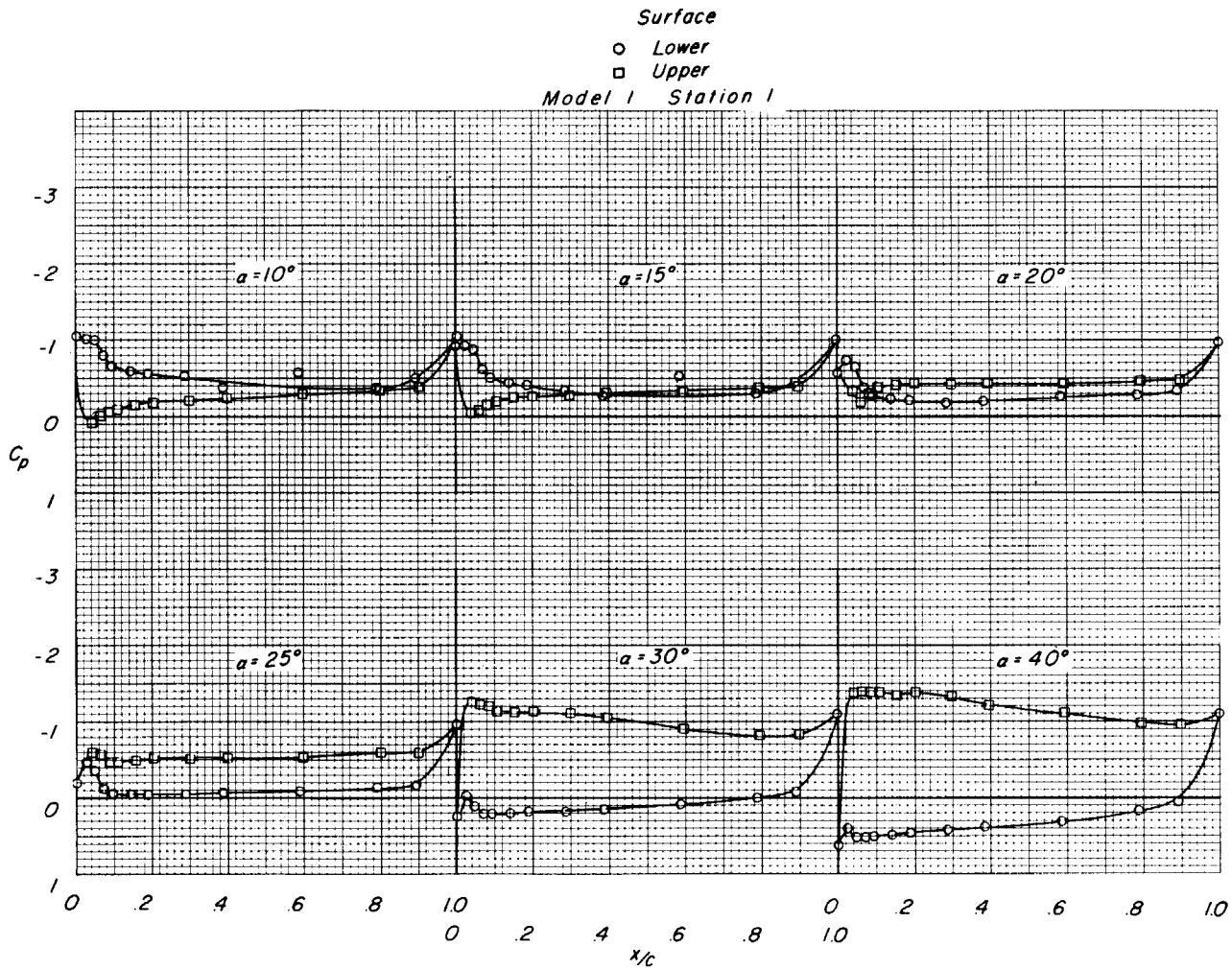

(c) M = 0.98.

Figure 6.- Continued.

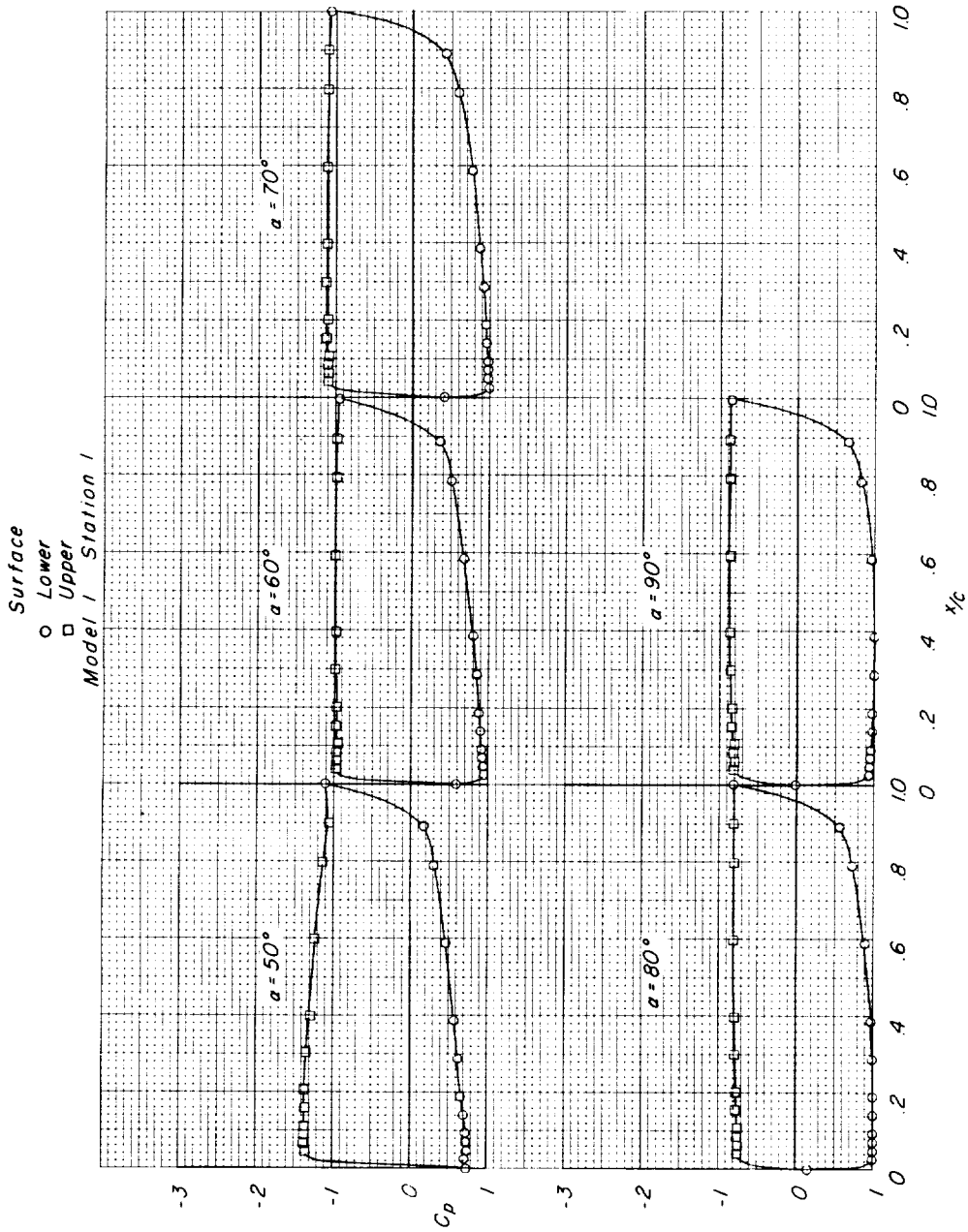

(c) M = 0.98. Continued.

Figure 6.- Continued.

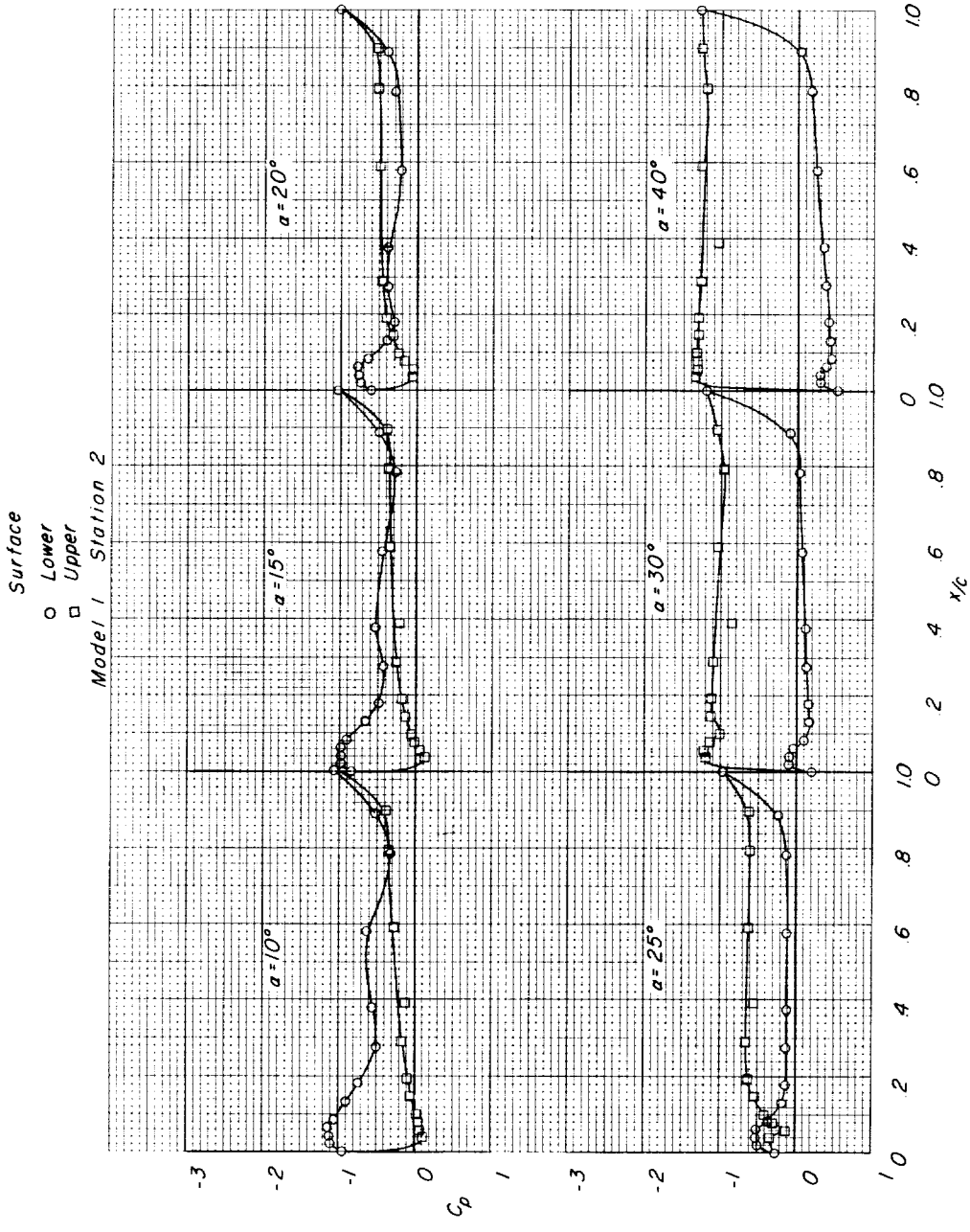

(c) M = 0.98. Continued.

Figure 6.- Continued.

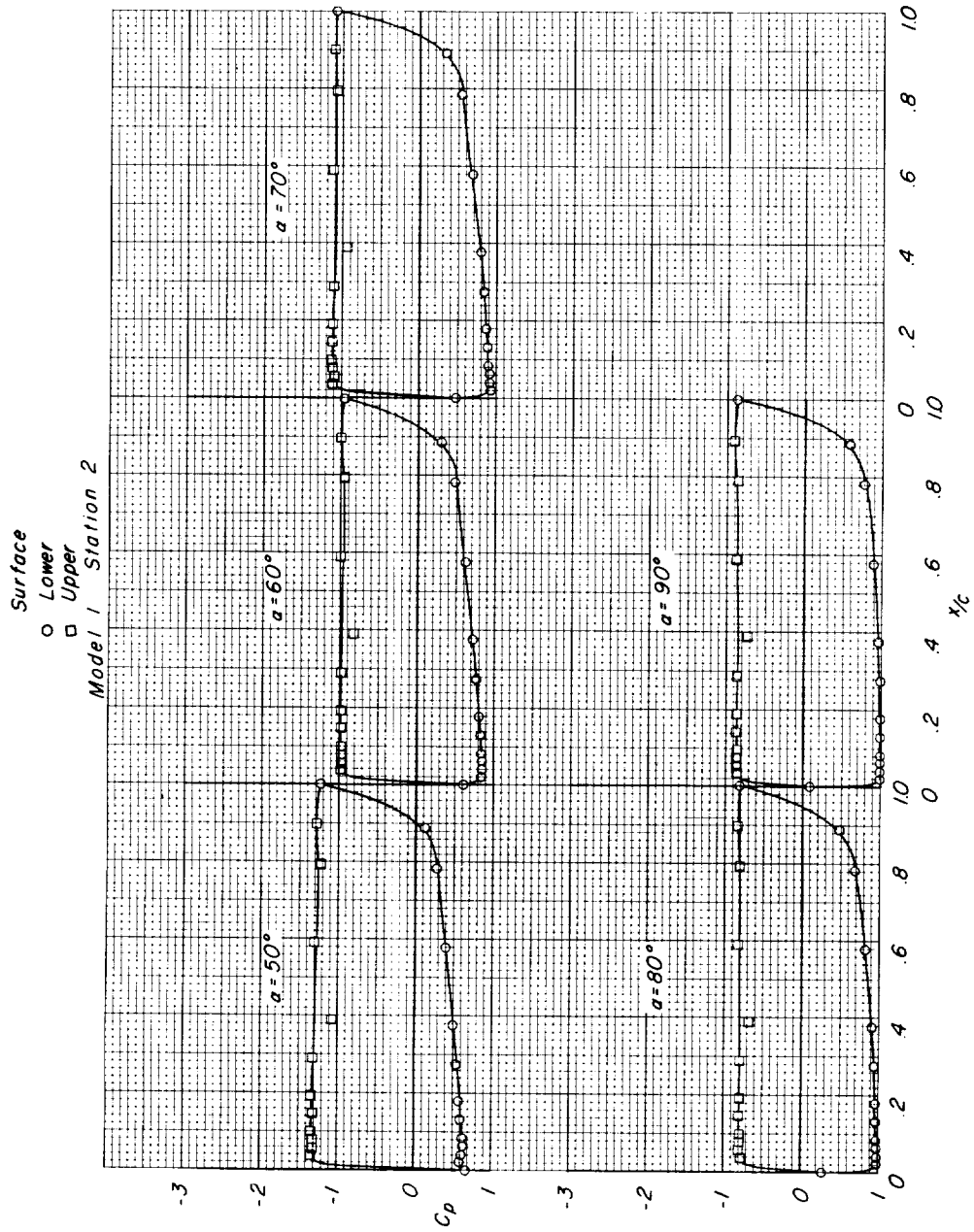

(c) M = 0.98. Continued.

Figure 6.- Continued.

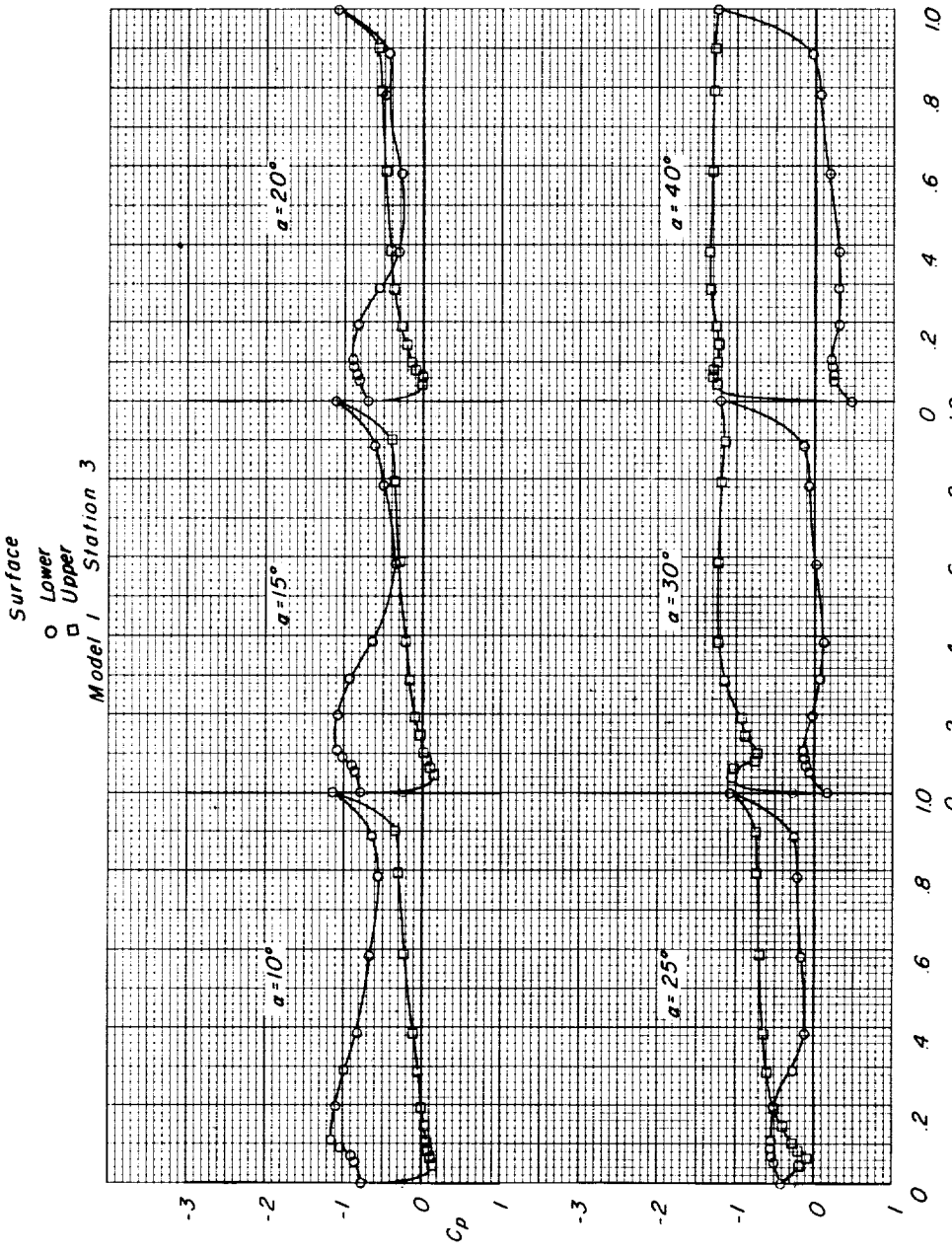

(c) M = 0.98. Continued.

Figure 6.- Continued.

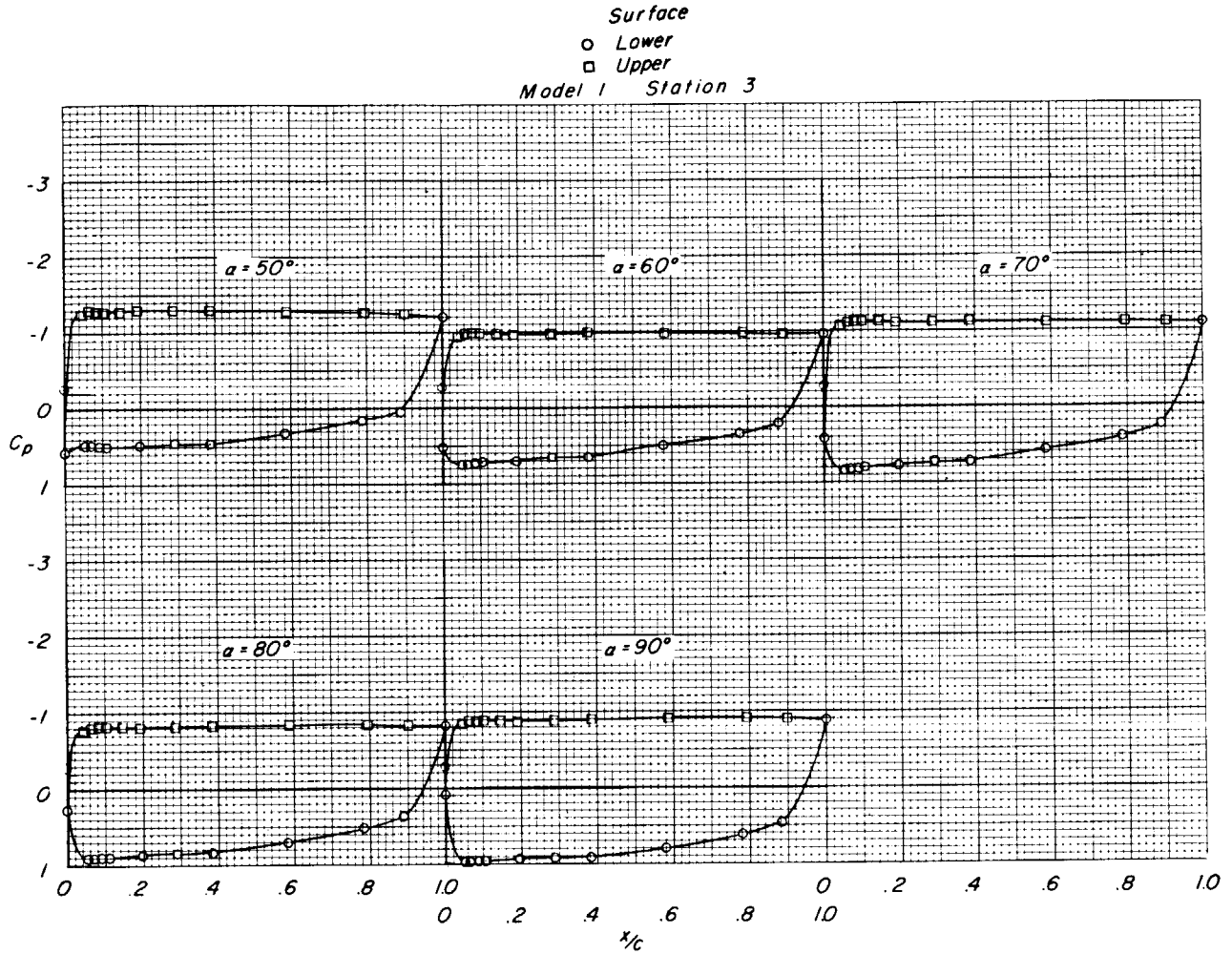

(c) M = 0.98. Continued.

Figure 6.- Continued.

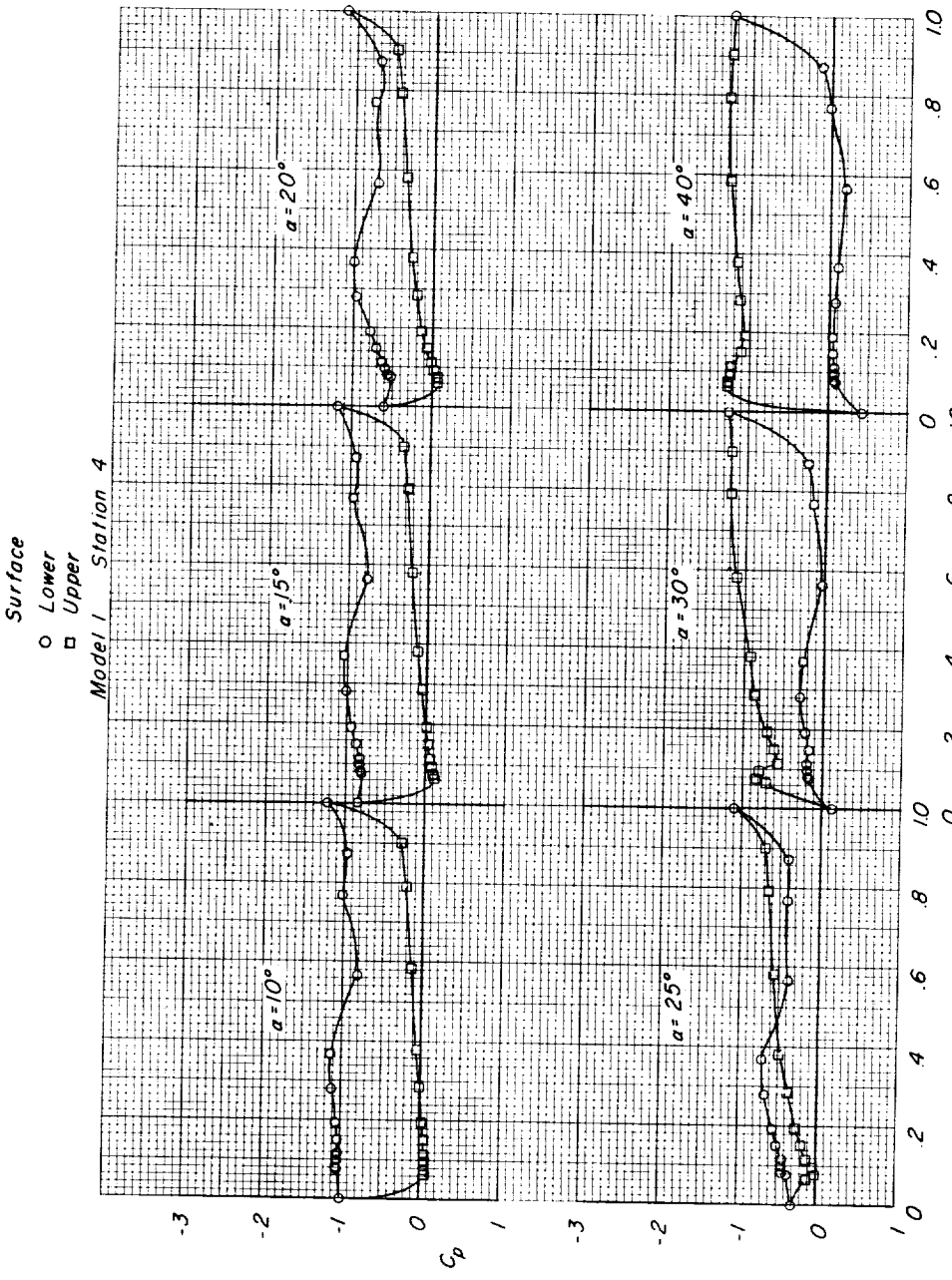

(c) M = 0.98. Continued.

Figure 6.- Continued.

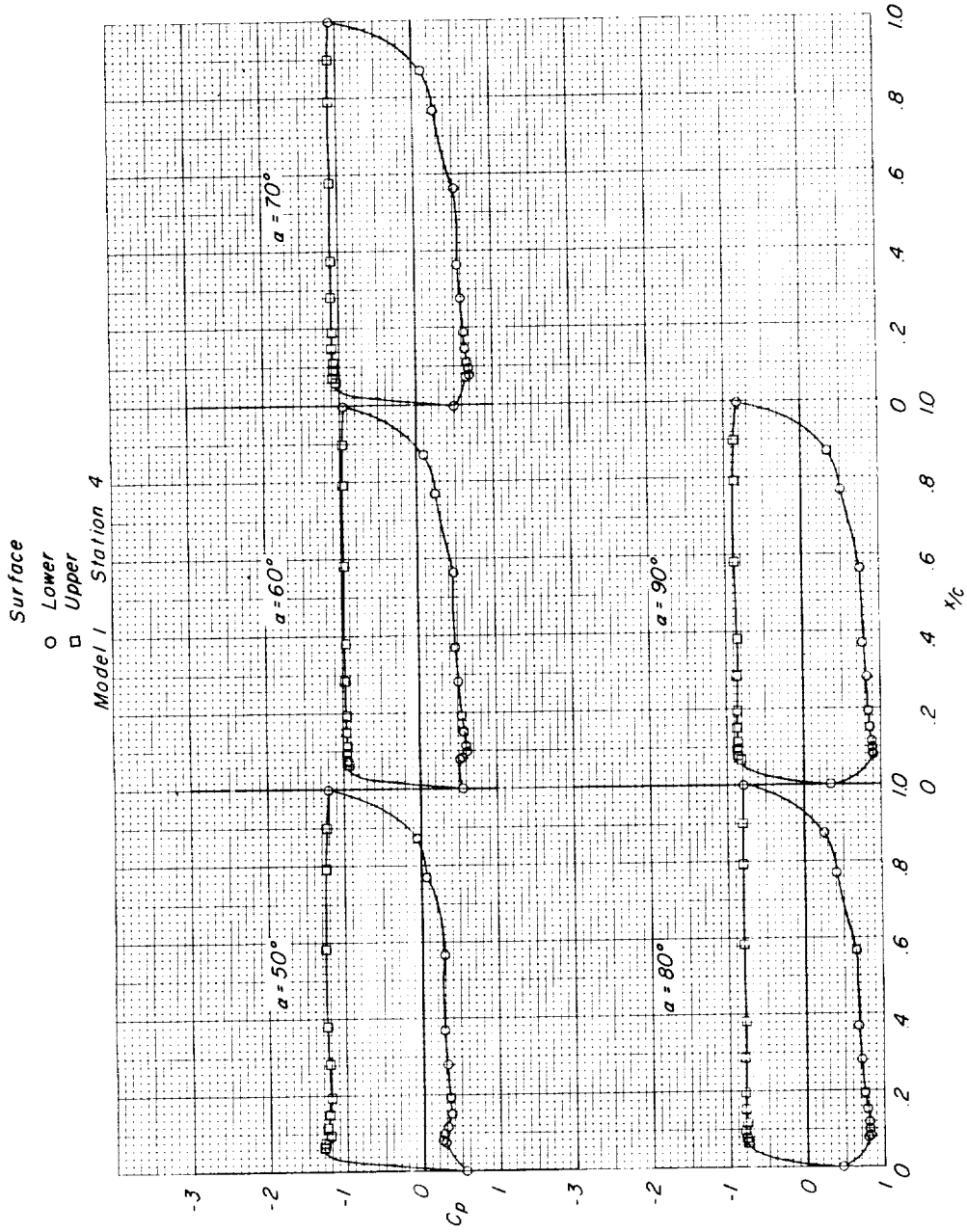

(c) M = 0.98. Concluded.

Figure 6.- Continued.

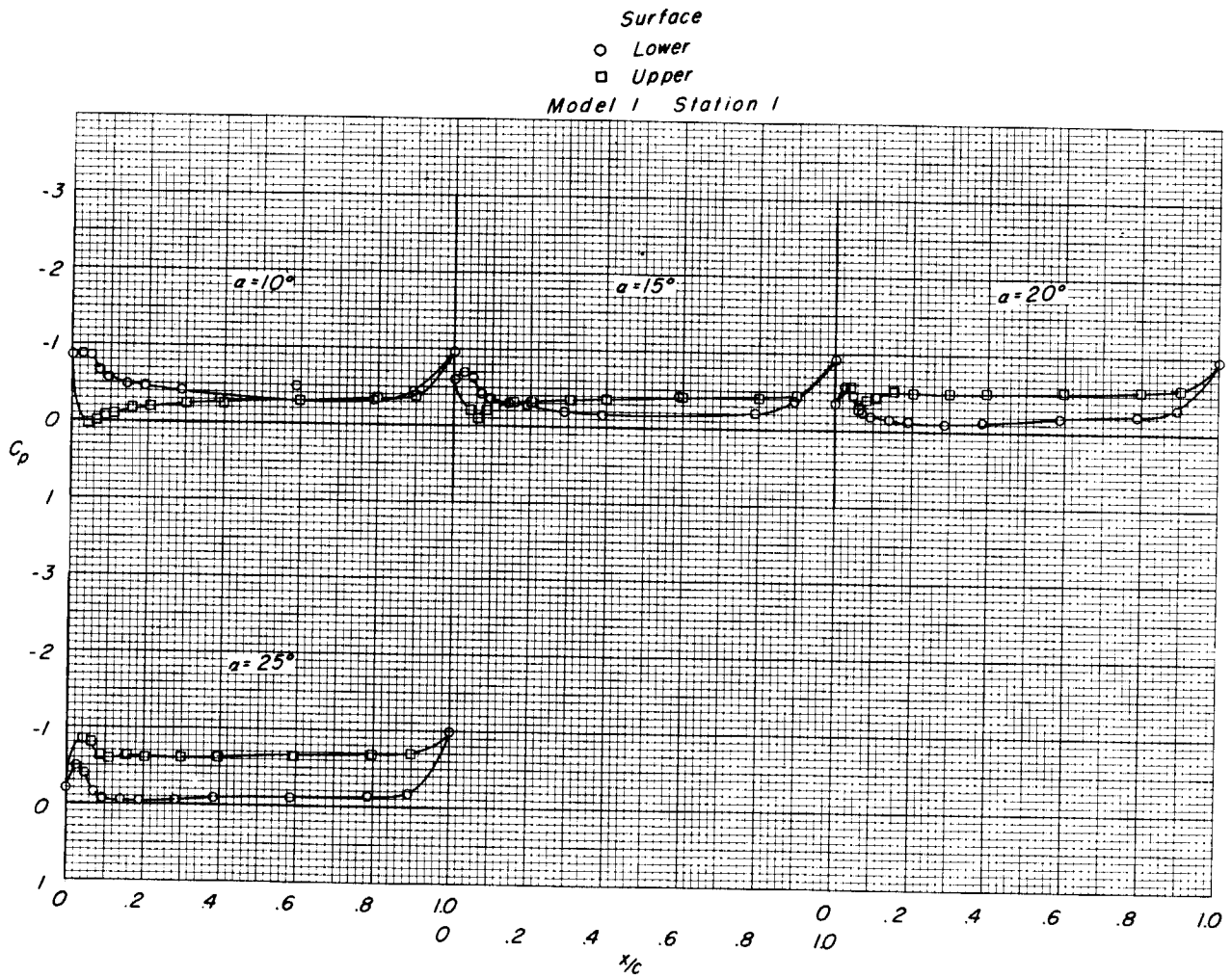

(d) M = 1.02.

Figure 6.- Continued.

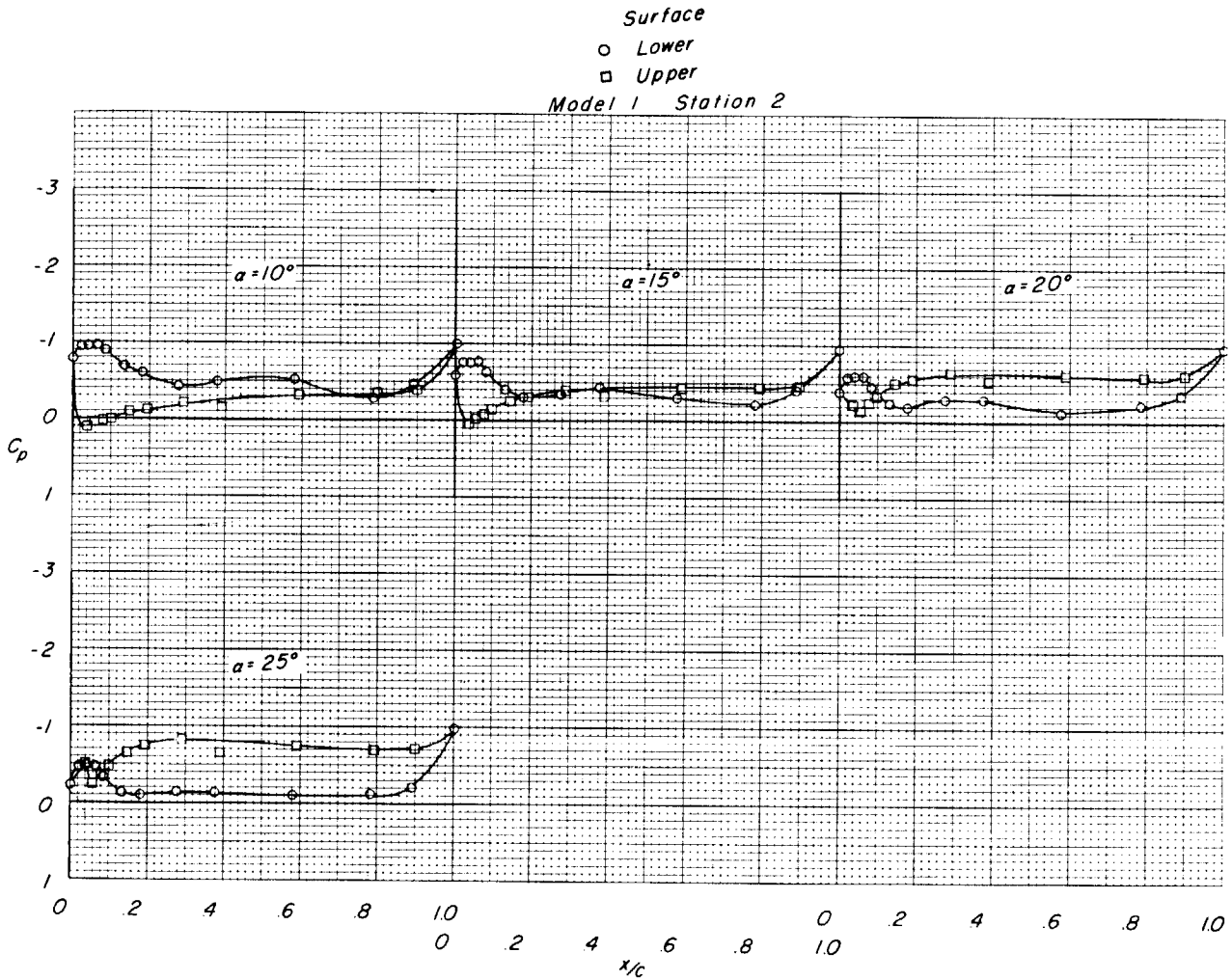

(d) M = 1.02. Continued.

Figure 6.- Continued.

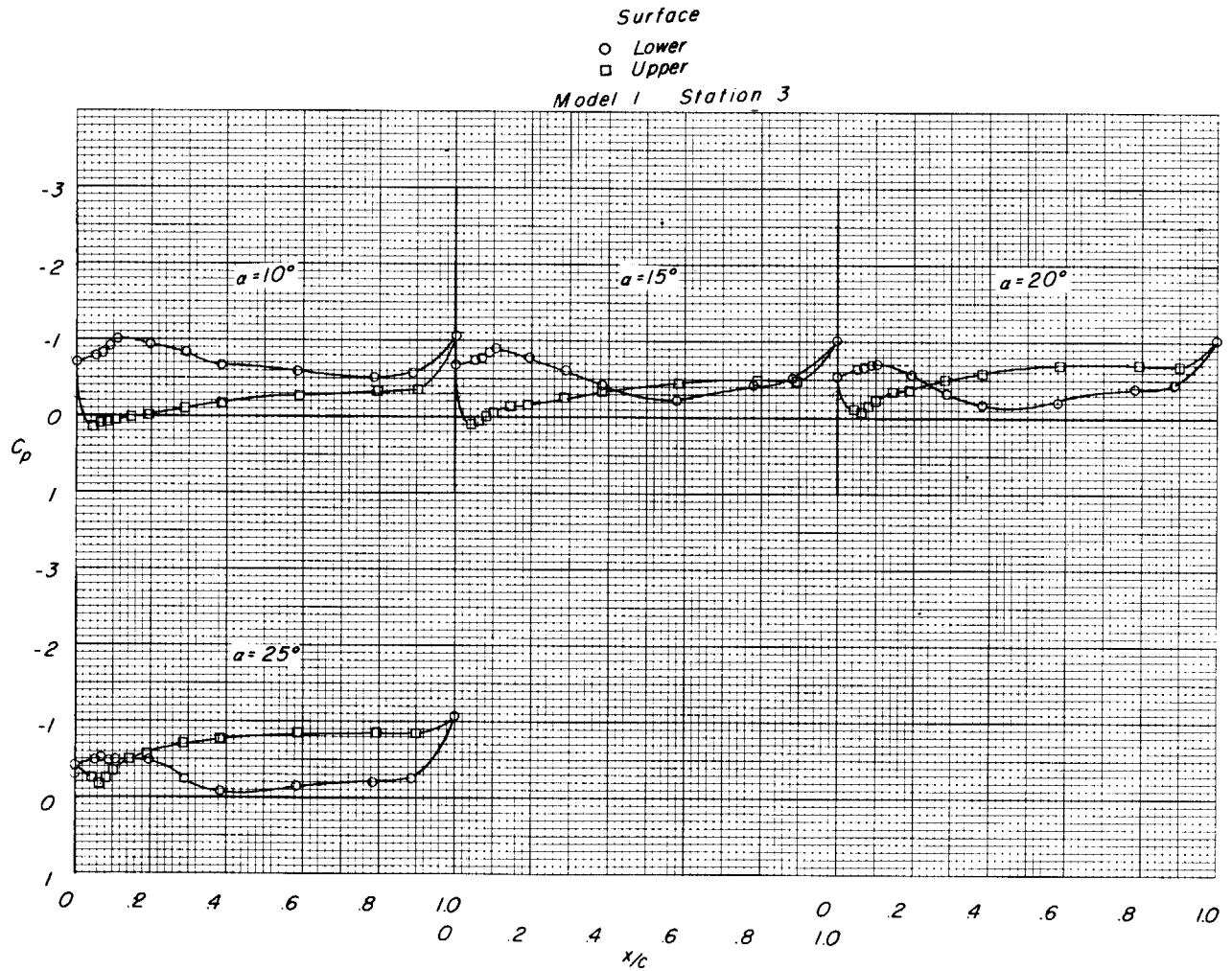

(d) M = 1.02. Continued.

Figure 6.- Continued.

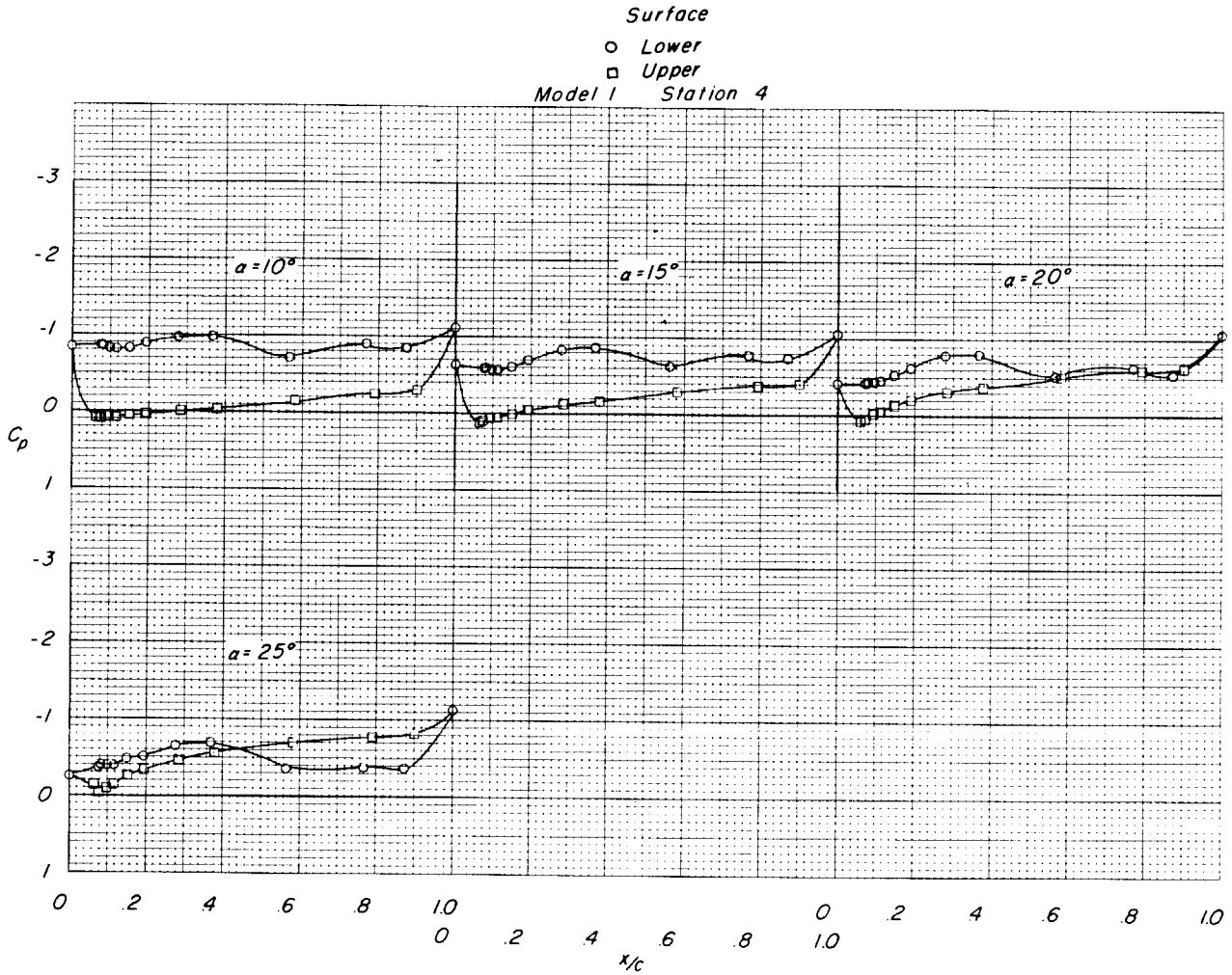

(d) M = 1.02. Concluded.

Figure 6.- Continued.

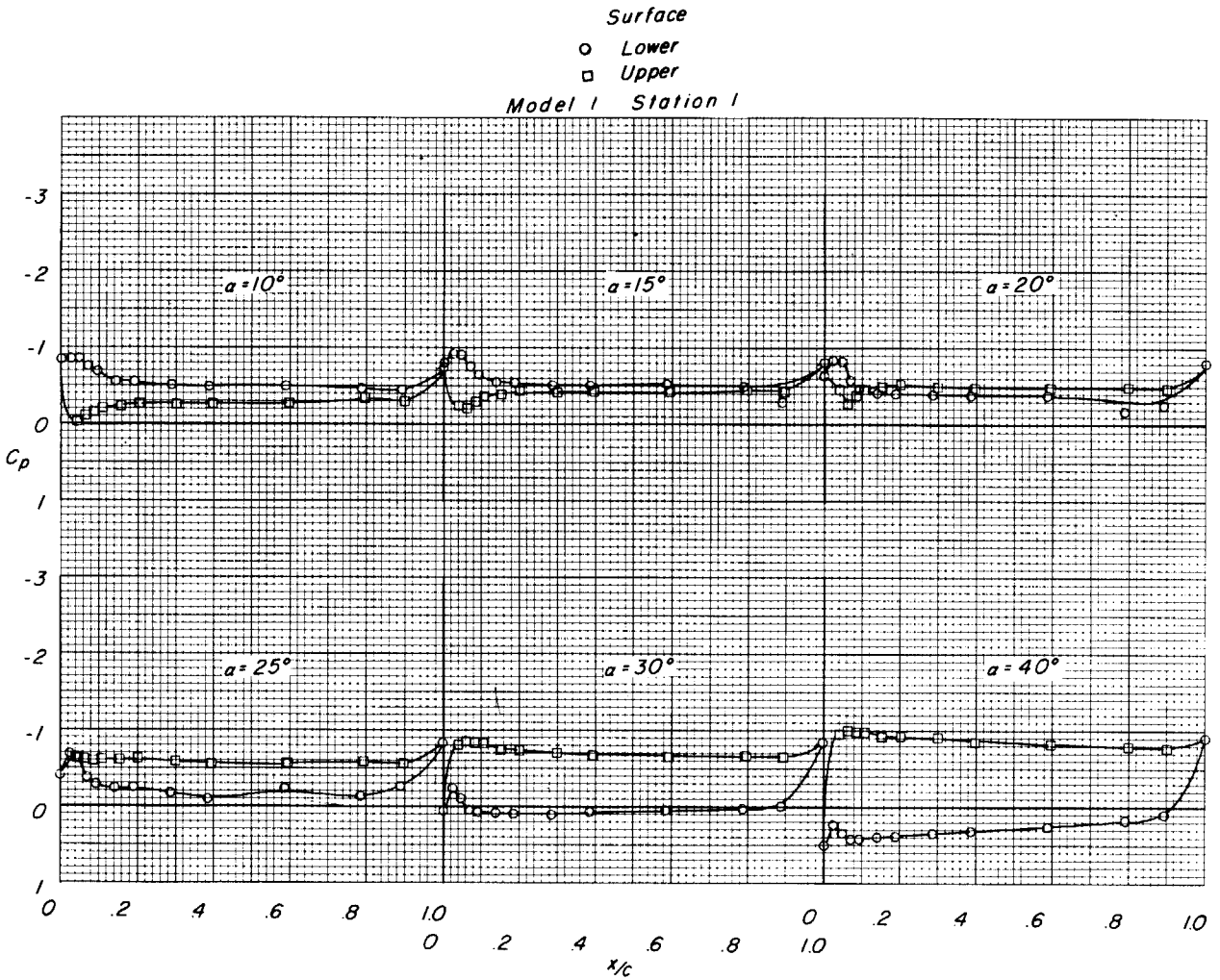

(e) M = 1.20.

Figure 6.- Continued.

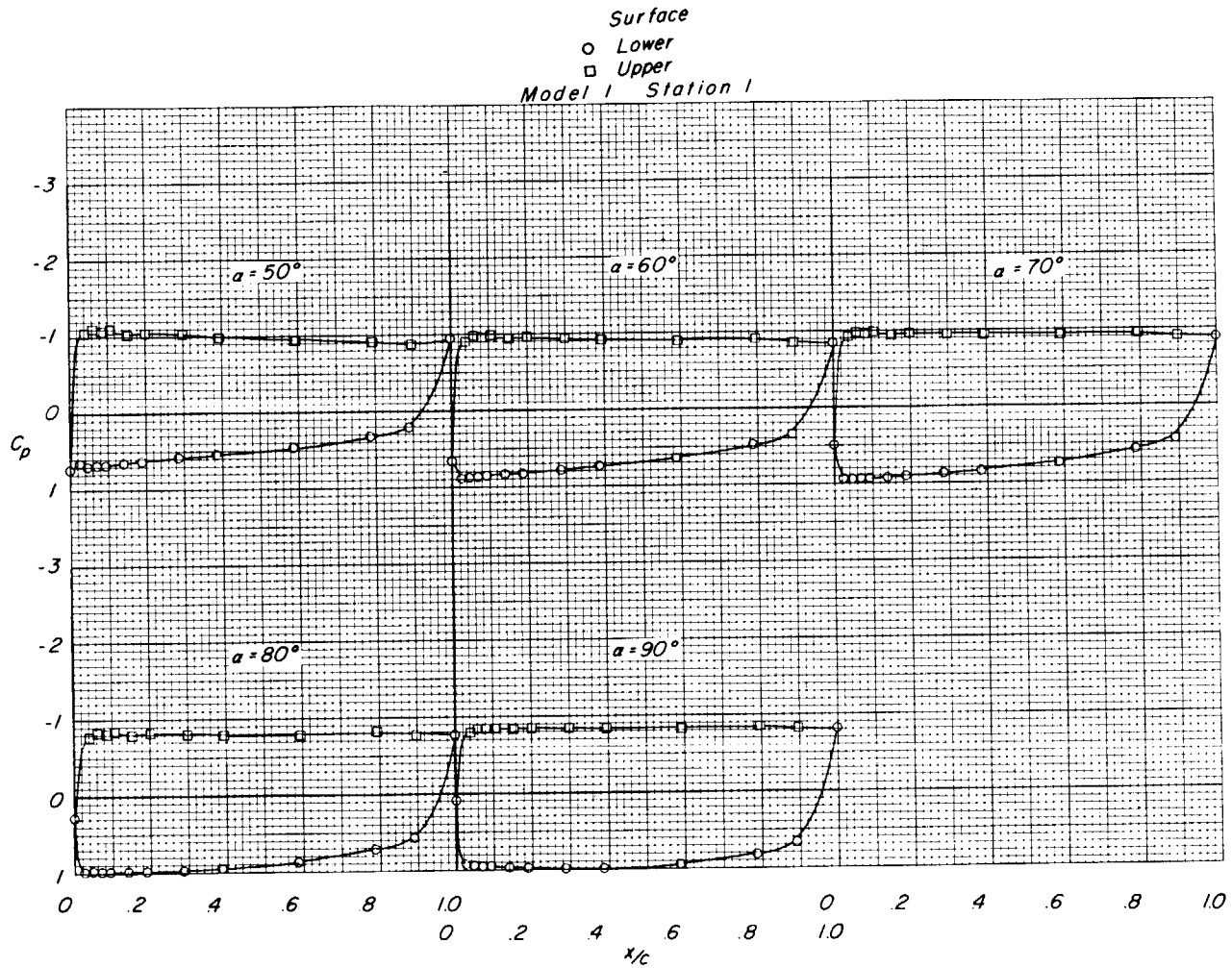

(e) M = 1.20. Continued.

Figure 6.- Continued.

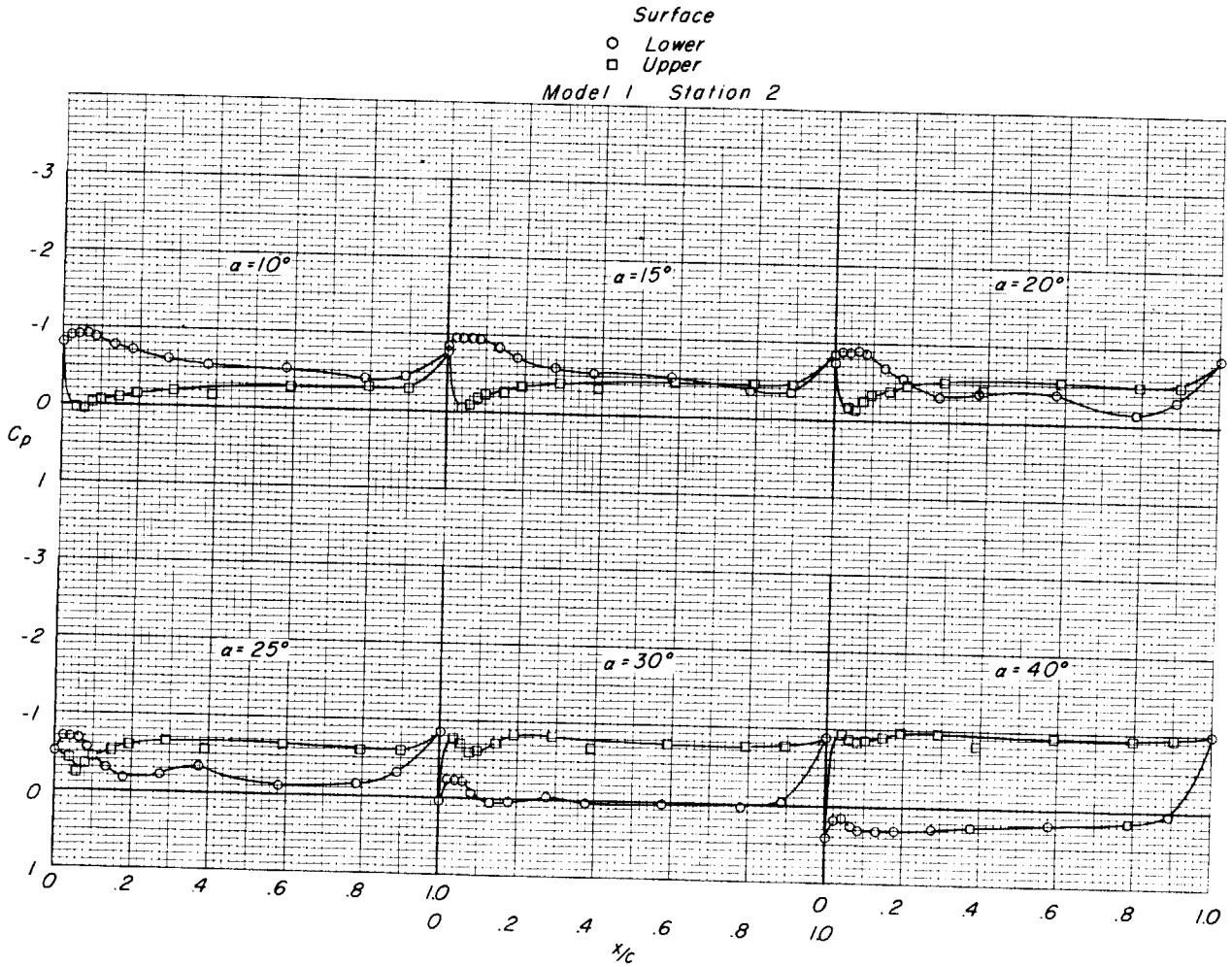

(e) M = 1.20. Continued.

Figure 6.- Continued.

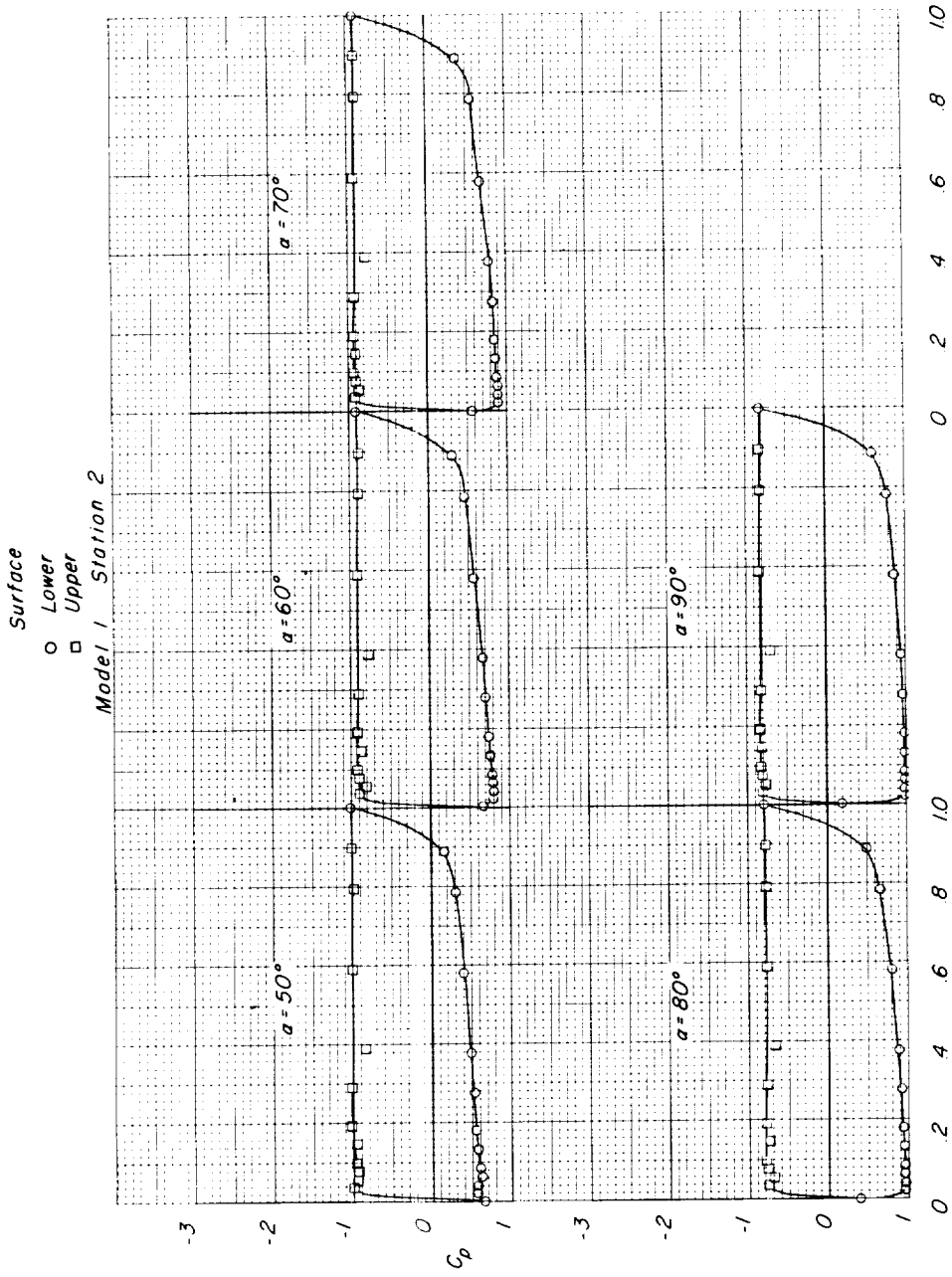

(e) M = 1.20. Continued.

Figure 6.- Continued.

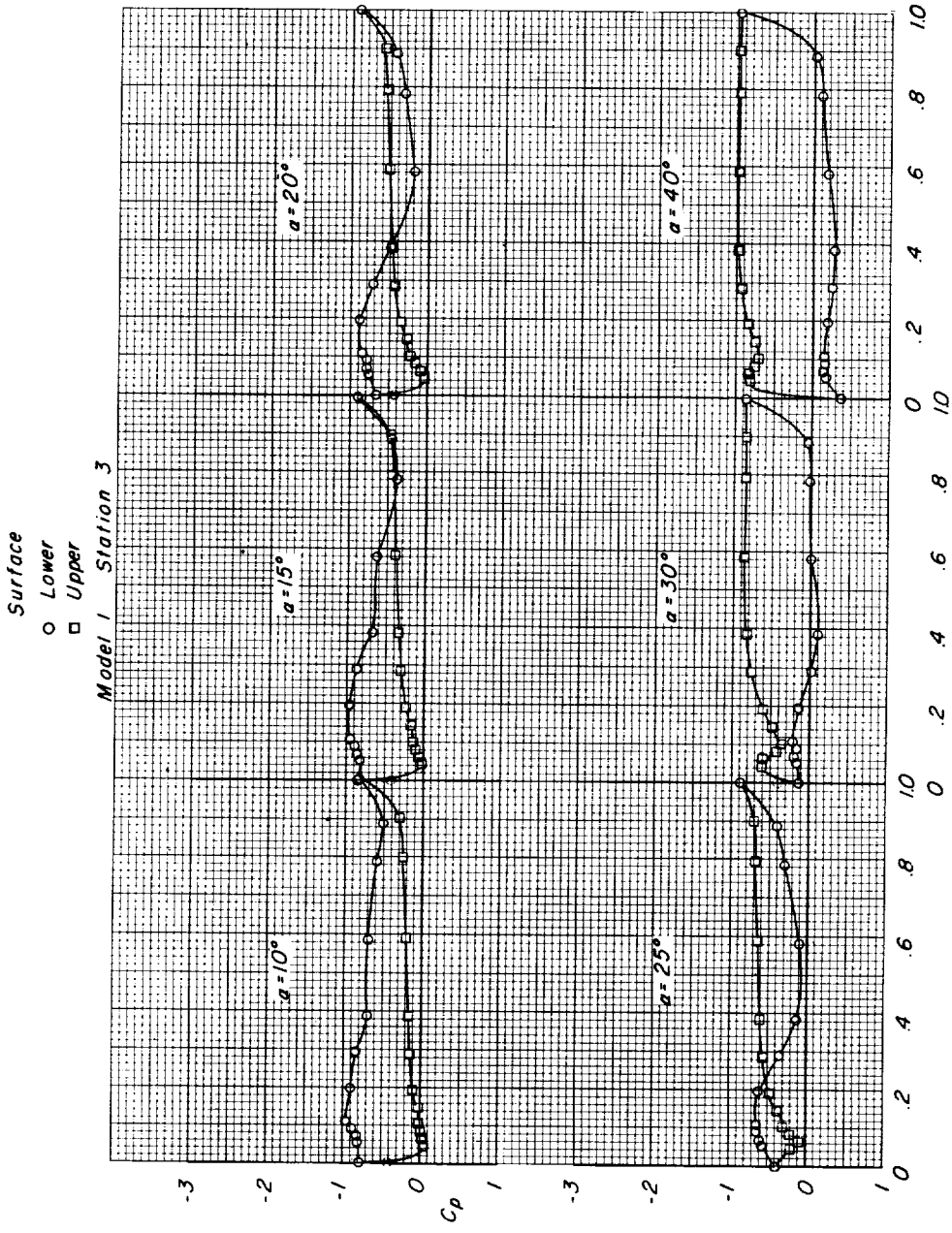

(e) M = 1.20. Continued.

Figure 6.- Continued.

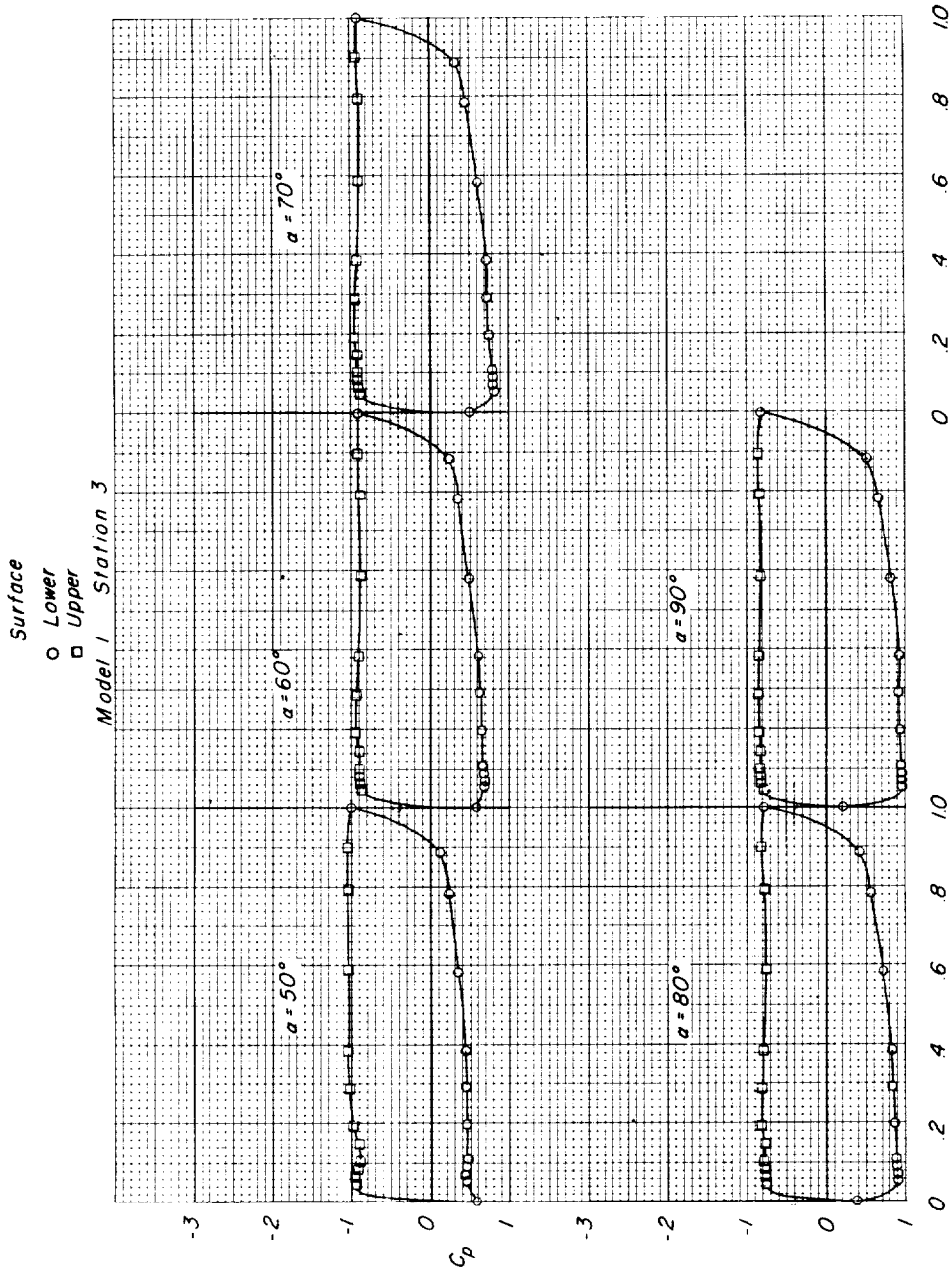

(e) M = 1.20. Continued.

Figure 6.- Continued.

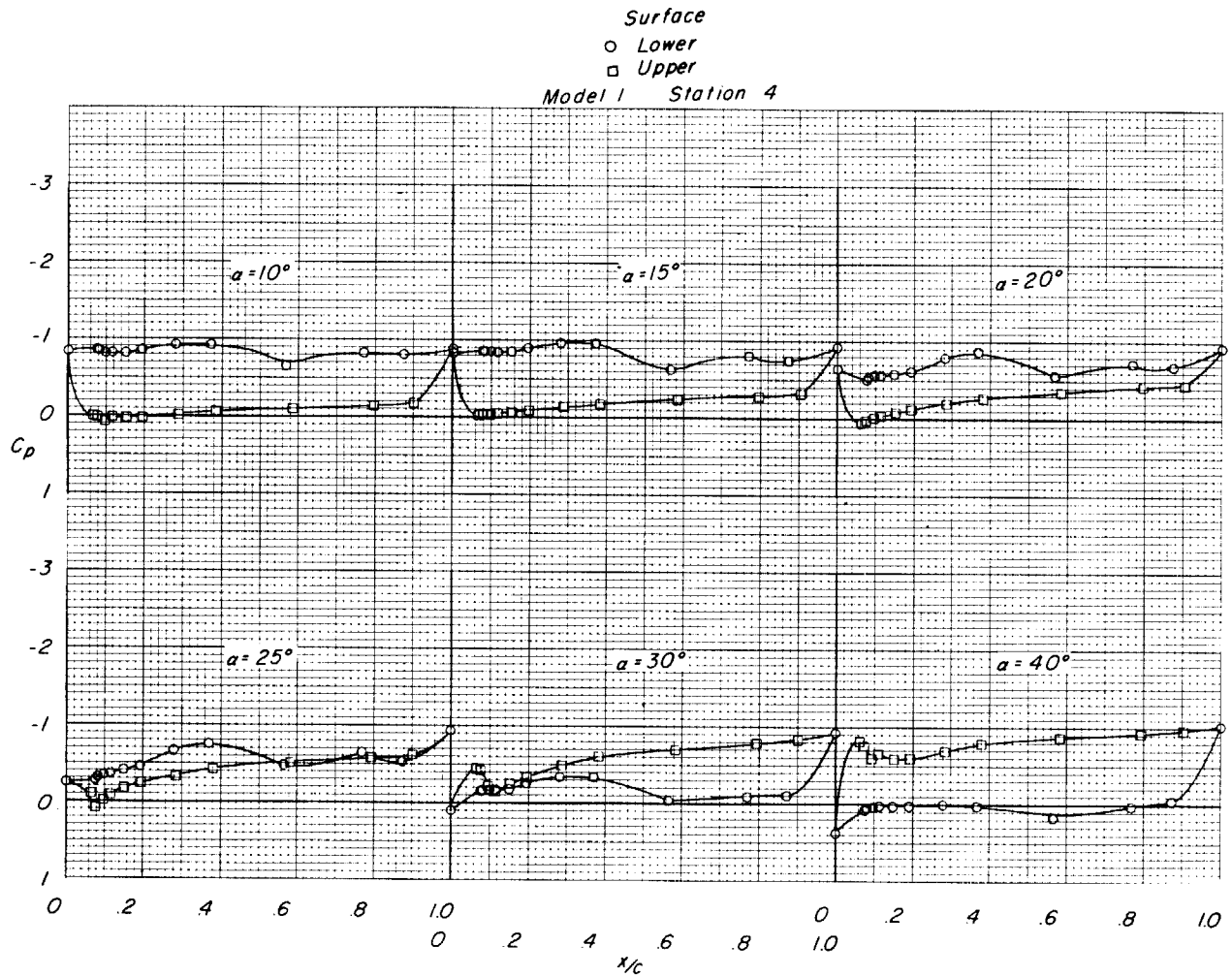

(e) M = 1.20. Continued.

Figure 6.- Continued.

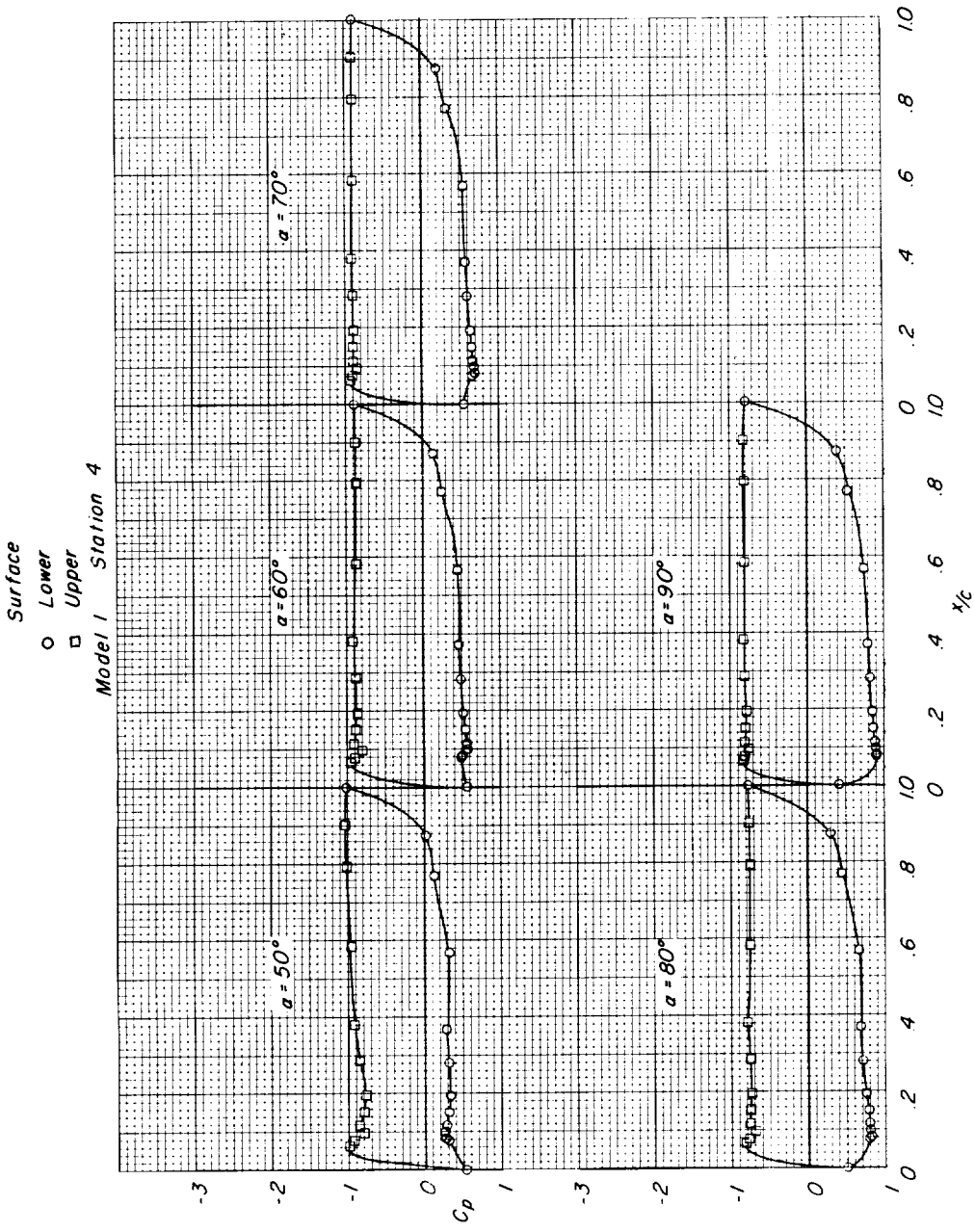

(e) M = 1.20. Concluded.

Figure 6.- Concluded.

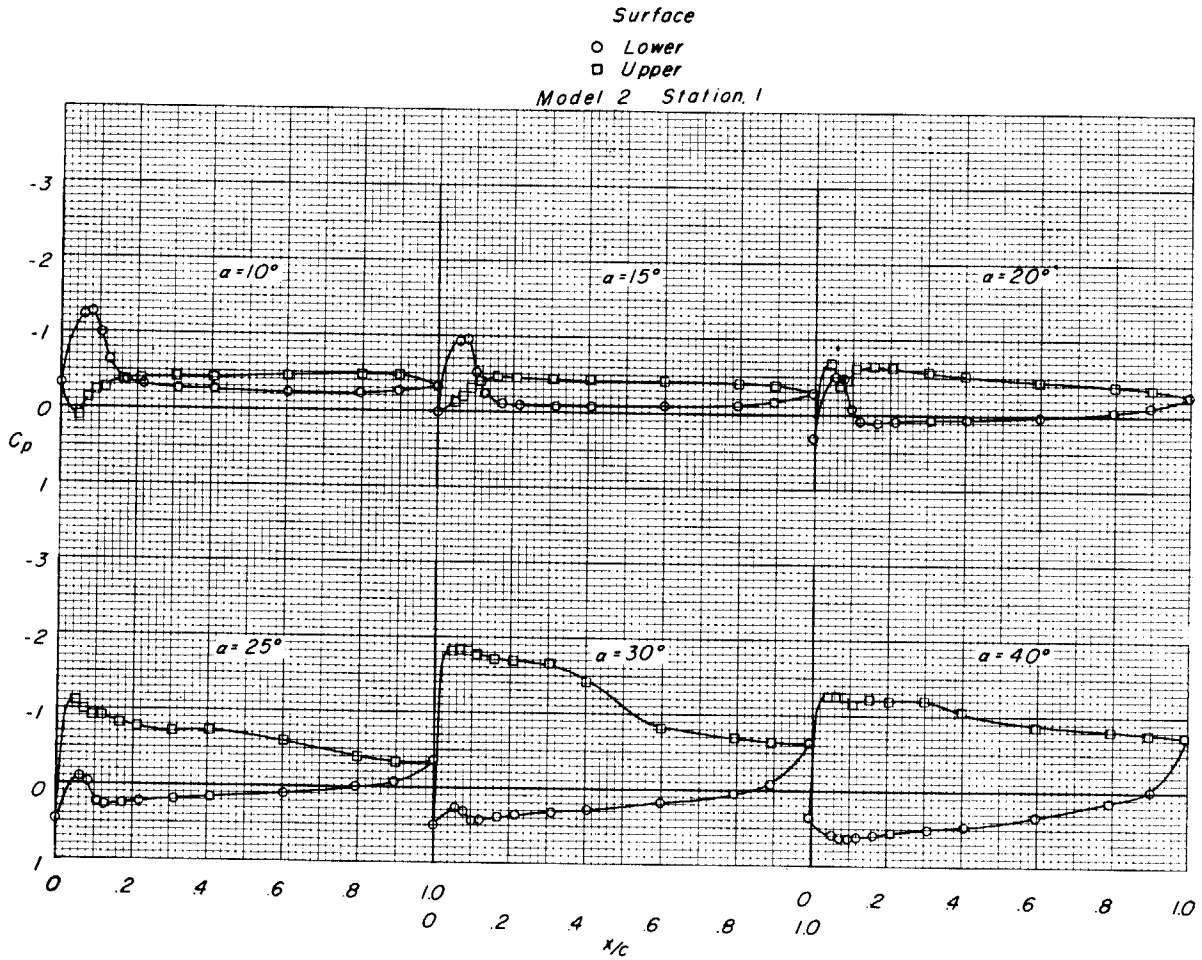

(a) M = 0.80.

Figure 7.- Pressure distributions on model 2 at various angles of attack.

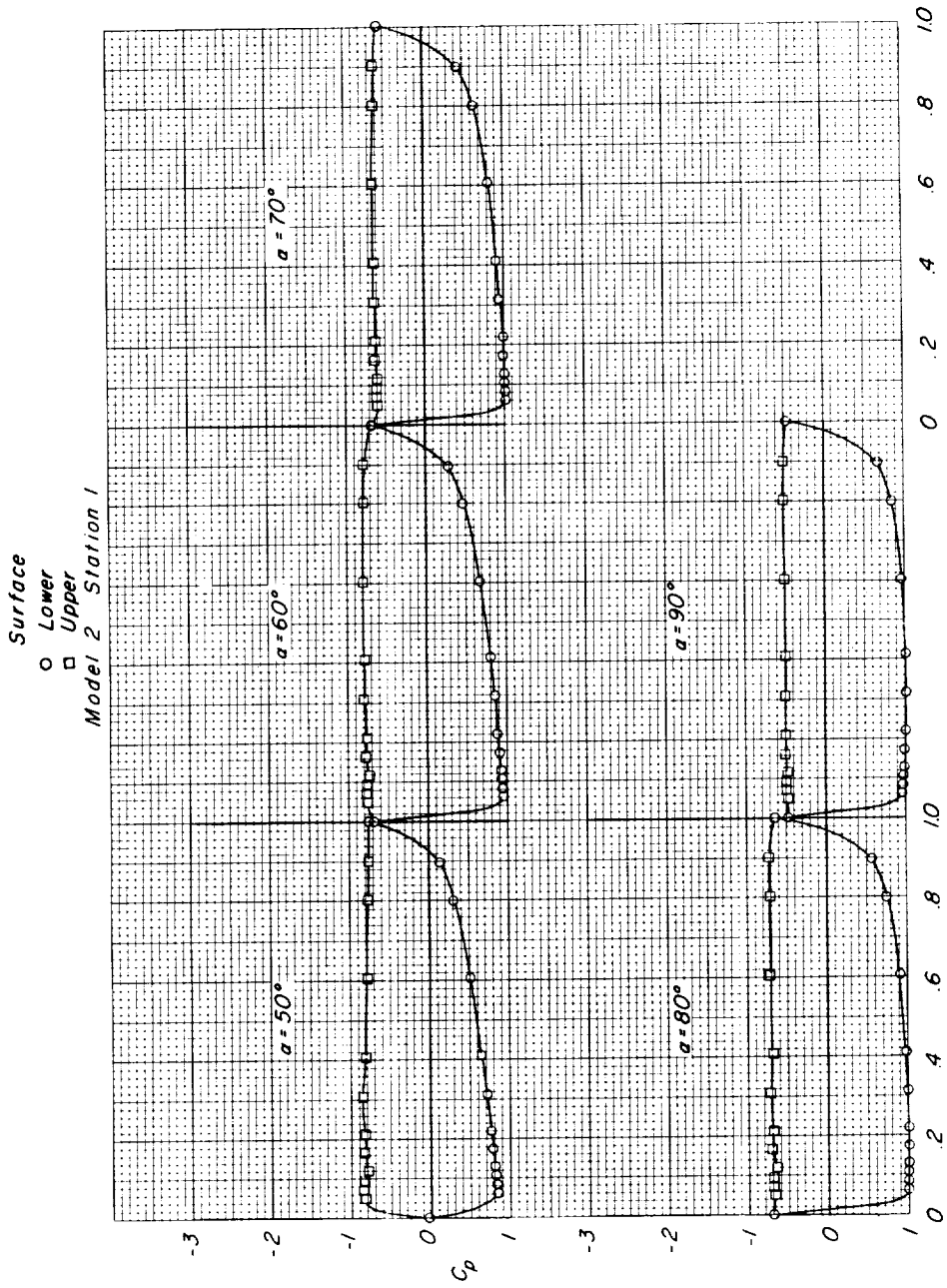

(a) M = 0.80. Continued.

Figure 7.- Continued.

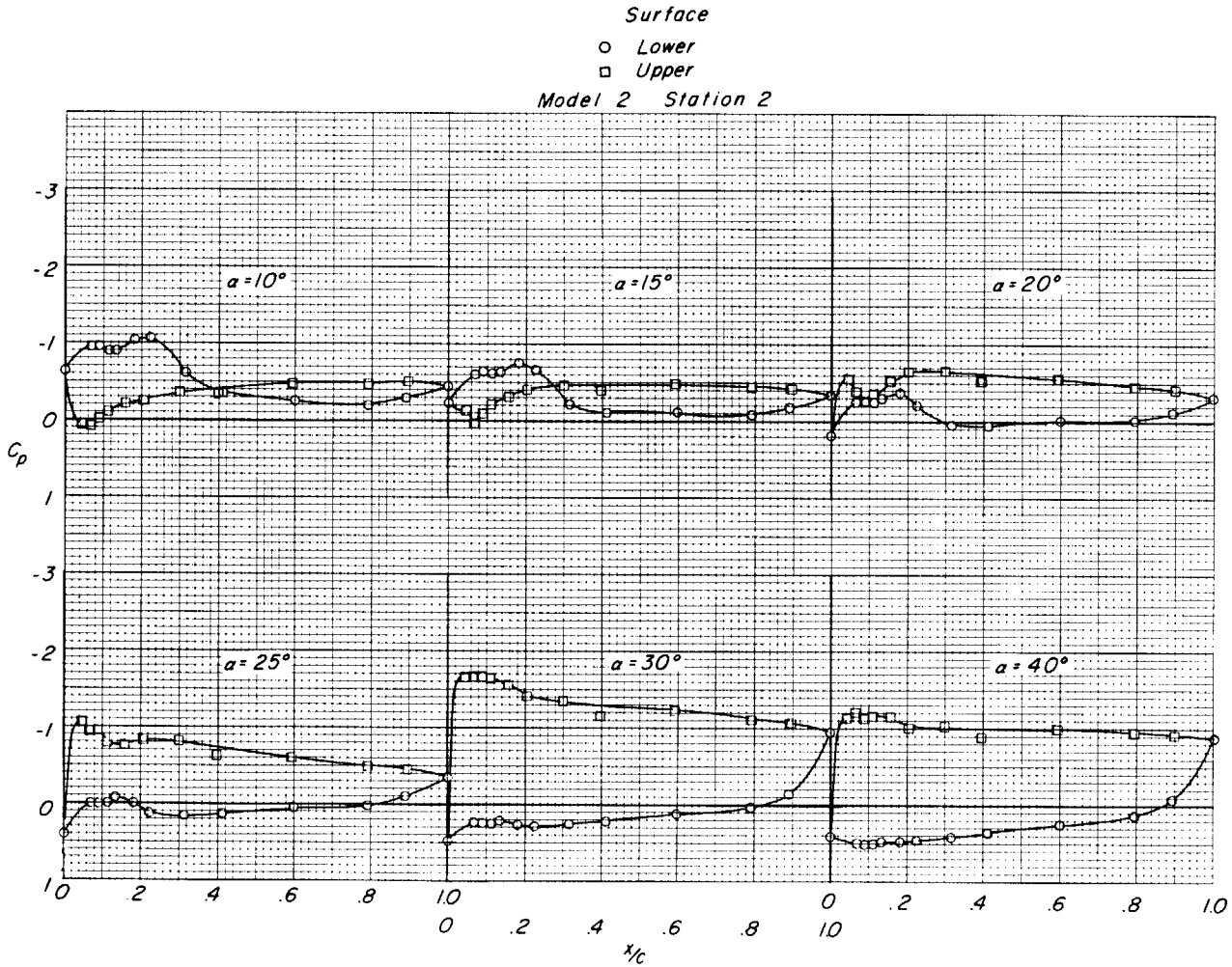

(a) M = 0.80. Continued.

Figure 7.- Continued.

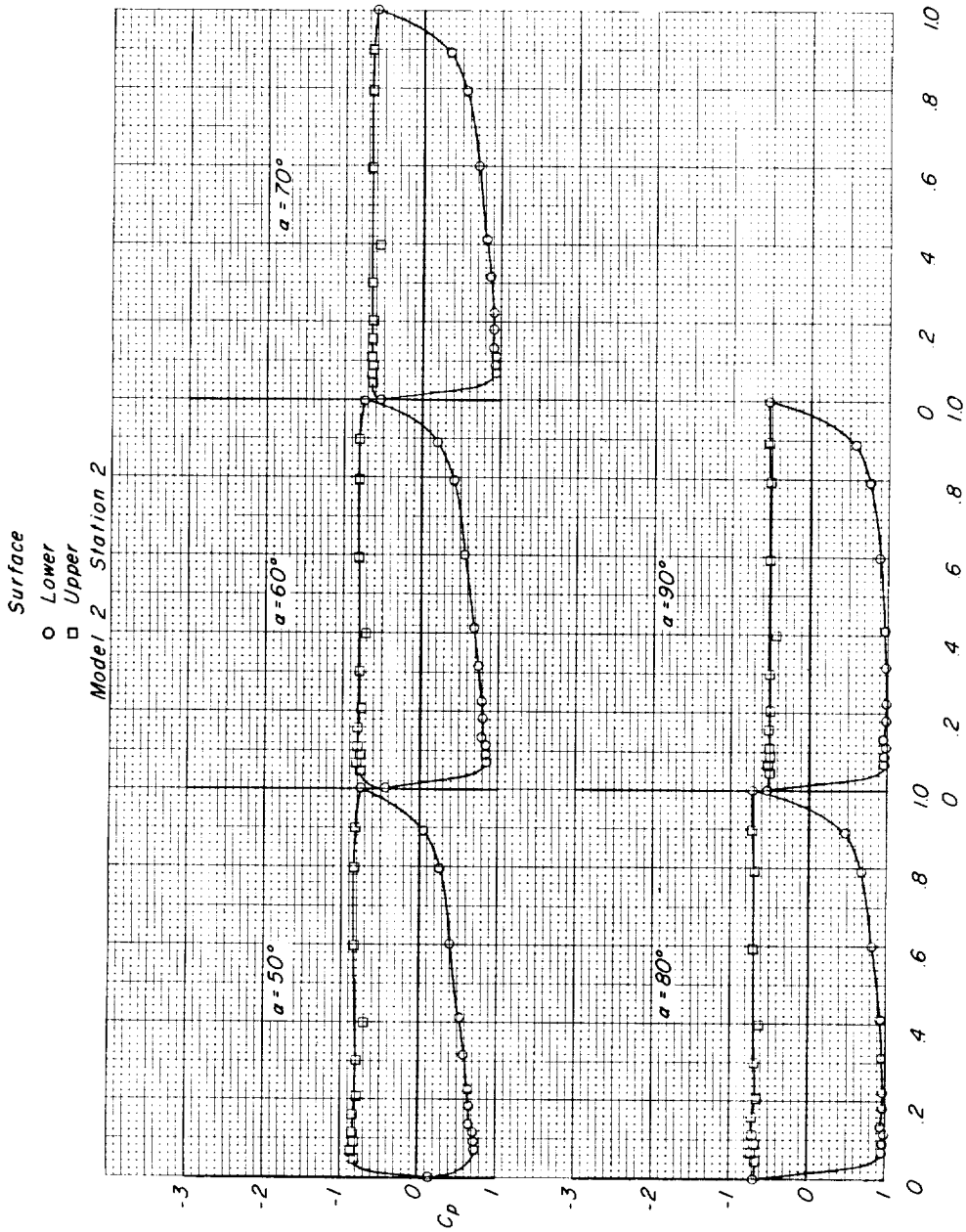

(a) M = 0.80. Continued.

Figure 7.- Continued.

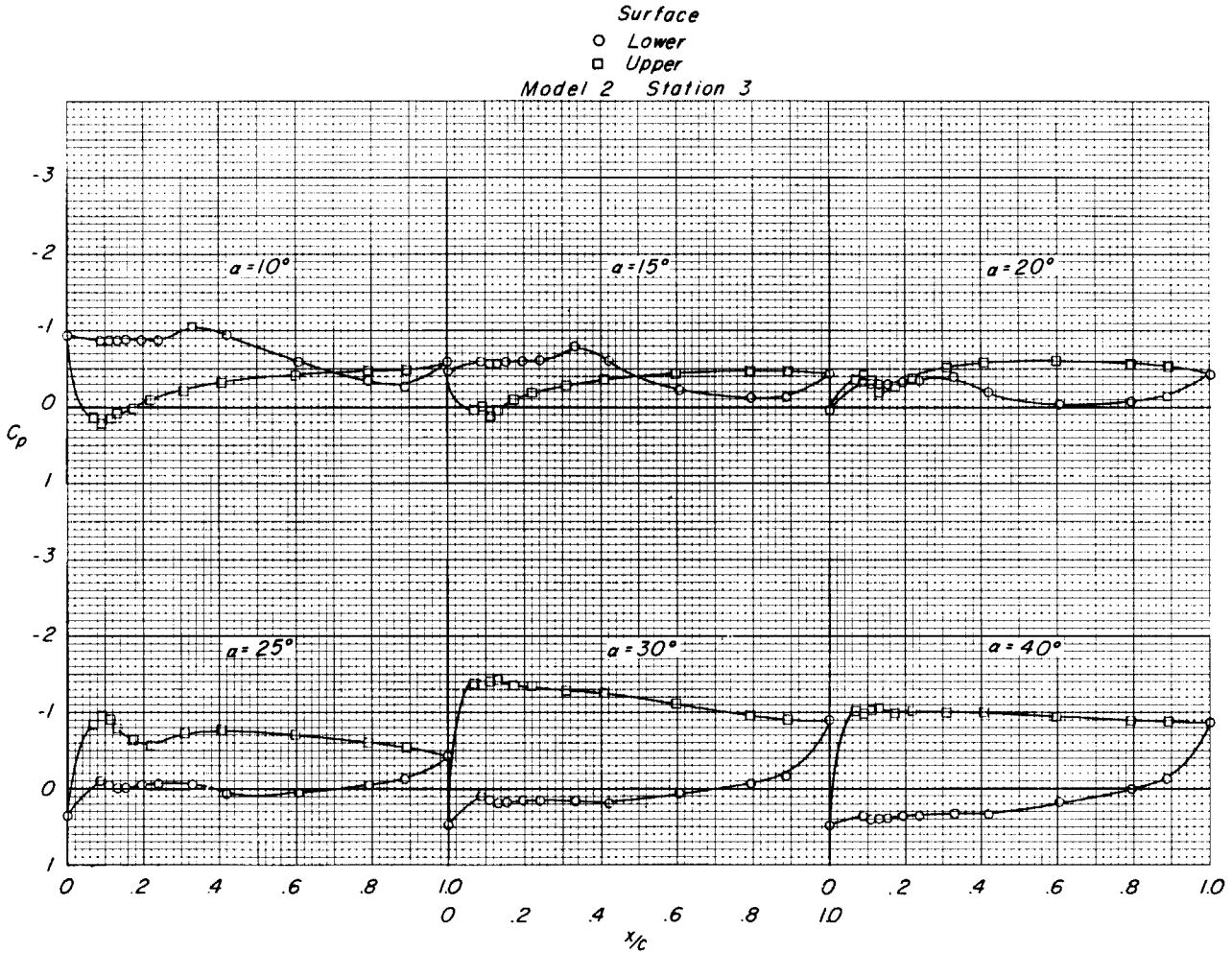

(a) M = 0.80. Continued.

Figure 7.- Continued.

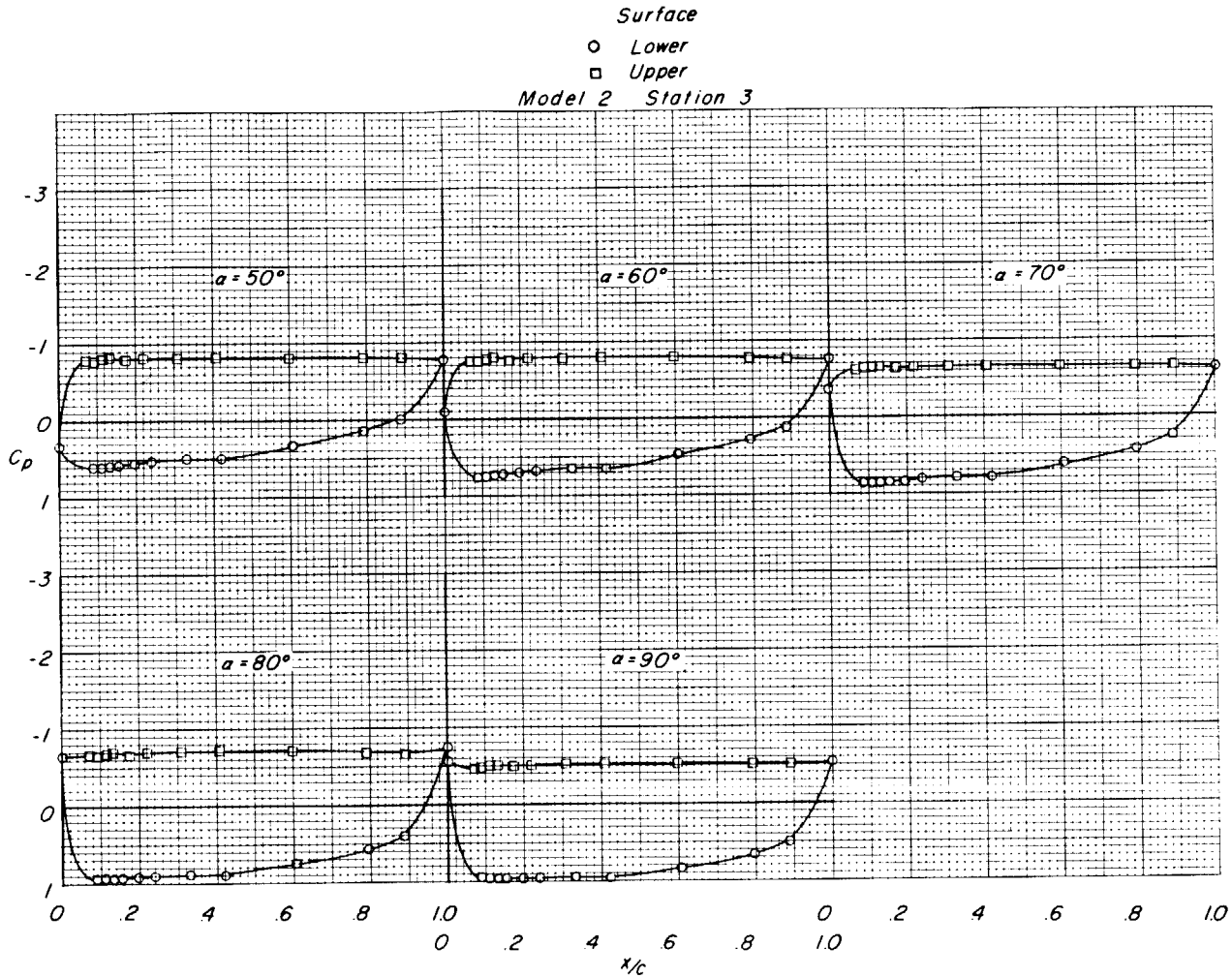

(a) M = 0.80. Continued.

Figure 7.- Continued.

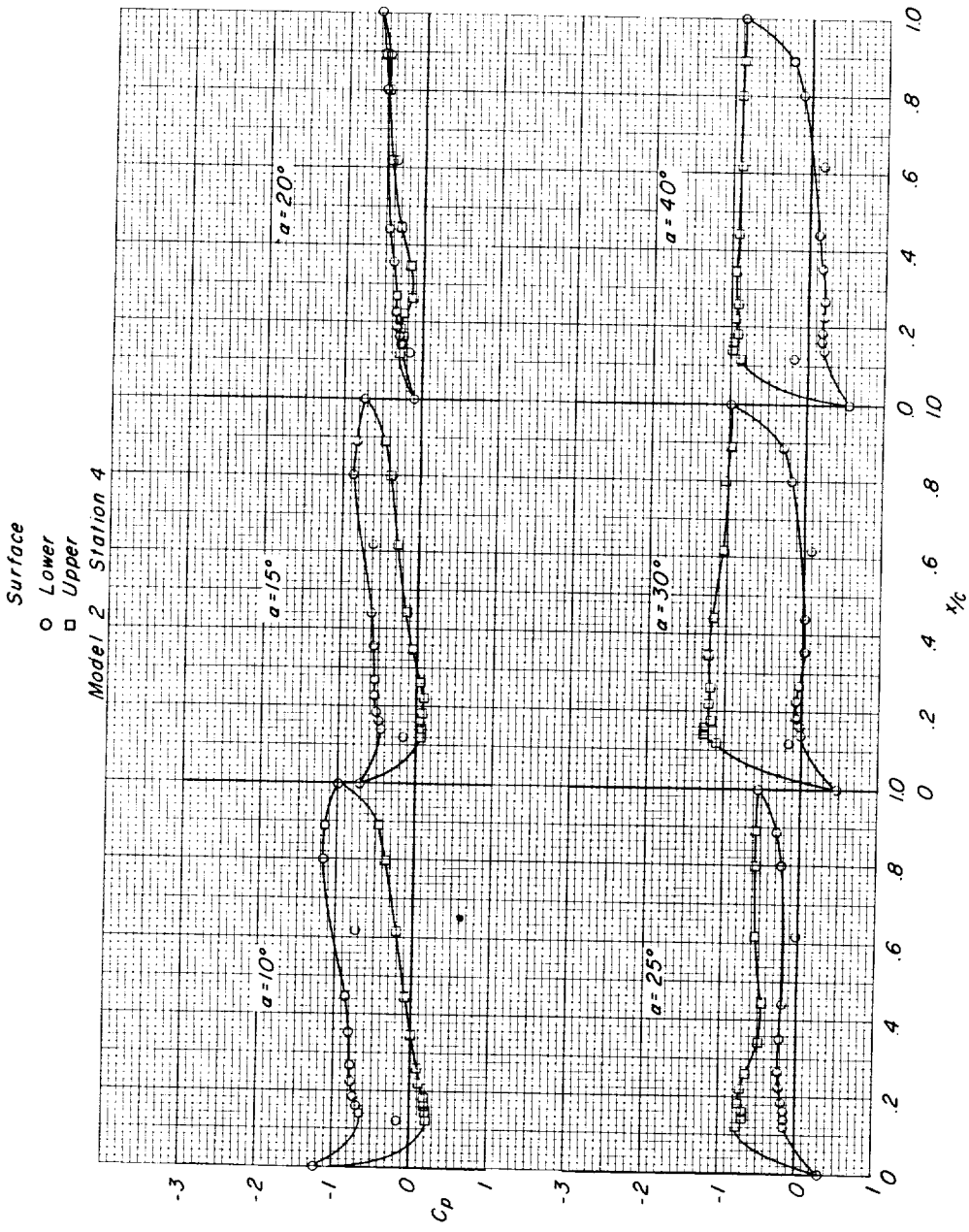

(a) M = 0.80. Continued.

Figure 7.- Continued.

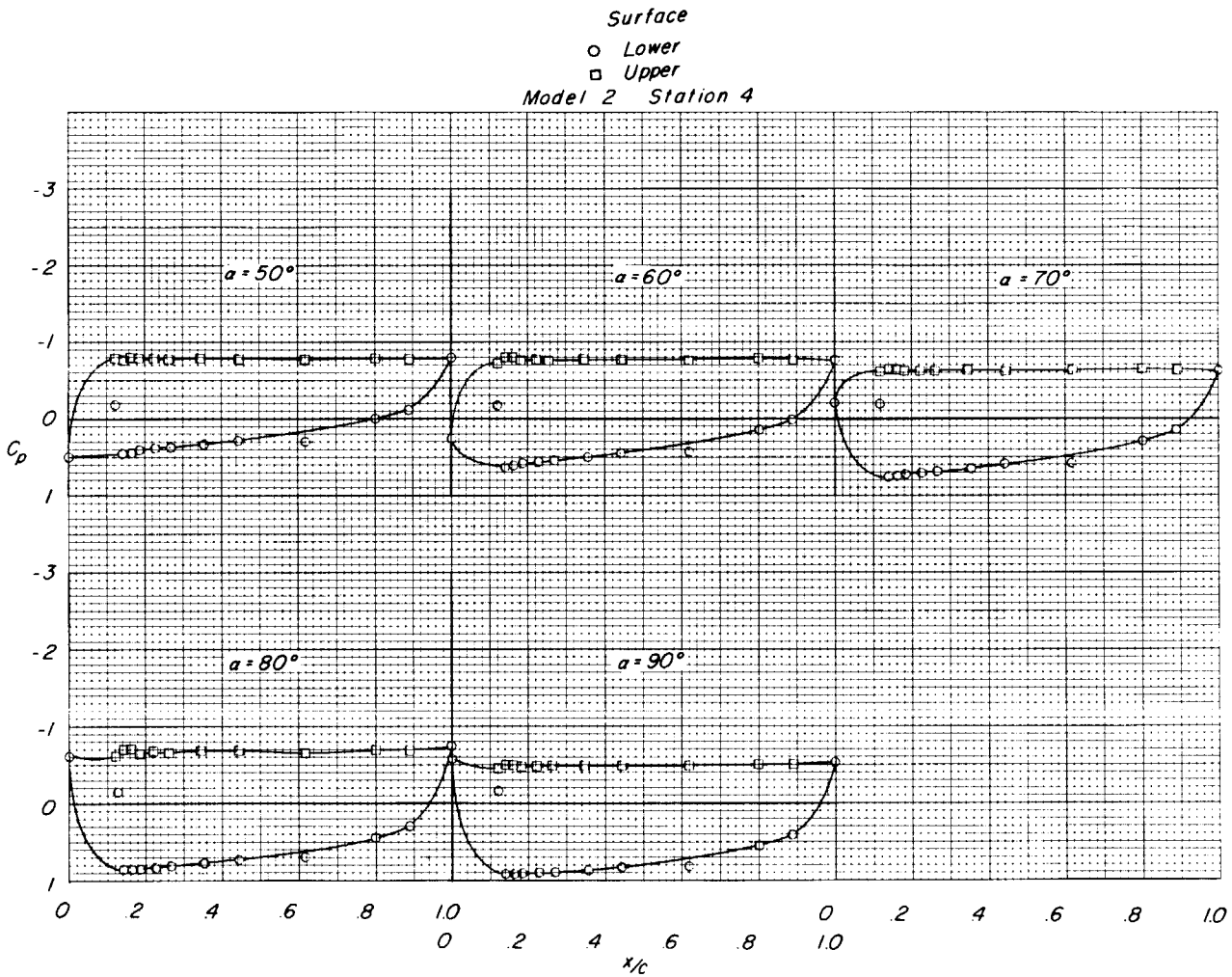

(a) M = 0.80. Concluded.

Figure 7.- Continued.

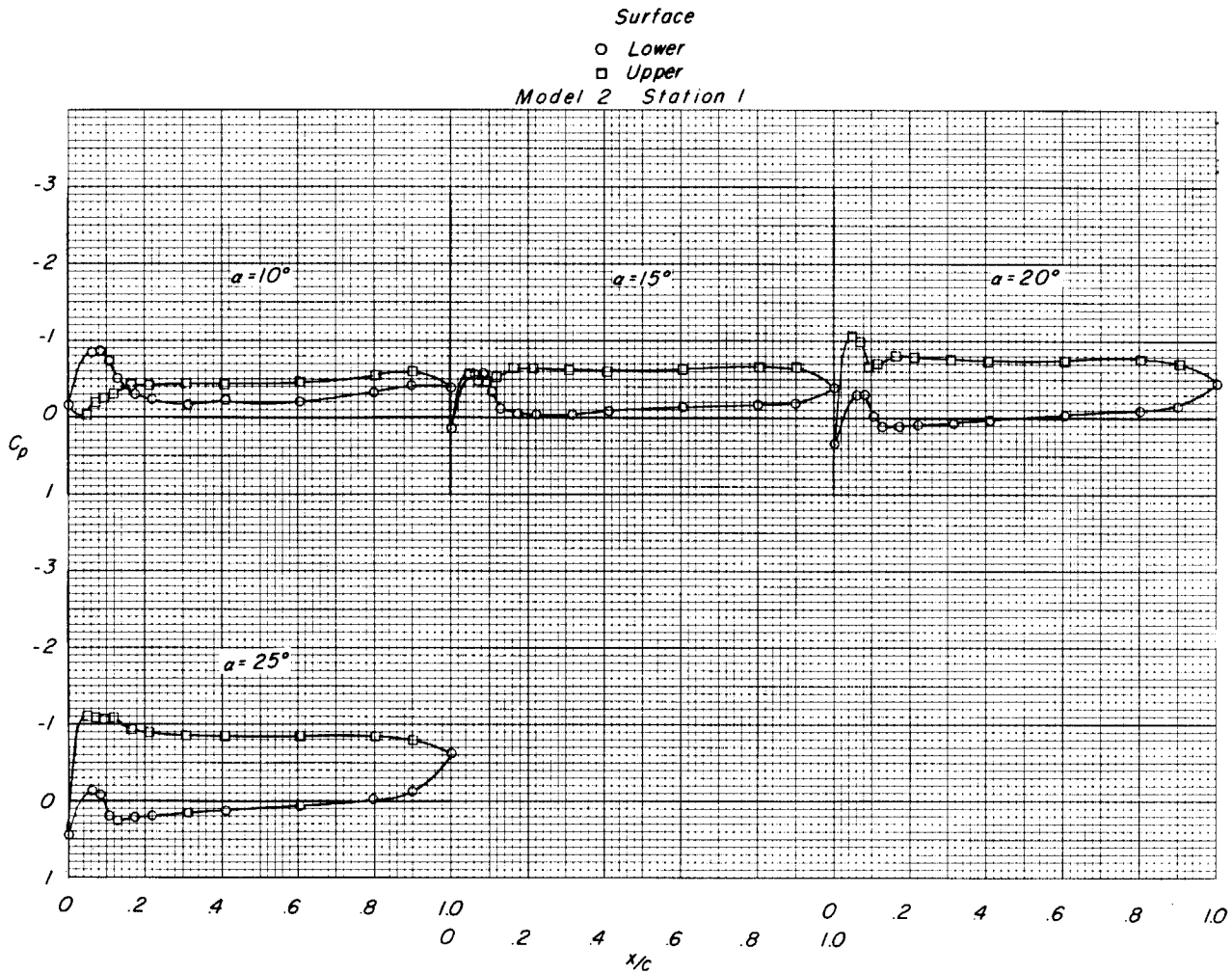

(b) M = 0.94.

Figure 7.- Continued.

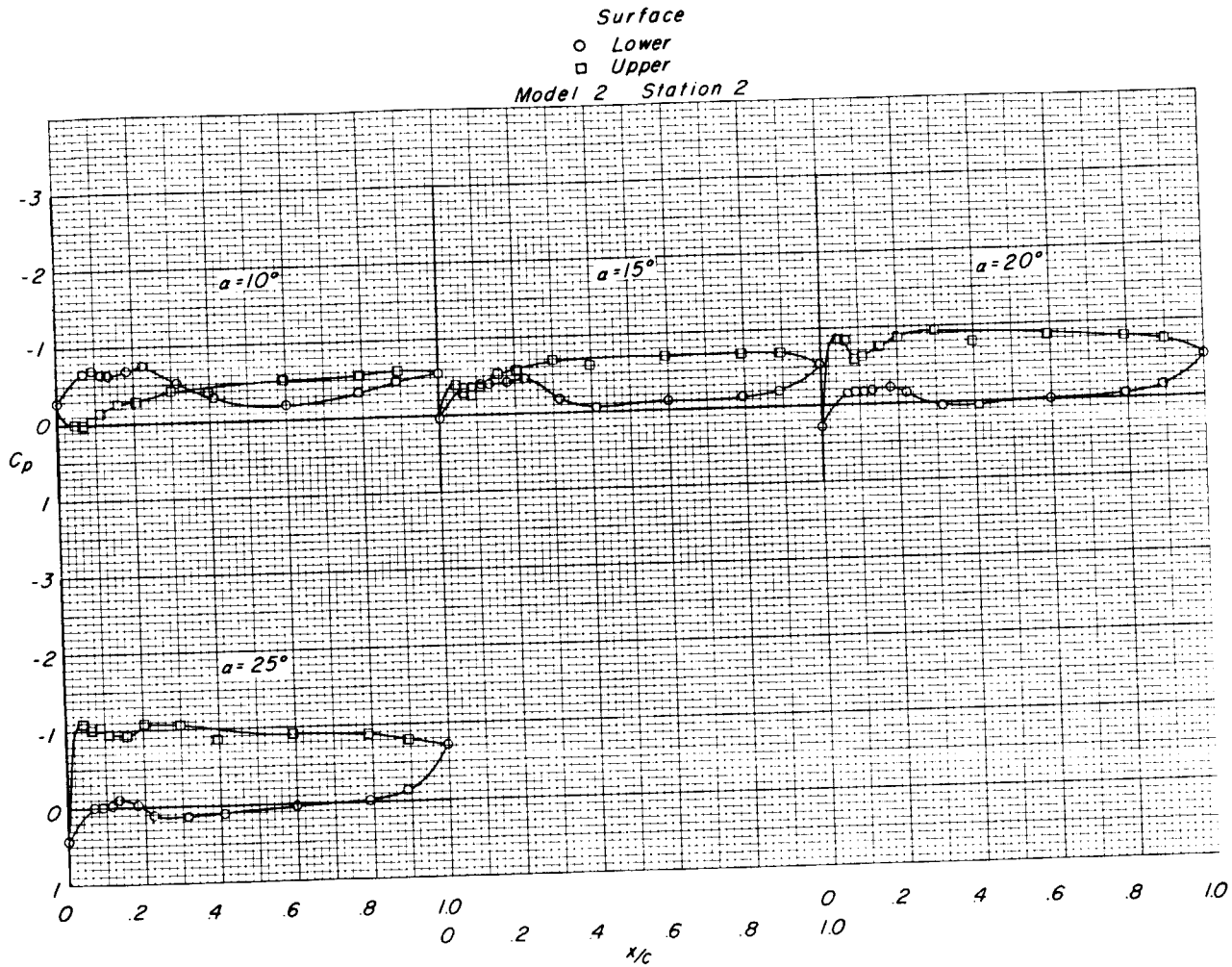

(b) M = 0.94. Continued.

Figure 7.- Continued.

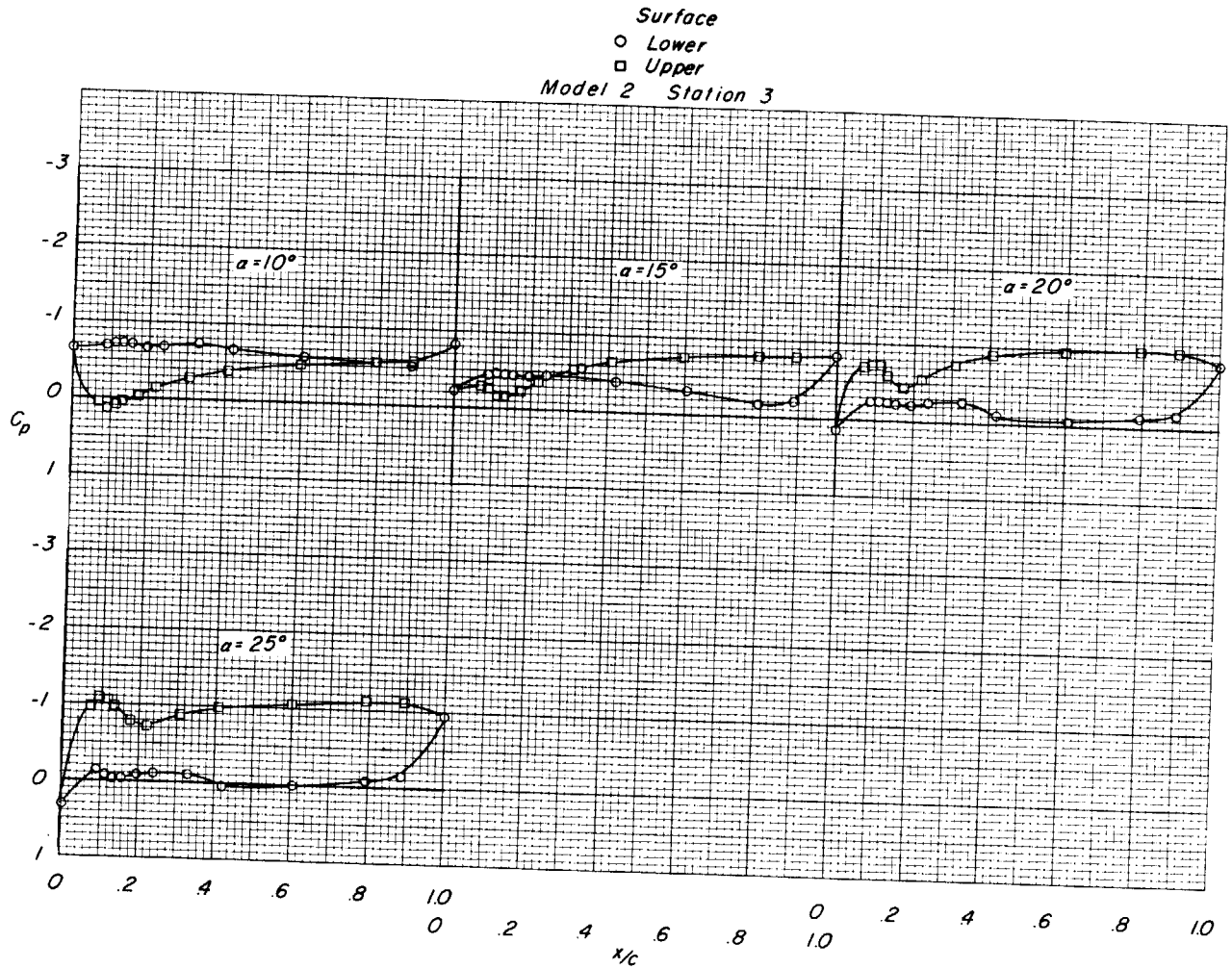

(b) M = 0.94. Continued.

Figure 7.- Continued.

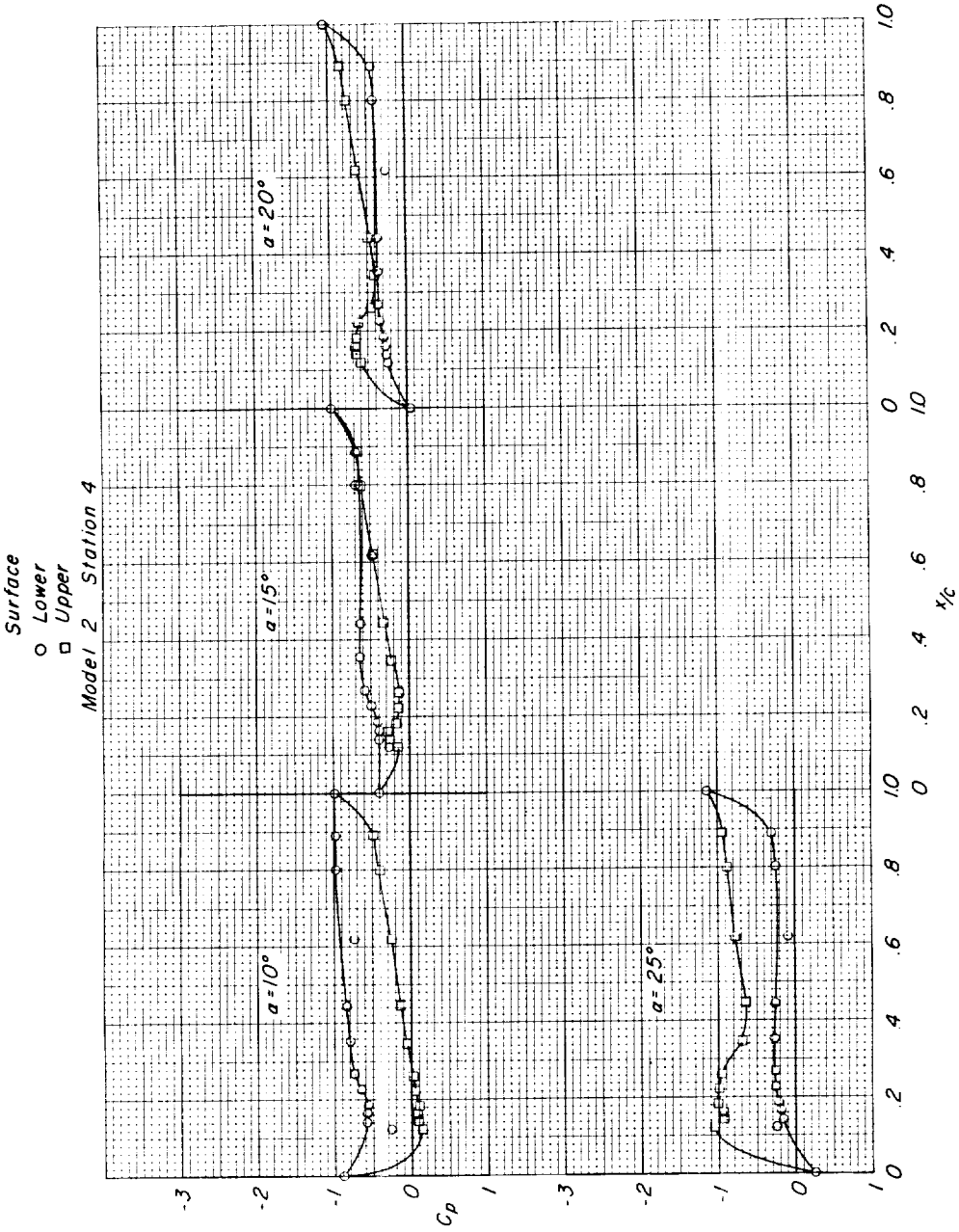

(b) M = 0.94. Concluded.

Figure 7.- Continued.

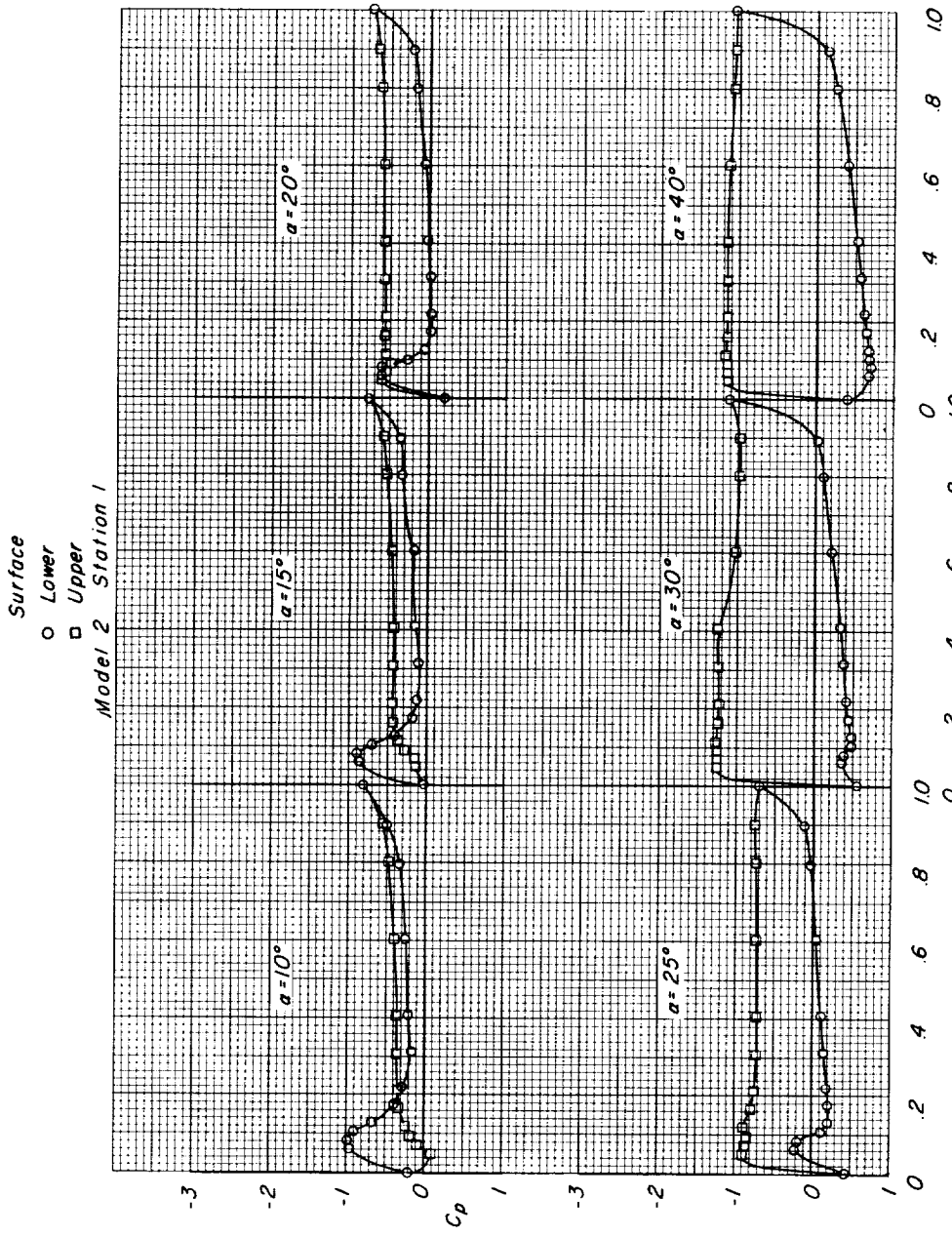

(c) M = 0.98.

Figure 7.- Continued.

L-1865

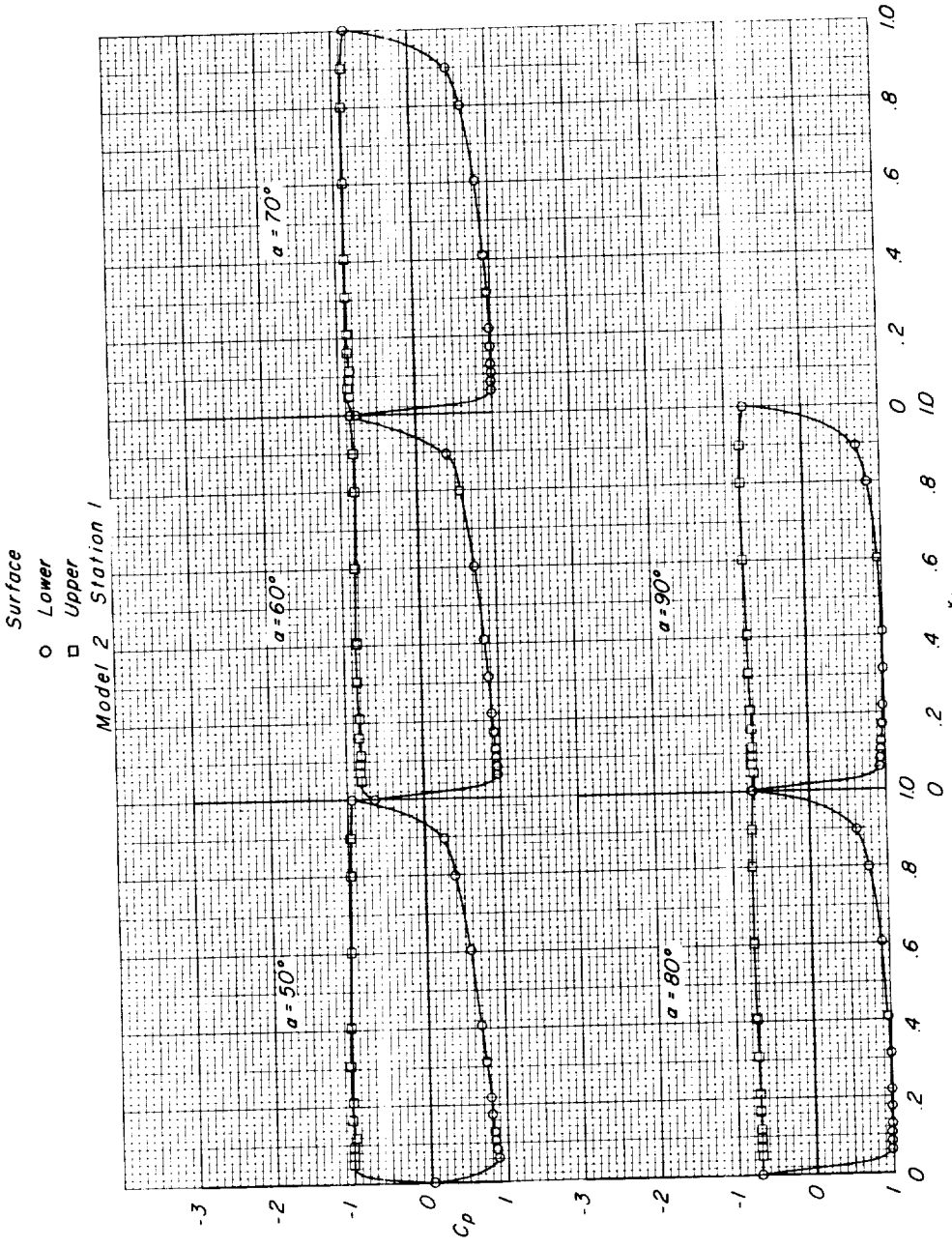

(c) M = 0.98. Continued.

Figure 7.- Continued.

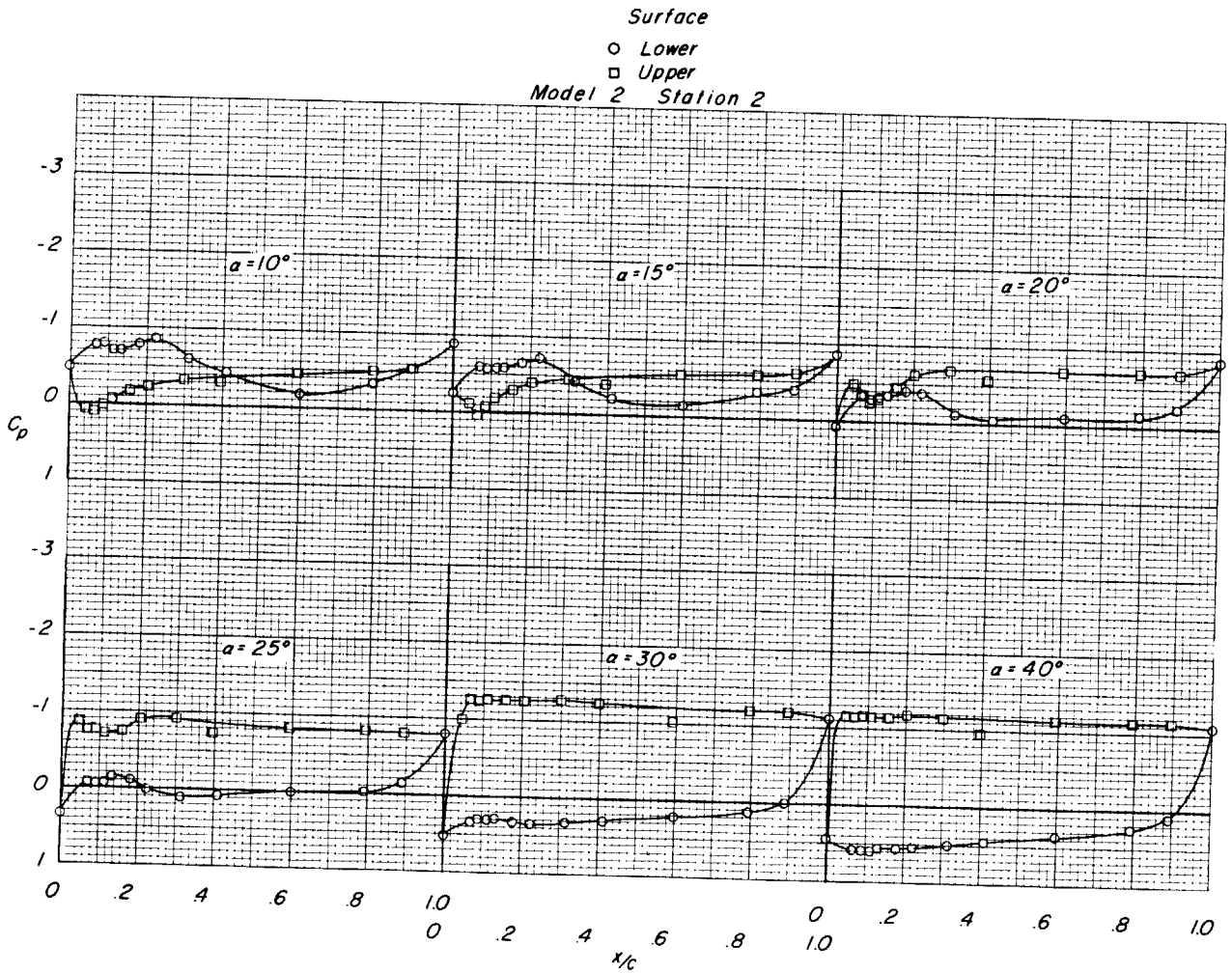

(c) M = 0.98. Continued.

Figure 7.- Continued.

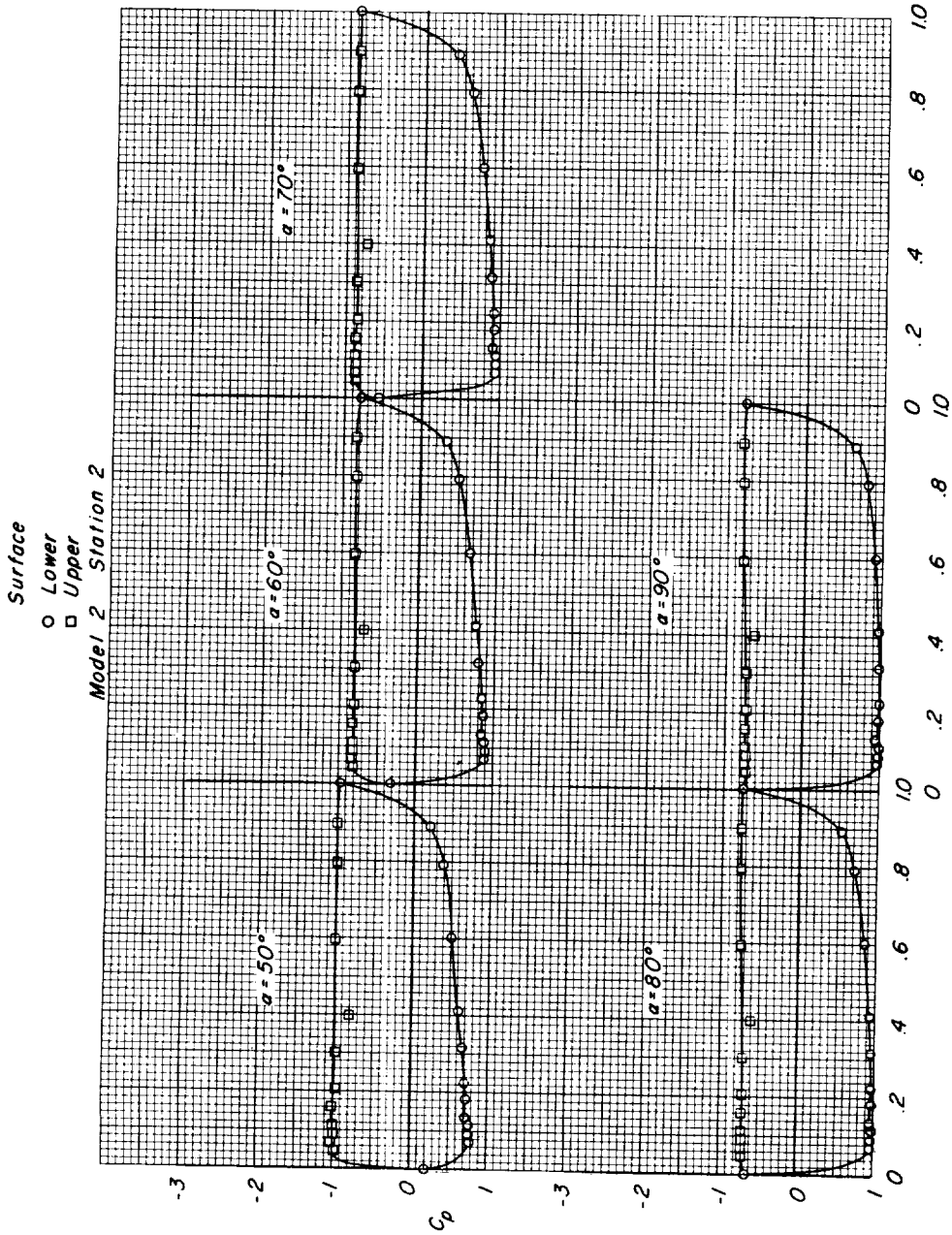

(c) M = 0.98. Continued.

Figure 7.- Continued.

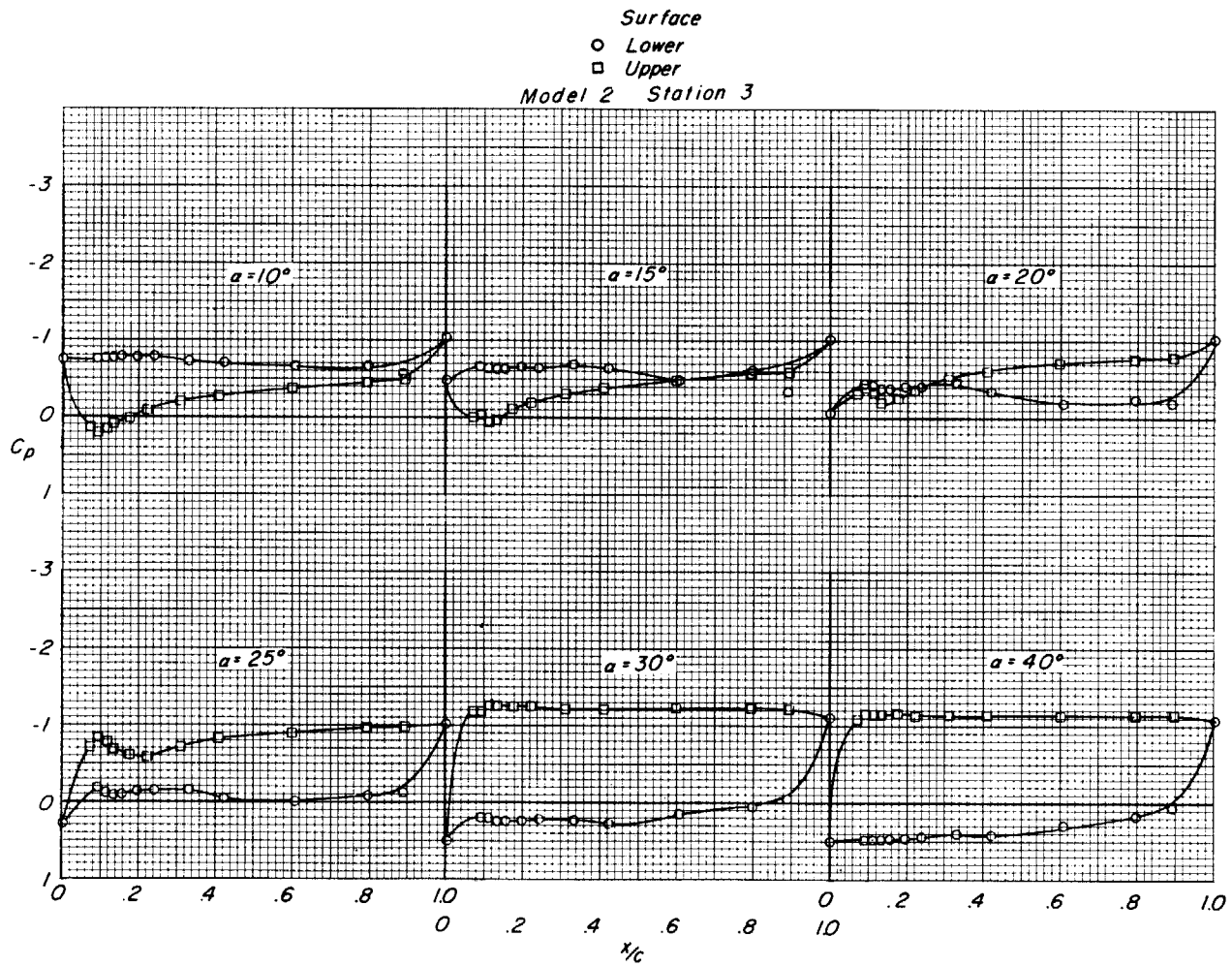

(c) M = 0.98. Continued.

Figure 7.- Continued.

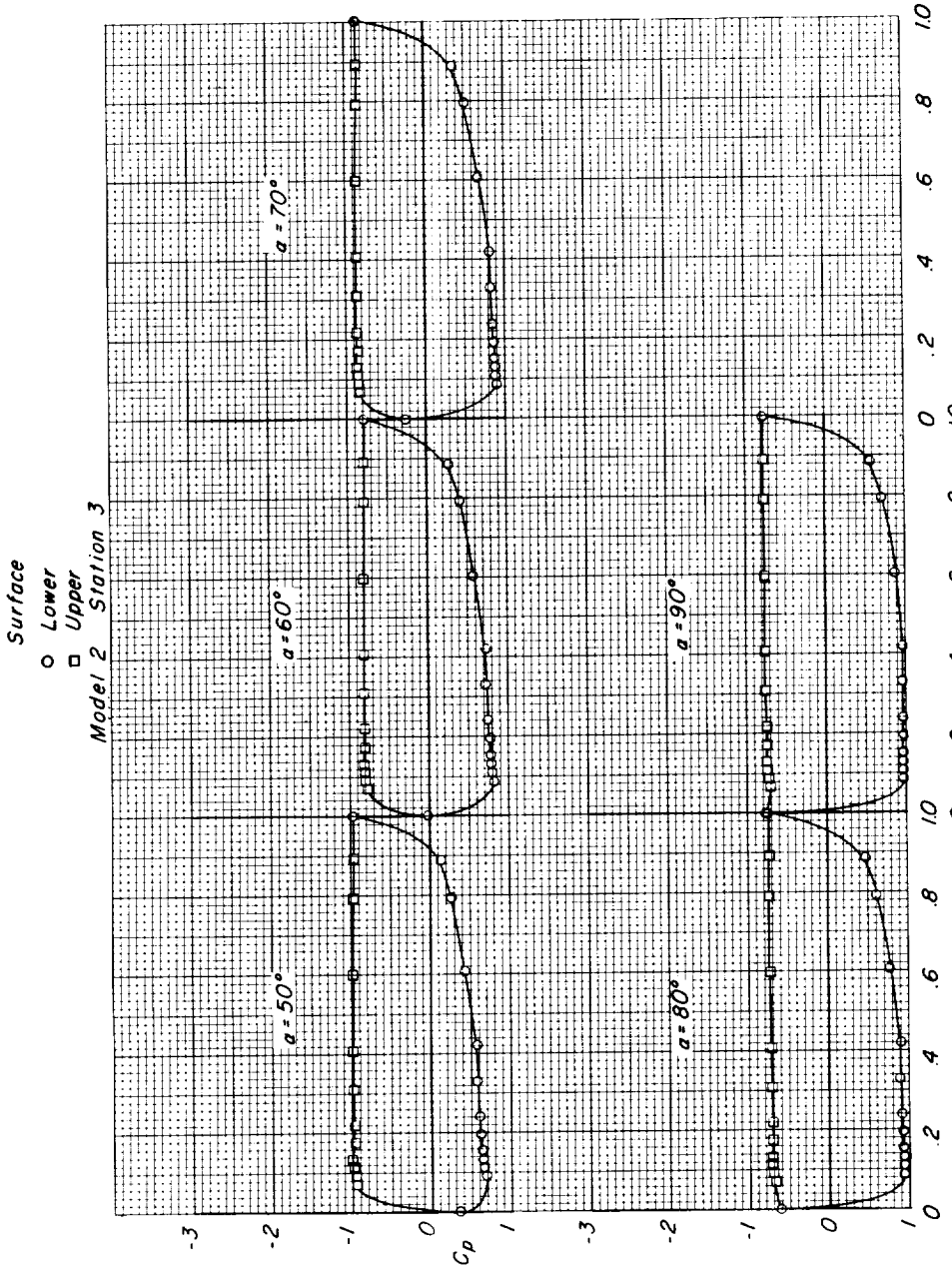

(c) M = 0.98. Continued.

Figure 7.- Continued.

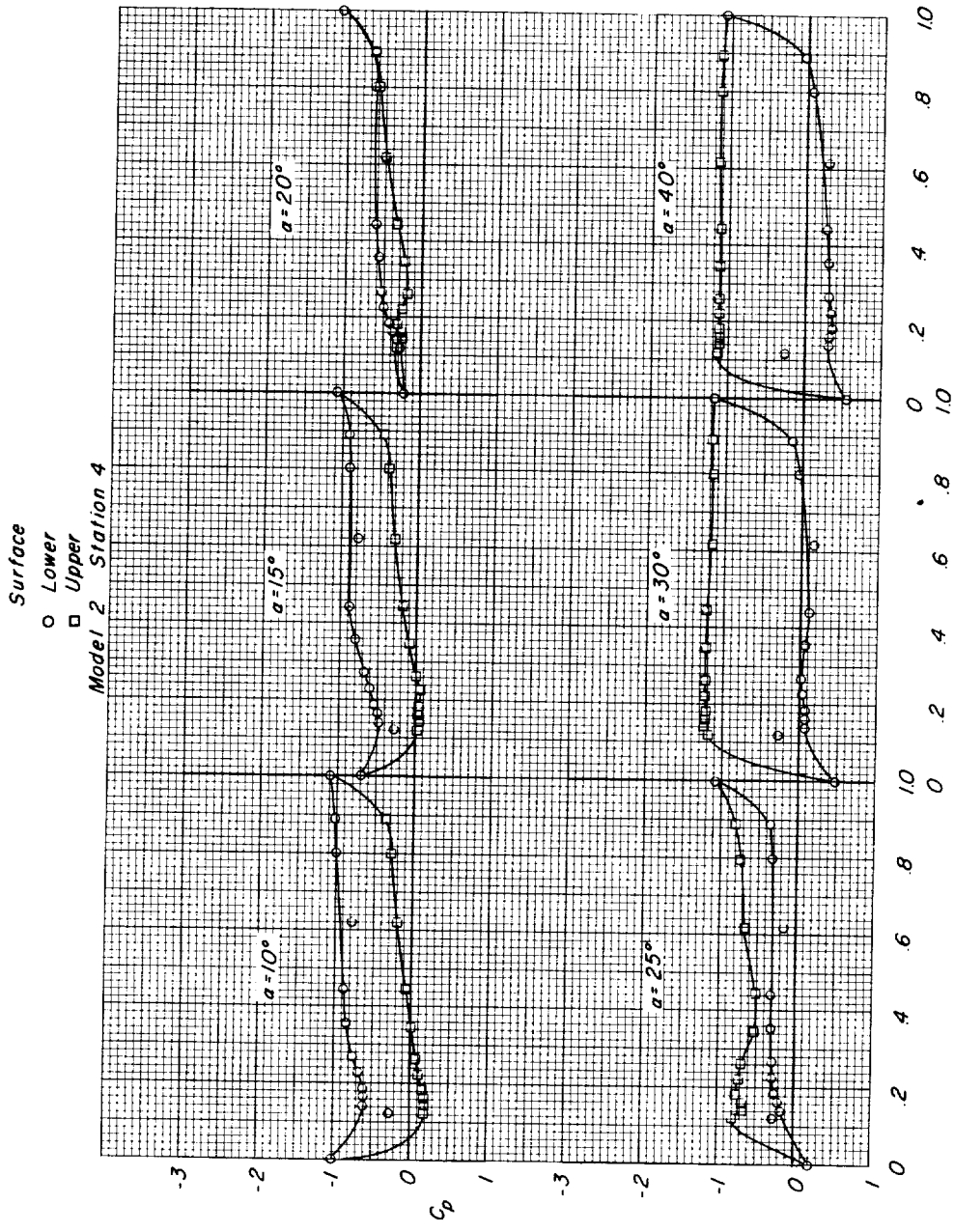

(c) M = 0.98. Continued.

Figure 7.- Continued.

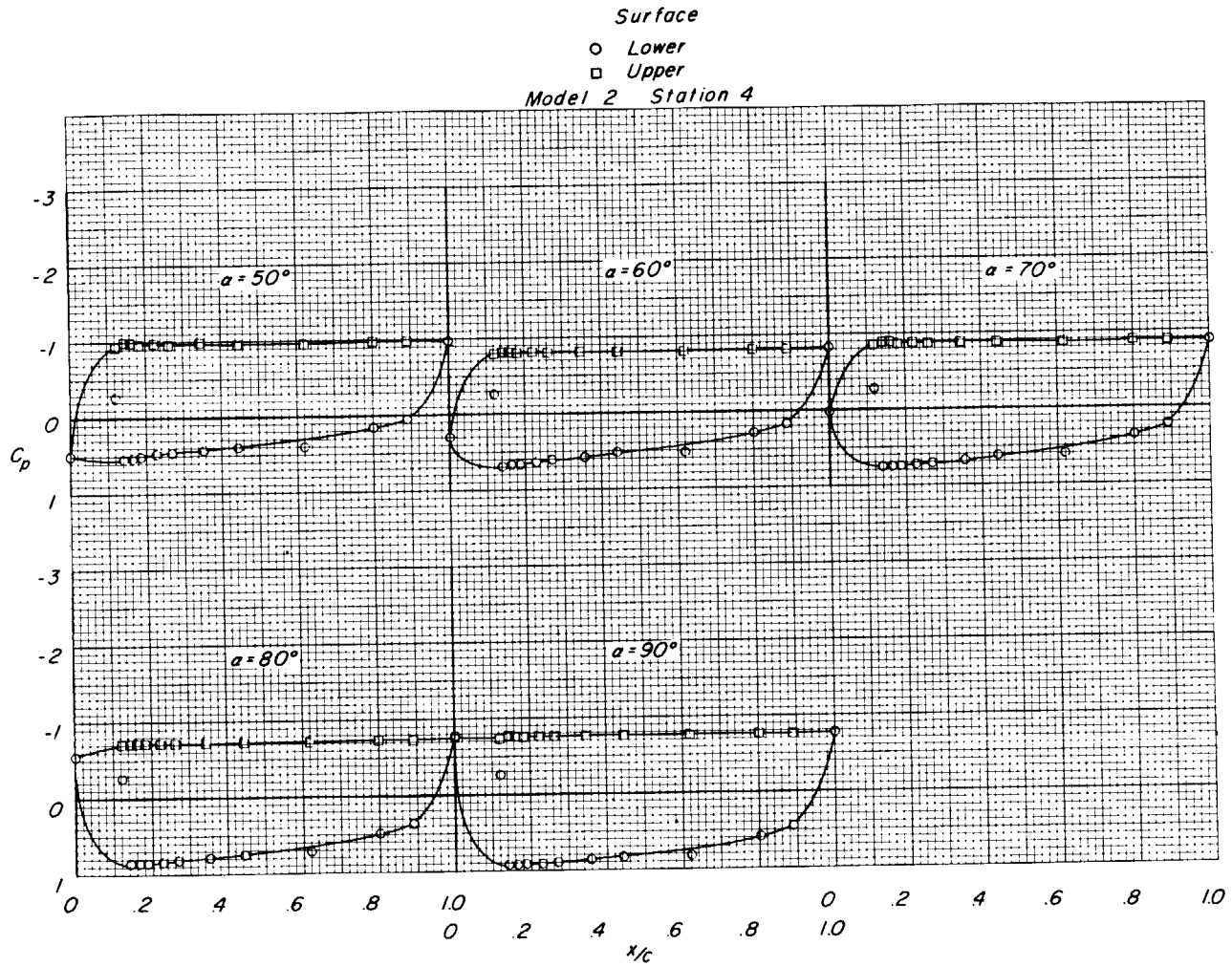

(c) M = 0.98. Concluded.

Figure 7.- Continued.

(d) M = 1.02.

Figure 7.- Continued.

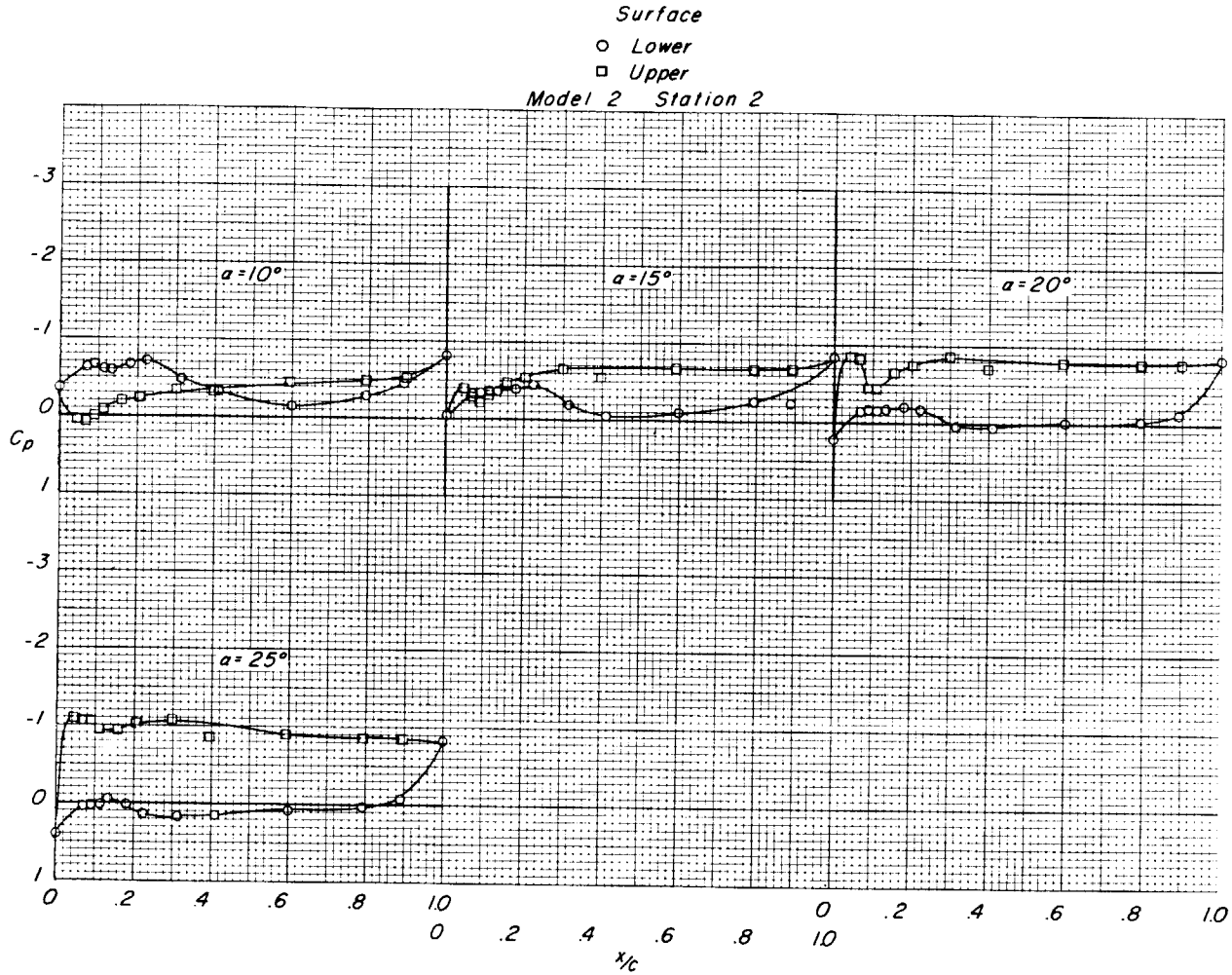

(d) M = 1.02. Continued.

Figure 7.- Continued.

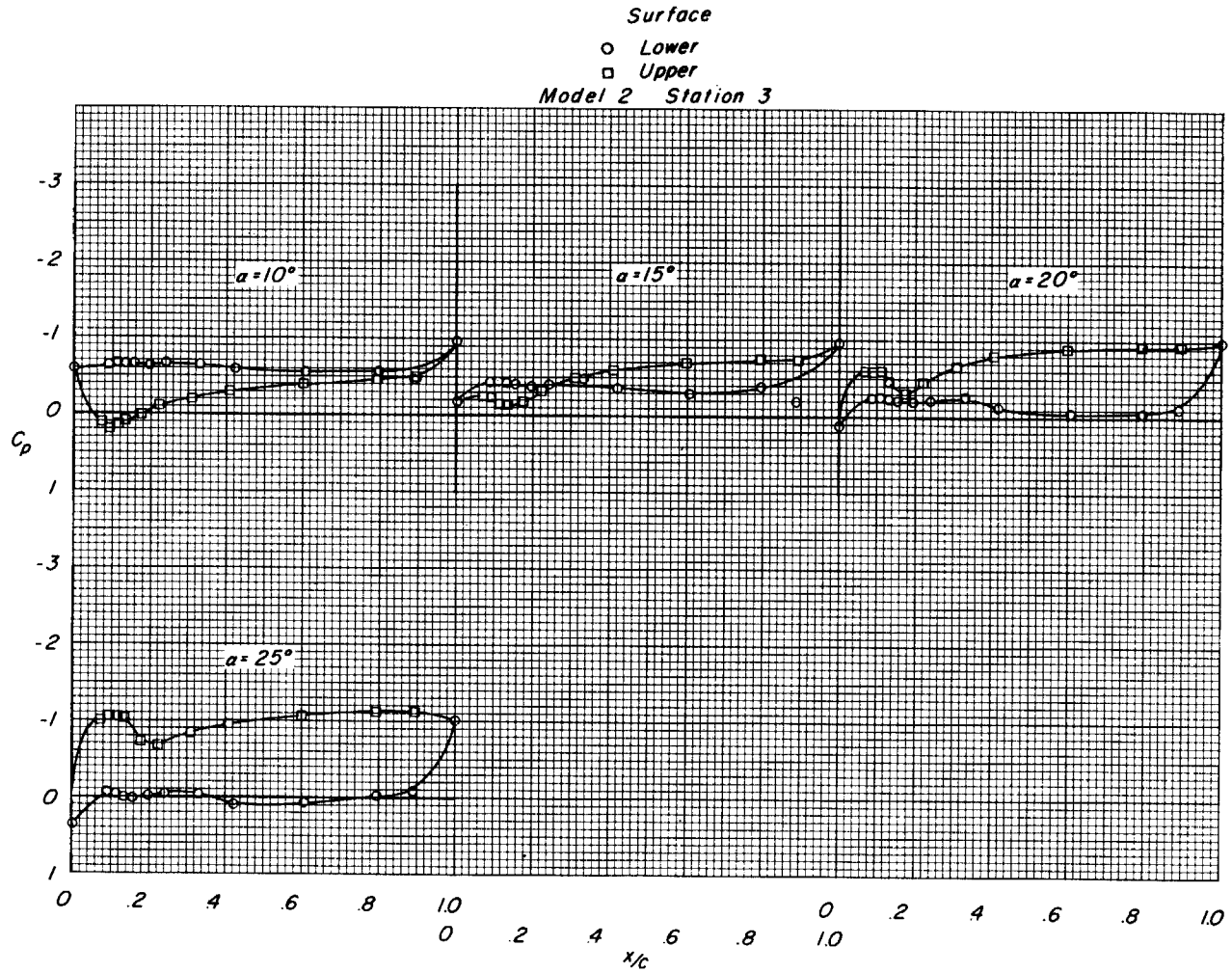

(d) M = 1.02. Continued.

Figure 7.- Continued.

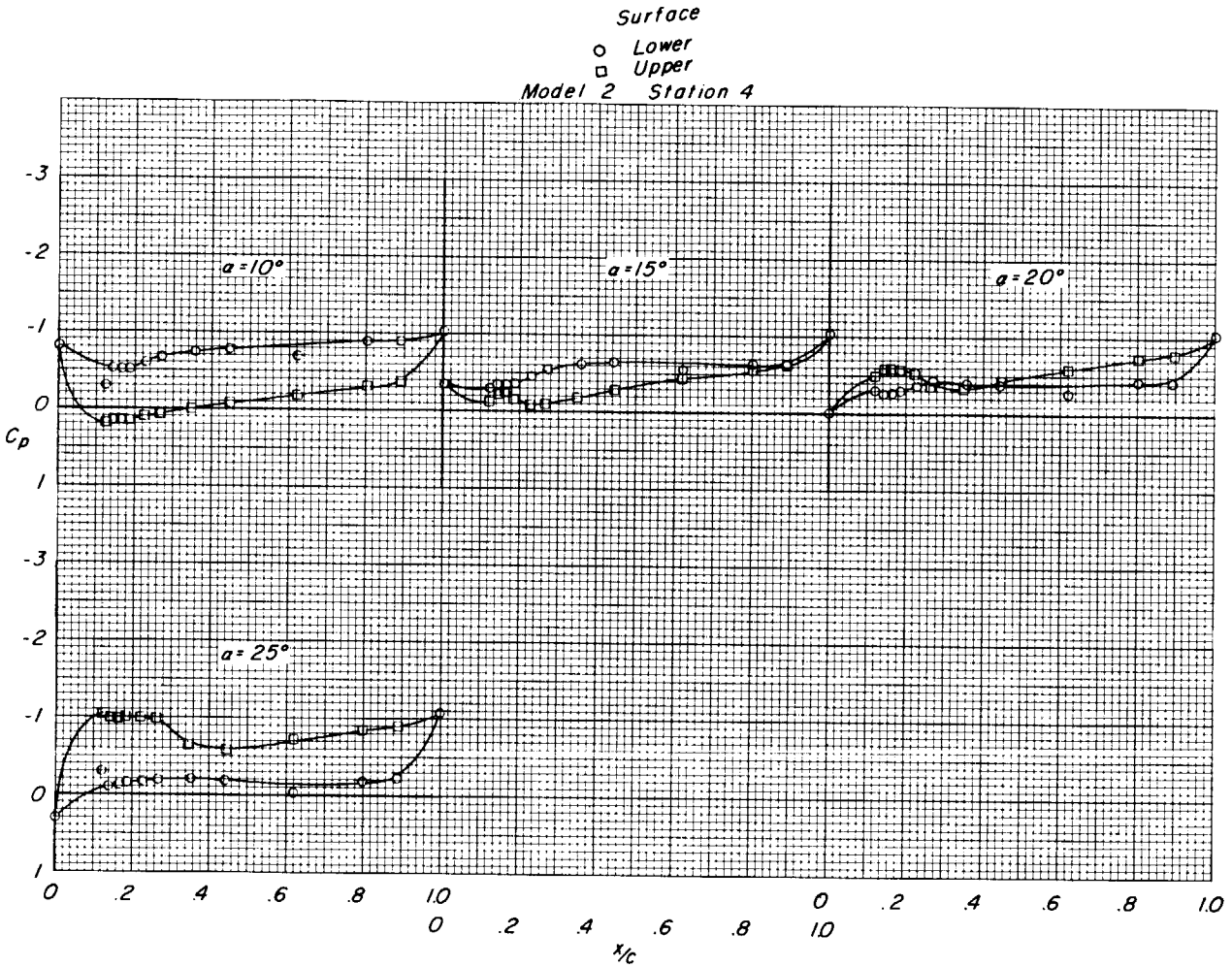

(d) M = 1.02. Concluded.

Figure 7.- Continued.

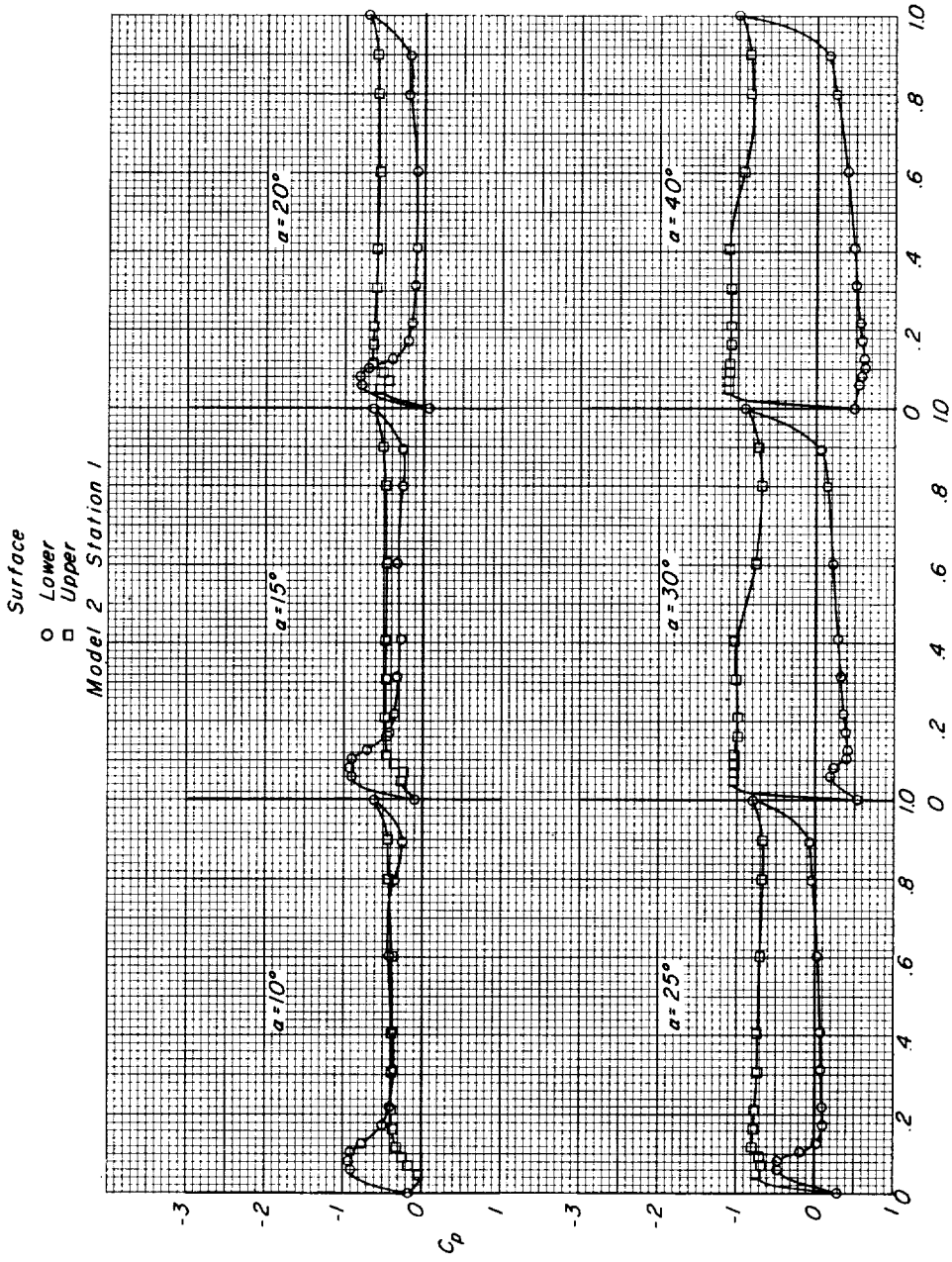

(e) M = 1.20.

Figure 7.- Continued.

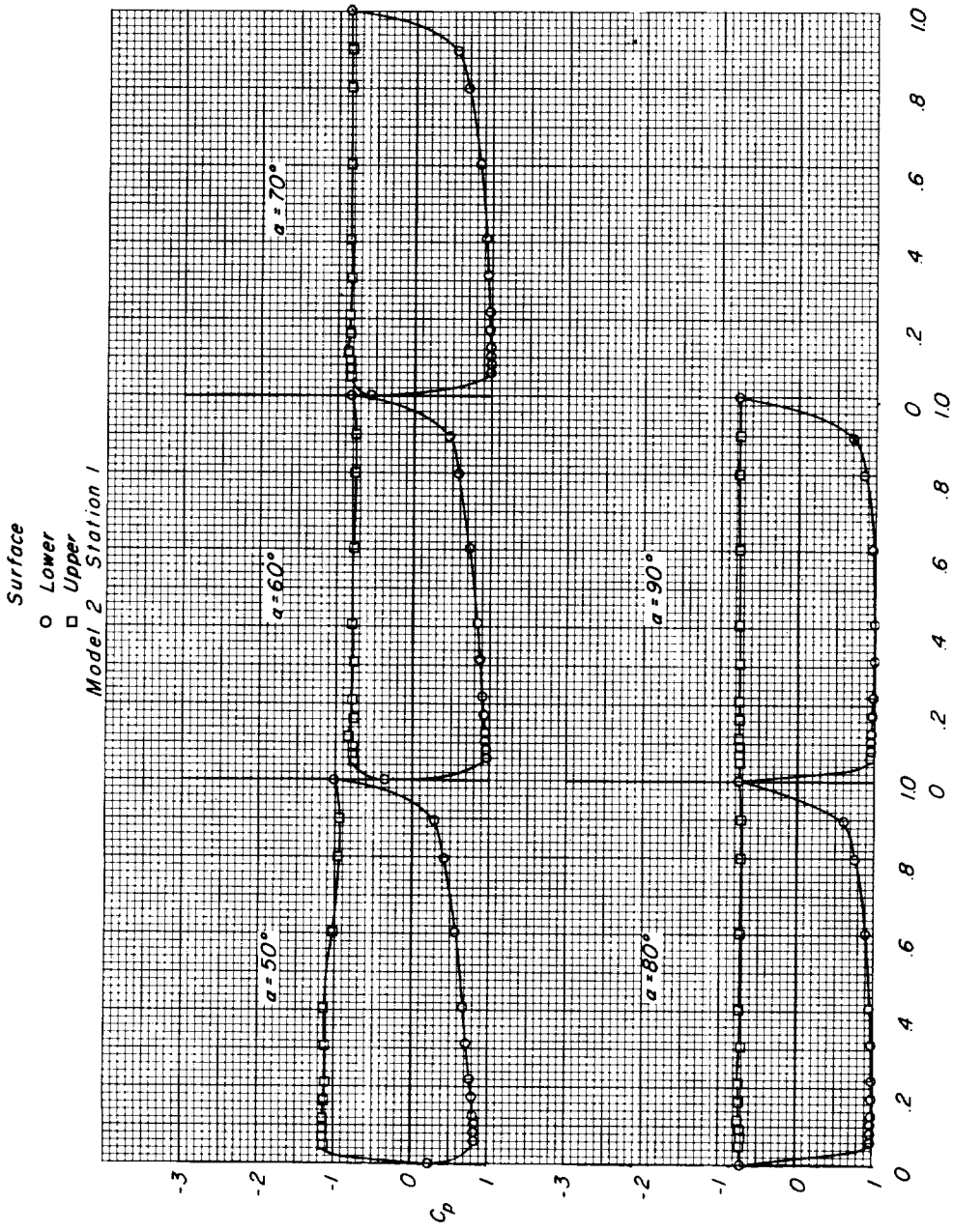

(e) M = 1.20. Continued.

Figure 7.- Continued.

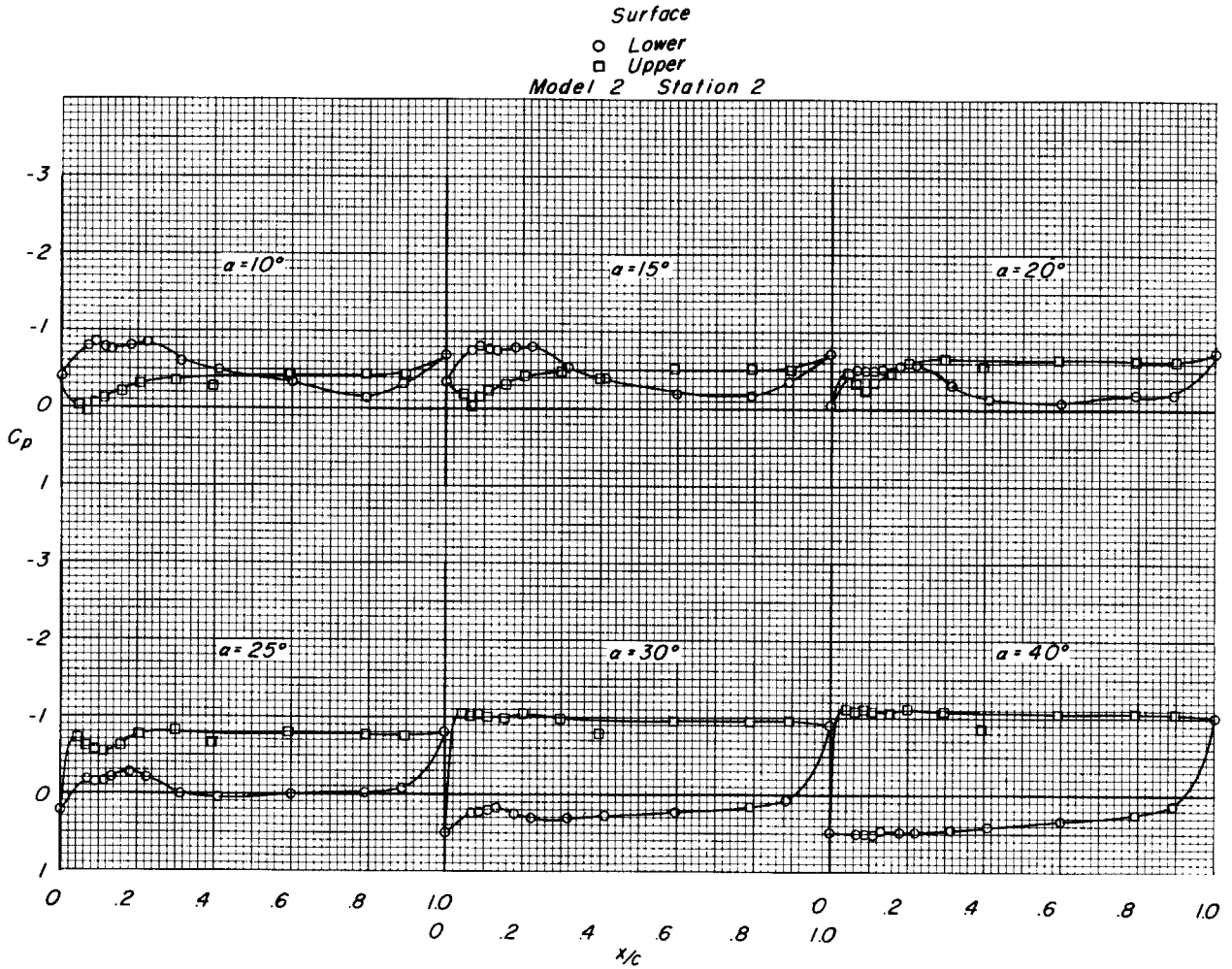

(e) M = 1.20. Continued.

Figure 7.- Continued.

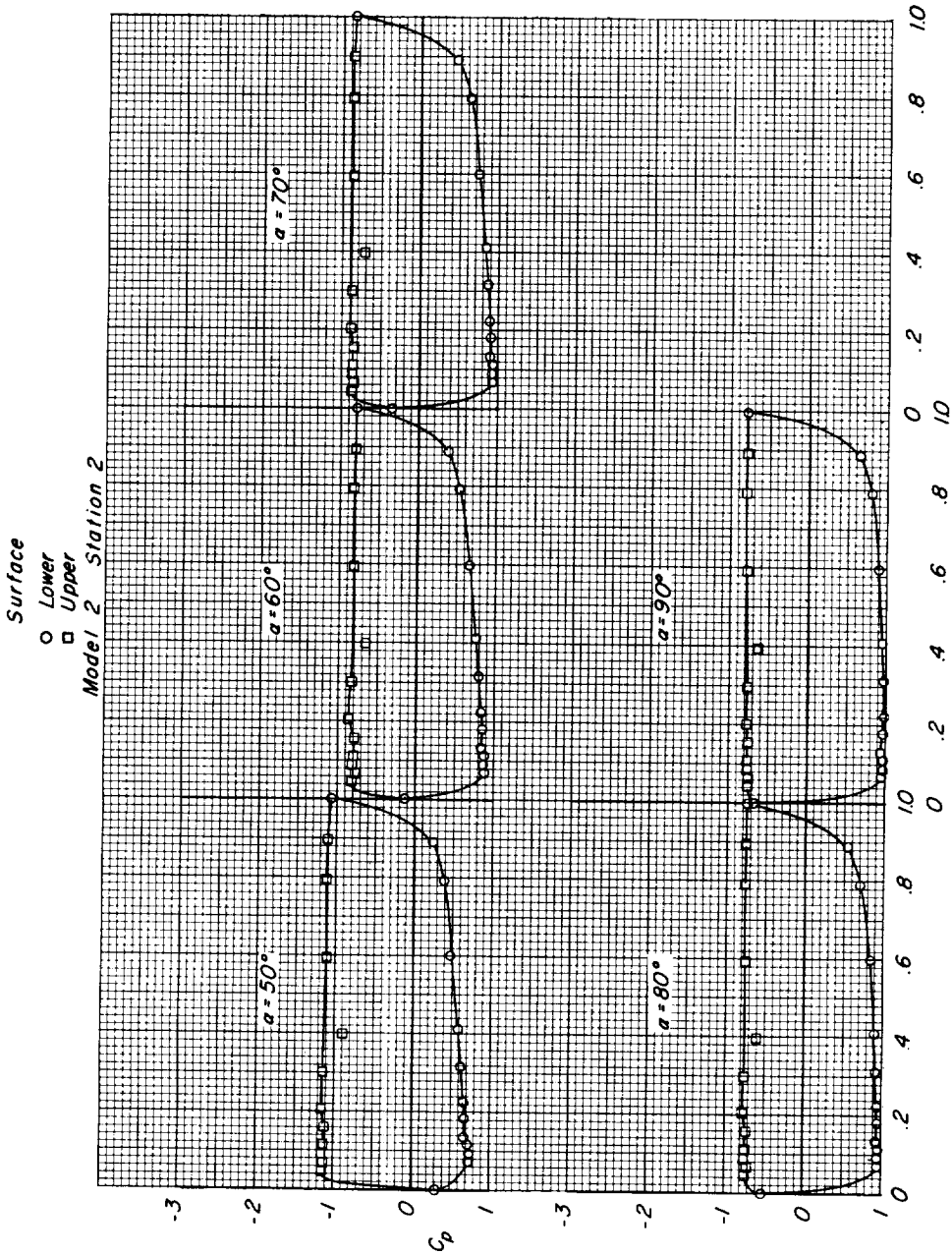

(e) M = 1.20. Continued.

Figure 7.- Continued.

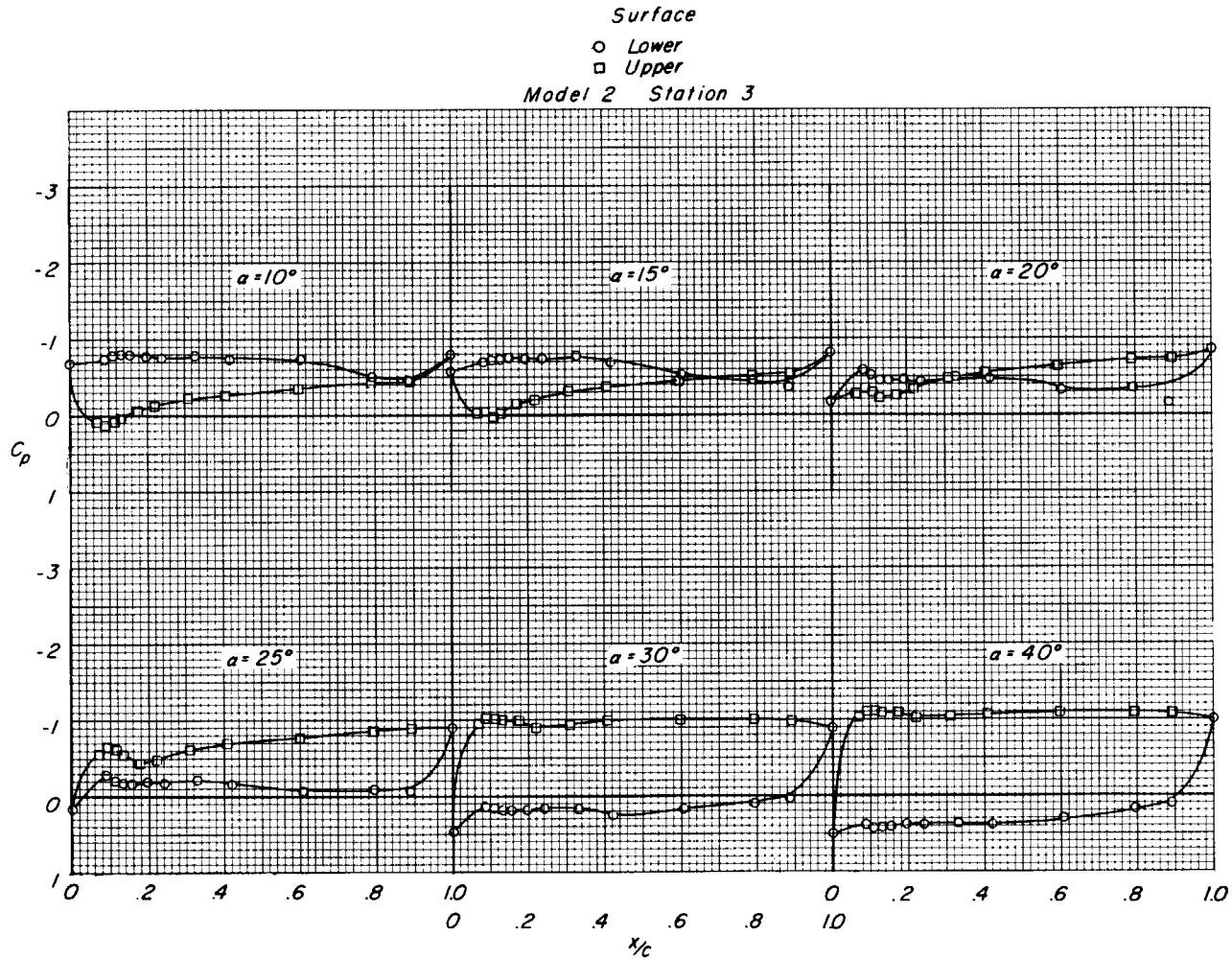

(e) M = 1.20. Continued.

Figure 7.- Continued.

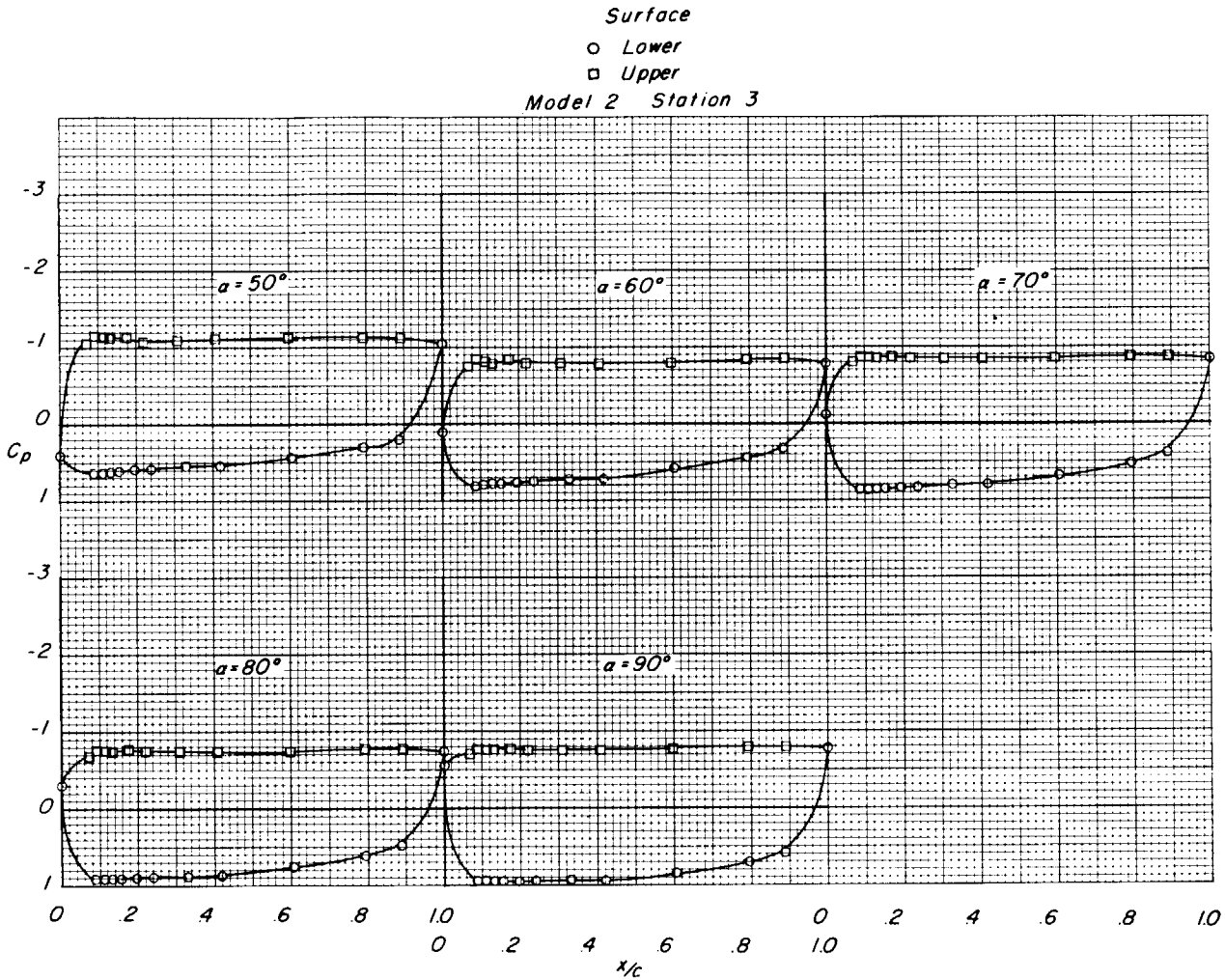

(e) M = 1.20. Continued.

Figure 7.- Continued.

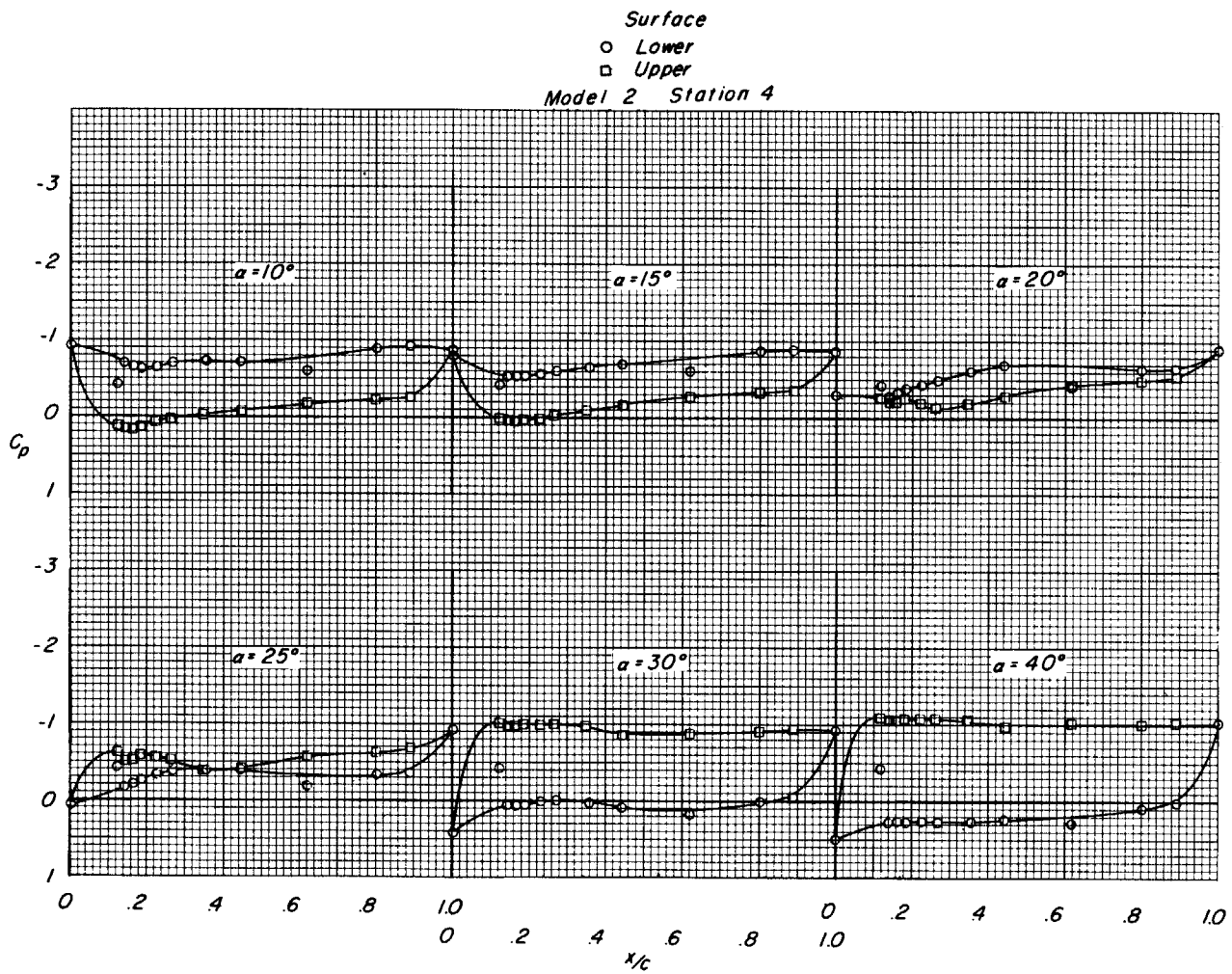

(e) M = 1.20. Continued.

Figure 7.- Continued.

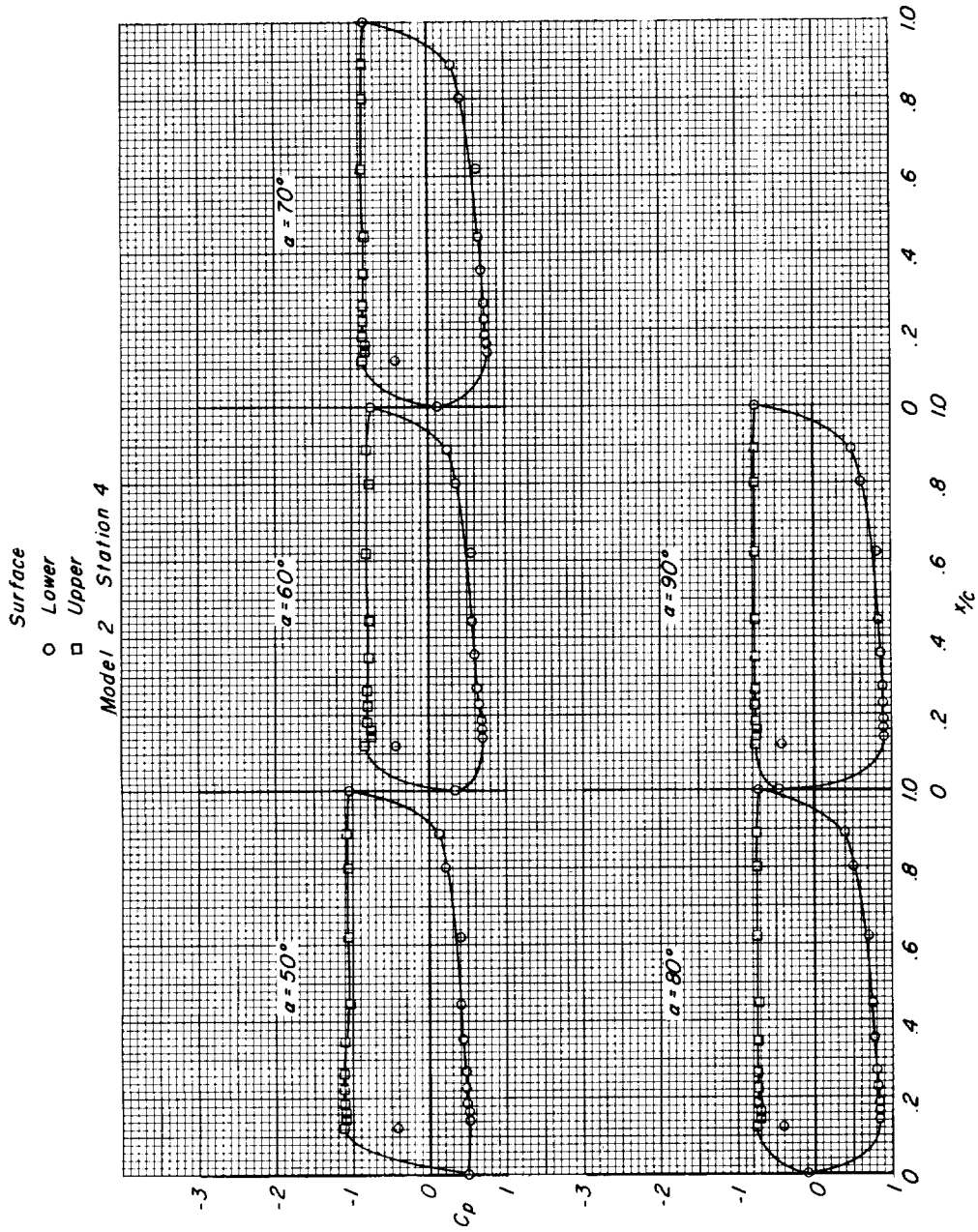

(e) M = 1.20. Concluded.

Figure 7.- Concluded.

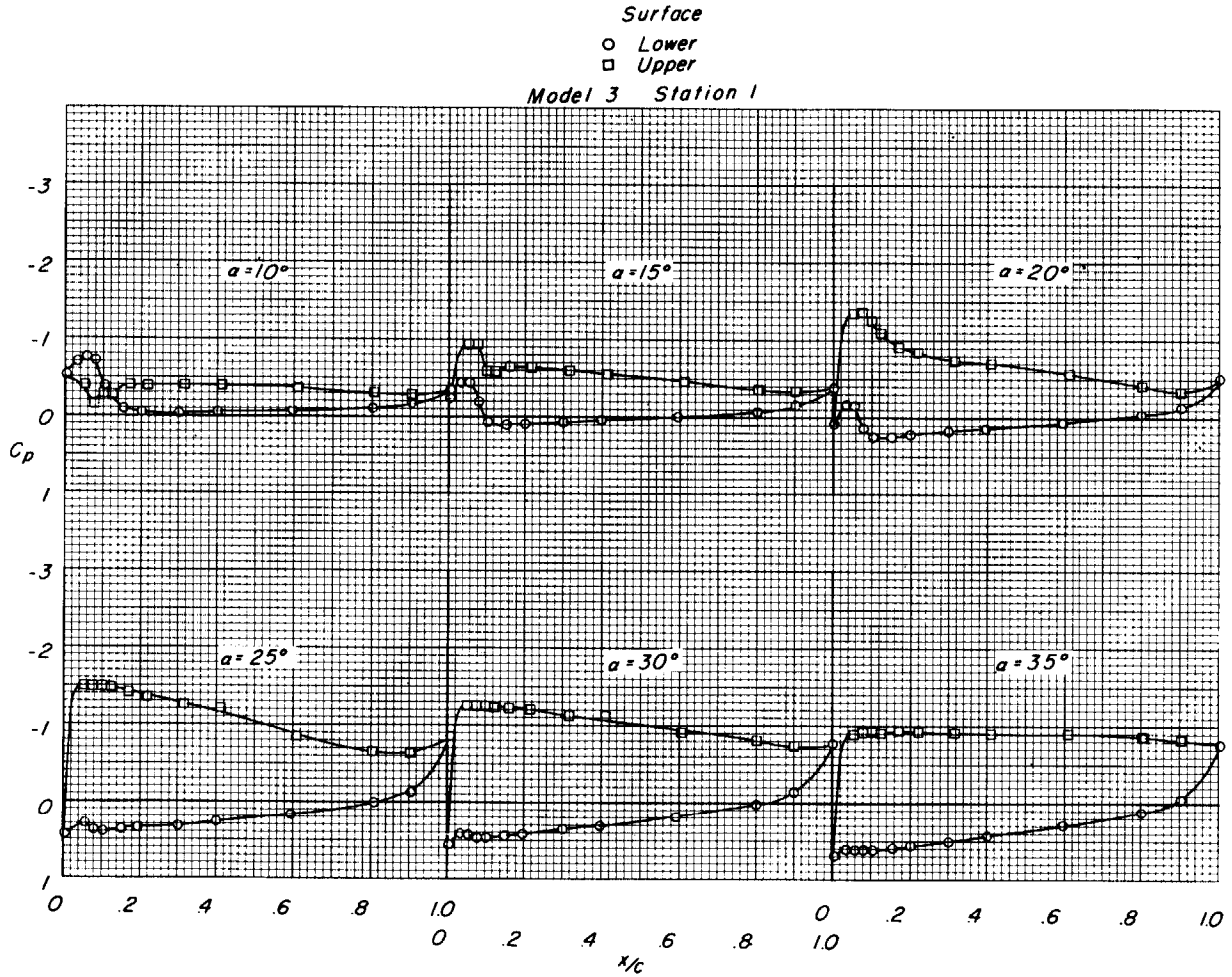

(a) M = 0.80.

Figure 8.- Pressure distributions on model 3 at various angles of attack and Mach numbers.

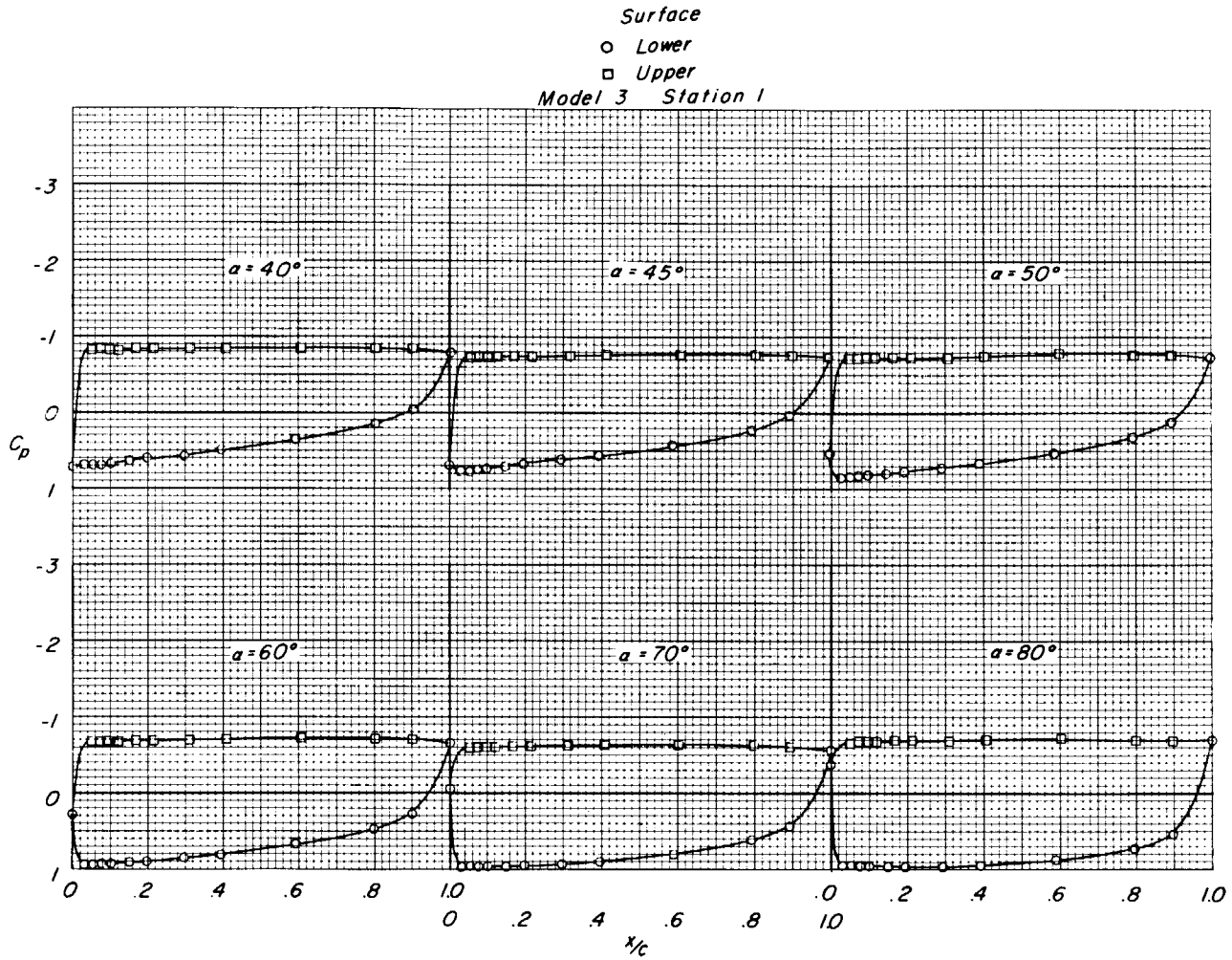

(a) M = 0.80. Continued.

Figure 8.- Continued.

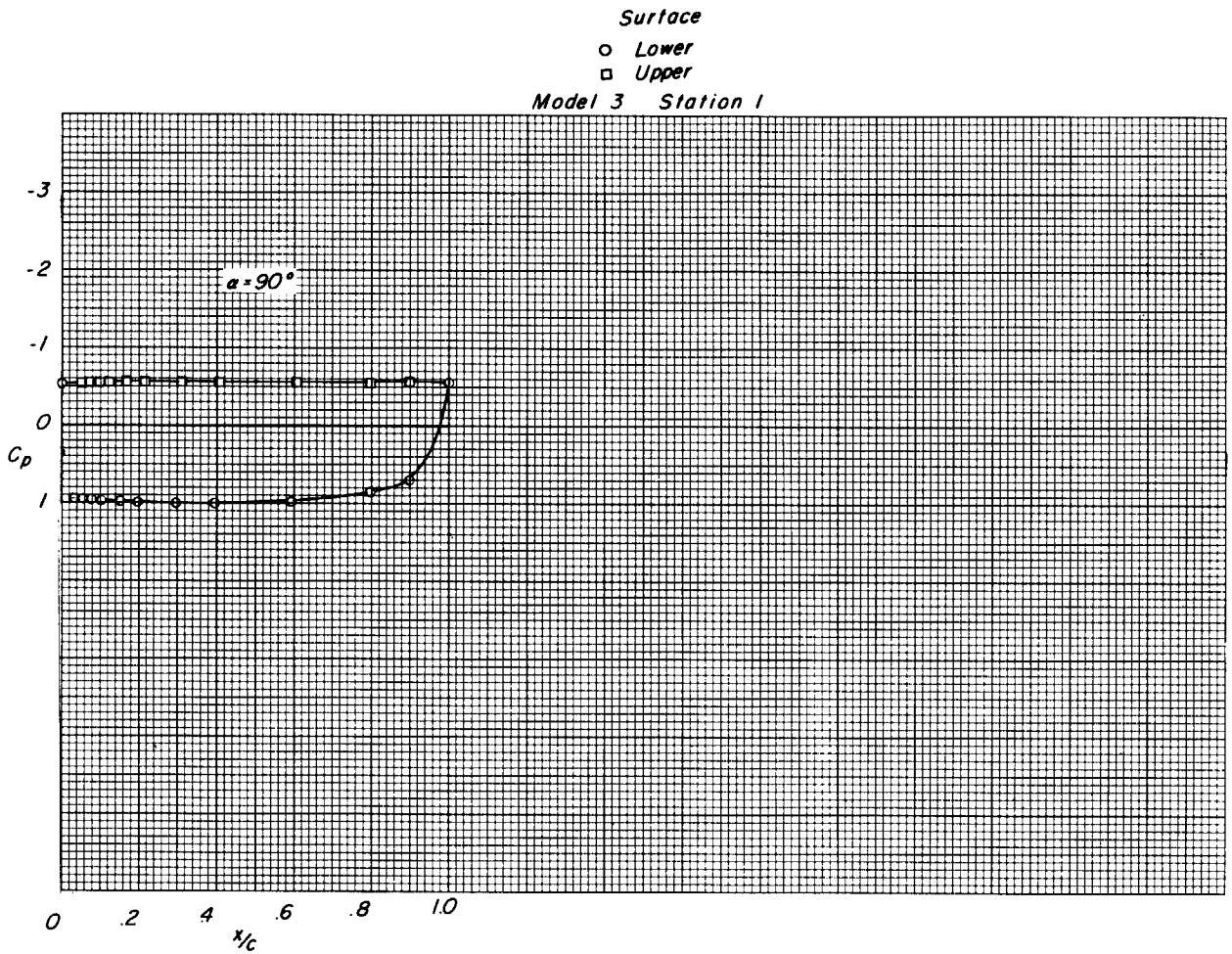

(a) M = 0.80. Continued.

Figure 8.- Continued.

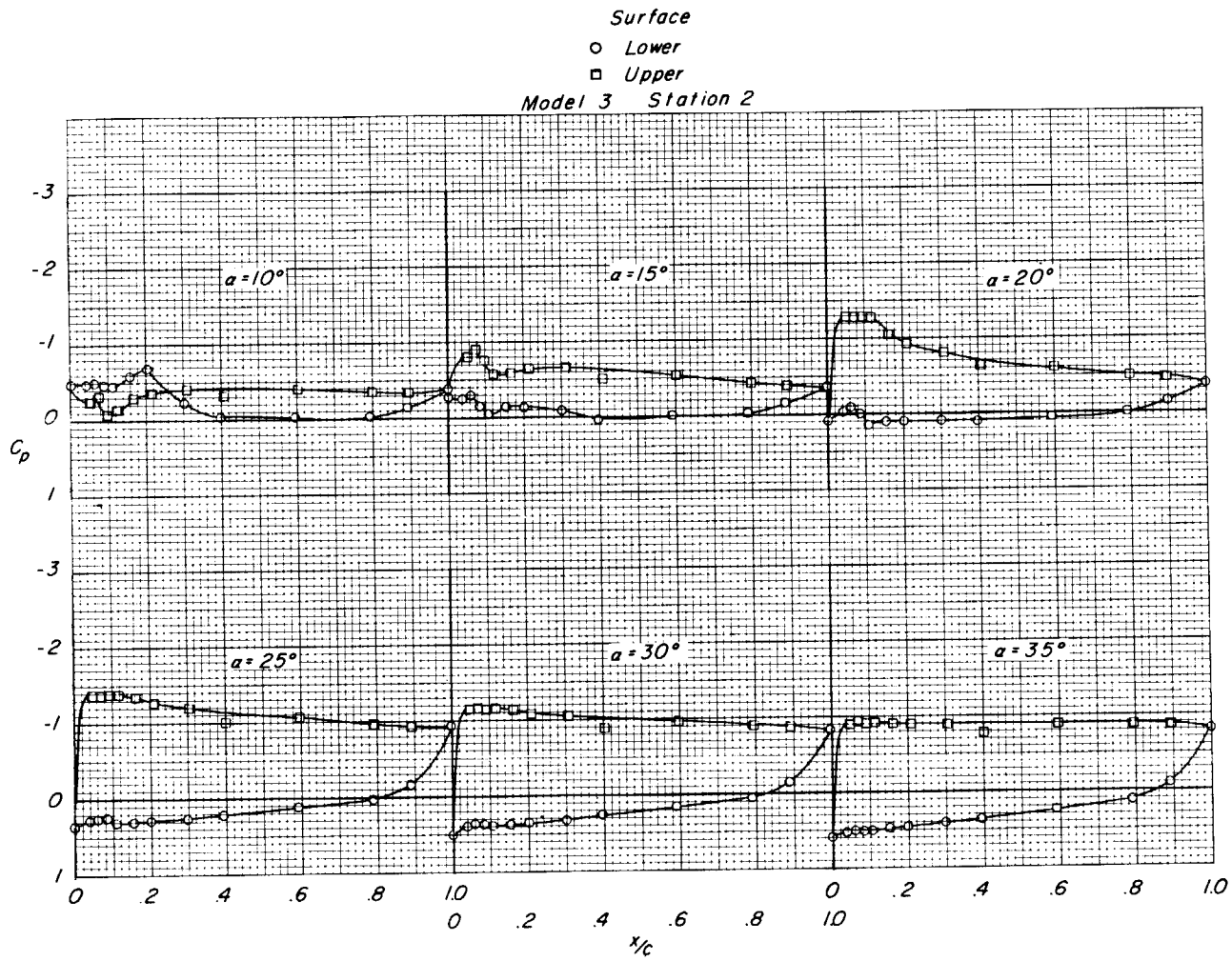

(a) M = 0.80. Continued.

Figure 8.- Continued.

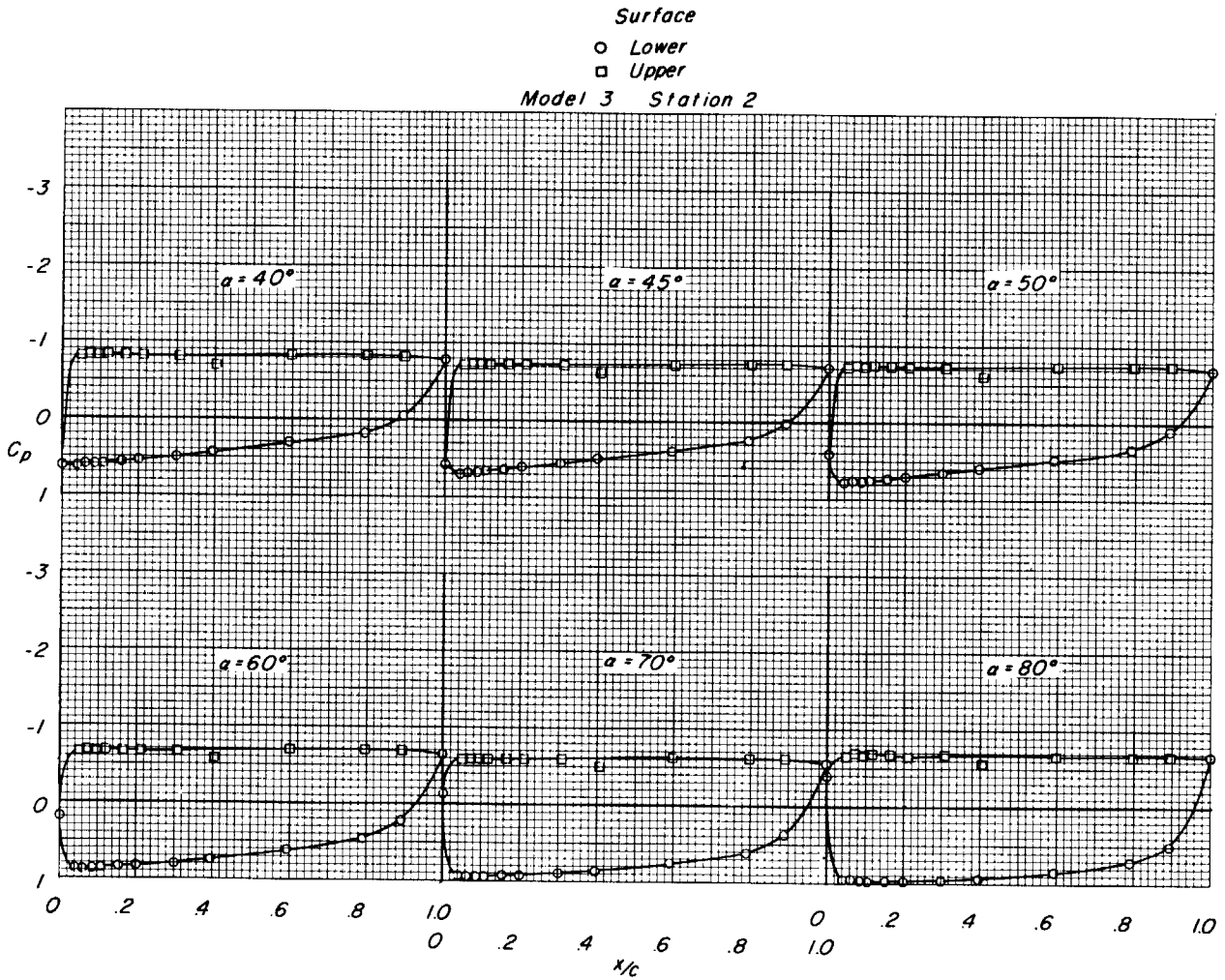

(a) M = 0.80. Continued.

Figure 8.- Continued.

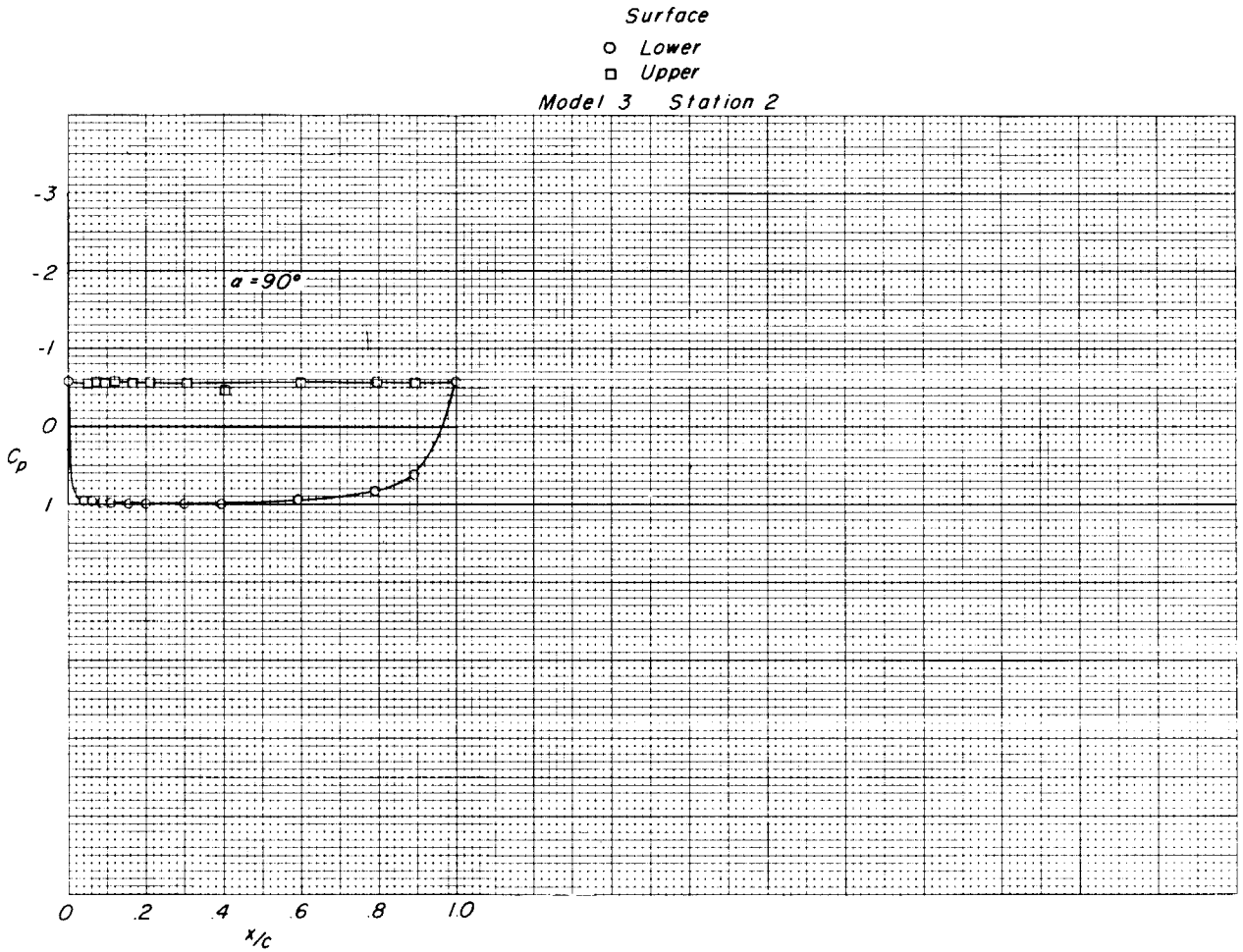

(a) M = 0.80. Continued.

Figure 8.- Continued.

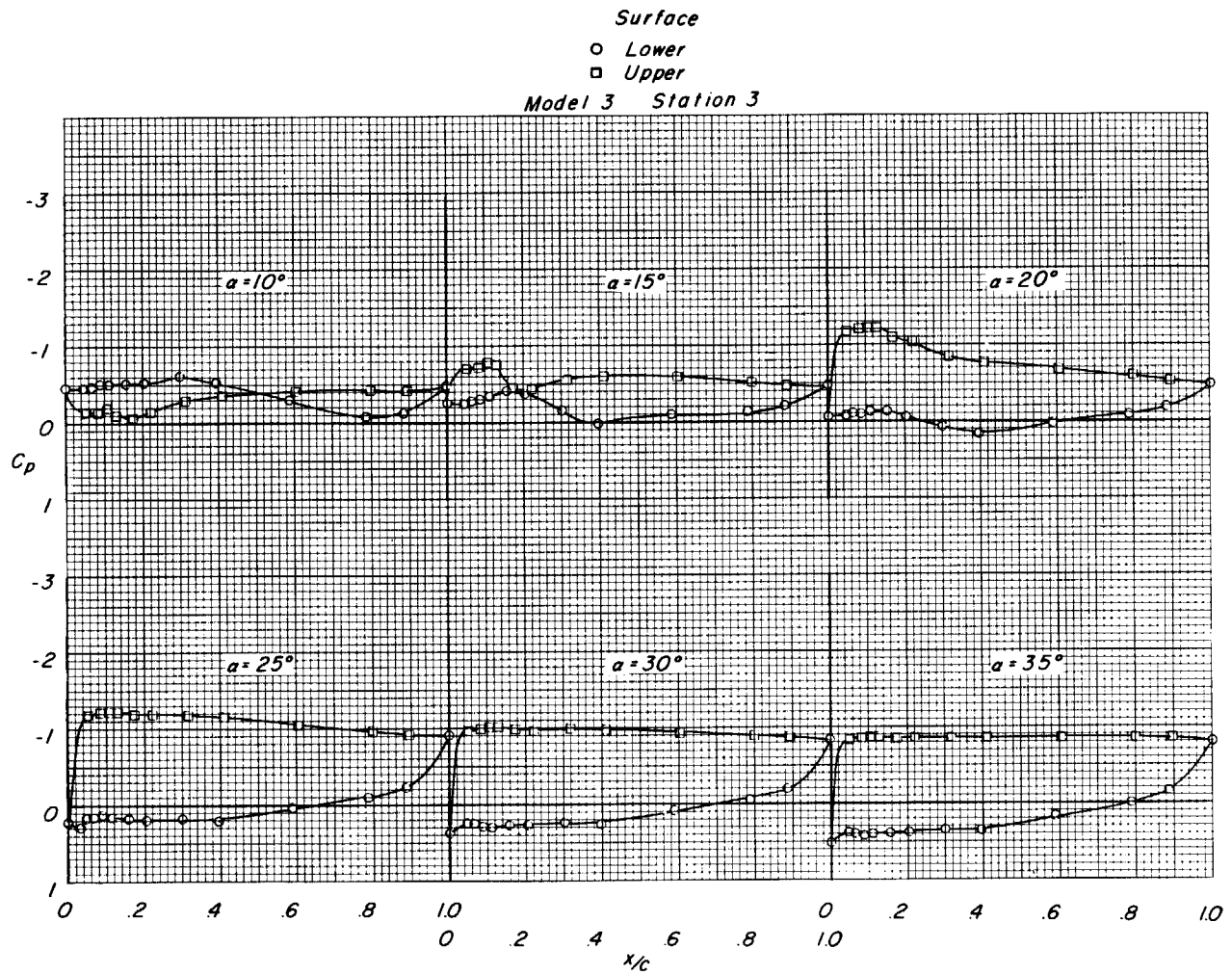

(a) M = 0.80. Continued.

Figure 8.- Continued.

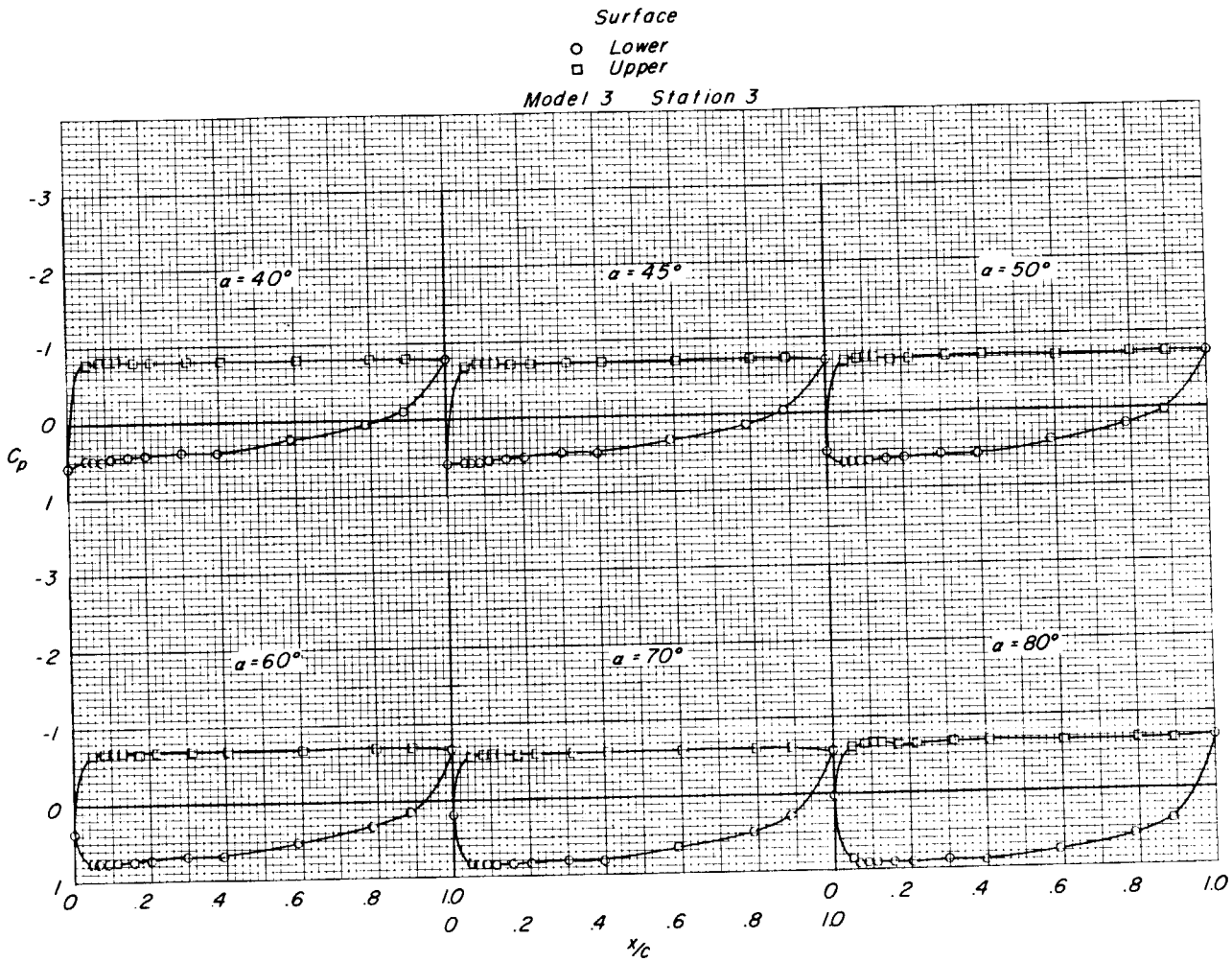

(a) M = 0.80. Continued.

Figure 8.- Continued.

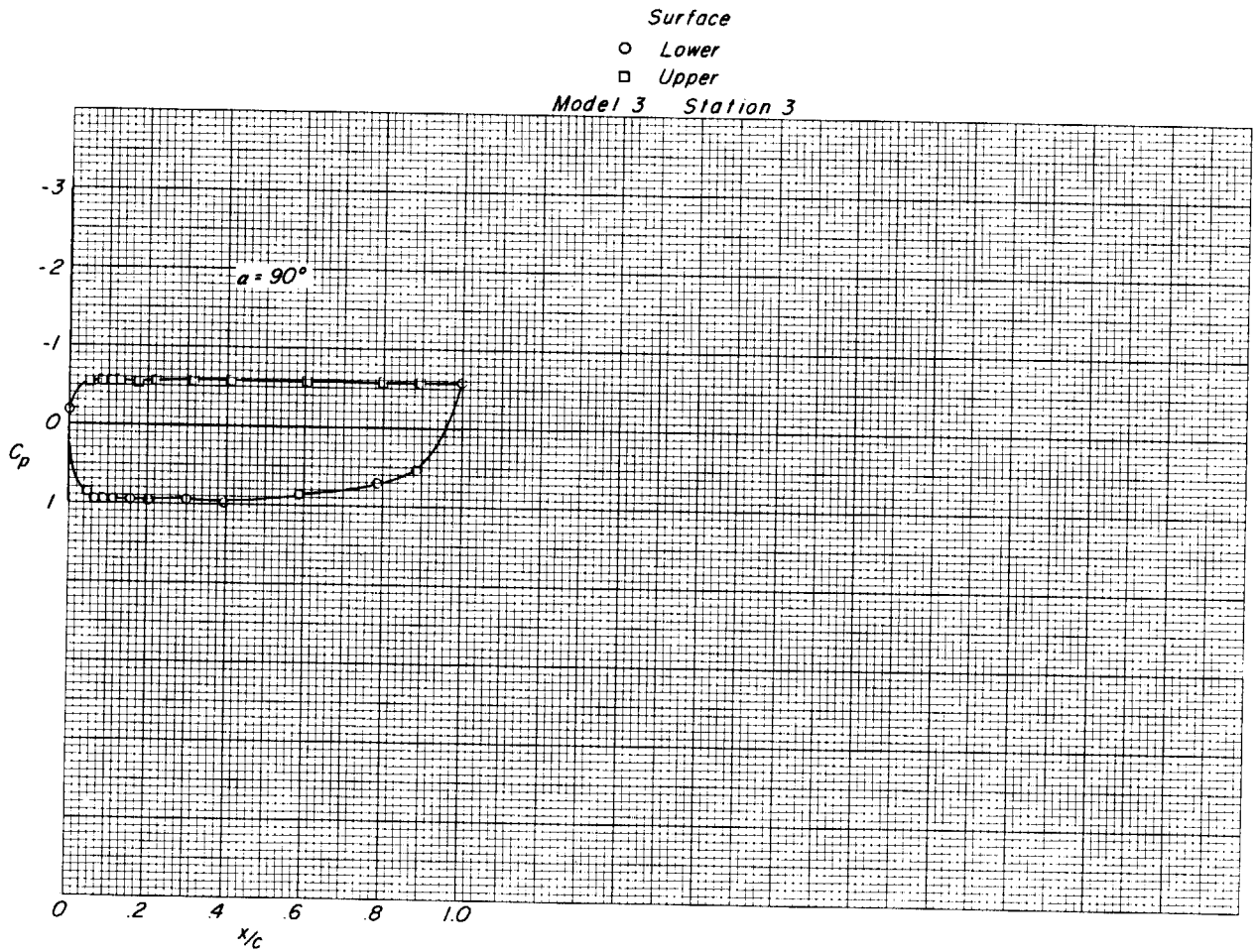

(a) M = 0.80. Continued.

Figure 8.- Continued.

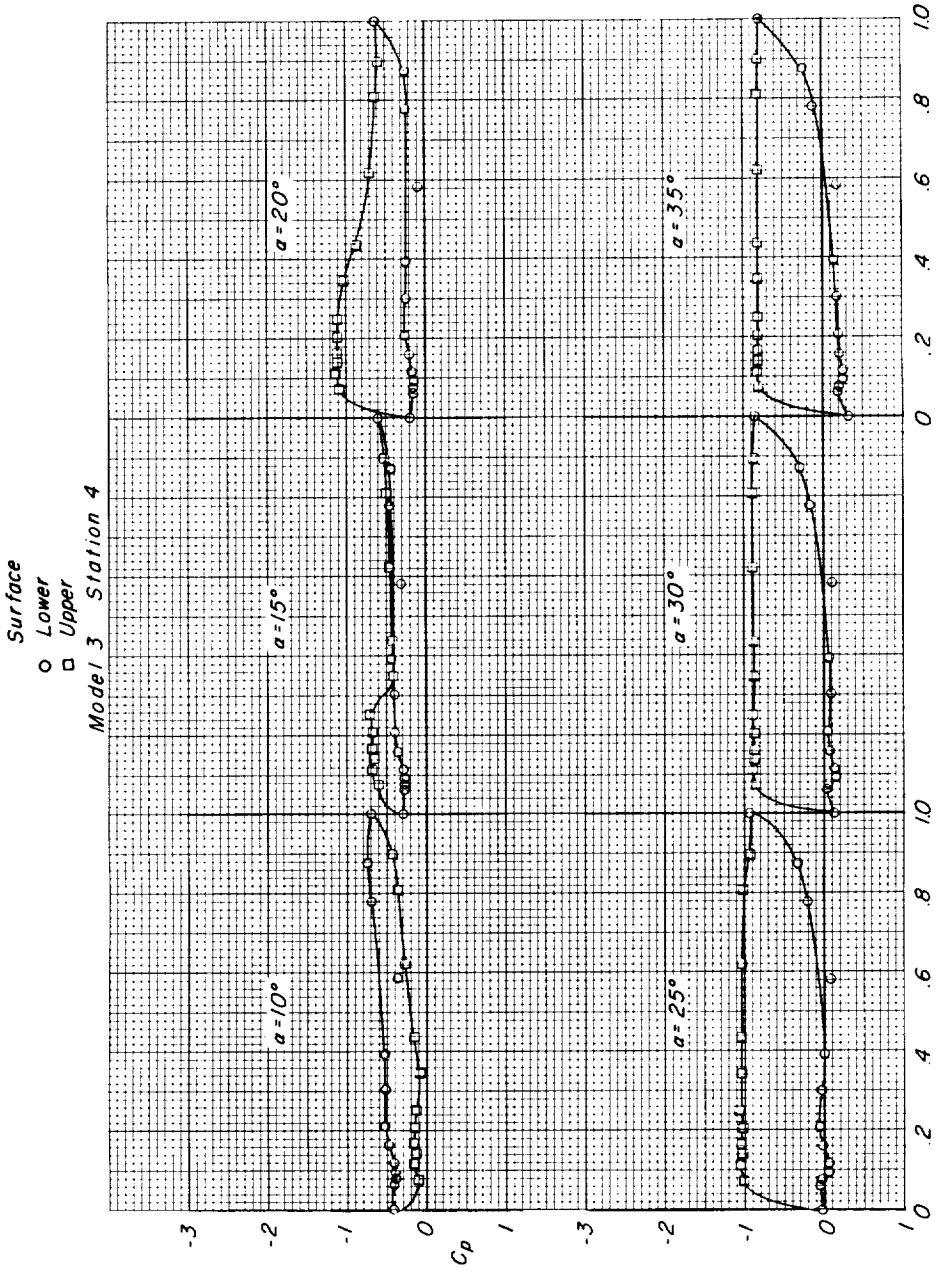

(a) M = 0.80. Continued.

Figure 8.- Continued.

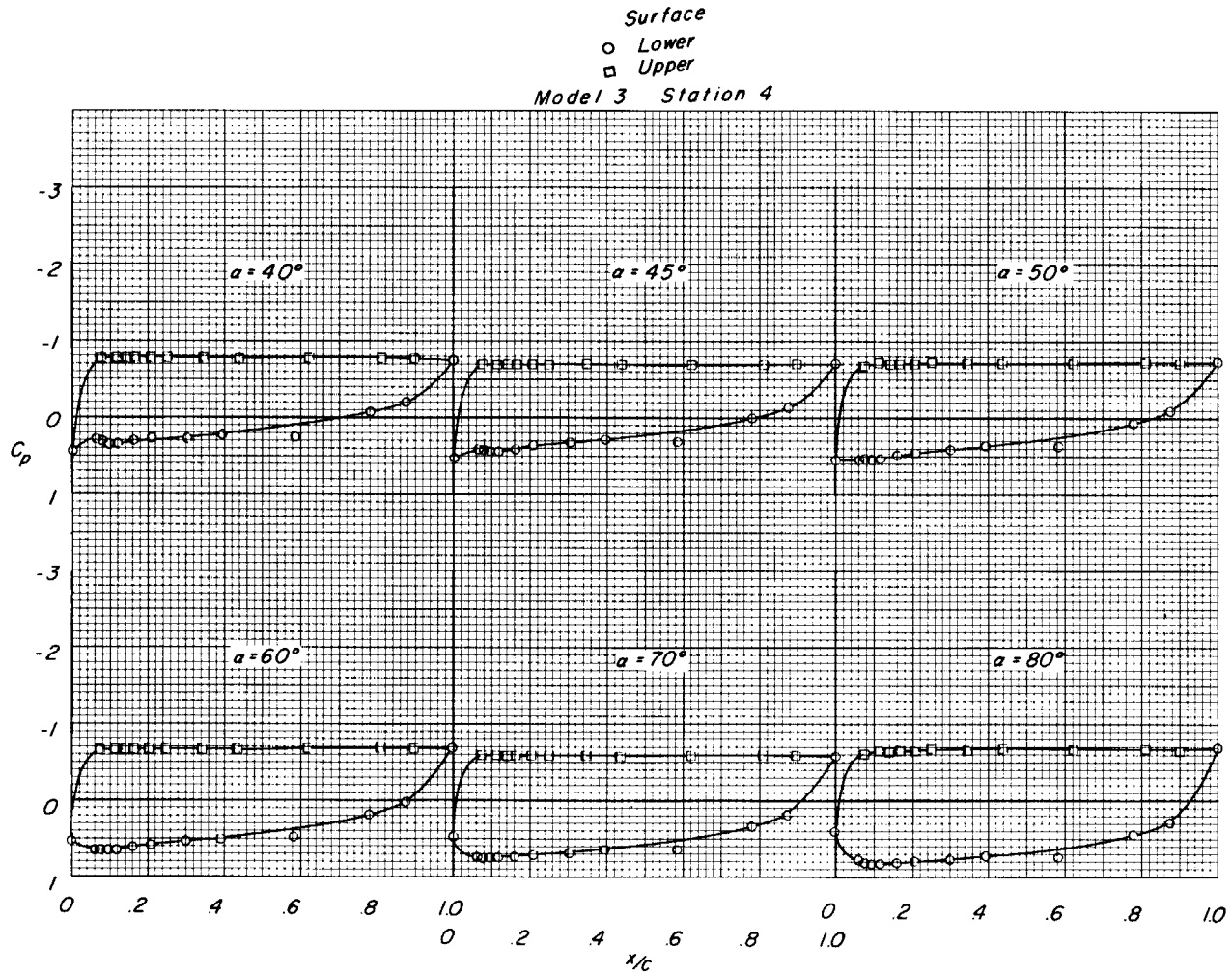

(a) M = 0.80. Continued.

Figure 8.- Continued.

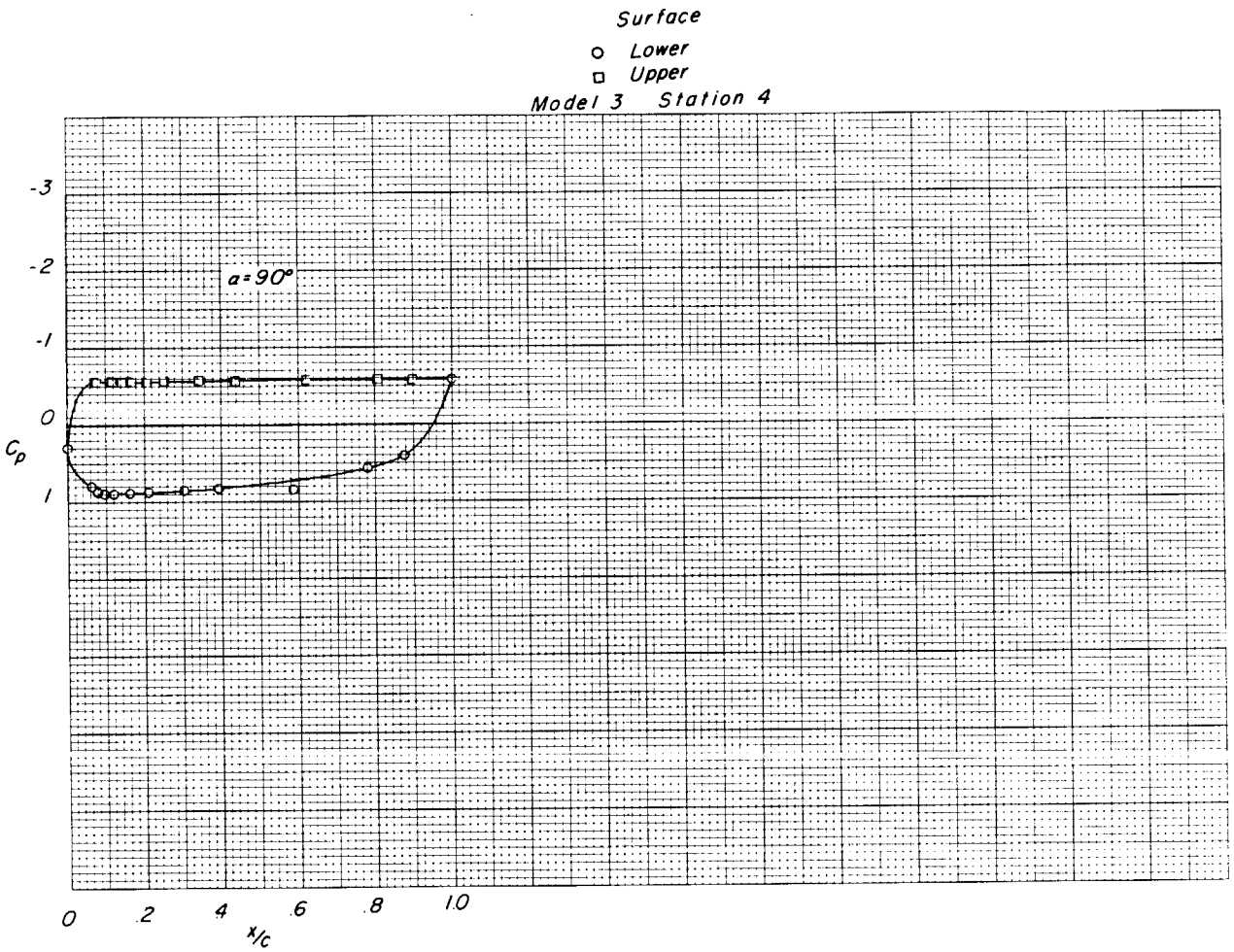

(a) M = 0.80. Concluded.

Figure 8.- Continued.

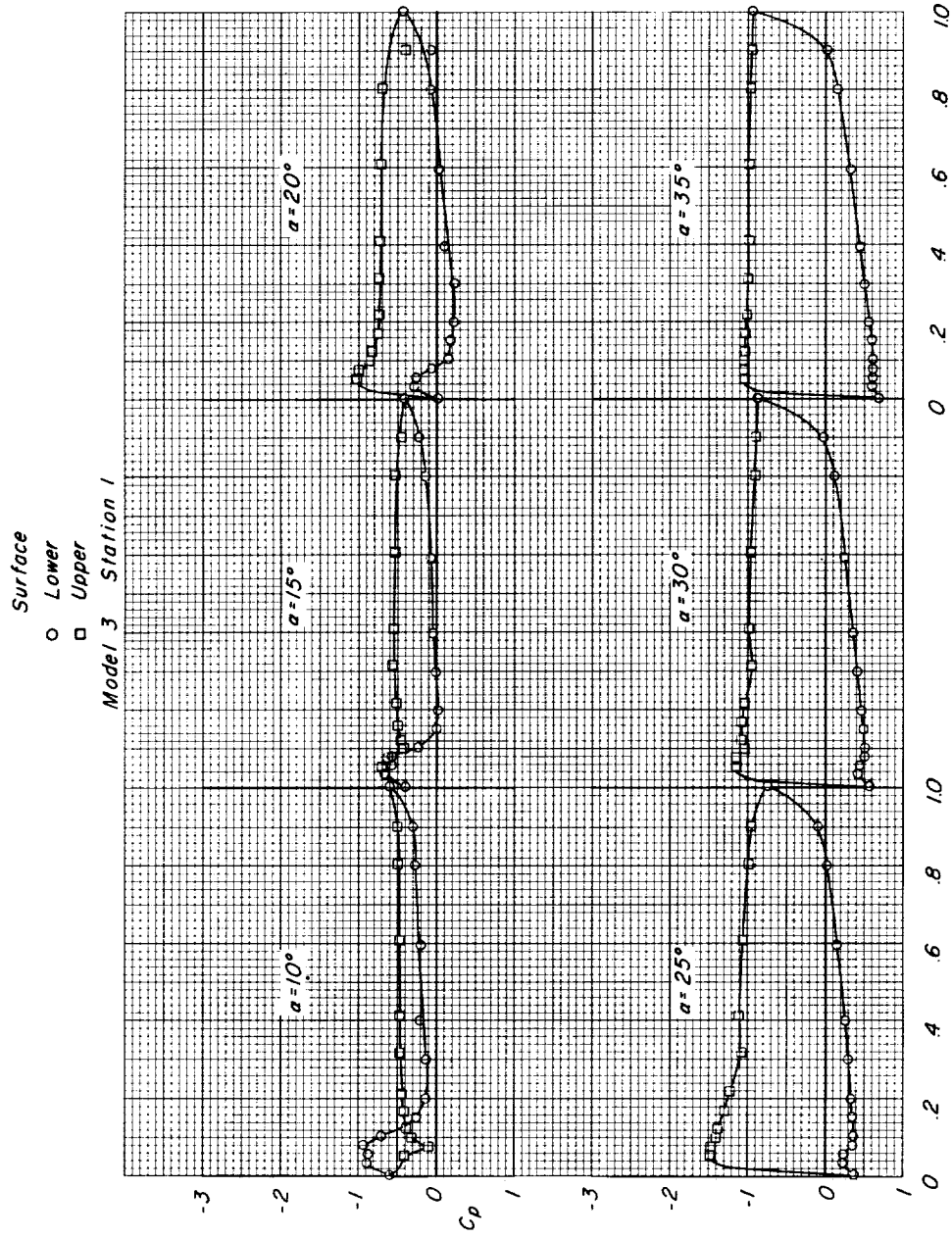

(b) M = 0.94.

Figure 8.- Continued.

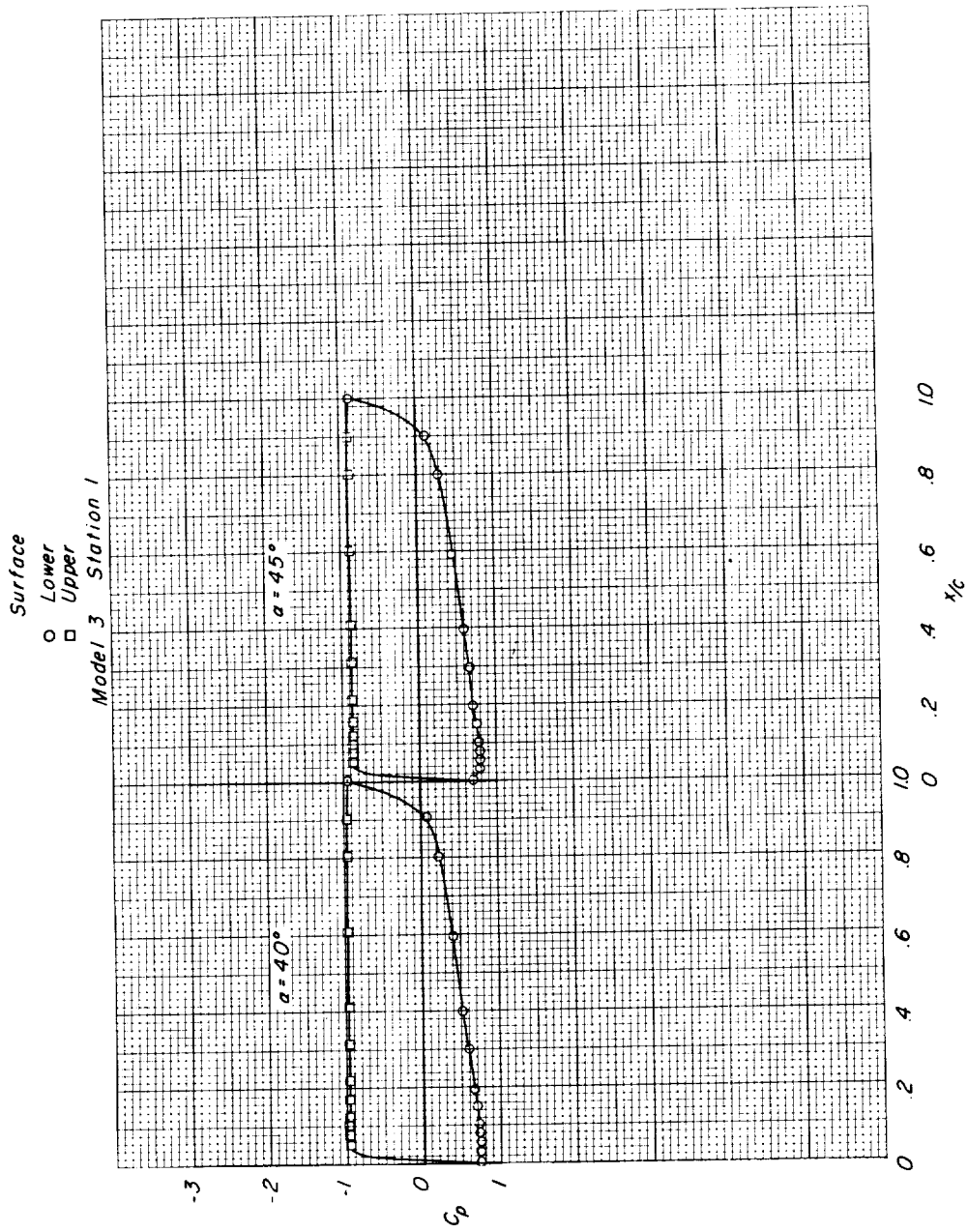

(b) M = 0.94. Continued.

Figure 8.- Continued.

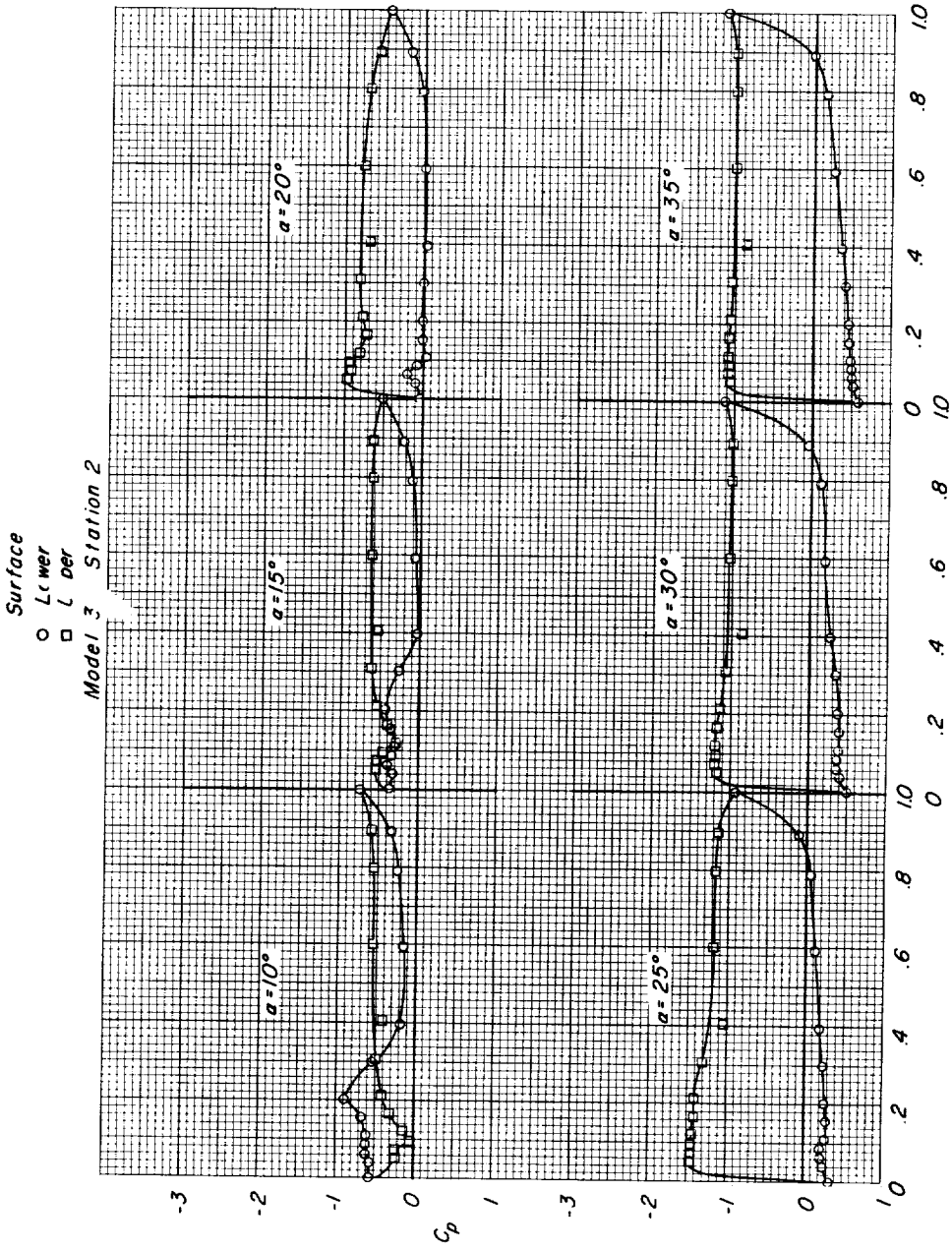

(b) M = 0.94. Continued.

Figure 8.- Continued.

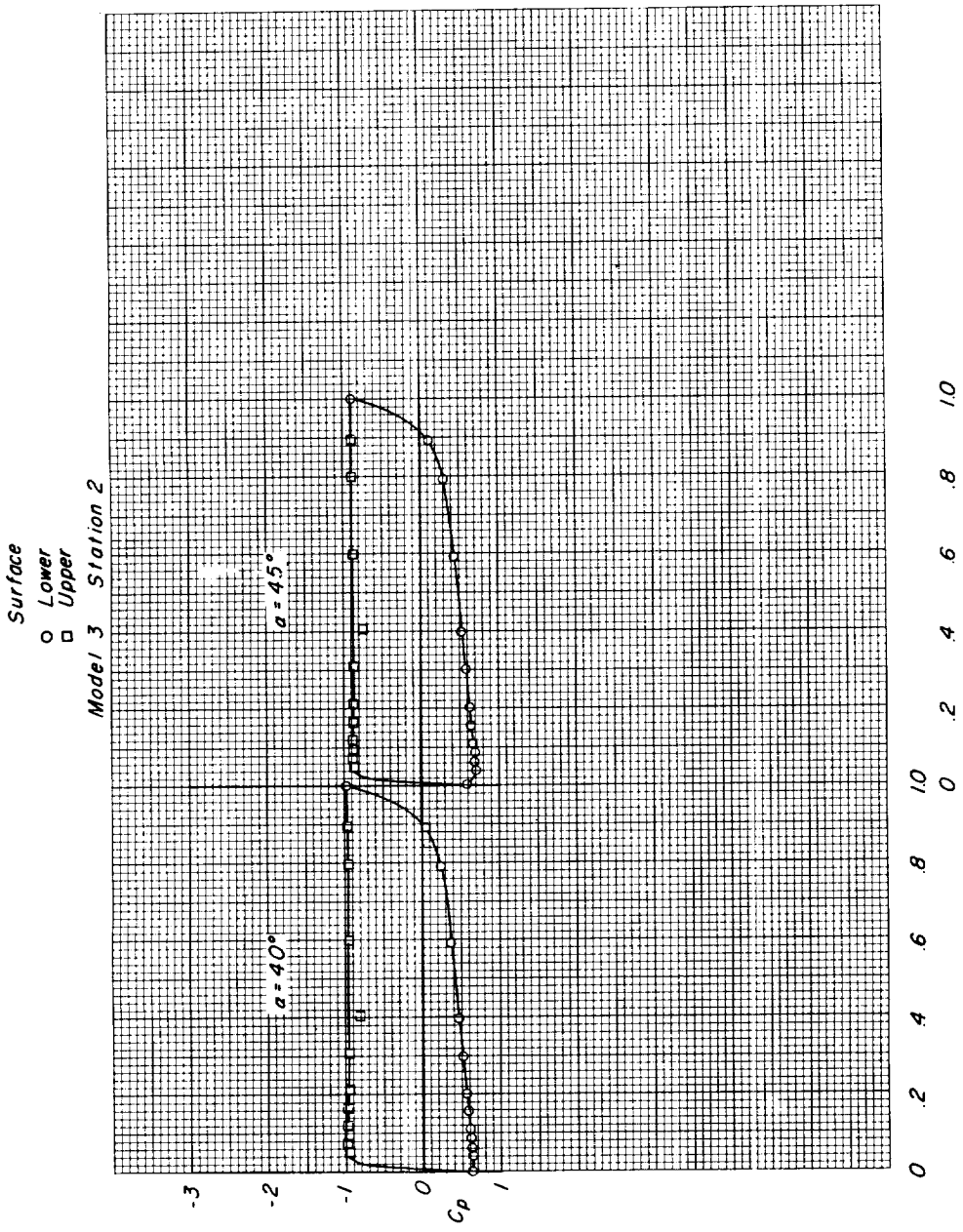

(b) M = 0.94. Continued.

Figure 8.- Continued.

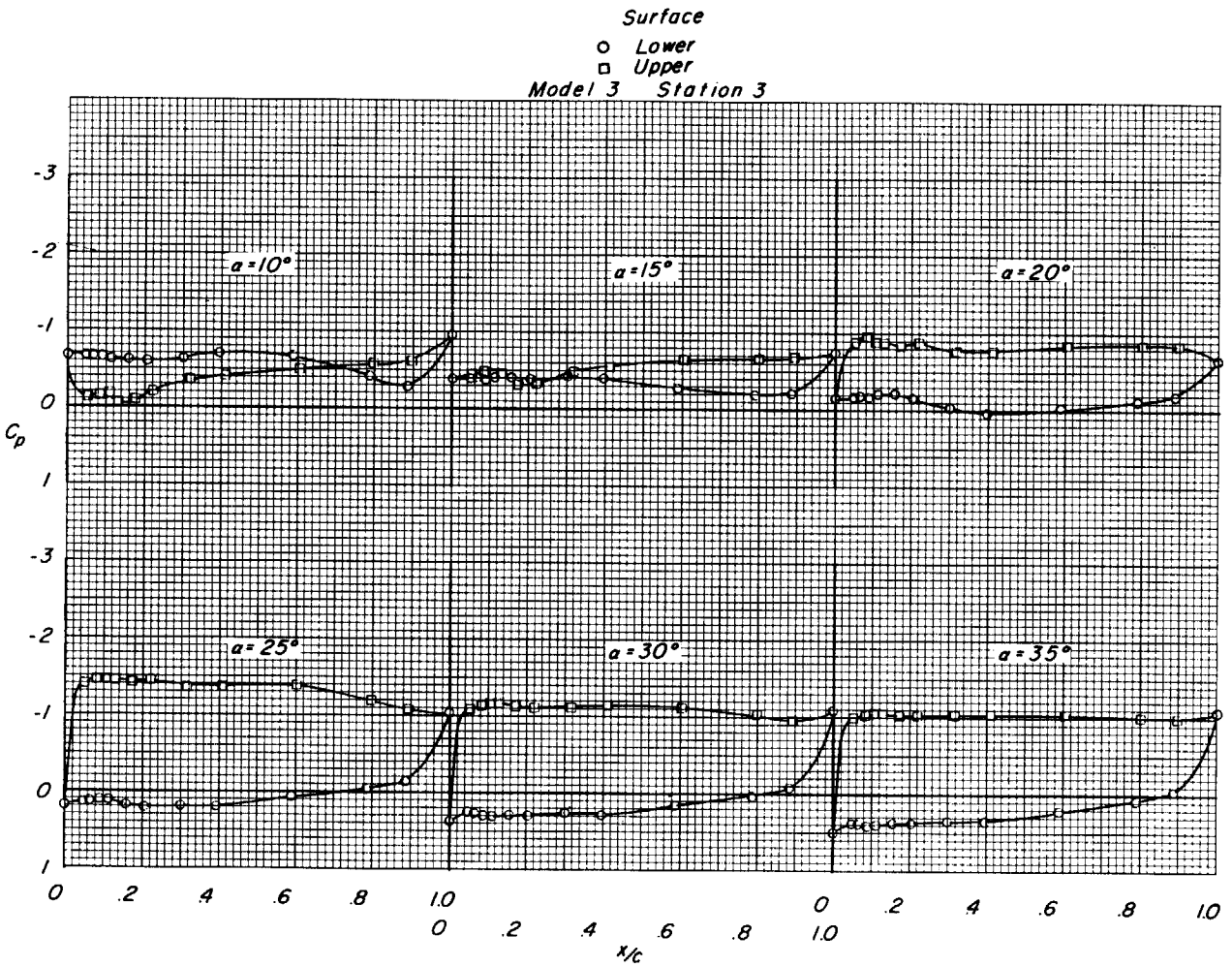

(b) M = 0.94. Continued.

Figure 8.- Continued.

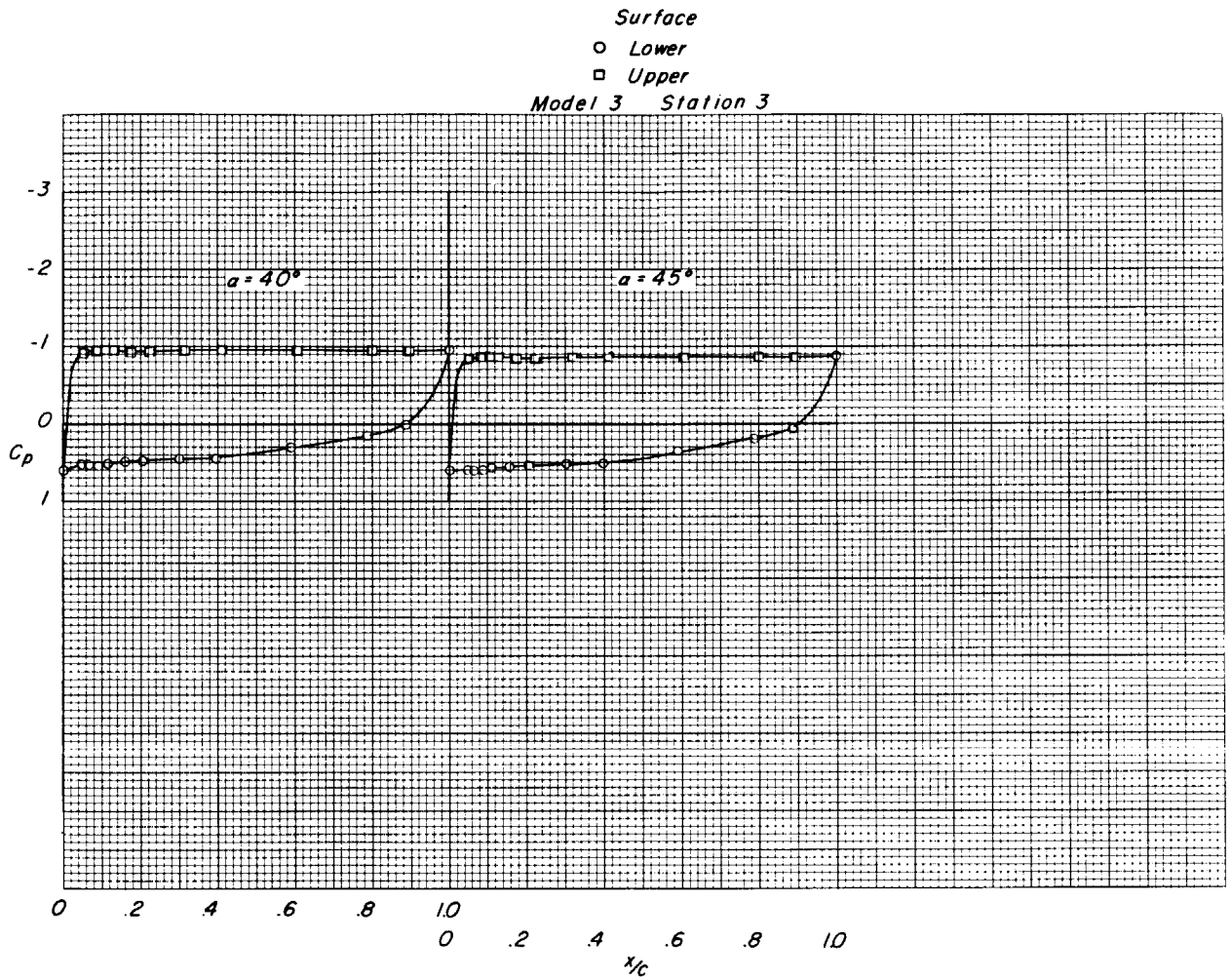

(b) M = 0.94. Continued.

Figure 8.- Continued.

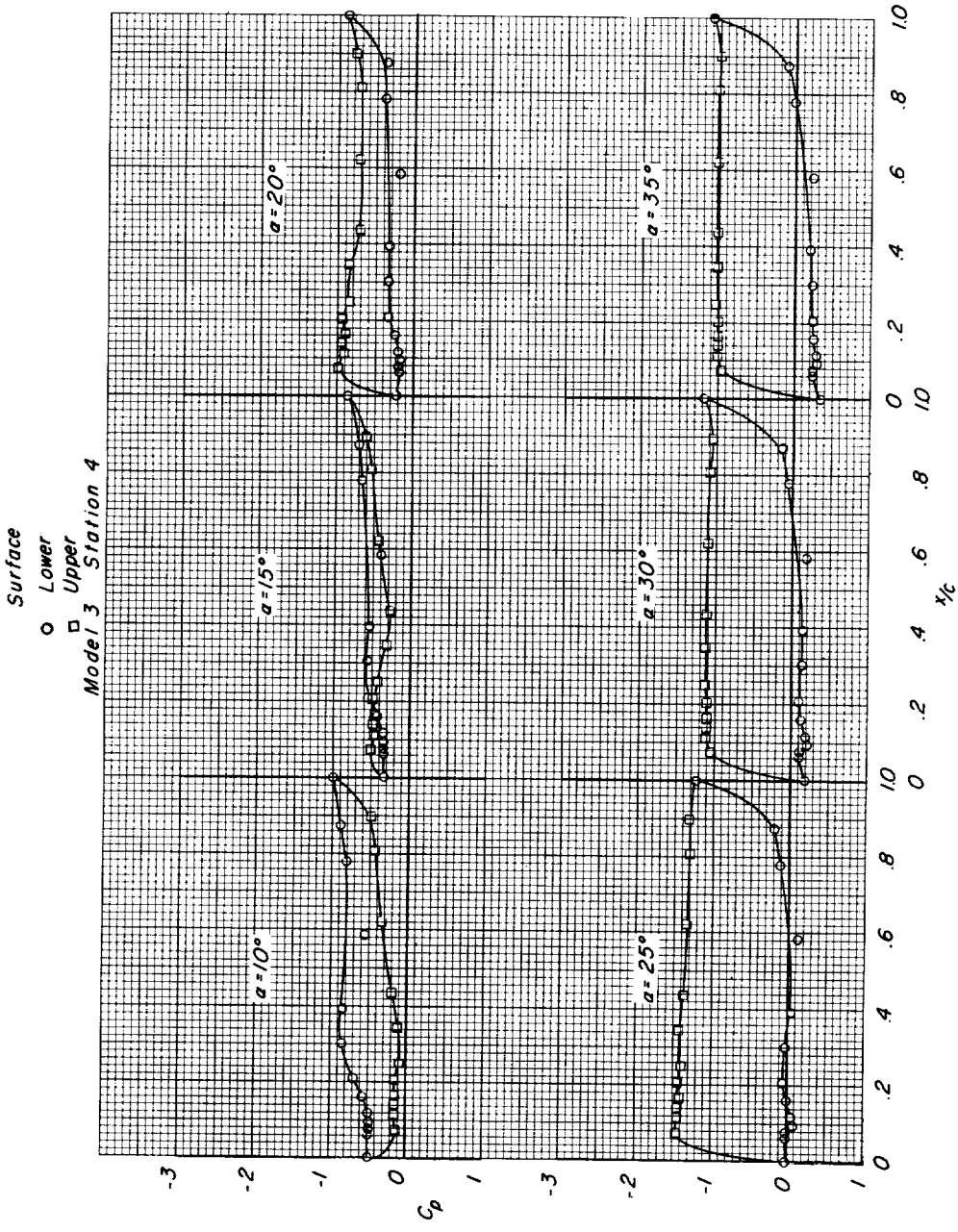

(b) M = 0.94. Continued.

Figure 8.- Continued.

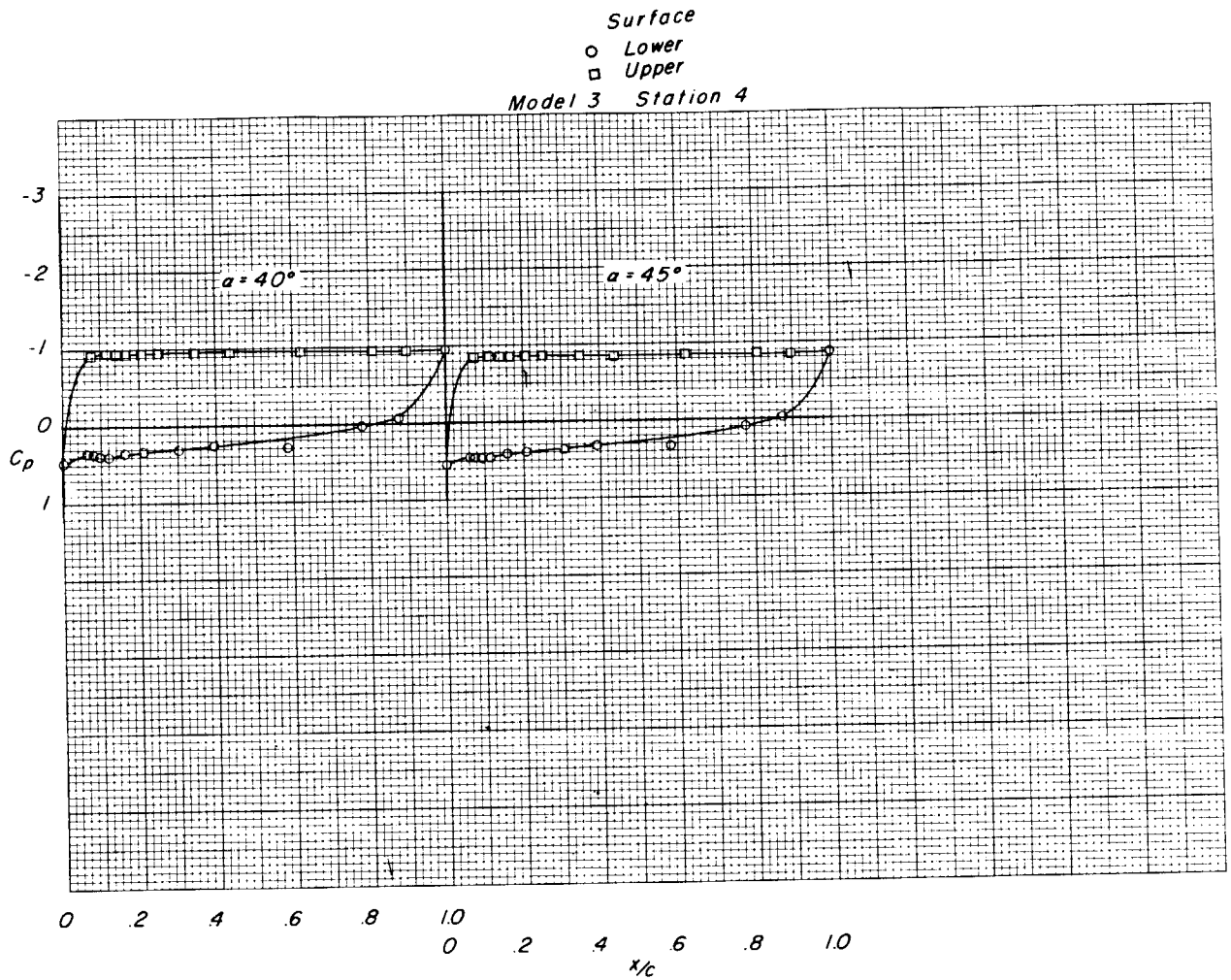

(b) M = 0.94. Concluded.

Figure 8.- Continued.

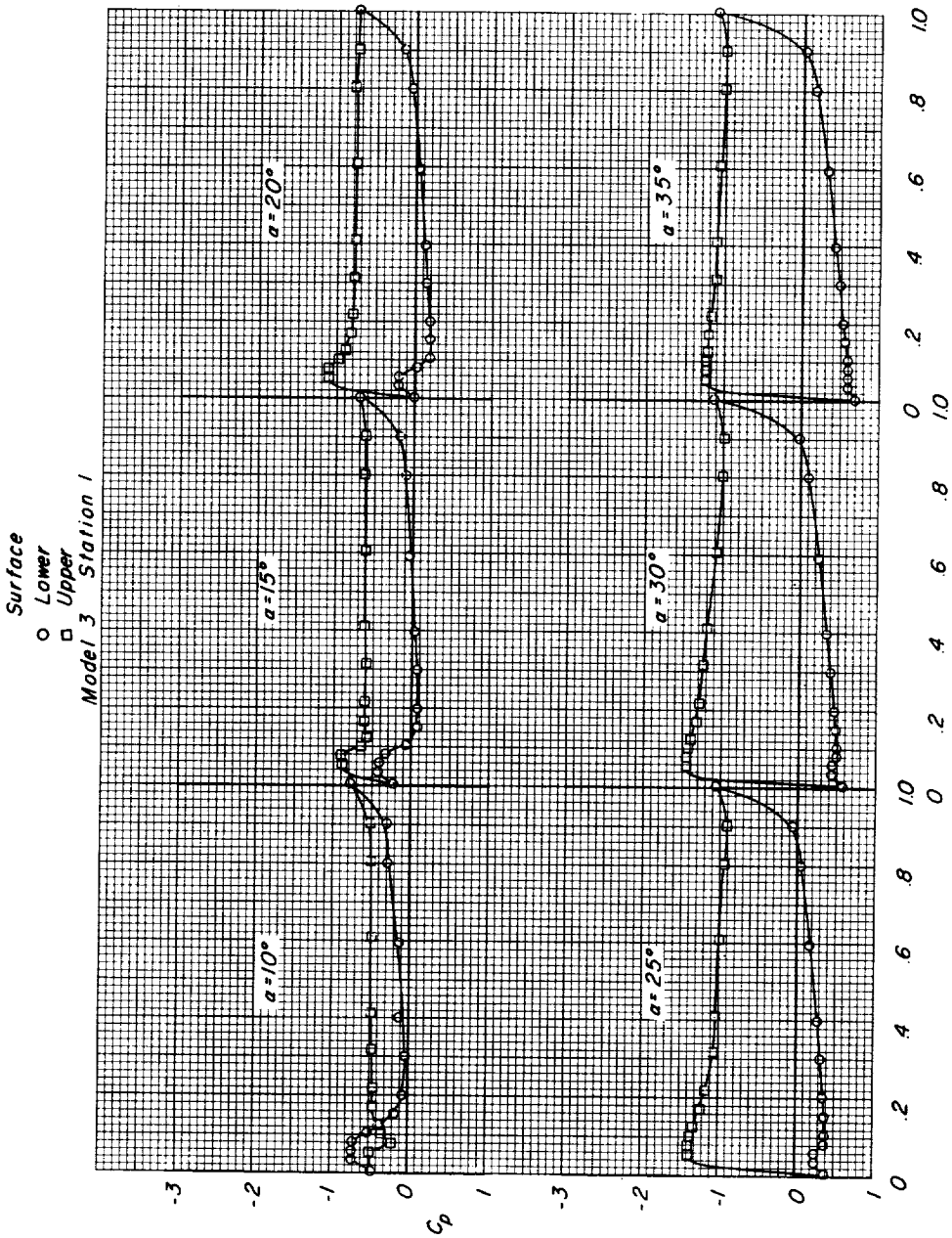

(c) M = 0.98.

Figure 8.- Continued.

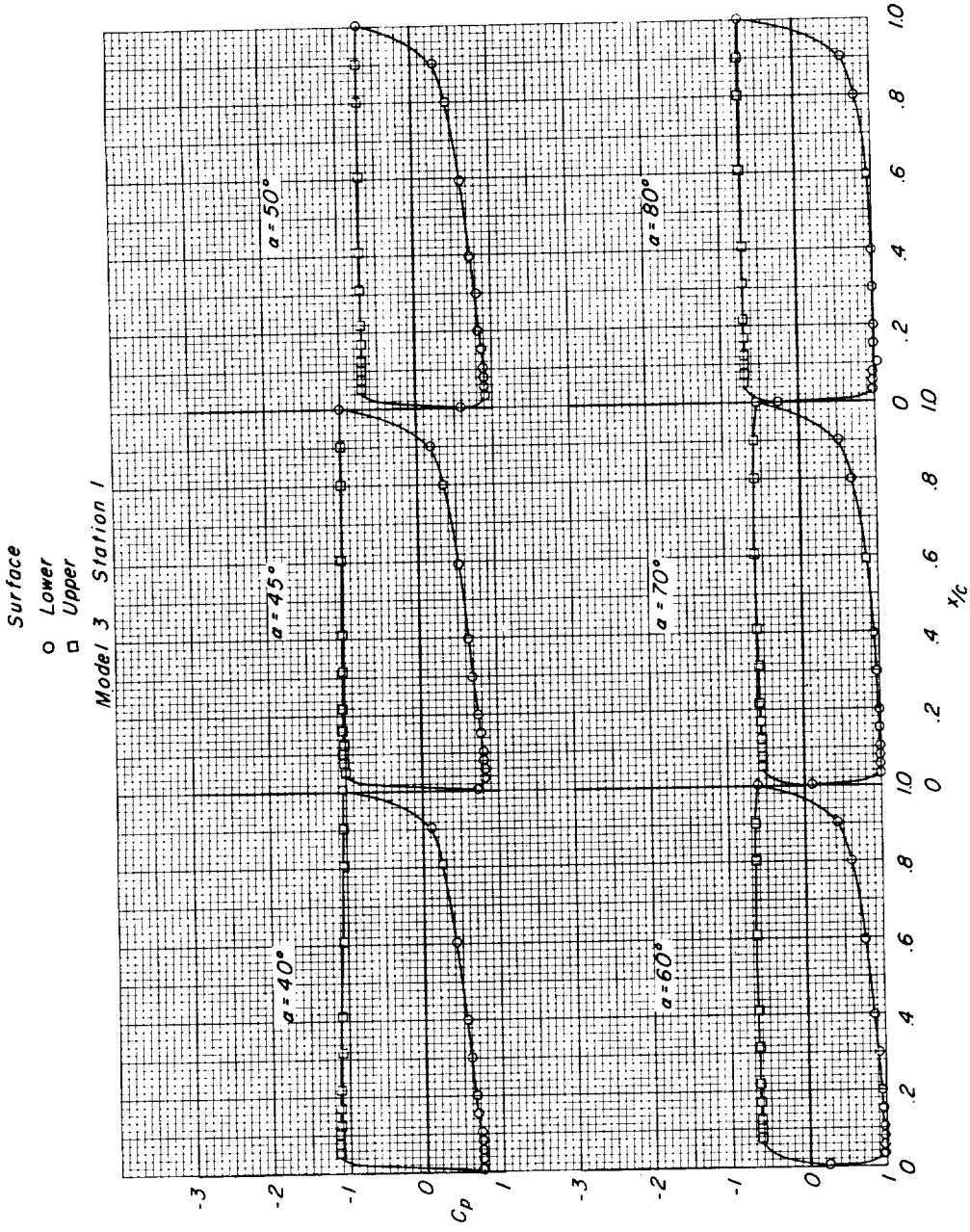

(c) M = 0.98. Continued.

Figure 8.- Continued.

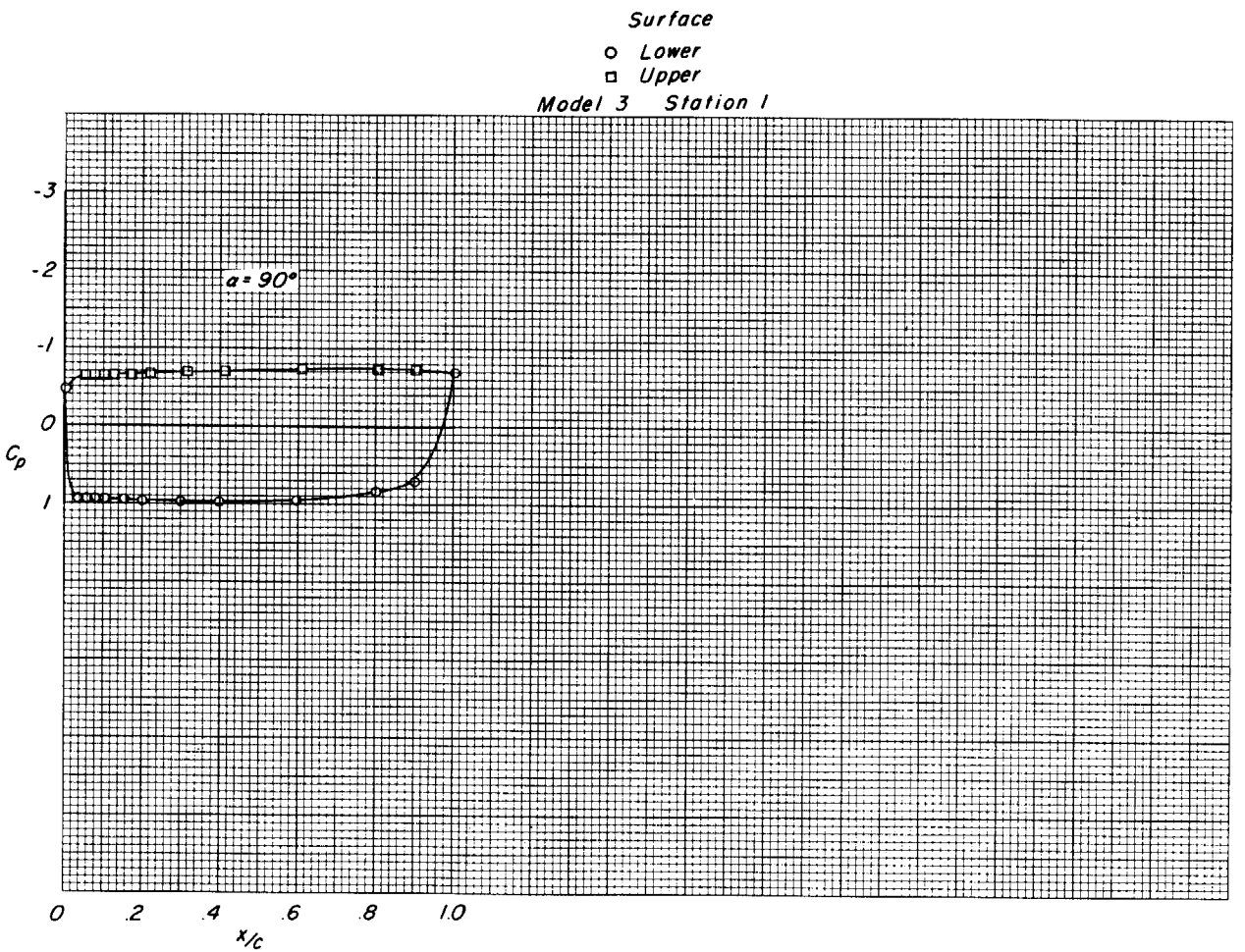

(c) M = 0.98. Continued.

Figure 8.- Continued.

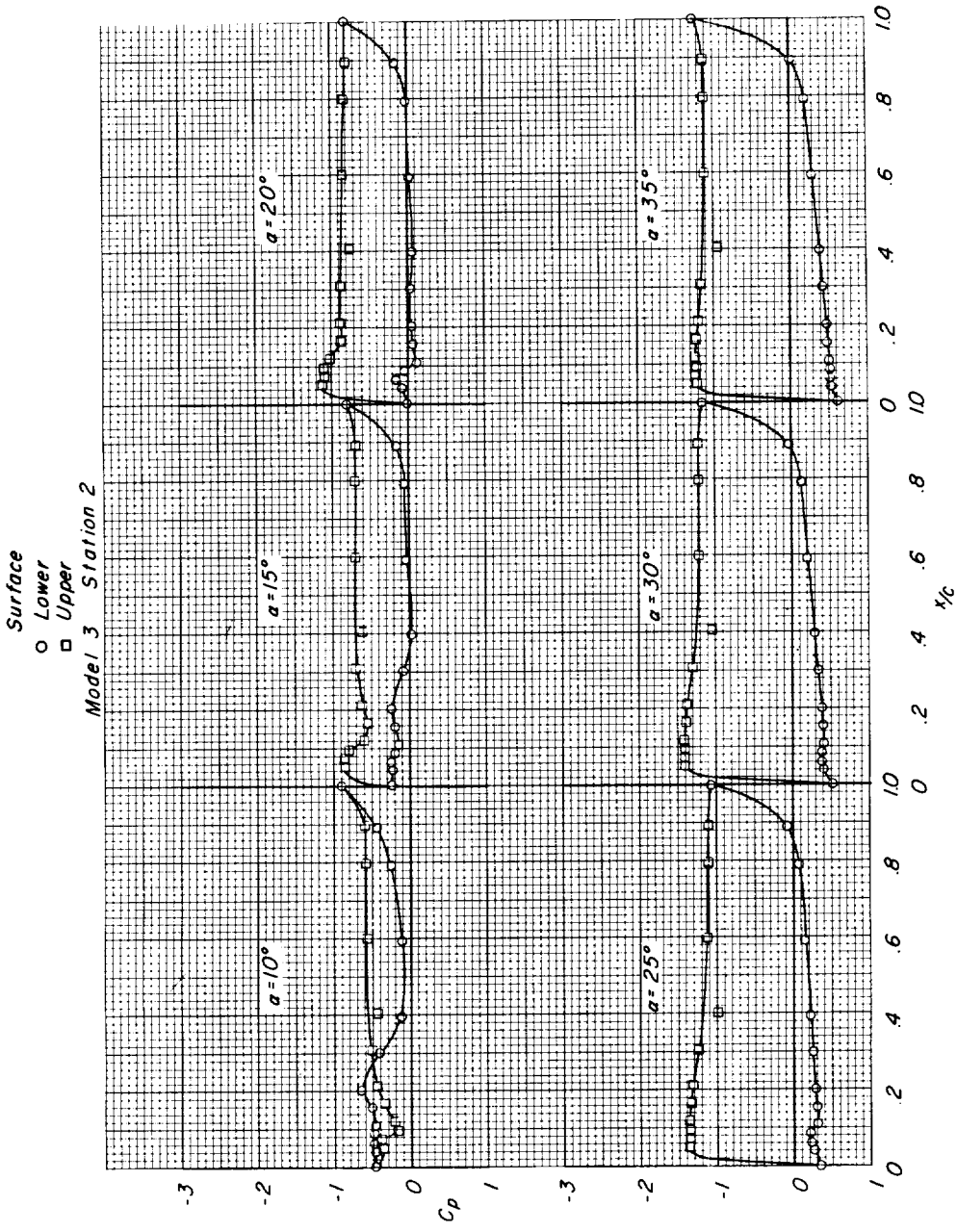

(c) M = 0.98. Continued.

Figure 8.- Continued.

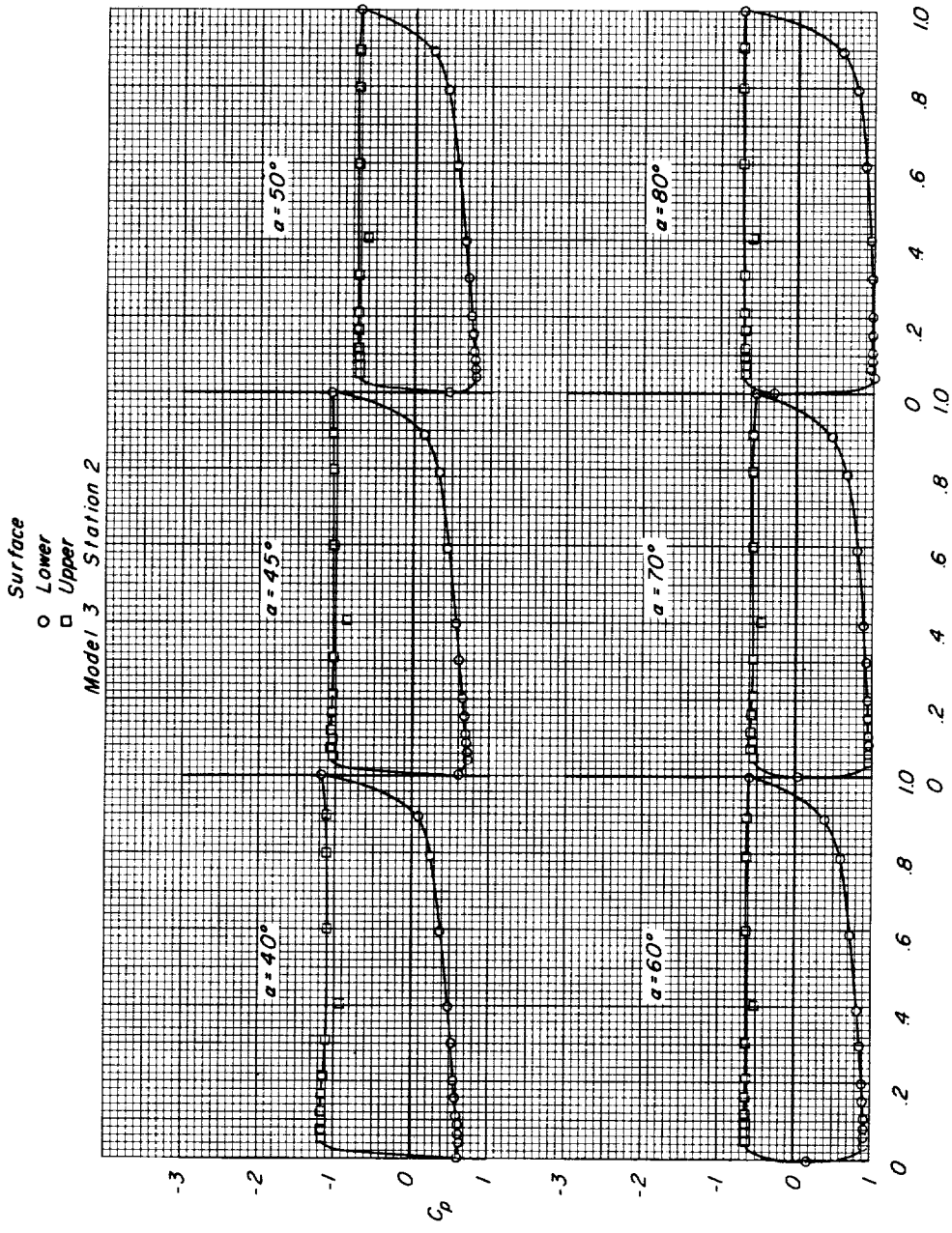

(c) M = 0.98. Continued.

Figure 8.- Continued.

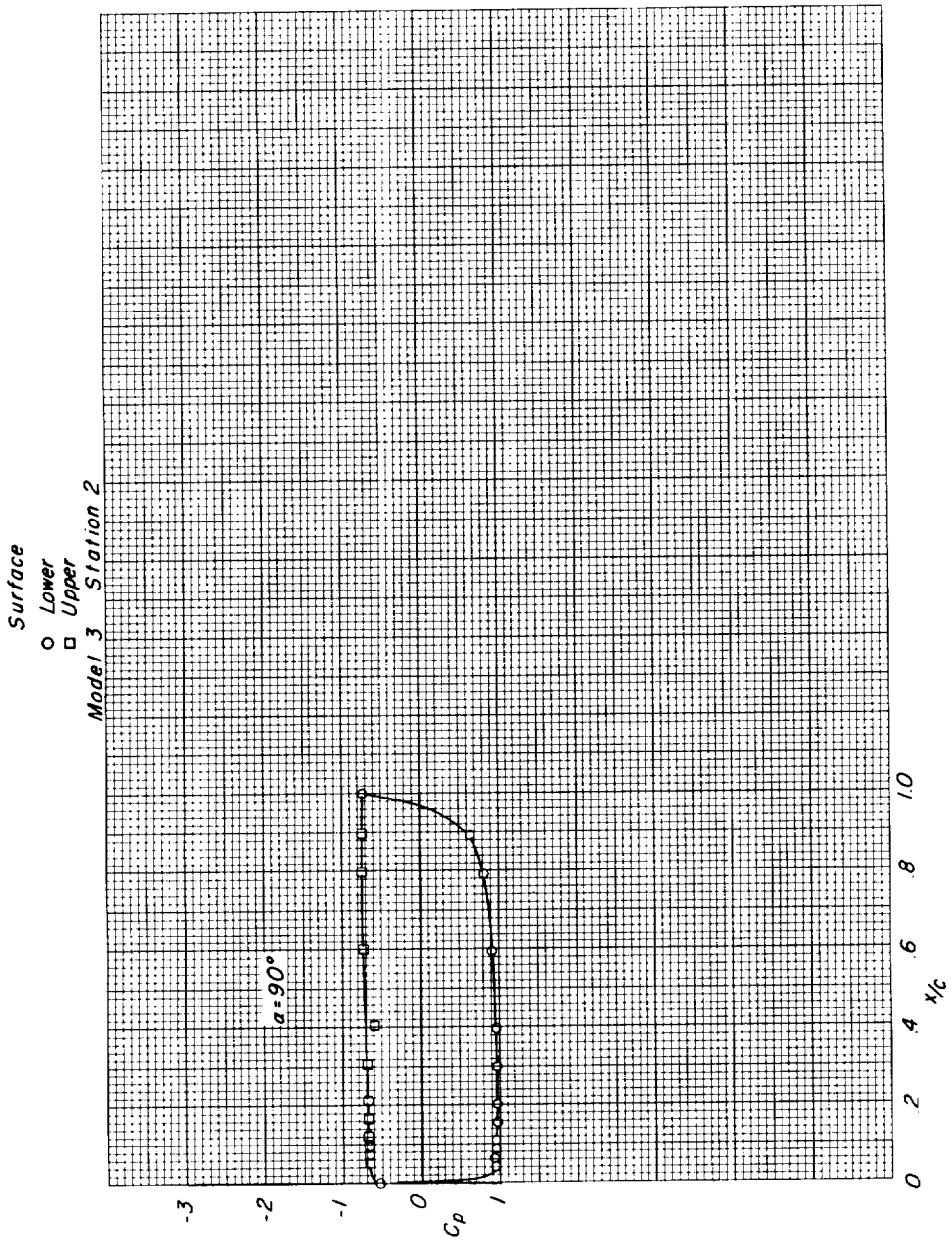

(c) M = 0.98. Continued.

Figure 8.- Continued.

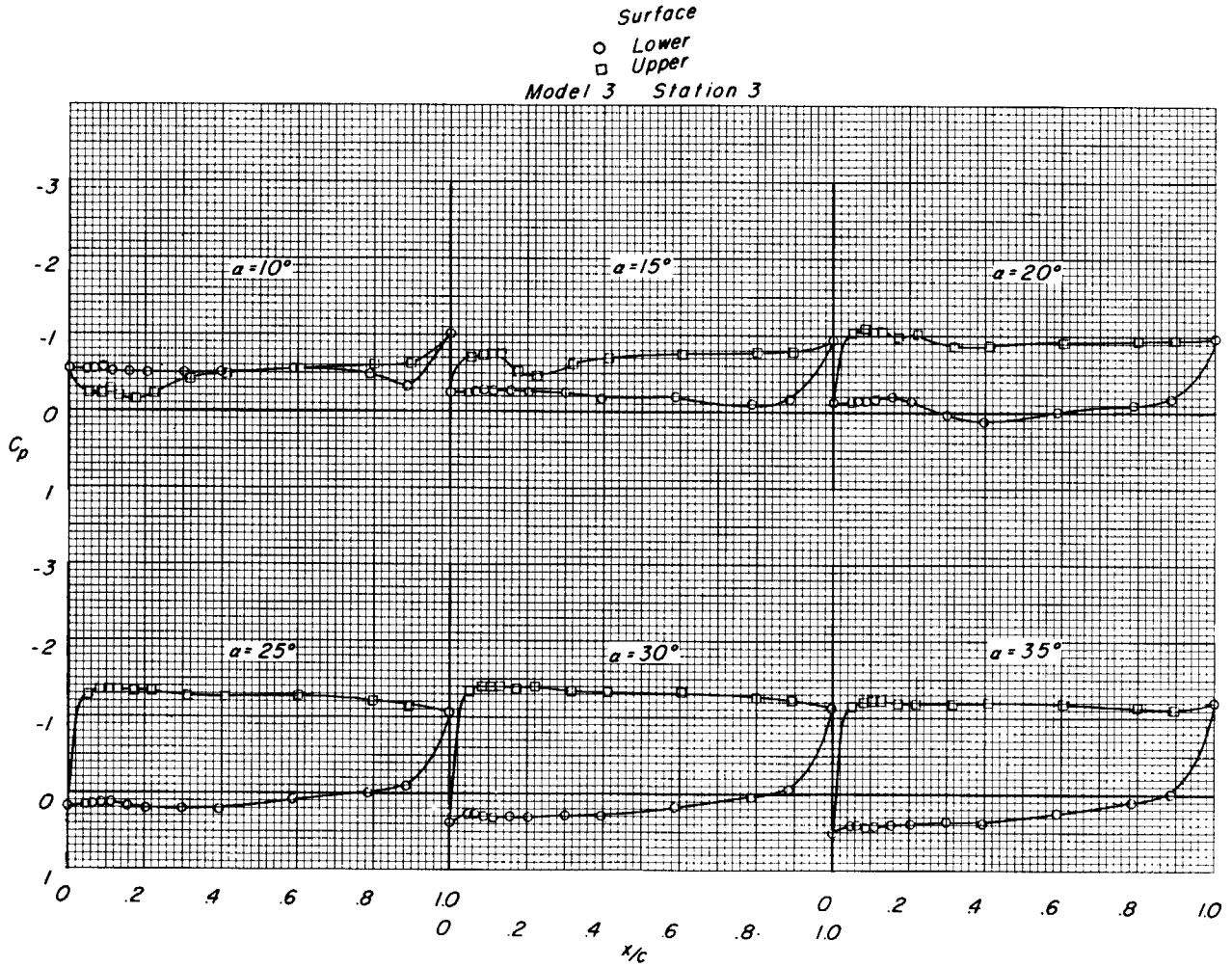

(c) M = 0.98. Continued.

Figure 8.- Continued.

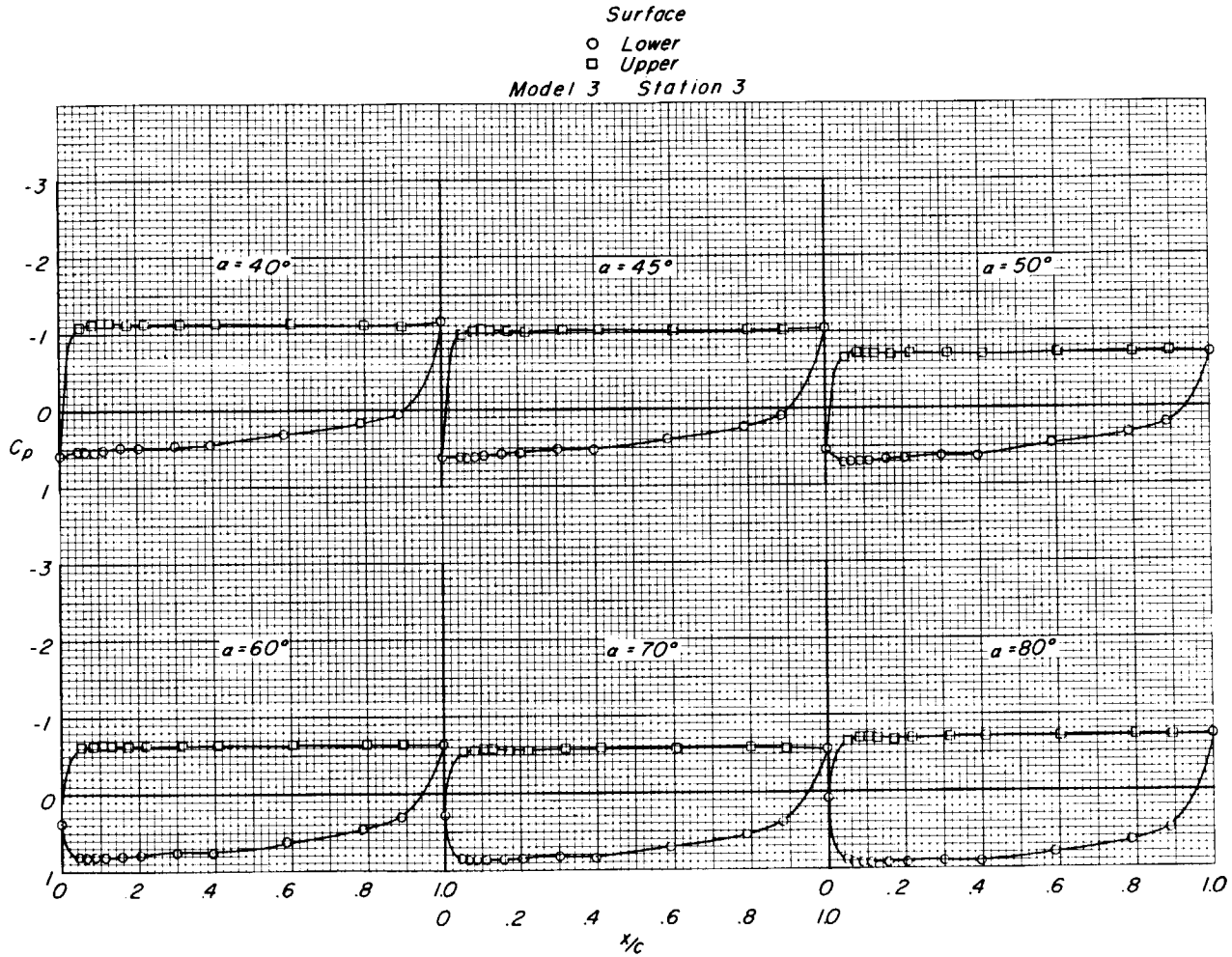

(c) M = 0.98. Continued.

Figure 8.- Continued.

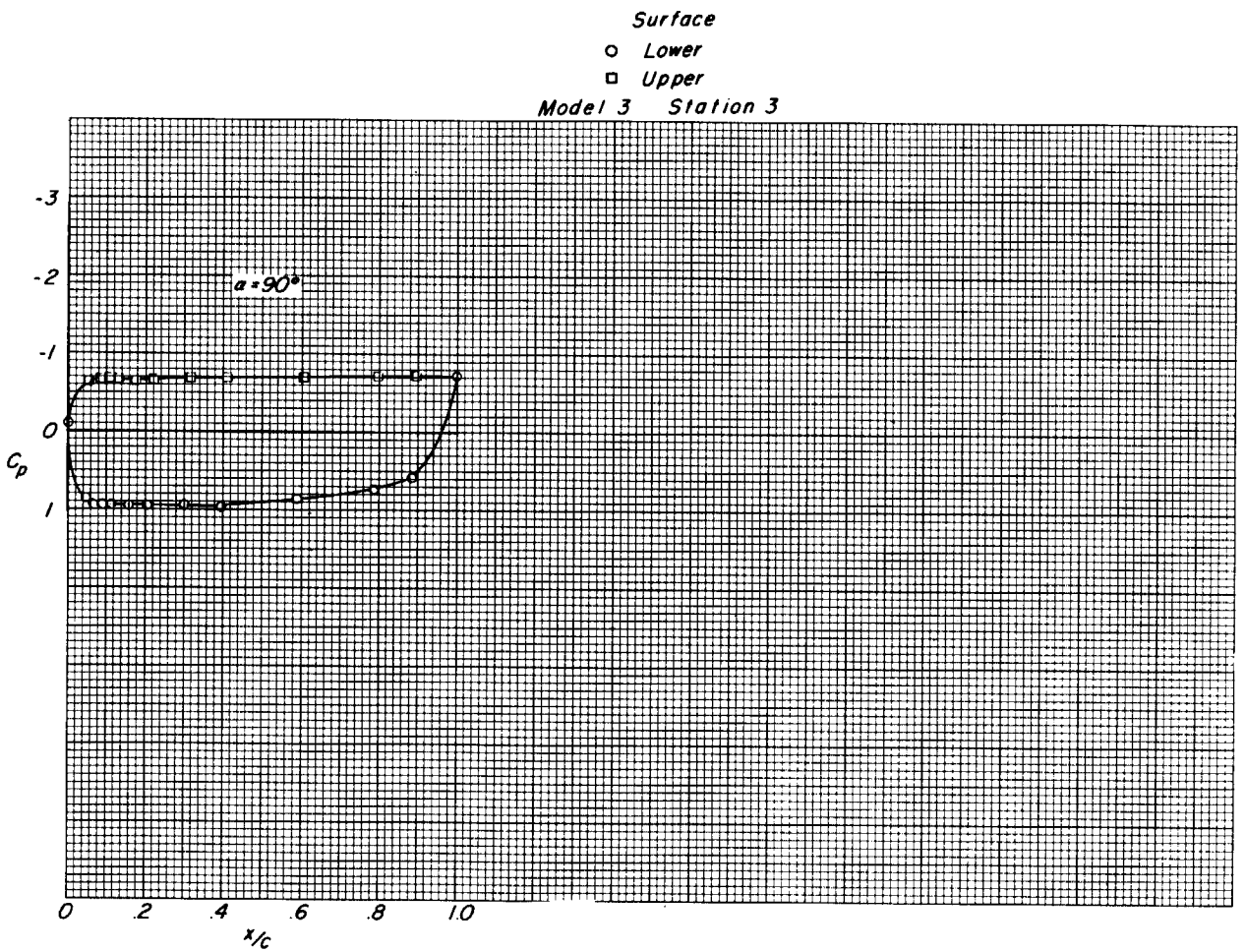

(c) M = 0.98. Continued.

Figure 8.- Continued.

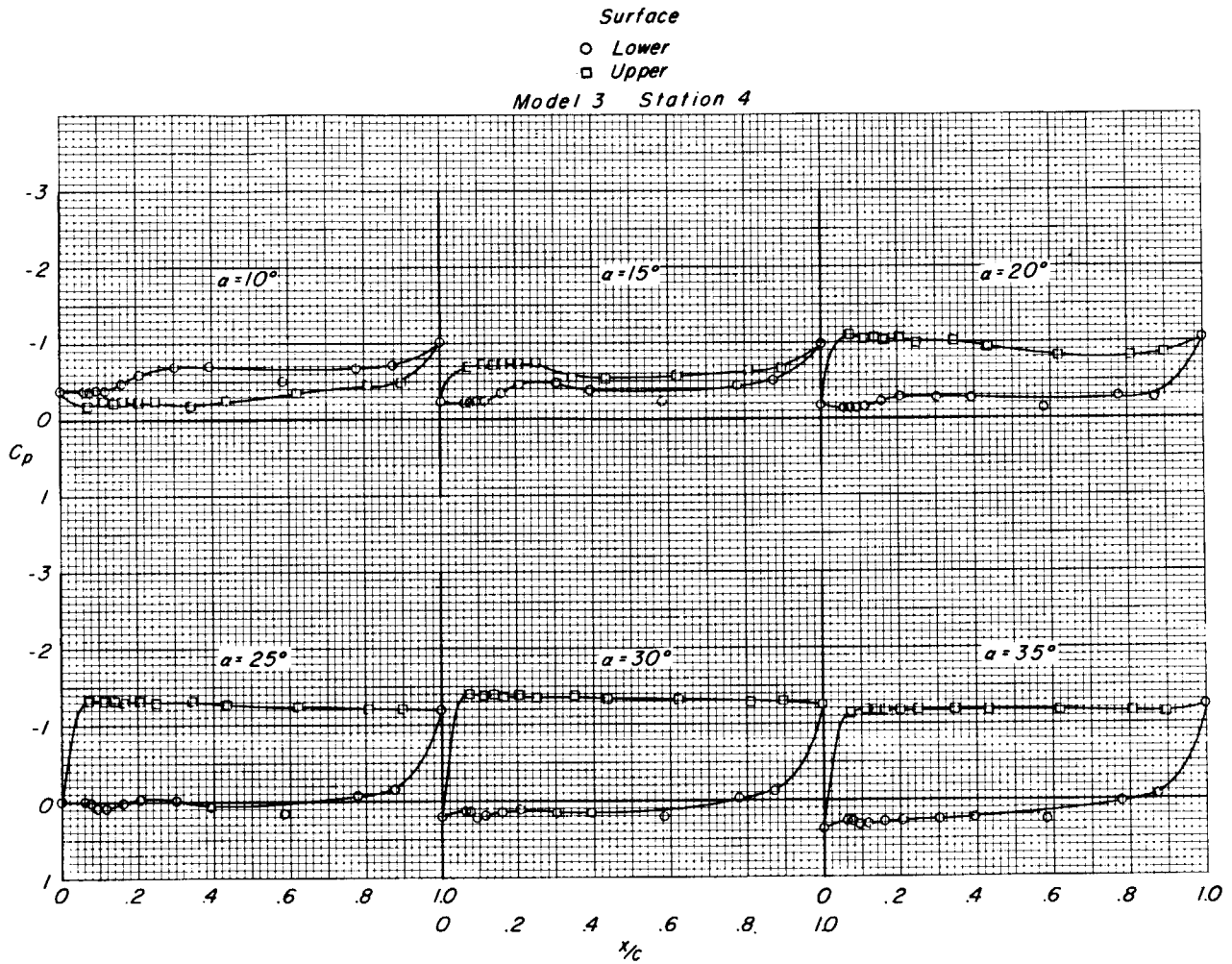

(c) M = 0.98. Continued.

Figure 8.- Continued.

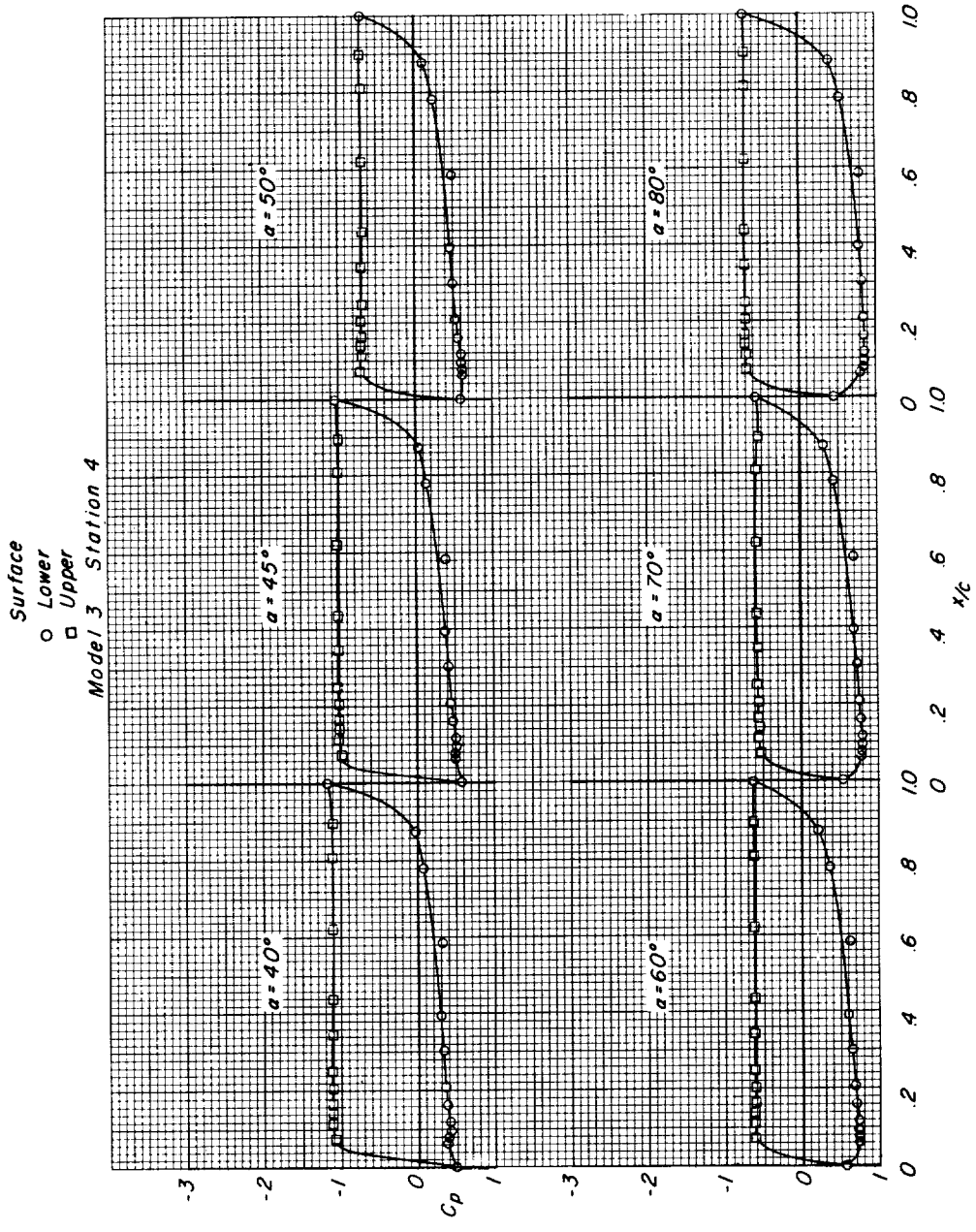

(c) M = 0.98. Continued.

Figure 8.- Continued.

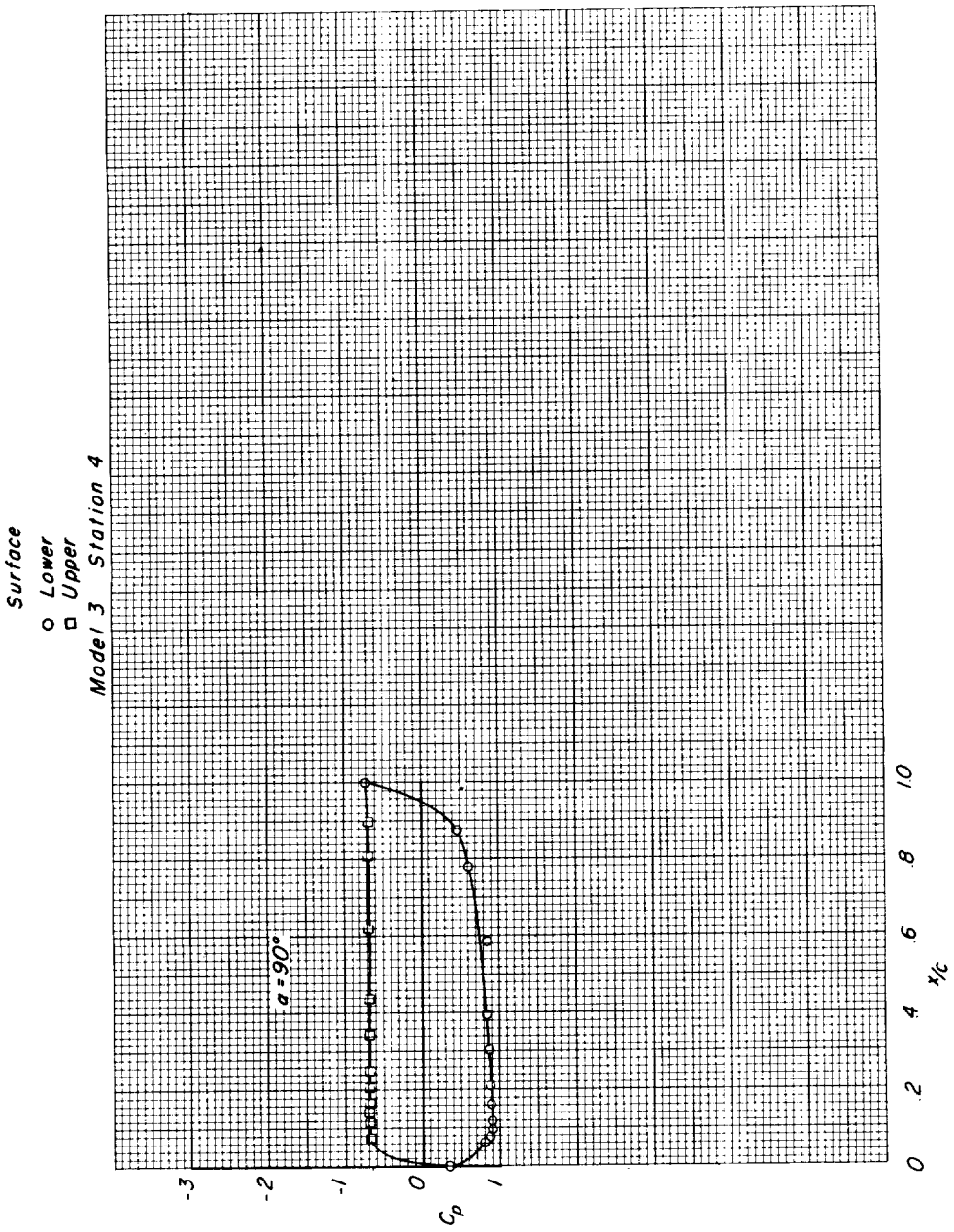

(c) M = 0.98. Concluded.

Figure 8.- Continued.

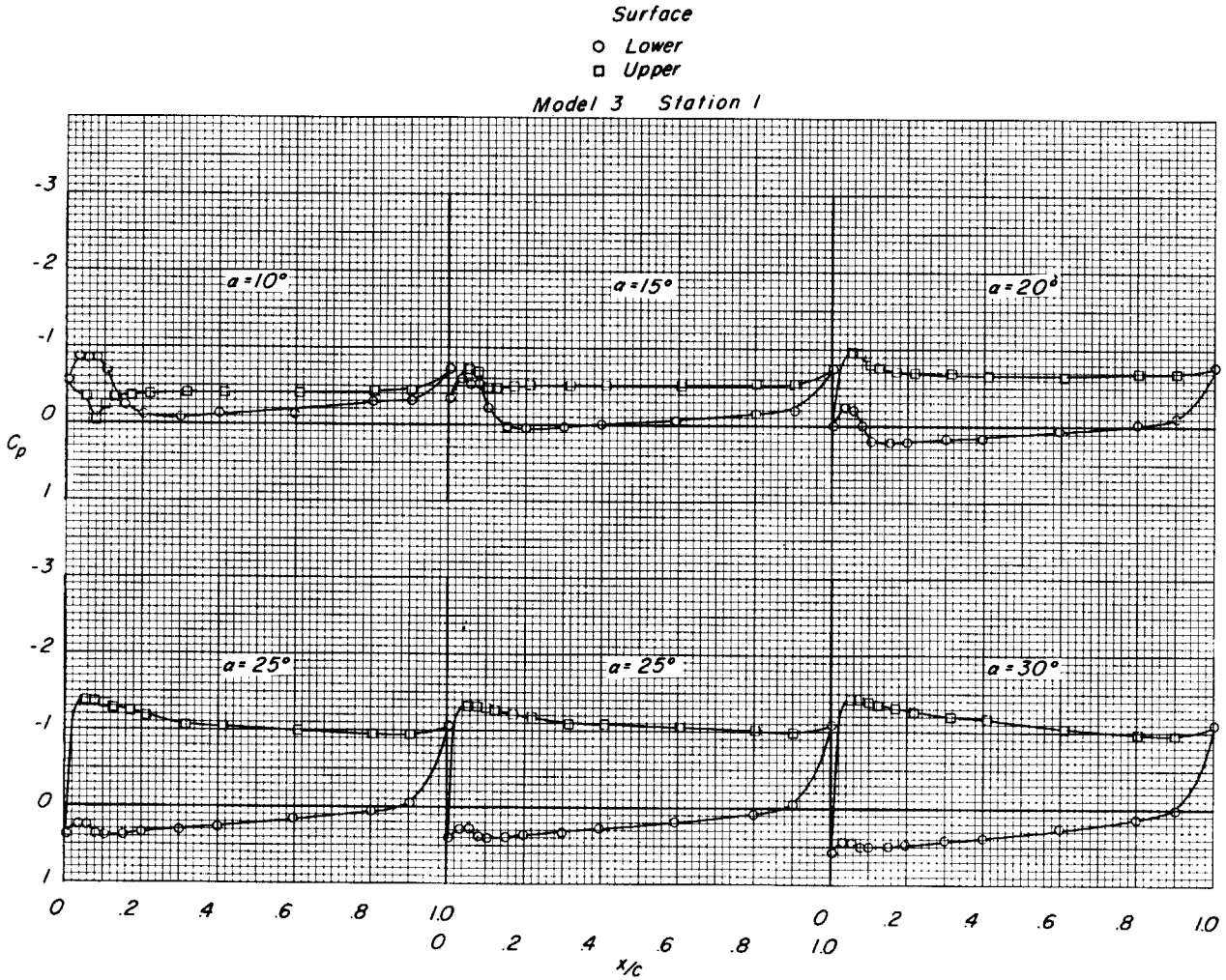

(d) M = 1.02.

Figure 8.- Continued.

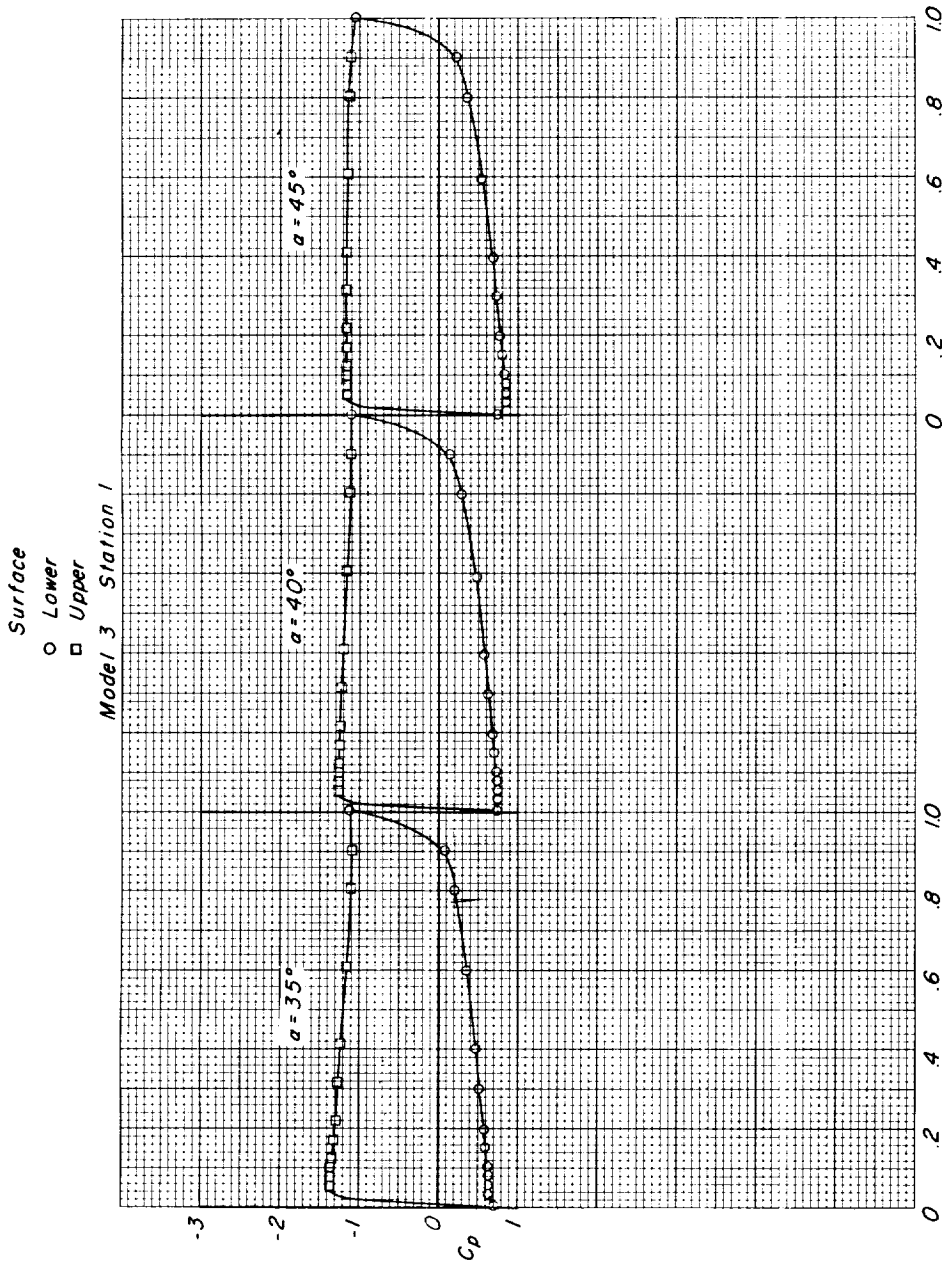

(d) M = 1.02. Continued.

Figure 8.- Continued.

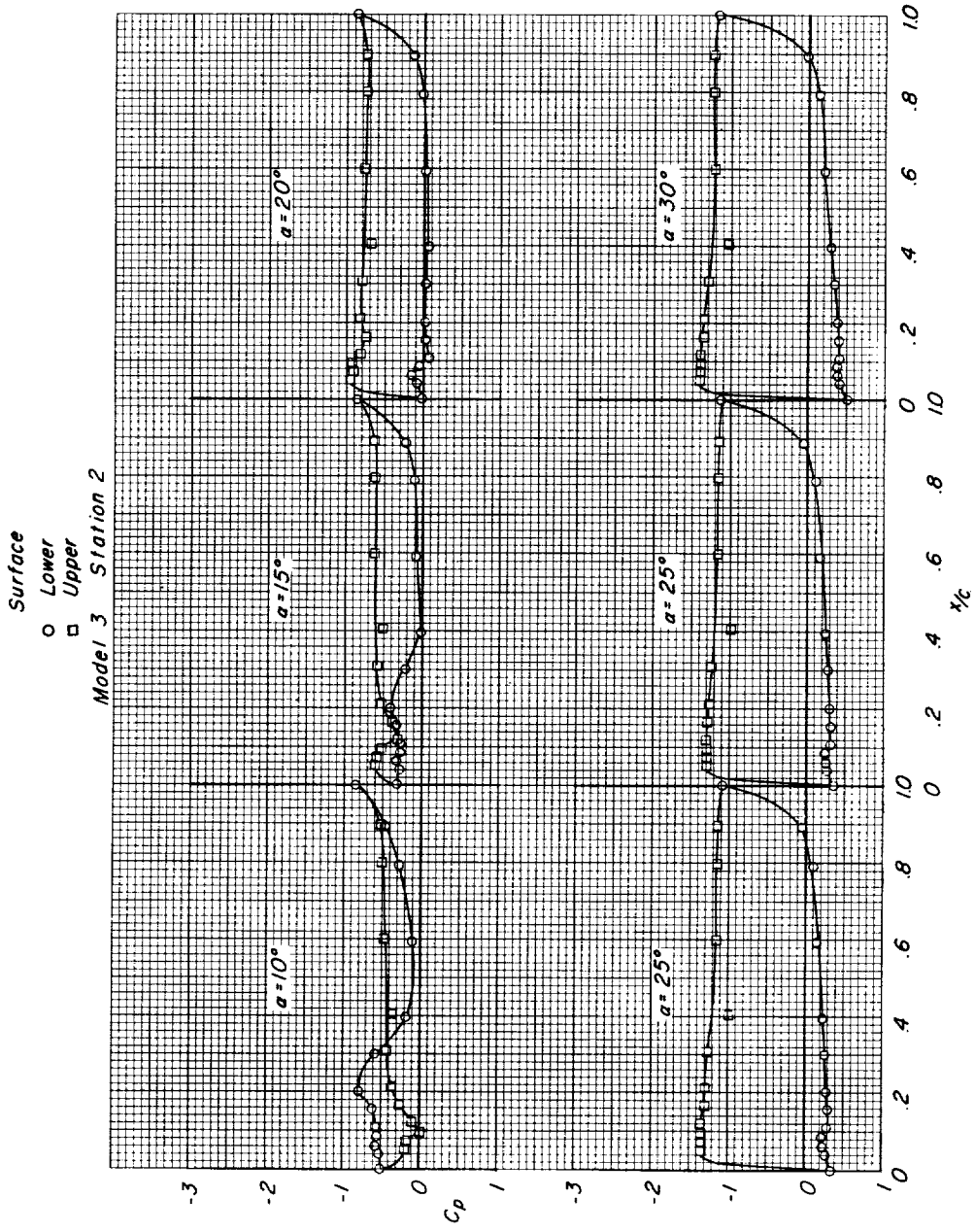

(d) M = 1.02. Continued.

Figure 8.- Continued.

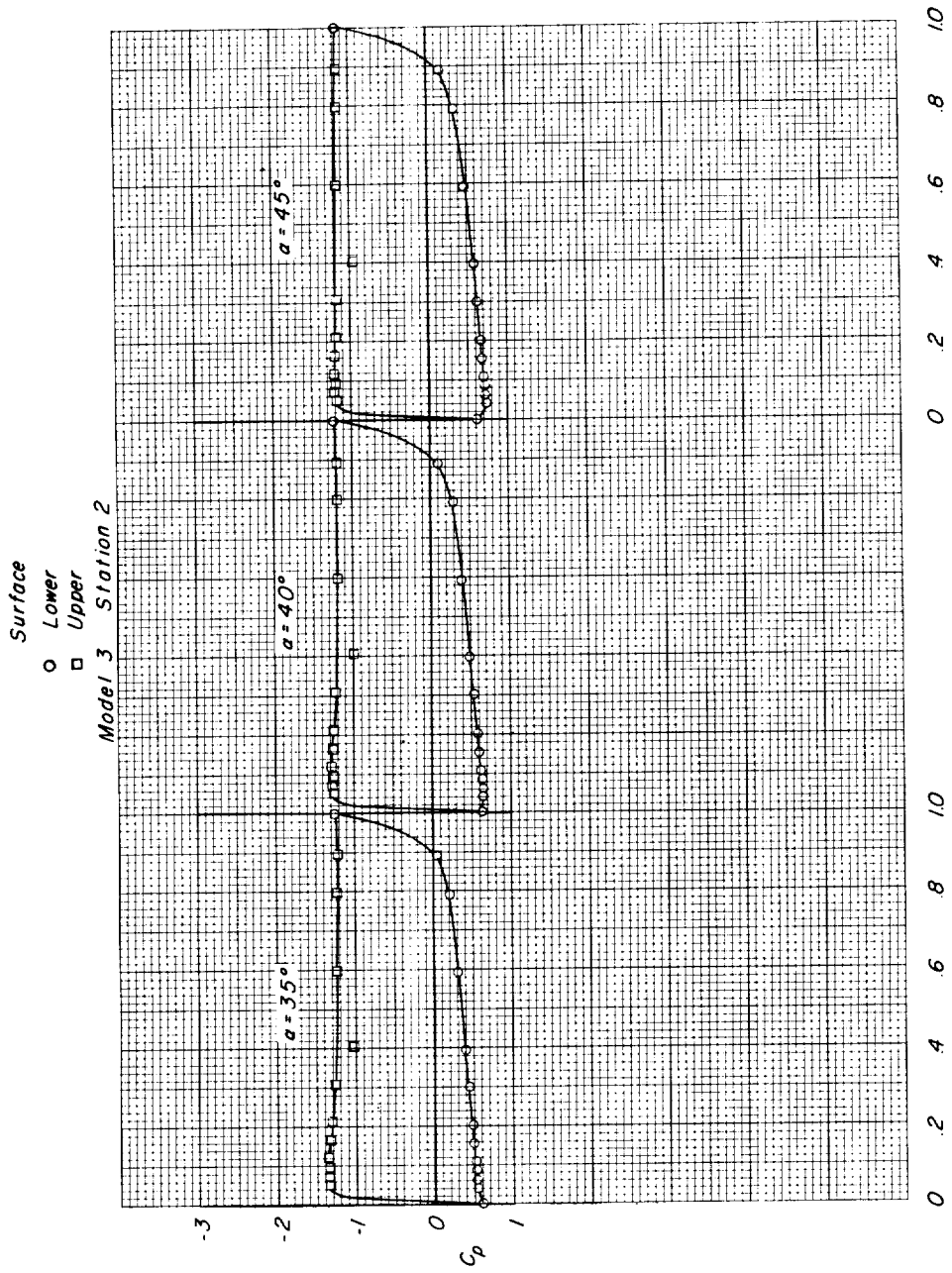

(d) M = 1.02. Continued.

Figure 8.- Continued.

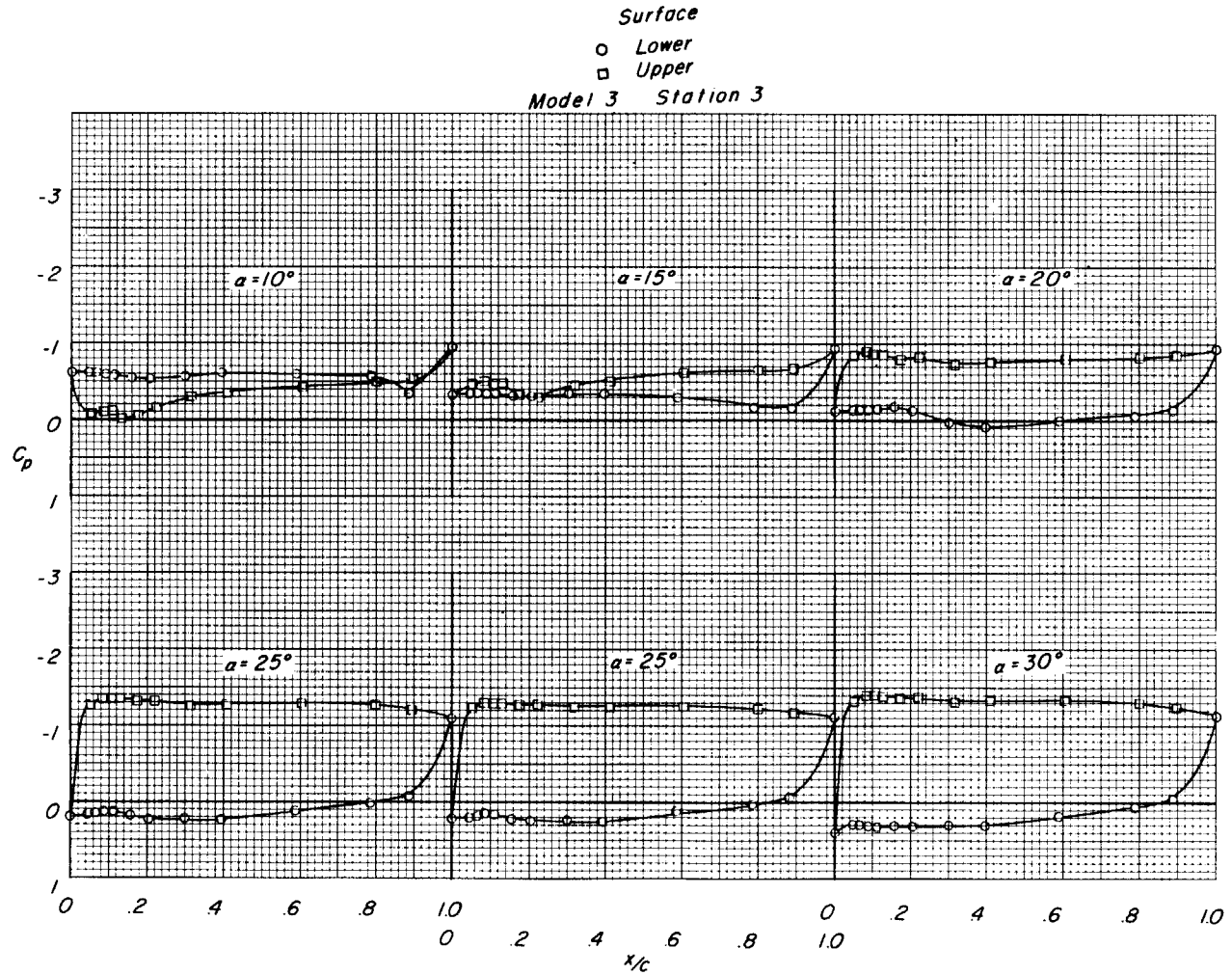

(d) M = 1.02. Continued.

Figure 8.- Continued.

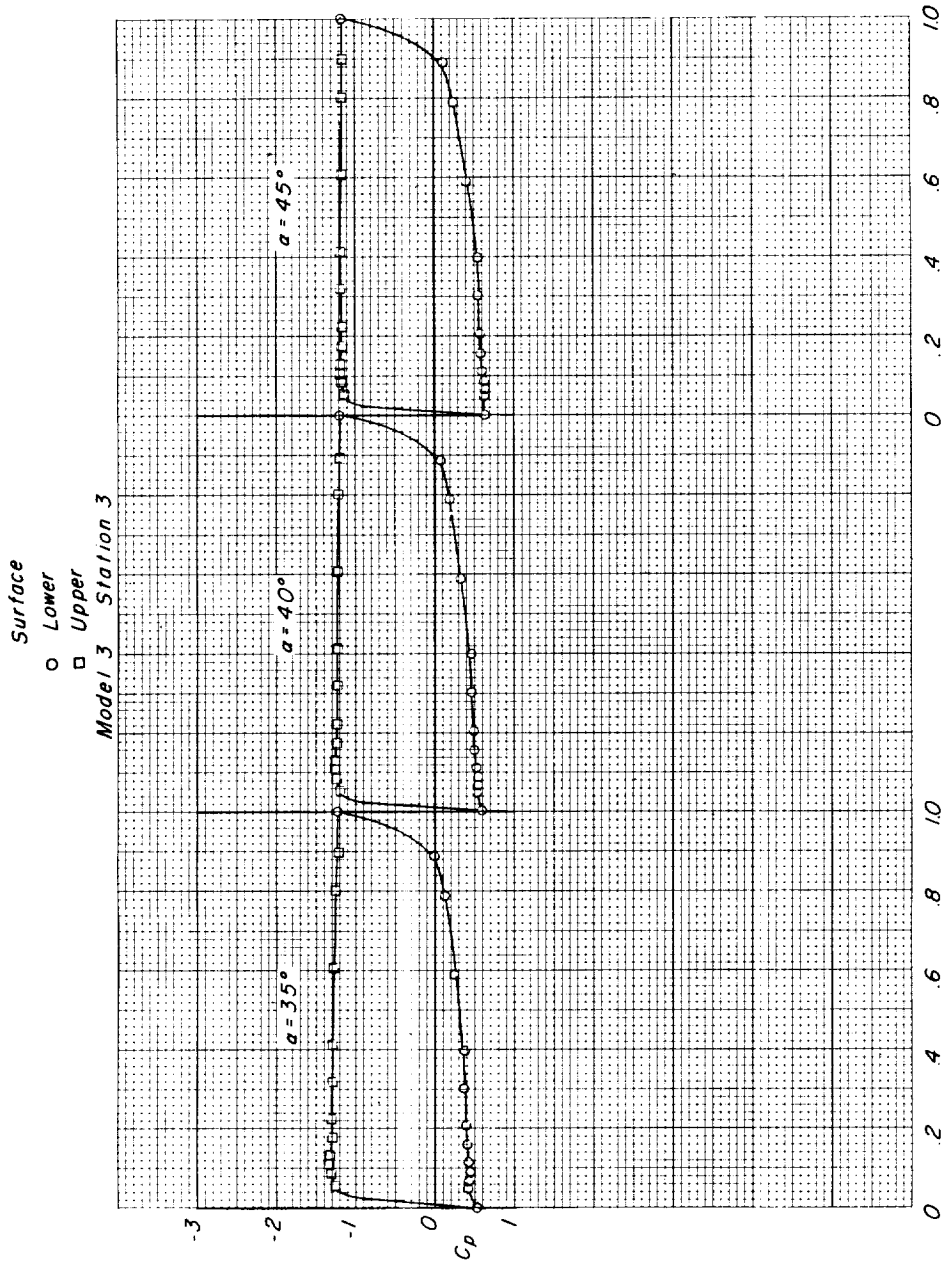

(d) M = 1.02. Continued.

Figure 8.- Continued.

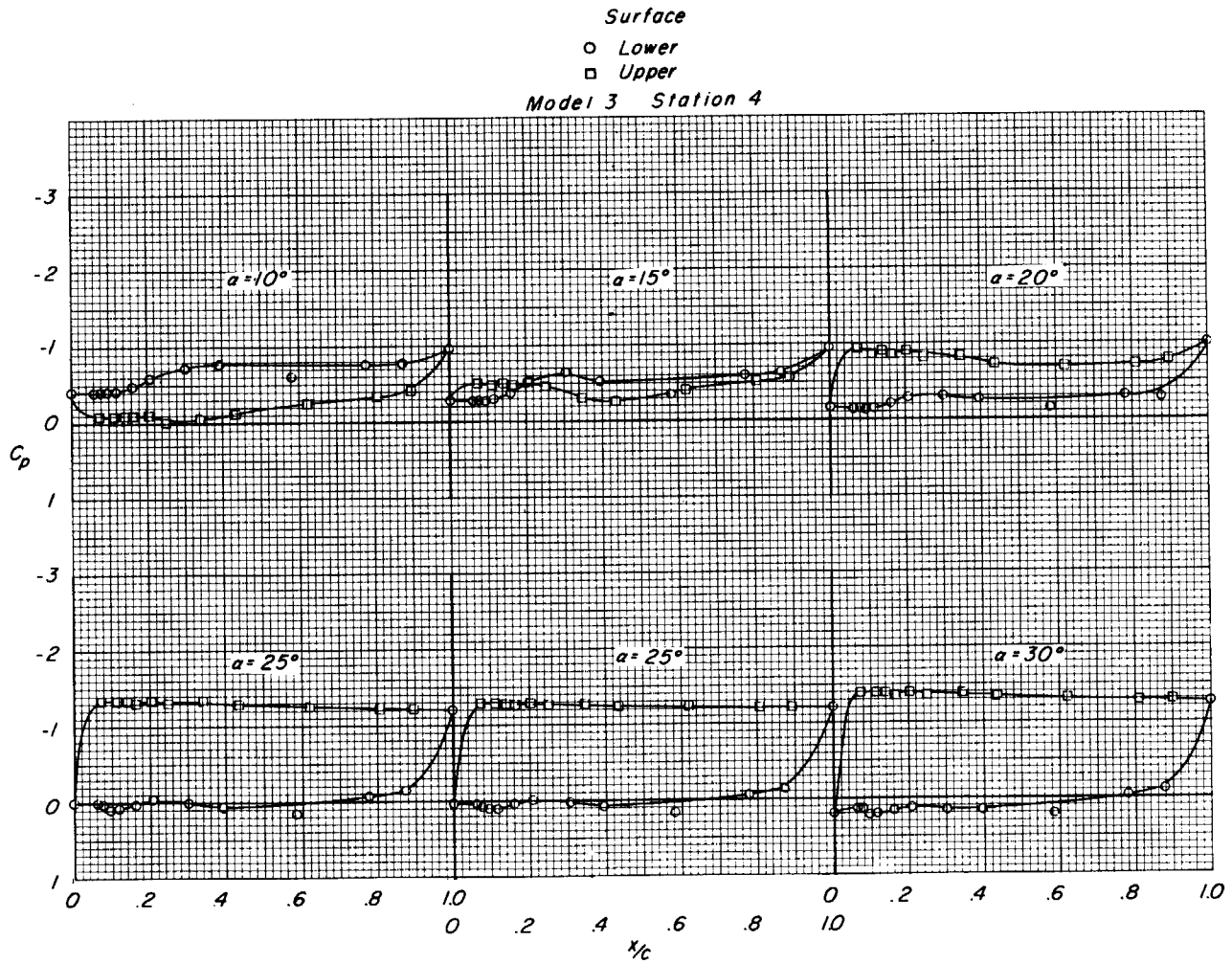

(d) M = 1.02. Continued.

Figure 8.- Continued.

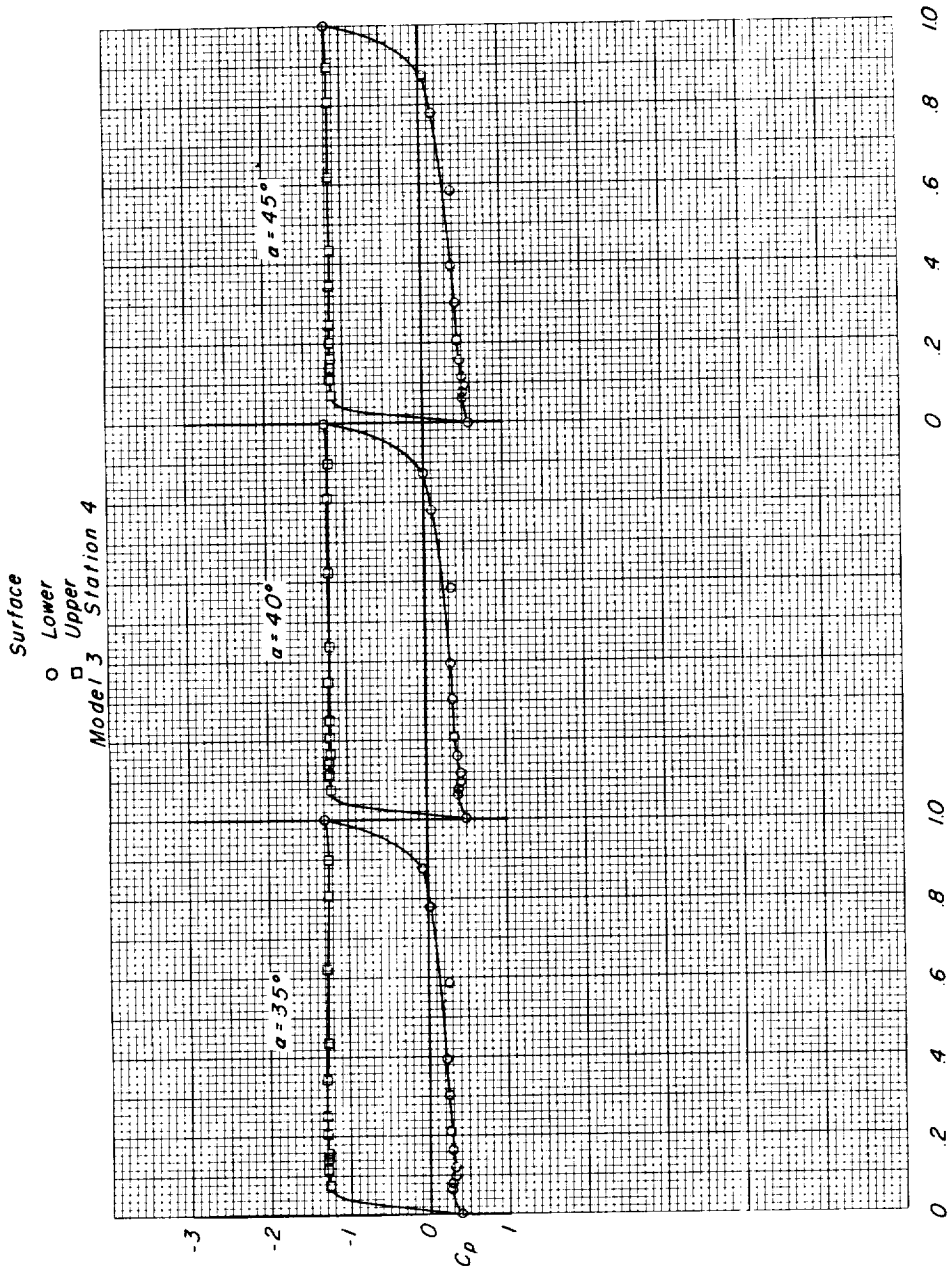

(d) M = 1.02. Concluded.

Figure 8.- Continued.

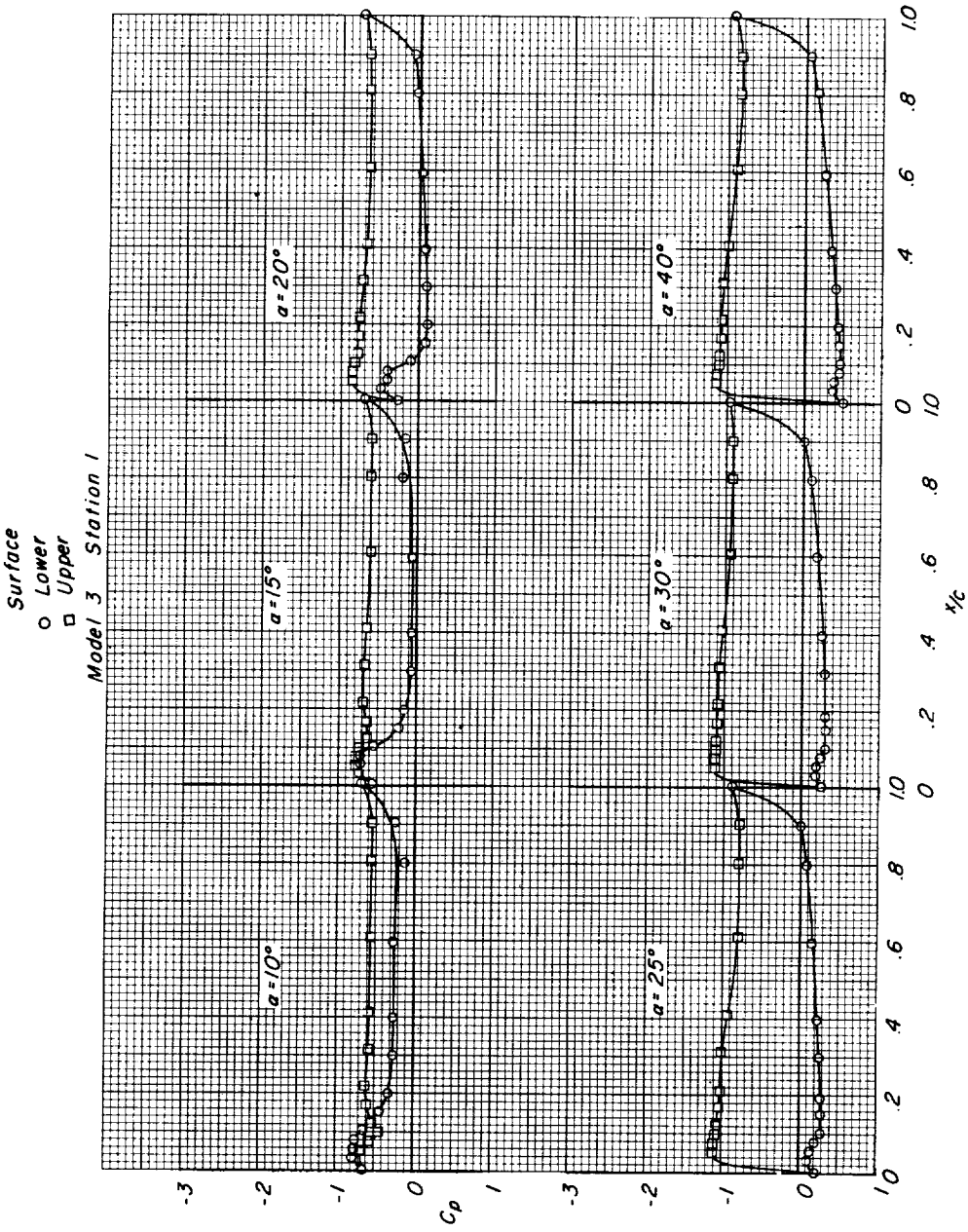

(e) M = 1.20.

Figure 8.- Continued.

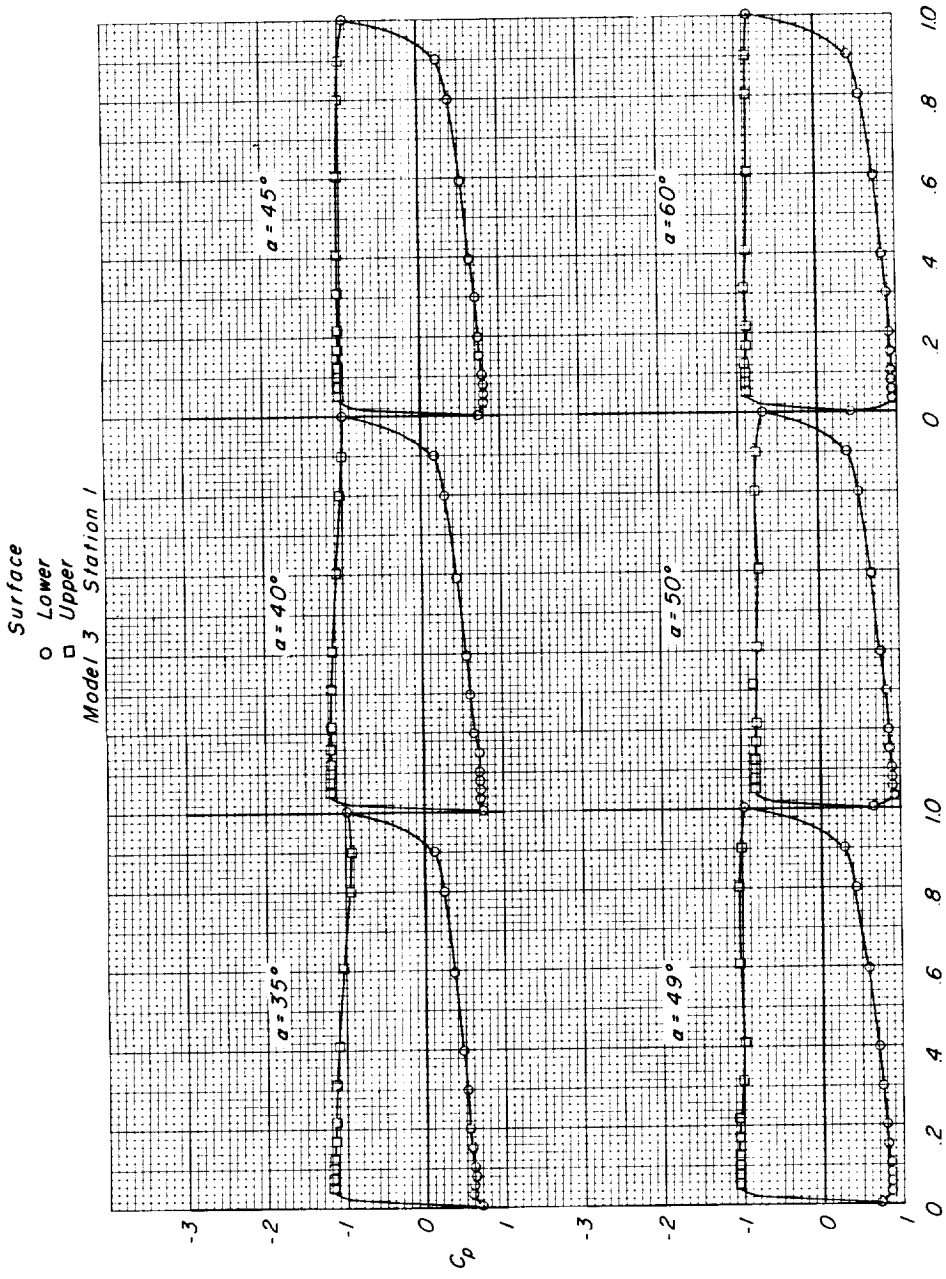

(e) M = 1.20. Continued.

Figure 8.- Continued.

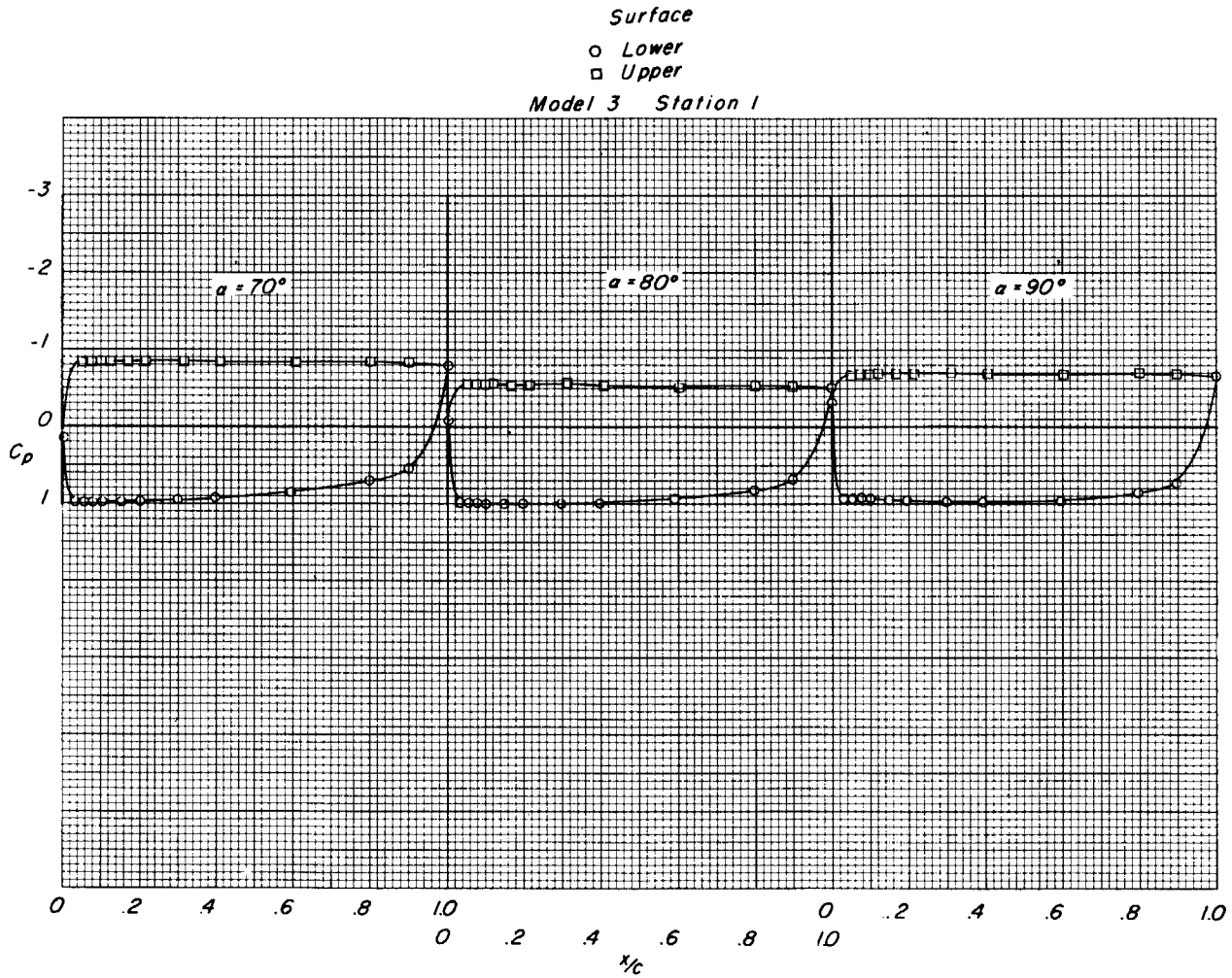

(e) M = 1.20. Continued.

Figure 8.- Continued.

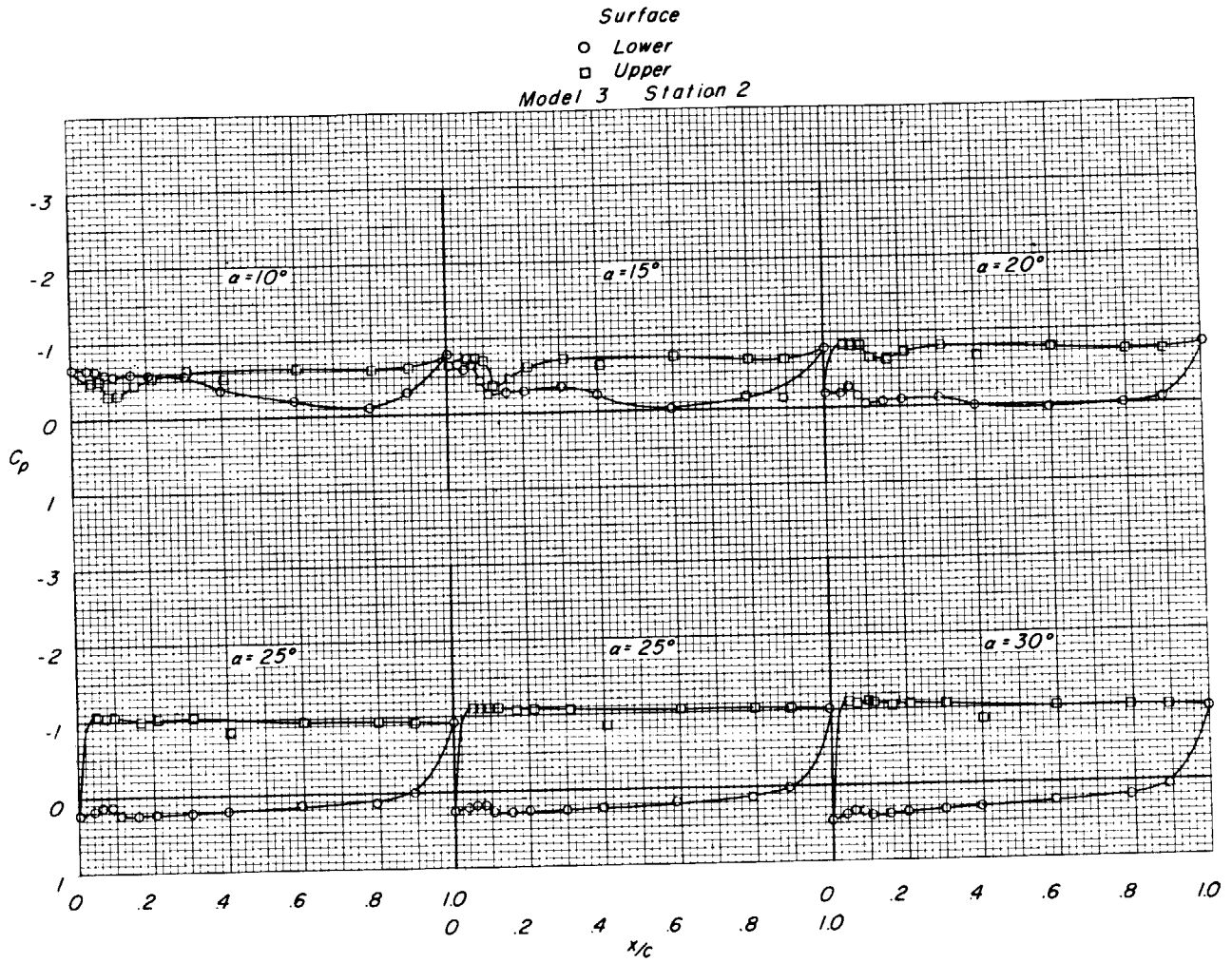

(e) M = 1.20. Continued.

Figure 8.- Continued.

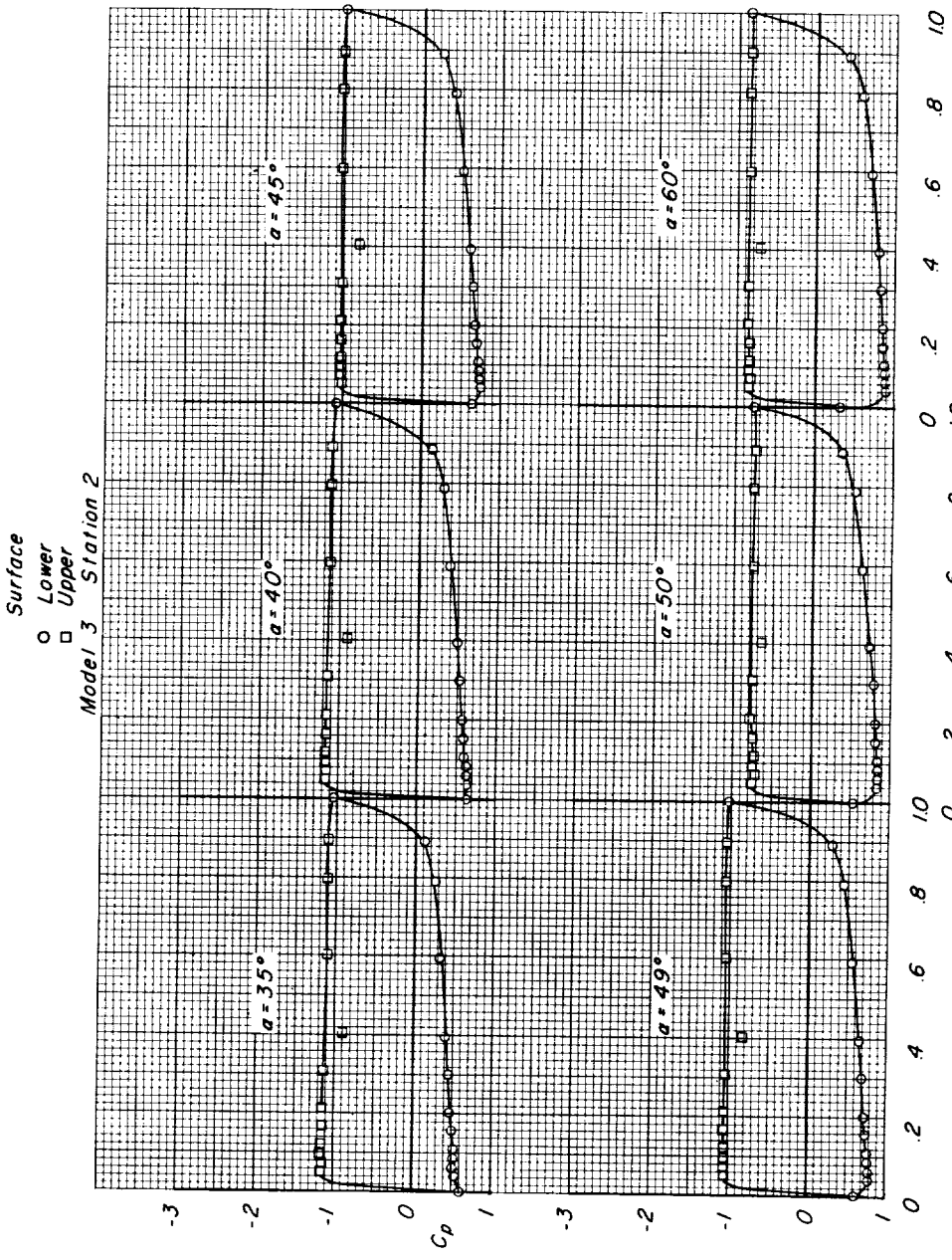

(e) M = 1.20. Continued.

Figure 8.- Continued.

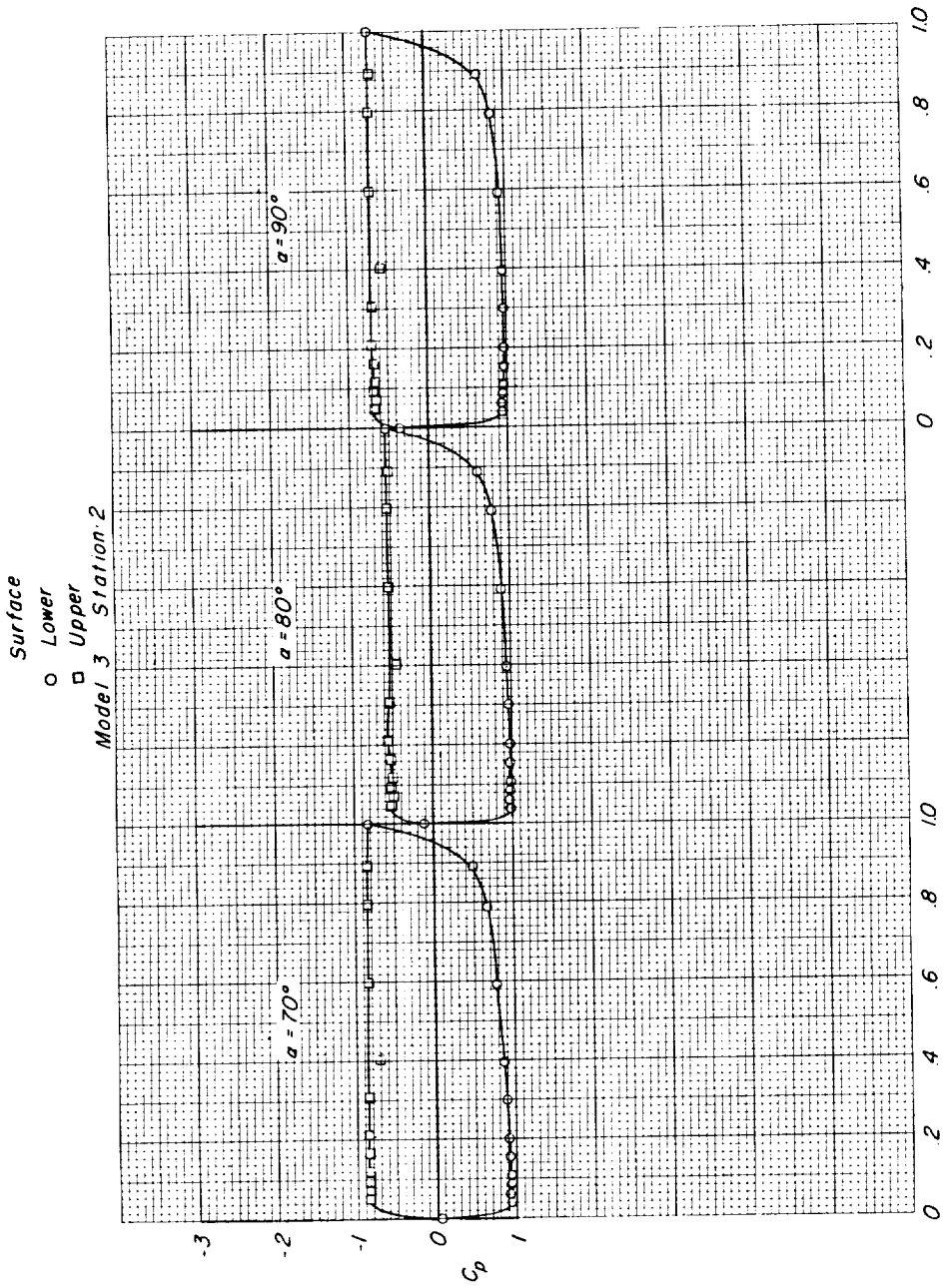

(e) M = 1.20. Continued.

Figure 8.- Continued.

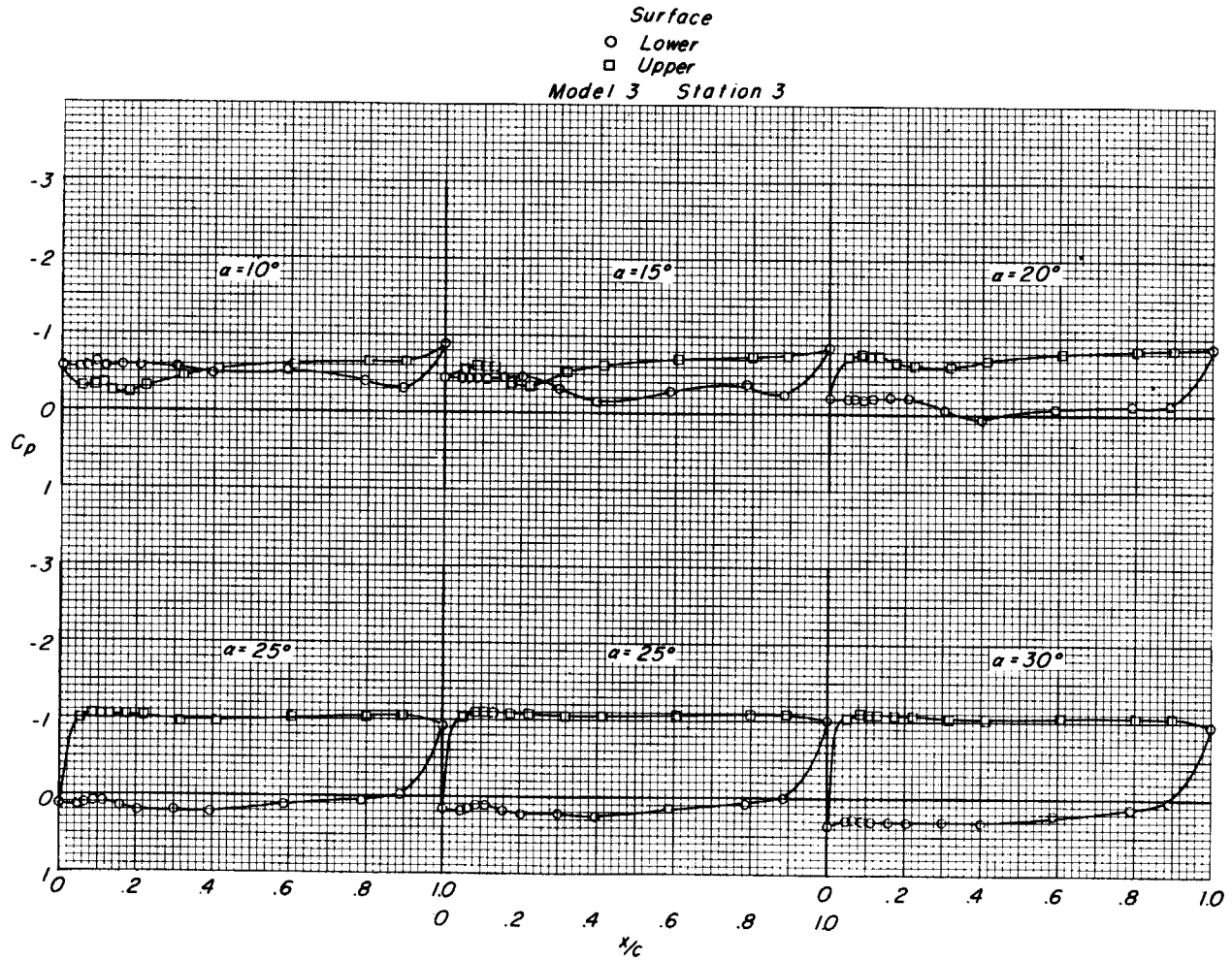

(e) M = 1.20. Continued.

Figure 8.- Continued.

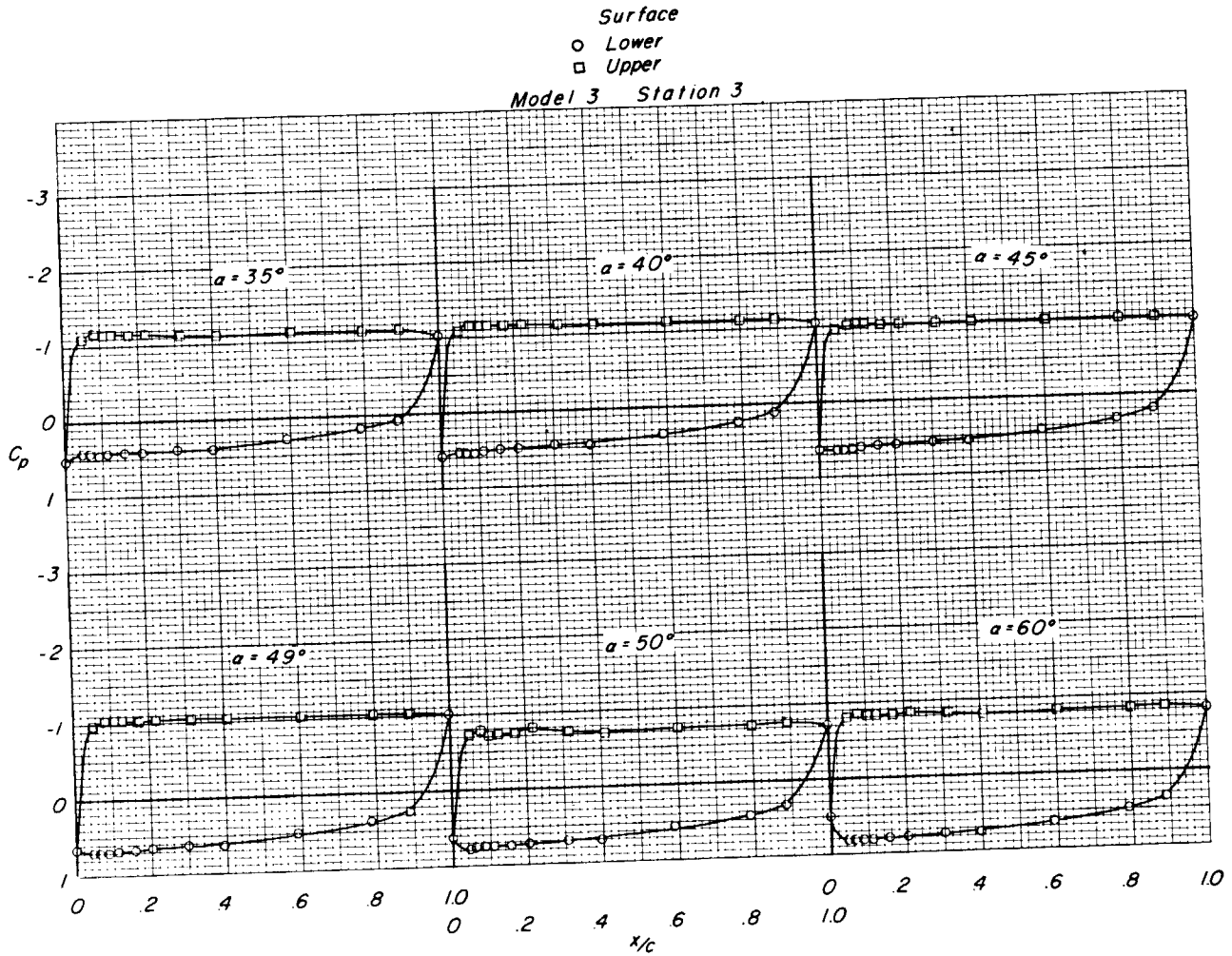

(e) M = 1.20. Continued.

Figure 8.- Continued.

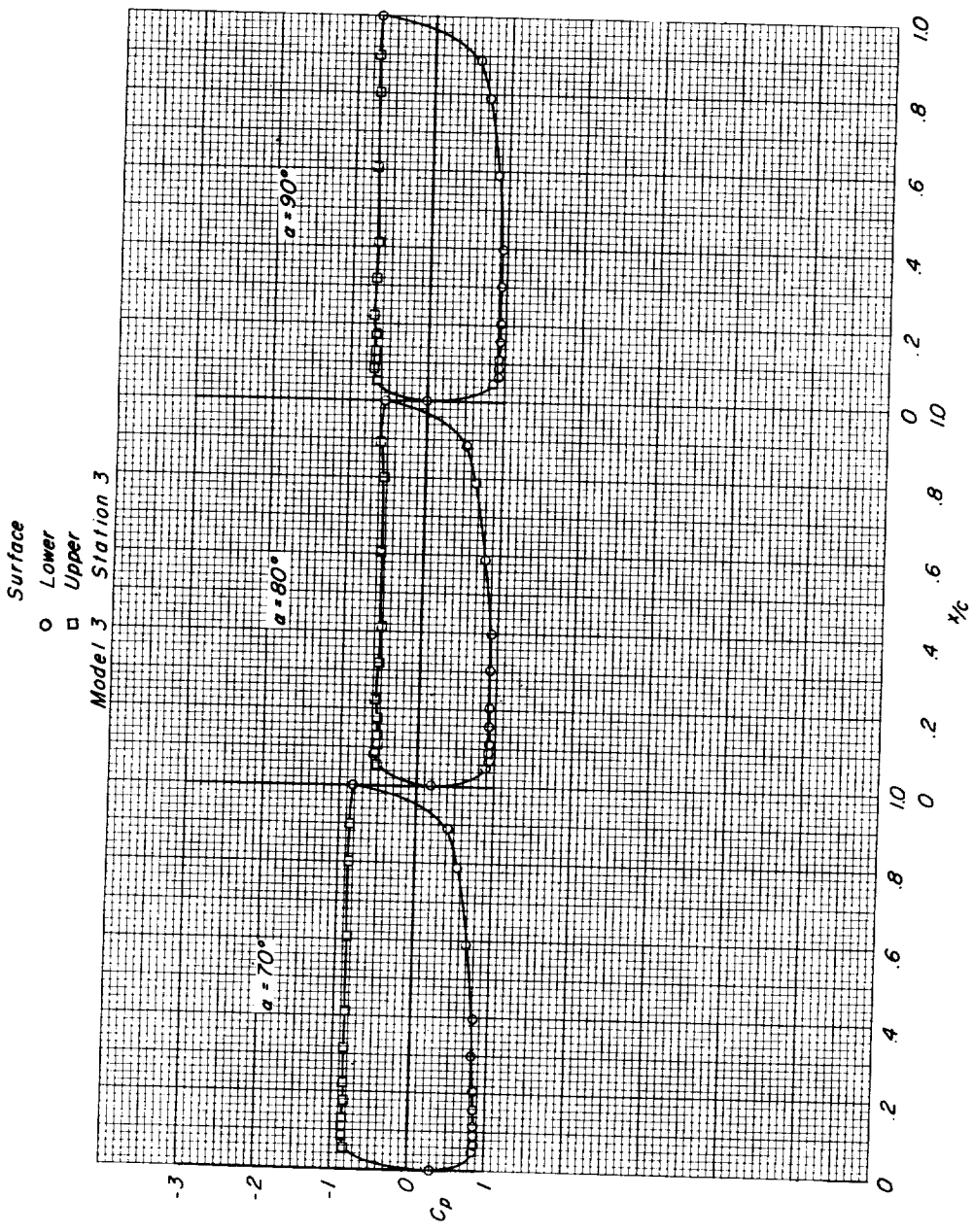

(e) M = 1.20. Continued.

Figure 8.- Continued.

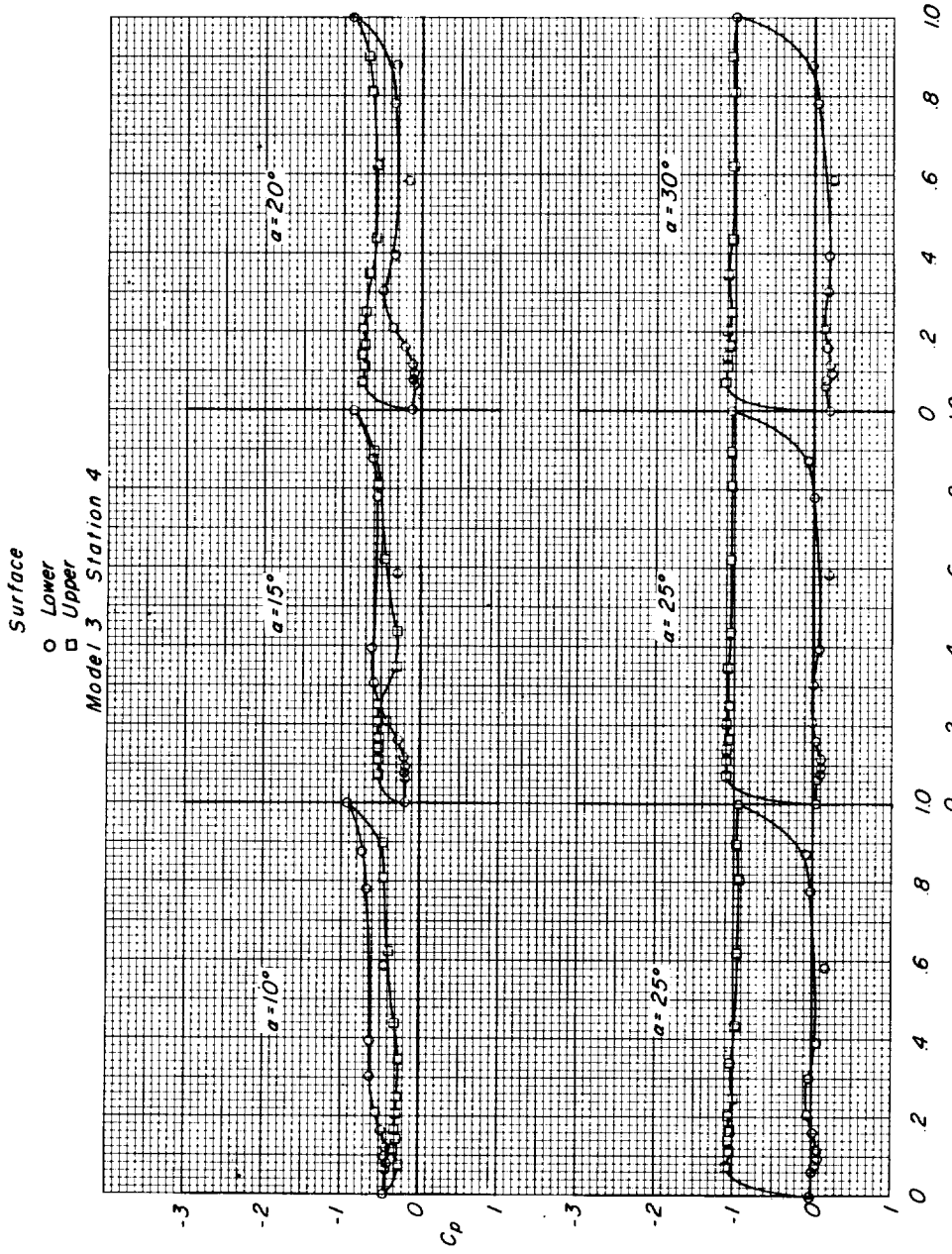

(e) M = 1.20. Continued.

Figure 8.- Continued.

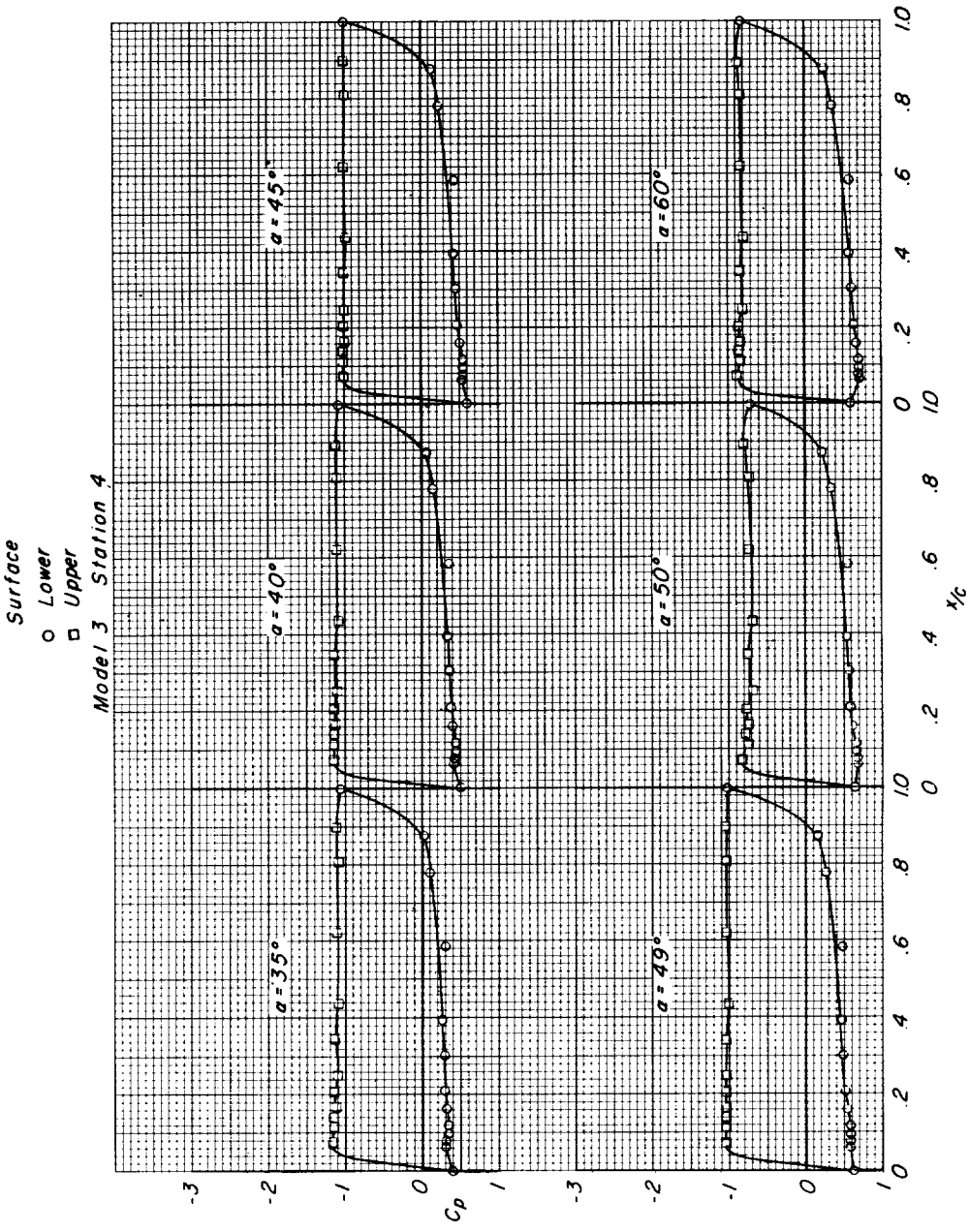

(e) M = 1.20. Continued.

Figure 8.- Continued.

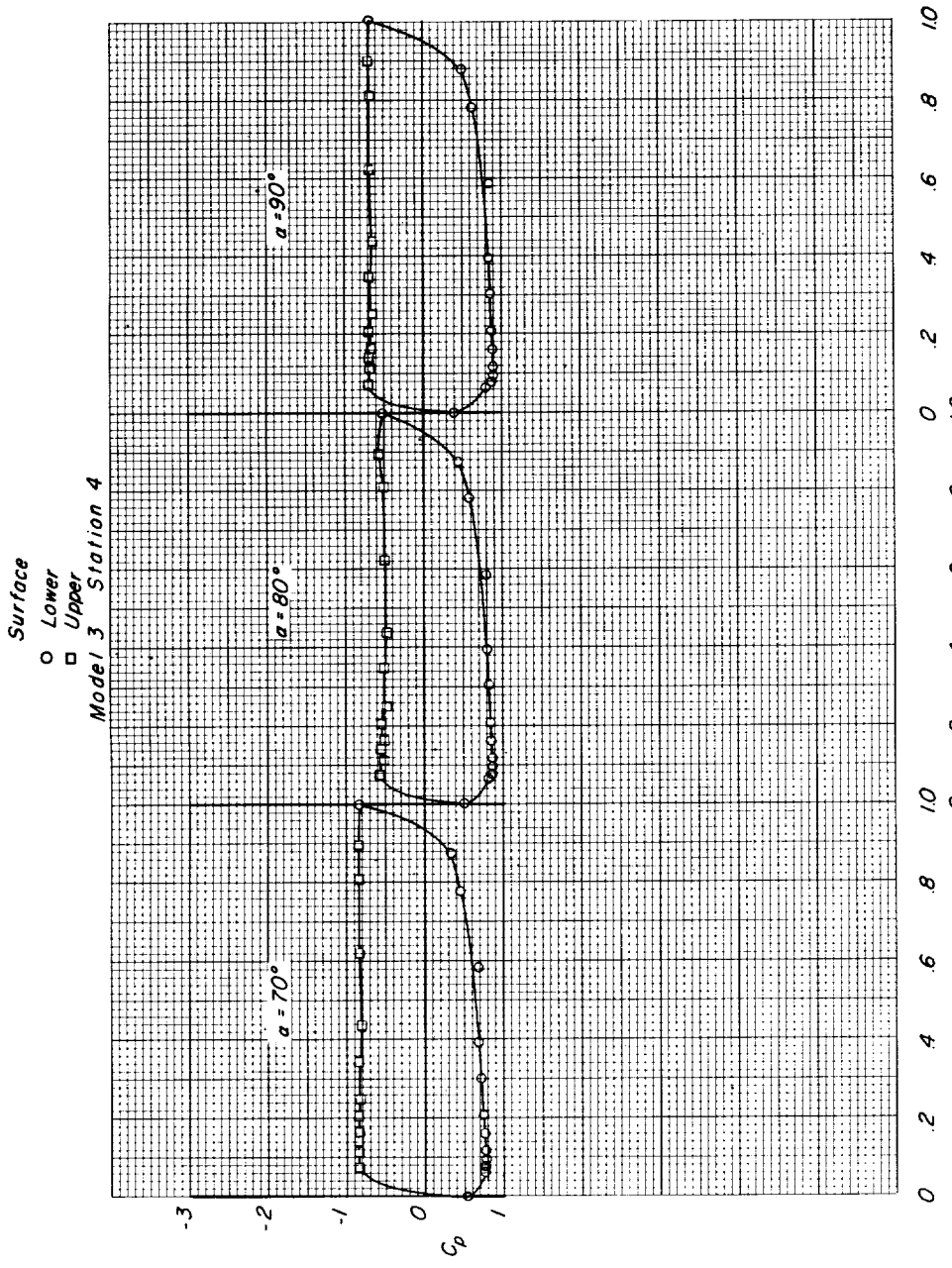

(e) M = 1.20. Concluded.

Figure 8.- Concluded.